Tectonic, Climatic, and Sedimentary Processes Recorded by Pleistocene Fold Growth Strata, The South Caspian Basin, Azerbaijan

RICHARDSON, STEPHEN,EDWIN,JONATHAN

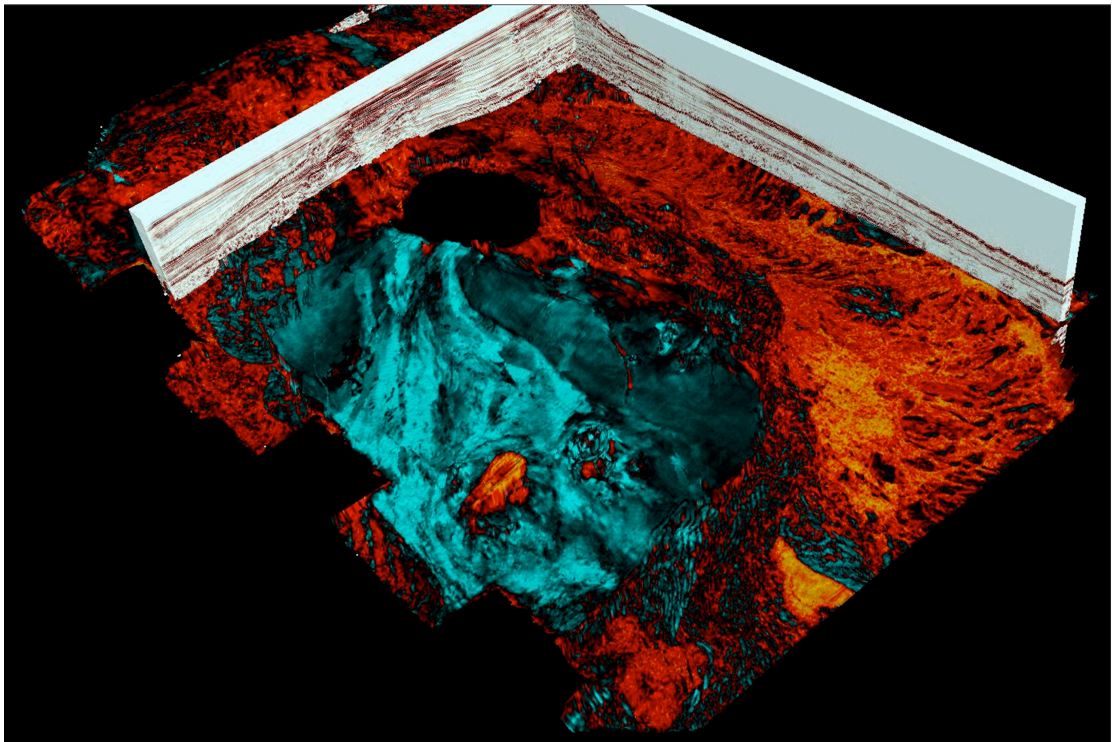

Tectonic, Climatic, and Sedimentary Processes Recorded by Pleistocene Fold Growth Strata, The South Caspian Basin, Azerbaijan

Steve E J Richardson

2012

Cover Photo:
This Pleistocene seismic horizon overlaps the Shah Deniz Fold, and forms part of its growth strata. It has been coloured by the amplitudes of the seismic reflections that lie immediately above it. The amplitude map images a mud flow(coloured in light blue) emanating from a large mud volcano crater, and two mass transport deposits, (coloured in orange), which wrap around the flanks and tips of the fold. The mass transport deposits are a spectacular example of syntectonic sedimentation, which forms the topic of this thesis.

The perspective view image is oriented to the North, and covers an area of approximately 30 x 20 km. the horizon is coloured by a root mean squared amplitude extraction of 30 m.

Tectonic, Climatic, and Sedimentary Processes Recorded by Pleistocene Fold Growth Strata, The South Caspian Basin, Azerbaijan

Steve E J Richardson

Centre for Research into Earth Energy Systems (CeREES)
Department of Earth Sciences, Durham University

2012

Supervised by

Mark B Allen

Richard J Davies
Stuart J Jones
Simon F Grant

This thesis is submitted for the qualification of a doctorate in geology

The material has not previously been submitted for a degree.

_____

Stephen Edwin Jonathan Richardson 08/03/2012

Notes for printing:
For proper layout, this document should be printed with each page on a separate sheet of A4 paper (non duplex). Several detailed figures should ideally be printed on landscape oriented, A3 paper, these are pages: 3, 5, 29, 30, 32, 33, 34, 40, 53, 55, 78, 96, 128, and 144

Acknowledgements

I would like to gratefully acknowledge the teaching, patience and support of my main supervisor: Mark Allen, and of my additional supervisors: Richard Davies, Stuart Jones and Simon Grant. Their wide-ranging expertise, and clear explanations, discussions and criticisms were essential in shaping and developing the ideas presented in this thesis and also taught me many geological and scientific fundamentals.

A NERC CASE studentship (number NE/F008007/1) funded this research. BP Exploration (Caspian Sea) Limited, the Shah Deniz Partnership and the Azerbaijan International Oil Company are thanked for providing the seismic data used in this thesis and for logistical support during my field work in Azerbaijan. The Landmark University Grant Program is thanked for providing seismic interpretation software. I would especially like to thank Dave Stevenson, Gary Wilkinson and Dave Moy for the technical support in using this software.

I would like to thank the many people who provided help and assistance during my fieldwork in Azerbaijan; Elmira Aliyeva, Mark Ireland, Husseyn Hussinov, Faig Mehdiyev, Azeem Ramzan, Greg Riley, Katie Roberts, Michael Pinter, Rauf Sautanov and Valida Zamanova all helped to implement safe fieldwork logistics and were of great assistance in my initial orientation of the local geology.

My research benefitted greatly from conversations with regional and technical experts; in particular I would like to thank Nazeem Abdullayev, Juliette Buis-Wegerif, Ken McCaffrey, Thomas Gray, Kieth Richards, Katie Roberts and Hannah Rogers, for their insights and advice on the regional geology and processes investigated in this thesis. A version of Chapter 4 has been published and was greatly improved by comments from prof. Brian Horton, Dr. Lorena Moscardelli and an anonymous reviewer. I would also like to thank my fellow PhD students and friends for their ever-present support and humour and for coaching me in several of the topics presented in this thesis. Regarding this last point I would especially like to thank Peter Gatt, Aaron Howie, Peter Holt, Mark Ireland, Dominic Maloney, David Moy, Juan Carlos Laya-Pereira, Amelie Leduc and Jennifer Pless, who have taught me a huge amount of geology during my study, and Will & Gwen Bergius, Mark Fletcher, and Jasper Koops who kept me in good spirits.

My family and friends have always been encouraging and understanding throughout my studies for which I'm very grateful. I would especially like to thank my mother, Helen Richardson, who proof-read the thesis manuscript for spelling and grammar errors.

Finally I would like to thank Rachel, my wonderful field assistant, for her support and fearlessness in the face of attacking dogs, and then for agreeing to marry me after our field season in the hills of Azerbaijan.

Thank you all so much.

♬

Abstract

The Pleistocene – Present-day sedimentary succession of the South Caspian Basin was deposited syntectonically alongside growing anticlines in an under-filled, rapidly subsiding basin. The combination of ample sediment supply from surrounding mountain belts, fast sedimentation rates (variously estimated at between 0.4 and 1.7 m/kyr) and high accommodation space has resulted in an exceptionally thick succession (up to 3000 m) which documents structural growth and regional tectonics at a high temporal resolution. The succession additionally records the palaeo-water level history of the Caspian Sea —an internally drained lake— which has fluctuated at much higher magnitudes and frequencies throughout the study interval than along comparable marine settings. The Pleistocene – Present-day Caspian stratigraphy therefore represents an ideal geological dataset with which to study depositional processes along syntectonic fold 'growth strata' and to investigate the relative impacts of tectonics and climate change on syntectonic sedimentation.

This thesis presents three studies which describe South Caspian Basin fold growth strata at a variety of scales using offshore seismic data from the north-eastern portion basin and field data from western Azerbaijan. The studies examine; [1] the vertical spacing and regionally lateral synchronicity of angular unconformities within late Pliocene – Present-day growth strata; [2] Pleistocene basin margin syntectonic sedimentology, and: [3] the process of large scale slope failure from submarine landslide deposits along folds located in the basin interior.

The results of these studies add to the scientific understanding of the regional geology and of tectono-sedimentary processes in general. However the main finding —recurrent in all three studies— is the presence of repetitive sedimentary patterns and correlations. These are suggested to represent orbital Milankovic cycles of 40,000 years (obliquity) and 100,000 years (eccentricity). Orbitally driven climate change appears to have been a major control on South Caspian fold growth strata architecture and sedimentary processes within anticline mini-basins. Fold growth effects are also observed but these are relatively subdued as tectonic uplift was outpaced by high sedimentation rates.

Table of Contents

1. Introduction 1
1.1. Objectives 1
1.2. Thesis structure 2
1.3. Geological history of the South Caspian Basin 4
Quaternary tectonic and sedimentary configuration 4
Triassic/Tertiary; basin formation 6
Jurassic – Miocene; Tethys and Paratethys marine basins 6
Late Miocene – End Pliocene; lacustrine conditions first established 7
End Pliocene – present; marine flooding followed by renewed lacustrine conditions 8
1.4. Current regional research topics 9
Oligocene – Pliocene hydrocarbon play 9
Mud volcanoes and gas hydrates 10
Climatic cyclicity and controls 11
1.5. Syntectonic fold burial 12
Origin and significance of growth strata 12
Established controls on growth strata architecture 12

2. Climatically forced progressive unconformities in folds 15
2.1. Introduction 15
Aims and overview 15
Growth strata 17
Geological setting 21
Study rationale 23
2.2. Data and Methods 24
Seismic data 24
Interpretation strategy 25
2.3. Results 28
Observations 28
Interpretations 35
2.4. Discussion 39
Climatic forcing and progressive unconformity generation 39
Sedimentation rates and climatic controls during relative lake level cycles 42
Kinematic evolution and sedimentary controls on fold growth 43
2.5. Conclusions 45

3. Sedimentology of the Apsheron Formation 46
3.1. Introduction 46
Aims and objectives 46
Geological setting 47
3.2. Methodology 51
3.3. Results 51
Lithofacies 51
Facies associations and depositional environments 51
Stacking patterns, lateral correlation of logs and lake level fluctuations 77
3.4. Discussion 82
Correlation with regional lake level curves and dating of outcrops 82
Climatic controls on sedimentology 82
Tectonic controls on sedimentation 87
Summary: Fold growth vs. climate forcing 88
3.5. Conclusions 89

4. Mass Transport Deposits in Fold Growth Strata 90
4.1. Introduction 90
Submarine slope failures and mass transport deposits 91
Geological setting 92
4.2. Data and methods 93
4.3. Results 95
Structural setting 95
Description of a representative mass transport deposit 97
Extensional domain syndepositional structures 97
Translational domain syndepositional structures 104
Compressive domain syndepositional structures 109
Location and kinematics of the South Caspian slope failures 114
4.4. Discussion and conclusions 117

Morphology and kinematics of the South Caspian mass transport deposits 117
Novel structures 120
Geological controls on the unstable South Caspian Basin margin 121

5. Discussion, Summary and Conclusions 122
5.1. Discussion 122
Climatic and tectonic controls on growth strata development 122
Recommendations for further work 130
5.2. Summary and Conclusions 132

6. Reference list 134

7. Appendices 143
Appendix 1. Comparisons between published seismic lines and Chapter 2 144
Appendix 2. Handheld gamma ray tool and specifications 146
Appendix 3. Munsell colour chart 147
Appendix 4. Photographic specimens of Apsheron Formation fossils 148
Appendix 5. Apsheron Formation dip-corrected palaeocurrent measurements 149
Appendix 6. Geological slope stability processes and seismic mapping methodology 150
Appendix 7. Alternative views along mass transport basal shear surfaces 151
Appendix 8. Kinematic indicators of South Caspian Mass Transport Deposits 152

List of Figures

Figure 1.1 Geological overview of the South Caspian basin. [a] Stratigraphic log showing ages and names of local sedimentary 'suites' (roughly equivalent to geological formations) modified from Devlin *et al*., (1999). Intervals of research presented in this thesis are highlighted along the right of the figure. The ages presented along the left of the figure are poorly constrained in the Quaternary formations, and are discussed in later sections of this thesis. [b] Structural map of the South Caspian Basin region showing fold traces and location of the Apsheron Ridge. Modified from Jackson *et al*., (2002). The structures investigated in this thesis are shown on the figure: *SD* = Shah Deniz Anticline, *ACG* = the Azeri Gunashli Chirag Structure, *Ch3* = the folded region presented in Chapter 3, encompassing the Quaradag Anticline, Kerkesdag Anticline, and Yasamal Anticline. [c] Conceptual sketch showing the present-day active tectonics of the South Caspian Basin, modified from Jackson *et al*., (2002). [d] Seismic isochore map of the Akchagyl – present-day sedimentary succession. Map shows locations and outlines of the folded succession. Modified from Green *et al*., (2011). *To be printed on A3 landscape oriented paper* 5

Figure 1.2 Stacking patterns of growth strata along kinematically different fold types. This figure is repeated in chapter 2 13

Figure 1.3 Stacking patterns and locations of growth strata terminations along buckle folds deforming at different burial/uplift ratios. This figure is repeated in chapter 2 14

Figure 2.1. [a] Cartoon showing configuration and location of seismic data. Bathymetry and structure map of the study area. Fold traces are shown in black and white, locations of figures are shown in yellow. Fold locations modified from Jackson *et al*., (2002), bathymetry map from Hall (2002) and GeoMapApp (2011) [b] Stratigraphic log showing main geological formations (locally termed 'suites'), and significant events in the basin's history. Modified from Devlin *et al*., (1999). 16

Figure 2.2. Unconformities observed in Apsheron Formation syntectonic growth strata along the Quaradag anticline (described in detail in chapter 3). Bedding dips steepen down-section in a fanning geometry. Location of photo mosaic is approximately: 40°15'28.06"N, 49°31'21.57"E, looking towards the north. 17

Figure 2.3. Stacking patterns of growth strata along kinematically different fold types. 18

Figure 2.4. Stacking patterns and locations of growth strata terminations along buckle folds deforming at different burial/uplift ratios. 20

Figure 2.5. Different types of progressive unconformities and their generation mechanisms. 22

Figure 2.6. Correlated progressive unconformities between folds. Unconformities are either unique to a fold, probably driven by localised tectonic activity, or regionally synchronous, driven by a basin-wide process. 24

Figure 2.7. Idealised lake level curve and sequence stratigraphy, adapted from Kendall (2003). An idealised sequence is shown with all systems tracts and significant surfaces. 27

Figure 2.8. Seismic sections taken through individual flanks of the Shah Deniz [a] and ACG [b] anticlines. In the interpretation panel below each seismic section, onlapping reflections are shown as white lines. Onlaps are shown as red dashed. Progressive unconformities are multi-coloured. Pretectonic strata are coloured red. *To be printed on A3 landscape oriented paper* 29

Figure 2.9. Vertically exaggerated (x 2.5) seismic section, arranged into a correlation loop (from left to right: dip section – strike section – dip section – strike section – dip section) around the Shah Deniz anticline. Progressive unconformities (multi coloured) are correlated around the anticline crest using a loop which intersects less deformed areas. The upper map shows the location of the loop, the yellow arrow shows the start of the loop. *To be printed on A3 landscape oriented paper* 30

Figure 2.10 Correlated progressive unconformities between the Shah Deniz and ACG structures. [a] Line drawing of 2D seismic section, with progressive unconformities and onlapping reflections (black triangles). [b] close-up of onlapping reflections against each fold flank. Reflections are between folds and are either unique, synchronous or truncated by mass transport deposits. Vertical exaggeration is estimated as ~2.5x. *To be printed on A3 landscape oriented paper* 32

Figure 2.11. 2D seismic section correlating the NW shelf margin of the South Caspian Basin, with the Shah Deniz anticline. [a] location of all sequence boundaries and maximum flooding surfaces, mapped onto the SW flank of the Shah Deniz anticline. Progressive unconformities are interpreted along the NE flank. [b] Detailed view of sequence boundaries on line 1, showing onlaps and downlaps of reflections contained with the sequence boundaries. Inflection points, locations of the palaeoshelf break, are indicated by black circles, and their motion paths are highlighted in blue. [c] Correlation between

sequence boundaries and progressive unconformities along the SW flank of the Shah Deniz structure. Seismic sections are displayed in two way time and are vertically exaggerated by approximately 2.5x.. *To be printed on A3 landscape oriented paper* 33

Figure 2.12. Large scale seismic megasequences (Ms-1 to MS-3) comprised of sequences (A to L). Megasequence boundaries are highlighted in thick red. Vertical exaggeration is estimated as ~2.5x. *To be printed on A3 landscape oriented paper*..... 40

Figure 2.13. Growth strata wedge showing vertical position of time picks, and idealised age distributions for episodic and constant fold growth scenarios..... 45

Figure 3.1 Geological outline. [a] Stratigraphic log , showing ages and sedimentary 'suites' (formations) modified from Devlin et al., (1999). [b] Structural map of Azerbaijan region showing fold traces, and location of the Apsheron Ridge. Modified from Allen et al., (2002) [c] estimations of the location of the Apsheronian palaeoshelf break, modified from Grant (2010 , pers. comm.). [d] Geological map of the study area (modified from Geospatial Research Limited, 2008 and reproduced with permission from BP), showing Apsheron, Akchagyl and Productive Formations and traces of the main folds in the area. 48

Figure 3.2. Summary of published age estimates and dating methods for the Pleistocene South Caspian Stratigraphy 50

Figure 3.3 Field localities and log traces, (yellow), separated along marker beds (green); [a] Quaradag anticline, [b] Kerkesdag Anticline, [c] Yasamal Anticline. North arrows (in black) and position of Caspian Sea marked on images. Satellite imagery and elevation data from GeoEye, TerraMatics and DigitalGlobe (2011). GPS coordinates of logs are shown in figure 3.5. 52

Figure 3.4 Summary and lateral relationships of facies associations and depositional environments. ... 54

Figure 3.5 Vertically extensive logs taken along the Quaradag and Kerkesdag anticlines, incorporating facies, colour and bulk gamma ray data, and showing interpretation of relative depths [a] Log 1.1: lower portion of Quaradag, also contains lamination data which was ultimately not used in the study. [b] Log 1.2: upper portion of Quaradag. [c] Log 2: Kerkesdag . *To be printed on A3 landscape oriented paper* 55

Figure 3.6. Field photos of FA1 outcrops: [a] Photomontage of the Kerkesdag anticline, showing thick FA1 succession, displaying coloured banding (1 – 9). [b] Quaradag anticline, showing coloured banding, picked out in the adjacent cartoon. Approximate location of number '1' on figure a is: 40°17'48.23"N 49°37'54.99"E. Base of gully on figure b is: 40°15'4.41"N, 49°31'30.57"E 57

Figure 3.7. Representative logs of facies association FA 1: [a] (previous page) showing low energy offshore self (FA1a), and [b] high energy offshore shelf. Top of log contains turbidite beds from facies association FA2 59

Figure 3.8. Field photos of FA1 facies: [a] Ferric stained silt bands pick out cm-scale bedding in M_B muds. [b] Silt banding and cm-scale bedding more apparent in weathered outcrop. [c] Silt stained blebs, possibly trace fossils in M_B. [d] Thick ribbed bivalve and horizontal traces in M_B. [e] Isolated clusters of shell valves in M_B. [f] Anastomosing, horizontal trace fossils in M_B. [g] Branching horizontal trace fossils in M_B. [h] Fossilised wood in M_B. [i] Contorted folded lamination in M_B 60

Figure 3.9. Field photos of FA1 facies: [a] faint, graded laminations in M_{FL}. [b] Graded contact between M_B and M_{FL}. [c] well developed colouration lamination in M_{St}. [d] close up of M_{St}, showing silt lenses (dashed lines) and cm-scale colour changes between muds. [e] Undulating silt laminations, truncating lower fabric along white dotted line. [f] cm-scale sand beds in M_{St}. [g] cross laminated concave-upwards sandy bedding structures in M_{St}, interpreted as isolated ripples. [h] J, or U shaped burrow in M_{St}, below sandy horizon, visible at top of photograph, and filled with sand. [i] Convex-upwards structures in M_{St}, interpreted as bivalve resting traces..... 61

Figure 3.10. Field photos of FA1, FA2 and FA3 type facies: [a] Layer of ash tuff at base of photograph, with laminations of ash in overlying MFL facies. [b] Convoluted bedding in Tf_A ash bed, interpreted as dewatering flame structure. Arrow shows tip of flame structure [c] Iron staining to top of ash bed. [d] Shell valves and fragments (white specks seen in photo) in Cq_M facies. [e] close up of shelly bands some show grading (band nearest base of photo, shown with white triangle). [f] Beds of Cq_{Sn} showing rip up clasts at bed base (RUC), and grading into laminated sand grade particles, and laminated silts. Interpreted as Bouma sequences A – D. [g] Cq_{Sn} in trough cross bedded unit, confined to a single trough (T). [h] Graded isolated bed of Cq_{Sn}. Grading shown by white triangle [i] Cq_{Sn} showing moderate sorting, cm-scale lamination and grading. 62

Figure 3.11 Sketches of outcrops along the Stonepay roadcutting. [a] partial exposure of St_O silts and sands arranged into horizontal topsets and inclined foresets. [b] location sketch of the two outcrops along the roadcutting. Note that figure a is viewed looking towards the W – SW, and figure b looking towards the E – NE [c] inclined St_O muds and silts incised by large channel filled with shelly Cq_C gravels

and Sn_M sands. Metre-scale crossbeds migrate away from the Caspian shoreline. Location of roadcutting is 40°21'28.50"N, 49°47'46.72"E 65

Figure 3.12. Type logs of FA2: Lower shoreface. [a] log 3.1 showing lower shoreface silts and sands, and a submarine channel. [b] log 3.2 showing lower shoreface silts and FA3 type (upper shoreface), trough cross bedded shelly sands 67

Figure 3.13 Field photos of Fa2 and FA3 type facies: [a] Wavy heterolithic bedding in StO facies. [b] Cross bedded, convex structure in SnO. [c] Vertical trace fossils in flaser (F) and lenticular (L) bedding, in SnO. [d] Muddy sandstone SnM, showing faint horizontal lamination. [e] graded sets of SnO, containing abundant ripples, and rare, cross laminated gravels (G). Ripples show bidirectional up-building at (B). Apparent palaeocurrent directions (white arrows) estimated from ripple asymmetry and cross lamination. [f] Beds of SnO overlying SnCS over an undulating contact. Contacts between SnO are also undulose and erosive. [g] SnCS overlying SnO facies over an angular and erosive contact. [h] muddy climbing ripple, ripple trough is filled with coarser shell fragments. 68

Figure 3.14. Photomontage showing stacked FA3 type (shoreface) facies, overlain by FA1 type (offshore shelf) facies over an angular unconformity, interpreted as a growth strata boundary. Taken at Quaradag Anticline, approximately 30meters SE of GPS waypoint 40°15'28.06"N, 49°31'21.57"E 69

Figure 3.15 Type log of facies association FA3: Shoreface. From the westerly tip of the Quaradag Anticline 70

Figure 3.16. Field photos of FA3 type facies: [a] scalloped bedding, dune scale trough cross bedding, or hummocky cross stratification, in SnMD sands. [b] cm-scale cross bedding in SnMD sandstone. [c] mm-scale cross bedding in SnMD showing reactivation surfaces (dotted lines). [d] Muddy ripple crests in SnMD. [e] Muddy gutters in SnMD, outcrop is faulted and offset by 10cm to the right of the photo (red dots show marker bed). [f] Liesegang rings in SnMD. [g] Rip up clasts in poorly sorted massive bed of SnCS, overlying SnO along undulose erosive contact. 2 have been circled, many more are seen on photo. [h] Trough cross bedding in SnCS. Note angular discordance of the laminations in the lower half of the photo. [i] Cylindrical structures weathered out of SnCS, interpreted as vertical trace fossils. 71

Figure 3.17 Photomontage showing FA4 type (high energy, coastal) facies, exposed along the northern tip of the Kerkesdag Anticline. Photo is annotated with an angular unconformity (dotted line), scalloped (S) and planer (P) bedding. Photo is taken at base of Log 2a, at 40°17'46.19"N, 49°37'34.34"E. 74

Figure 3.18 Type log of facies association FA4 75

Figure 3.19. Field photos of FA4 and minor FA1 and FA2 type facies: [a] Close up of CqC, coquina, predominantly consisting of carbonate matrix, which shows aragonite dissolution moulds of bivalve fragments. [b] dark grey mottling to CqC (picked out by white dotted line). [c] Faint horizontal lamination in CqC. [d] Horizontal lamination in SnCS and CqC, carious weathering picks out vertical structures, interpreted as burrows. [e] faint cross lamination in CqC. [f] Trough cross bedding in CqC picked out by weathering. [g] Muddy contorted Cq_M coquina FA1 interbed. The bed is disharmonically folded (dashed lines) and contains blocky layers of mudstone within it (arrows). 76

Figure 3.20 Projections of hillside exposures, annotated to show the relative position of sand beds (sections of FA3 and FA4 type facies). [a – c] perspective views over all three localities. Satellite imagery and elevation data property of GeoEye, TerraMatics and DigitalGlobe (2011). [d] Chart showing lateral position and relative height of each sand bed and hillside. *To be printed on A3 landscape oriented paper* 78

Figure 3.21 Relationship between facies associations and relative lake level. Blue line shows the lake level curve associated with sequences, the grey line shows fluctuating parasequences. Systems tracts are abbreviated to 'ST'. 80

Figure 3.22 Summary of field data and interpretations. [a] All sedimentary logs, in relative stratigraphic order, showing correlated sand bodies. [b] Constructed relative lake level curve, based on depositional environments (Figure 3.4) and lateral extent and position of sand bodies (Figure 3.20). [c] Published lake level curves from Jones and Simmons (1996) and Abreu and Nummendal (2007), matched to this study's constructed relative lake level curve. [d] Seismic stratigraphy along the South Caspian Basin margin (chapter 2), a large regression is also observed in the seismic data, coloured in yellow. [e] idealised progradational parasequence stacking patterns from Van Wagoner *et al*., (1988). Colour changes represent, terrestrial, proximal and distal sediments. 81

Figure 3.23 Two types of stacking pattern related to differing interactions between depocentre uplift and relative lake level changes 85

Figure 4.1 (1a) Structural elements of the study area and location of seismic surveys. Fold and fault traces adapted from (Jackson, J. et al., 2002). (1b) Outlines of the seismic surveys with the location of fold traces, basin margin and mud volcanoes shown. (1c) Lithological log of the interval of interest and

stratigraphic position of mass transport deposits. (1d) Oriented outlines of both seismic surveys used in this study showing orientations of maps (grey shading) and seismic profiles (black lines). 93

Figure 4.2 Domains of a representative mass transport deposit. [a] Vertically exaggerated (x 2) seismic section running down slope, showing major surfaces and characteristic syndepositional structures in each domain [b] Plan view of the palaeolake bed and mass transport deposit upper surface showing main components of a mass transport deposit. Cross-cutting flow units are numbered I – IV. Faint lineations are dashed white. Image is illuminated from the SW (2c) Shaded depth map of the mass transport deposit basal shear surface showing main components. Faint lineations have been dashed white. Image is illuminated from the SW. Images taken from mass transport deposit 1 from Shah Deniz. *To be printed on A3 landscape oriented paper* 96

Figure 4.3 Divergently oriented headwall scarps [a] Composite depth map of a mass transport deposit upper surface, illuminated from the north. Convex upslope headwall scarp lobes are oriented 90 degrees away from the lateral margin. The left of the image is coloured with a root mean square (RMS) amplitude extraction. The extraction window is 30 m tall and taken 25 m beneath the upper surface. [b] Vertically exaggerated (x 5) seismic section through the deposit showing basal ramp and drape of material following the ramp outline, highlighted with a pink marker horizon. [c] Perspective view of the basal shear surface showing the outline of the ramp, The image is located at the edge of the seismic survey and contains a square gap of no data. [d] Interpretation; multiple, divergently retrogressive failures, translated material along two basal shear surfaces linked by ramps. The ramp from figure 3b is an older headwall scarp of an earlier failure. Images taken from deposits MTC-4 and MTC-6, along the Shah Deniz fold. 99

Figure 4.4 Headless canyons located along the shelf break. Dip magnitude map of a palaeolake bed. Dip magnitude is a dimensionless variable that picks out changes in slope along a seismic horizon. The shelf break runs approximately E – W to the left of the map. Material alongside the canyons is disrupted. A circular mud volcano edifice and its mudflow lie to the right of the image. The canyons are contemporaneous with the larger mass transport complex MTC-1 from the Shah Deniz anticline, shown on Figure 4.2. 101

Figure 4.5 Mass transport deposit without a conventional headwall scarp. [a] 3D view of a mapped coherent reflection within the mass transport deposit (Horizon A) and a lower horizon, corresponding to the basal shear surface. Horizon A is coloured by depth , the basal shear surface is blue. Horizon A pinches out onto the basal shear surface, the location of pinch-out falls towards the centre of the mass transport deposit where material displacement is the greatest. [b] Vertically exaggerated (x 6) seismic section through the deposit, up-dip of the upper surface pinch out, no scarp is observed. [c] Interpretive cartoon showing evolution of the mass transport deposit, leaving no headwall scarp. Example taken from mass transport deposit 1, from the ACG structure. 103

Figure 4.6 Individual mass transport deposits within a mass transport complex. Lateral shear zones and deposit frontal lobes are highlighted in dotted white, interpreted material transport directions are shown with white arrows. Amplitude extraction taken from mass transport deposit 6 on Shah Deniz, 30 m above the mass transport deposit basal shear surface, with an extraction window of 25 m. 105

Figure 4.7 mud volcano interaction structures [a] Erosional shadow remnant. Root mean square (RMS) amplitude extraction taken through mass transport deposit 6 on Shah Deniz from 20 m above the basal shear surface with an extraction window of 30 m [b] Mass transport deposit frontal margin obstructed by a mud volcano crater. Low amplitude, concave downslope pressure ridges are visible in the mass transport deposit. Several more mud volcanoes (low amplitude, circular features) are shown to the bottom right of the image. Arrow shows the material transport direction. RMS Amplitude extraction taken from mass transport deposit MTD-14 on the Shah Deniz fold, 25m above the basal shear surface with a 25 m extraction window. 106

Figure 4.8 Translational domain structures. [a] Amplitude extraction taken though a mass transport deposit and the adjacent stable slope. The deposit contains sigmoidal lateral shear traces. Upslope of the mud volcano, the slope failure is extruded over the lake bed. Volcano mud flow orientations show slope dip direction. Amplitude extraction taken through mass transport deposit MTD-8 on Shah Deniz, 60 m above the basal shear surface with an extraction window of 30 m. [b] Dip magnitude map of a basal shear surface showing incised grooves, which show the material transport direction. The longest groove is 9 km long, providing a minimum transport distance. Taken from mass transport deposit MTD-18 on Shah Deniz. 108

Figure 4.9 Root mean square (RMS) amplitude extraction maps showing outline and Internal structures of three compressive domains. [a] Wide frontal margin, containing fine-scale arcuate thrusts. The thrust sheet is segmented into four sections, A1 – 4, separated by flow unit boundaries B. Also present are translated blocks, C. [b] Elongate frontal margin displaying fault and fold traces at its tip. [c] Partially imaged compressive domain, containing a translated block, TB, and sinuous thrust lineations. Cartoon shows mass transport deposit evolution based on cross-cutting relationships of. [d] Vertically exaggerated (x 3) seismic section taken through the contorted compressive domain of Figure c. The

highlighted area is offset by two mass transport complexes travelling in opposite directions. Figure 4.9 a,b, and c – d taken through mass transport deposits 16, 7, and 6, respectively, along the Shah Deniz anticline . All amplitude extractions are taken 30 m above the basal shear surface with a 25m window length. 111

Figure 4.10 Compressive domain thrust belt. [a] Vertically exaggerated (x 6) seismic profile through a thrust sheet. Thrust hanging walls are picked out by tilted, moderate amplitude, negative (black – red – black) reflections. The section is oriented parallel to the material transport direction of the mass transport deposit (MTC-A, along the ACG structure), and is vertically exaggerated by a factor of 3. [b] Throw distribution of thrusts from Fig 8a. Throw along the thrusts increases downslope, though the toe of the failure lies off the extent of these data. 113

Figure 4.11 Translated blocks and basal shear surface scours. [a] Shaded depth map of the basal shear surface showing wide basal scours. Outlines of translated blocks shown in yellow, interpreted flow direction shown with arrow. Surface is illuminated from the west. [b] Vertically exaggerated (x 6) seismic profile through the block and scour, transport direction is apparent as seismic section is oriented oblique to scours. [c] Horizontal slice taken through a flattened attribute analysed volume. The example is taken from mass transport deposit MTC-13 along the Shah Deniz fold. The seismic volume has been processed with an edge detection algorithm and flattened along the mass transport deposit basal shear surface. The depth slice is taken 25 m above that surface. 116

Figure 4.12 Location and outlines of mass transport deposits in the study area. [a] Outlines of the seismic survey and mass transport deposits outlines. Arrows show sediment transport directions interpreted from kinematic indicators. [b] Interpretations regarding basin margin progradation and fold hinge growth, drawn from selected mass transport deposit outlines. 118

Figure 4.13 Cartoon of a Caspian mass transport deposit and a summary of all the syndepositional features contained within it relative to each structural domain. Broad white arrows show material transport directions. Modified from Bull & Cartwright (2009) and Prior et al., (1984). Key: (A) Layers of weakness. (B) Slope created by basin margin. (C) Slope created by fold uplift (D) Mud volcano crater. (E) Curved grabens emanating from mud volcano centre. Extensional domain (1) Headwall scarp (2) Crown cracks. (3) rotated blocks and residual debris (4) rafted blocks and sidewall fragmentation. (5) detached portion of the flow exposing evacuated basal shear surface. (6) arcuate scarps, showing divergent convex upslope orientations towards the fold flank and basin slope. (7) Headless canyons incising the headwall. (8) convex upslope lineations. (9) Normal ramps and flats in the basal shear surface located around fault traces. Translational domain (10) lateral margin (11) longitudinal shear zone. (12) Flow fabrics, convex downslope, and chaotic. (13) Normal ramp, with coherent drape of mass transport deposit facies. (14) Lateral ramp. (15) elongate strain shadow behind obstacle (16) restraining bend in the lateral margin. (17) Translated blocks Compressive domain (18) Blocks and basal shear surface scours. (19) Thrust sheet. (20) Pressure ridges. (21) Obstacle at mass transport deposit toe modifying frontal morphology. (22) Older mass transport deposit travelling along the old layer of weakness. (23) basal shear surface grooves. 119

Figure 5.1 Summary diagram of sedimentary and tectonic processes of the South Caspian Basin 126

Figure 5.2 Summary of age estimates for the South Caspian Basin 129

List of Tables

Table 1.1. Summary of South Caspian Basin geology (based on references cited in the text). Details of the Apsheron Formation (including its thickness) are presented in Chapter 3. *To be printed on A3 landscape oriented paper* 3

Table 2.1. Detailed descriptions and interpretations of each sequence and systems tract along the seismic line of figure 2.9. *To be printed on A3 landscape oriented paper*....34

Table 2.2. Correlation chart. Progressive unconformities are correlated between folds and stratigraphically significant surfaces along the basin margin 36

Table 2.3 Comparison chart of repetitive events observed in this study (top), published ages of the Pleistocene South Caspian succession (middle) , and possible Milankovic cyclicity (bottom) 41

Table 2.4. Hypothetical climatic conditions during lake level fluctuations (top), and a summary of the two opposing climatic models that have been proposed for the South Caspian Basin (bottom)....44

Table 3.1 Lithofacies descriptions from the Apsheron Formation *To be printed on A3 landscape oriented paper*....53

Table 3.2 Opposing climate models that have been proposed for the Caspian Sea....83

Table 3.3 Comparison chart of repetitive events observed in this study (top), published ages of the Pleistocene South Caspian succession (middle) , and possible Milankovic cyclicity (bottom) 86

Table 5.1 Comparison chart of repetitive events observed in this study (top), published ages of the Pleistocene South Caspian succession (middle) , and possible Milankovic cyclicity (bottom) *This table should ideally be printed on A3 paper*....128

1. Introduction

1.1. OBJECTIVES

Syntectonic sedimentary successions are of great academic and economic interest to geologists studying (regional) tectonics and hydrocarbon plays. A primary analysis of a structure's timing, growth rate and kinematic evolution can be obtained from studying the overlying, wedge-shaped sedimentary units, termed 'growth strata' (e.g. Mitra, 1990; Erslev, 1991; Suppe *et al.*, 1992; Hardy & Poblet, 1994; Poblet & Stuart, 1995; Schneider *et al.*, 1996; Verges *et al.*, 1996; Butler & Lickorish, 1997; Shaw *et al.*, 2004; Ghiglione & Ramos, 2005). Research into growth strata is commonly focussed on the tectonic signals contained within them (e.g. Masaferro *et al.*, 2002), yet climatic and autogenic sedimentary processes also operate during their deposition and their effects are not fully understood (Castelltort *et al.*, 2004; Pochat *et al.*, 2009).

This thesis presents work on growth strata from several anticlines along the western margin of the South Caspian Basin and addresses a key question:

- *Is it possible to identify climatic signals and autogenic sedimentary processes within fold growth strata, and if so, how do these control syntectonic sedimentation and sedimentary architecture?*

The Neogene and Quaternary strata from the South Caspian Basin are an ideal 'natural laboratory' to investigate this issue as both active tectonics and climate-driven relative water level changes operated at comparatively large magnitudes throughout their deposition. In addition to this, the thick sedimentary succession was deposited extremely rapidly, preserving a high-resolution record of regional tectonics, sedimentology and climate change.

The interval of research spans 2.5 million years (Figure 1.1a), from the earliest Pleistocene (2.58 Mya) to the earliest Holocene (0.01 Mya). Tectonic folding, which continues at the present-day, started in the basin during the late Pliocene (2.6 Mya), whilst its current hydrological configuration was established by the Pleistocene. Little research has been published on the Pleistocene geology of the South Caspian Basin, therefore a secondary aim of this thesis is to increase the understanding of this epoch in this region.

1.2. THESIS STRUCTURE

The main body of this thesis comprises chapters 2 – 4; these are three separate studies that investigate varying scales of syntectonic sedimentation. They are augmented by introduction and conclusion chapters, 1 and 5 respectively. To facilitate their publication, the main chapters are written in the style of academic papers. This organisation creates some unavoidable repetition which has been kept to a minimum.

The thesis is organised as follows:

Chapter 1 poses the thesis' main research question and reviews literature concerning the regional geology (Table 1.1), and the topic of fold burial. This is in addition to smaller reviews at the start of each chapter. The chapter highlights research questions that exist in the current scientific body of knowledge and which are explored in the later chapters.

Chapter 2 investigates basin-scale, syntectonic sedimentation and growth strata architecture along the western perimeter of the South Caspian Basin. The study interprets the stacking patterns of syntectonic strata from several fold mini basins and establishes a regional seismic stratigraphy using two-dimensional (2D) seismic data that transect the anticlines and the adjacent basin margin. By integrating both interpretations, the study investigates changes in fold burial during periods of relative water level fluctuation.

Chapter 3 examines syntectonic burial at the outcrop scale. The study uses sedimentary logs taken through Pleistocene growth strata along eroded folds, which outcrop in Azerbaijan. The study identifies facies associations and depositional palaeoenvironments within the sedimentary succession. The outcrop data are integrated with satellite imagery to create an interpretation of regional, depositional, and lake-level history. The effect of fold uplift on sedimentation is determined from field observations of changes in depositional palaeoenvironment.

Chapter 4 investigates sediment remobilisation along fold growth strata from the western basin margin. It presents work on Pleistocene submarine landslide deposits (termed 'mass transport deposits'), which are imaged in three-dimensional seismic data. The study uses seismic mapping techniques to visualise the deposits' internal structure and interpret landslide kinematics and slope configurations, whilst examining sedimentation and internal deformation during their emplacement.

A shorter version of chapter 4 has been published in 2011. A copy of this paper is bound at the back of the thesis.

Period	Outcrops	Regional name	Lithofacies	Thickness	Depositional Setting	Structural Setting
Pleistocene	-Sequences are exposed along the western Apsheron Peninsula, and the Greater Caucasus Mountains -Stratigraphy is regionally correlated between the Black Sea and modern Central Caspian Basin	-Apsheron Formation -Bakunian Formation	-Calcareous marine shales -Bioclastic limestones -Sands	-1000 – 1500 m thick	-Lacustrine setting -Onshore outcrops of Apsheron Formation contain littoral–offshore shelf facies associations -Gradual regressional trend throughout the Apsheronian	-South Caspian Basin begins to subduct beneath the Mid Caspian Basin along the Apsheron Ridge -Cretaceous–Pliocene sedimentary succession is deformed into large buckle folds. Earliest fold growth is onshore, in the youngest productive series sediments. -Deformation progresses from the west (the Greater Caucasus) and youngs eastwards.
Late Pliocene	-Sequences are exposed along the western Apsheron Peninsula and Greater Caucasus Mountains -Penetrated by offshore wells -Stratigraphy is regionally correlated between the Black Sea and modern day Central Caspian Basin	Akchagyl Formation	-Calcareous marine shales	-Akchagyl Formation is a condensed package < 100m thick	-Para-Tethyan connection(s) between the Caspian sea and world oceans re-opens via the Black Sea -Change from lacustrine to open marine conditions	
Pliocene	-Sequences are exposed along the western Apsheron Peninsula and Greater Caucasus Mountains - Penetrated by offshore wells	-'Productive Series' Consisting of smaller formations, from old to young: *-Kalin Formation* *-PK Sandstones* *-Kirmaky Formation* *-NKG shales* *-Perirev Formation (Also called the Fasila Formation)* *-Dalakhany Formation* *-Sabunchy Formation* *-Surakhany Formation*	*Lower productive series:* -Kalin Fm: fluvial–deltaic sandstones -PK Sandstones: fluvial–deltaic sandstones -Kirmaky Formation: Deepwater shales *Middle productive series* -Perirev Formation. : Fluvial, delta plain sandstones -Balakhany Fm. : Fluvial, delta plain sandstones -Sabunchy Fm. :Stacked, channelised, fluvial sands, separated by shale interbeds -Shaling-out in offshore areas *Upper productive series* -Surakhany Fm. : shales, isolated sand bodies and evaporites	-Sediment wedge 500–3000 m thick, thickening to the south of the Apsheron Peninsula -May be tectonic thickening	-Major environmental change coincident with the Messinian Salinity crisis -Basin becomes isolated from the world's ocean, and changes from marine to lacustrine setting -Caspian Sea reduces considerably in size -Deposition around the Apsheron Ridge is dominated by fluvial Volga delta facies which, since the Miocene, had migrated southwards by ~600 km. -The Paleo Volga becomes muddier, inputting less water and clastic sediment, and the input of muddier Kura river deposits increases. Lake level drops and playas develop along basin margins -A stratigraphic sequence is interpreted within the Productive series: Kalin Formation–PK Sandstones (lowstand and transgressive systems tracts); Kirmaky Formation–NKG sands (highstand systems tracts). Overall progradational trend -Retrogradational trend in NKG shales: transgression -Balkhany Formation is aggradational, indicating long term ~static, lake level. Flooding surface at top of formation -Sabunchy and Surakhany Formation, show a regressive, progradational trend	-SCB is trapped oceanic crust compressed between the Arabia and Eurasia sutre -Rapid basin subsidence
Oligocene-Miocene	-Sequences are exposed along the western Apsheron Peninsula and Greater Caucasus Mountains	-Maykop, Chockrak, and Diatom formations	-Brown–grey, calcareous, marine shales -Occasional thin sandstone inter-beds -Intervals of high Total Organic Carbon (TOC)	-Sediment wedge 500–3000 m thick, thickening to the south of the Apsheron Peninsula -May be tectonic thickening	-Deep water, marine environment -Stratigraphy is regionally correlated between the Black Sea and modern day Central Caspian Basin -The South Caspian Basin connected to the world's oceans via the Black Sea along E-W oriented seaways	The Palaoecene-Miocene stratigrapohy in Azerbaijan, is interpreted as a passive margin setting on the northern margin of the Para-Tethys. Some evidence for compressive tectonics is present in Seismic data, along the northern portion of the Apsheron Ridge, which shows Eocene inversion structures.
Paleocene-Eocene	-Sequences exposed along the eastern Greater Caucasus Mountains	-Greater Caucasus: Ihdag Formation (Paleocene) & Khoun Formation (Eocene)	-Deepwater and (quasi) marine shales	-Onshore: 200–2000 m -Offshore: thickness is not established but seismic mapping Shows a southwards thickening wedge (5000–20.000 m) of Jurassic–Eocene sediments	-Deep water, basin environment, possibly marine	
Jurassic-Cretaceous	-Penetrated by a single well in the Kura Delta -Rare deformed sequences outcrop along the Greater Caucasus, and Kopet Dagh Mountains		-Volcanics (basalt, andesite, diorite and tuff) lie beneath carbonate sequence, oolitic and coraline limestones. -The carbonate sequence is intruded and metamorphosed by the underlying basaltic sills	-Onshore: Jurassic seds: 600–2000 m Lower Cretaceous: 1500 m Upper Cretacous: 1500 m -Offshore: Jurassic volcanics: > 4400 m Jurassic–Cret. carbonates: 710m	-Carbonates: shelf–basin environments -Deepening upwards trend in the Jurassic; interpreted as subsidence around the Greater Caucasus -Compressive deformation may have began as early as the Cretaceous	Geochemical analysis shows magmas are calc-alkaline, island arc affinities. Closest analogue to South Caspian Basin Crust. Subsiding, passive margin setting, on the northern margin of the shrinking Tethys ocean

Table 1.1. Summary of South Caspian Basin geology (based on references cited in the text). Details of the Apsheron Formation (including its thickness) are presented in Chapter 3. *To be printed on A3 landscape oriented paper*

1.3. GEOLOGICAL HISTORY OF THE SOUTH CASPIAN BASIN

Quaternary tectonic and sedimentary configuration

The South Caspian Basin is located in the southernmost portion of the Caspian Sea (Figure 1.1b). The Caspian 'Sea' is technically a misnomer as, since the earliest Pleistocene, it has been an internally drained, lacustrine basin and disconnected from the world's oceans. Caspian lake level in the is governed by the balance between river input and evaporation and is extremely sensitive to climate. Lake level fluctuates at large magnitudes and at high frequencies, many times greater than along comparable marine margins (Kroonenberg *et al.*, 1997; Kroonenberg *et al.*, 2000; Kosarev, 2005).

The basin lies within the convergence zone of the converging Arabian and Eurasian plates (Jackson *et al.*, 2002). Its basement is rigid and aseismic, but is surrounded by tectonically active, compressive orogens along its margins: the Caucasus, Talysh, Alborz and Kopeh Dagh mountain belts (Allen *et al.*, 2003). The South Caspian Basin presently moves with a westward component of motion relative to Iran and Eurasia (Figure 1.1c), oblique to the north – south shortening of the Arabia – Eurasia collision (Priestley *et al.*, 1994; Jackson *et al.*, 2002; Allen *et al.*, 2003; Masson *et al.*, 2007; Hollingsworth *et al.*, 2008). This movement is accommodated by subduction and over-thrusting of the plate at the northern and western margins of the South Caspian Basin (Devlin *et al.*, 1999; Jackson *et al.*, 2002; Allen *et al.*, 2003; Knapp *et al.*, 2004; Green *et al.*, 2009). An accretionary prism runs along the subduction zone, which is topographically expressed as an elongate fold train and is named the Apsheron Ridge (Jackson *et al.*, 2002). The Miocene to present-day sedimentary cover is extensively folded into a series of large anticlines, which in map view run approximately parallel to their basin margins (Figure 1.1, b and d) and is detached along overpressured Miocene muds (the 'Maikop' Formation).

Although the Volga River is the main source of water to the lake, much of its sediment is confined to the present North Caspian Basin. Sediment in the current South Caspian Basin, is supplied by rivers that drain the surrounding mountain ranges (Kuprin, 2002), though this distribution is reduced in Pliocene and older sediments (Morton *et al.*, 2003). Sedimentation rates are extremely high (> 10 mm per year since the early Pleistocene, Allen *et al.*, 2002).

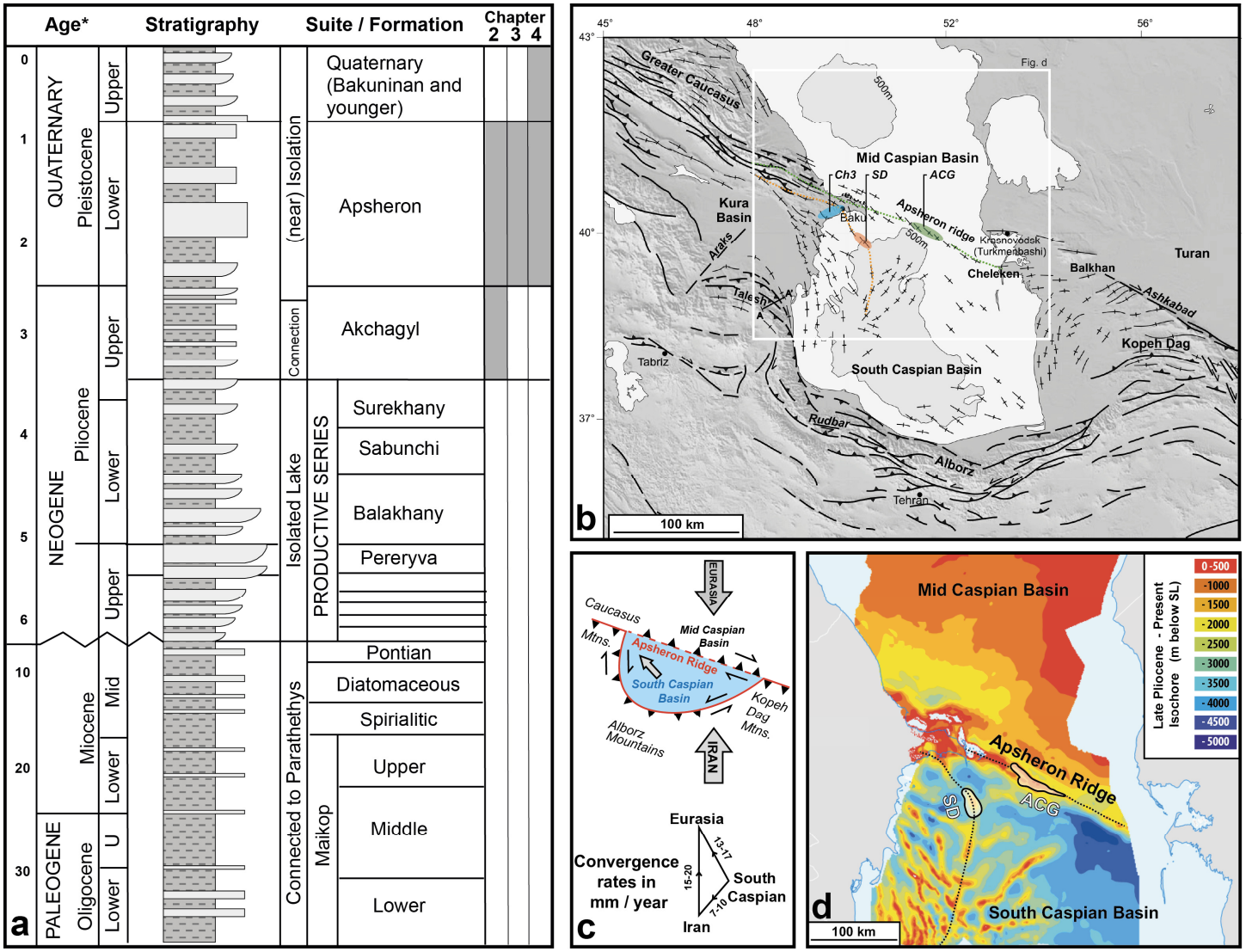

Figure 1.1 Geological overview of the South Caspian basin. [a] Stratigraphic log showing ages and names of local sedimentary 'suites' (roughly equivalent to geological formations) modified from Devlin *et al.*, (1999). Intervals of research presented in this thesis are highlighted along the right of the figure. The ages presented along the left of the figure are poorly constrained in the Quaternary formations, and are discussed in later sections of this thesis. [b] Structural map of the South Caspian Basin region showing fold traces and location of the Apsheron Ridge. Modified from Jackson *et al.*, (2002). The structures investigated in this thesis are shown on the figure: *SD* = Shah Deniz Anticline, *ACG* = the Azeri Gunashli Chirag Structure, *Ch3* = the folded region presented in Chapter 3, encompassing the Quaradag Anticline, Kerkesdag Anticline, and Yasamal Anticline. [c] Conceptual sketch showing the present-day active tectonics of the South Caspian Basin, modified from Jackson *et al.*, (2002). [d] Seismic isochore map of the Akchagyl – present-day sedimentary succession. Map shows locations and outlines of the folded succession. Modified from Green *et al.*, (2011). *To be printed on A3 landscape oriented paper*

Triassic/Tertiary; basin formation

The basement of the South Caspian Basin is covered by up to 30 km of sediment, and is not exposed at the surface. Its age is currently estimated at Mesozoic (Green *et al.*, 2009), and both continental (Shikalibeily & Grigoriants, 1980; Artyushkov, 2007; Golonka, 2007) and oceanic (Berberian, 1983) affinities have been proposed. Pre-Miocene rocks lie beneath the extremely deep and highly overpressured Maikop Formation shale interval and are poorly constrained. The combination of uncertain basement affinity, and undated, unexposed deep stratigraphy, has resulted in several interpretations regarding the early history and formation of the South Caspian Basin.

The basement beneath the western half of the basin has an ambiguous seismic character ; it has a seismic velocity consistent with oceanic crust but is anomalously thick (Mangino & Priestley, 1998). The debate regarding the nature of basement is ultimately of limited interest to the Quaternary research presented in this thesis, however the current consensus is that at least the western portion of the basin (the area investigated in this thesis) is floored by oceanic crust. The main supporting evidence for this is the basement's seismic velocity (Mangino & Priestley, 1998) and gravity signatures (Granath *et al.*, 2007), combined with earthquake focal mechanisms and deep seismic reflection imaging, which show the flexure and subduction of the South Caspian Basin beneath the Mid-Caspian Basin to the north (Priestley *et al.*, 1994; Jackson *et al.*, 2002; Knapp *et al.*, 2004). All this evidence is consistent with an oceanic crust interpretation. However, within this broad consensus, three competing models describe the basin's initial formation. The most commonly cited is that the South Caspian Basin formed as a back arc rift, North of the large Neo-Tethys ocean, sometime in the Mesozoic-Tertiary period (Zonensthain & Le Pichon, 1986). Alternative theories include a remnant of Tethys oceanic crust, which was trapped during the Tertiary (Berberian, 1983; Nadirov *et al.*, 1997), and formation in a Cretaceous pull-apart basin (Apol'skiy, 1974; Şengör, 1990).

Jurassic – Miocene; Tethys and Paratethys marine basins

The Neo-Tethys ocean was closed in the late Eocene (~35 Ma) due to the start of the Arabia Eurasia collision (Allen & Armstrong, 2008). "Paratethys" is the name given to a group of anoxia-prone basins to the north of Neo-Tethys, which became isolated from the world ocean system at about this time. The Paratethys seaway stretched from the Alps to the Aral Sea and encompassed the Aral-, Caspian-, and Black seas, and the Dacic Basin in Romania. It consisted of several narrow straits linking smaller intra-basin depocenteres; one of these lay above the South Caspian plate, (Popov *et al.*, 2006). Paratethys sub basins were separated from global ocean circulation patterns and were prone to periods of anoxia, resulting in the widespread deposition of highly organic muds during the Oligocene and early Miocene, (Allen & Armstrong, 2008; Krijgsman *et al.*, 2010) These form regionally significant source rocks (the Maikop Formation) in the current South Caspian hydrocarbon play (Devlin *et al.*, 1999; Gurgey, 2003).

Late Miocene – End Pliocene; lacustrine conditions first established

During the late Miocene, Messinian salinity crisis, lowering of the Mediterranean sea level, combined with compressive tectonics, separated the Paratethys seaway fully from the world's oceans, significantly changing its hydrological regime. The uplift of regional mountain belts separated and shrunk the seaway into several increasingly isolated, lacustrine, sub-basins such that between the Miocene and the earliest Pliocene, the water level in the Caspian portion of the Paratethys dropped between 600 – 1500 m, and the Caspian Sea reached its smallest aerial extent, approximately the size of the present-day South Caspian Basin area (Reynolds *et al.*, 1998; Popov *et al.*, 2006; Krijgsman *et al.*, 2010).

The Turkish-Iranian Plateau was thickened and elevated in the early stages of the Arabia – Eurasia collision. At some poorly-constrained time during the late Cenozoic, large areas reached a critical regional elevation of ~1 km, such that further continental shortening took place in adjacent, lower-lying areas: the Zagros mountains in Iran, and the Caucasus, Kopeh Dagh, and Talysh mountain belts surrounding the South Caspian Basin. This process was probably highly diachronous, and continues to the present (Allen *et al.*, 2004). The South Caspian Basin basement behaves as a rigid block in the collision zone, and has undergone little internal deformation (Allen *et al.*, 2003). The continental convergence was taken up by its subduction beneath the Mid Caspian Plate along the Apsheron Ridge subduction zone (Allen *et al.*, 2004).

Increased Cenozoic tectonism in the South Caspian area was accompanied by high rates of basin subsidence (Nadirov *et al.*, 1997), possibly driven by flexural down-warping of the crust (Allen *et al.*, 2002). Alternatively, the basin was initially sediment-starved with a surface hundreds of metres below sea-level during the Messinian, such that there was a great amount of accommodation space available. In this model, the basin had always been under-filled since initial rifting and during subsequent thermal subsidence (Guest *et al.*, 2007a; Egan *et al.*, 2009; Green *et al.*, 2009). In either case, the Pliocene South Caspian Basin became the depocentre of several large river deltas, which emptied into the basin from the surrounding, actively uplifting mountain ranges (Morton *et al.*, 2003). The largest, the Palaeo Volga Delta, entered the basin along its northern margin. The delta migrated 600 km to the south during the Messinian, incising a deep canyon into the Mid Caspian Basin and ultimately settling over the Apsheron Peninsula in Azerbaijan, depositing a range of fluvial and lake-marginal sands and shales, termed the 'Productive Series', which form the reservoir interval of the regional hydrocarbon play (Reynolds *et al.*, 1998; Devlin *et al.*, 1999; Hinds *et al.*, 2004). The combination of rapid basement subsidence, accommodation space creation and abundant sediment supply produced an extremely thick sedimentary succession, where approximately 6 km of sediment was accumulated in only 1.9 million years (Allen *et al.*, 2002) , a sedimentation rate several orders of magnitude higher than comparable large Quaternary lakes (e.g. Perissoratis *et al.*, 2000).

End Pliocene – present; marine flooding followed by renewed lacustrine conditions

In the late Pliocene, the fluvial – deltaic – lacustrine environment that had persisted in the South Caspian Basin since the Messinian was briefly punctuated by a flooding event, the 'Akchagyl flood' which connected the Mediterranean, Black, and Caspian Basins. Mediterranean waters from the west encroached and flooded the lake via the Black Sea, briefly establishing a marine connection (Degens & Paluska, 1979; Popov *et al.*, 2006). This ended at the start of the Pleistocene, locally termed the 'Apsheronian', apparently due to a spurt of basin subsidence which increased accommodation space and lowered water levels reducing the Caspian Lake to a similar size as today (Jones & Simmons, 1996). During the Pleistocene to present, the Caspian Sea has remained an endoheric, brackish lake with a few brief flooding events connecting it to the Black Sea (Nikiforova, 2004; van Baak, 2010).

Although the South Caspian Plate has been rapidly subducting since the early Pliocene (~5.5 Mya) (Allen *et al.*, 2002), or possibly even earlier (Hollingsworth *et al.*, 2008), folding only started along the Apsheron Ridge at the end Pliocene (~2.4 – 2.6 Mya) (Devlin *et al.*, 1999; Souque *et al.*, 2010). Fold growth may have commenced earlier to the west, where the Talysh and Greater Caucasus mountain structural trends are also expressed as fold trains along the basin margin. The folds in the South Caspian Basin lack a clear structural vergence when viewed in cross-section, and have been interpreted as buckle folds, deforming by layer-parallel shortening above a ductile detachment surface; the Maikop shales (Devlin *et al.*, 1999). However, several seismic investigations show thrust faults coring the anticlines at depth (Fowler *et al.*, 2000; Knapp *et al.*, 2004; Robinson *et al.*, 2005; Green *et al.*, 2009; Rogers, 2011), so the folds may also have developed with a component of passive growth.

1.4. CURRENT REGIONAL RESEARCH TOPICS

Oligocene – Pliocene hydrocarbon play

The South Caspian Basin lies within the Greater Caspian Hydrocarbon Province; one of the world's largest plays, with reserves estimated at 15 – 30 billion barrels of oil, and 230 – 360 trillion cubic feet of gas (Smith-Rouch, 2006; Belopolsky & Talwani, 2007). Consequently, much of the recent research in the area has focussed on hydrocarbon aspects. Historical records show the Azerbaijan region has been exploiting oil from natural seeps since the times of Alexander the Great (330 bc.) (Effimoff, 2000), whilst the area contains numerous archaeological sites from the ancient Zoroastrian religion (fire worshipping); a temple honouring 'the eternal fire' still survives above an ignited gas seep in Ateshgah, near the field locations described in this thesis (Terra Nova, 1990). The region experienced a major oil boom in the late 1800s when industrialised hydrocarbon extraction began in earnest onshore. Since the end of the Soviet Union oil exploration in the region has been enjoying a resurgence; fields in the offshore Caspian Sea region are being explored and developed in partnership with foreign oil companies, which has lead to 2D and 3D seismic data being collected on a basin scale. The seismic data used in this thesis images two folds in the Azerbaijan portion of the basin: the Shah Deniz anticline and the Azeri – Gunashli – Chirag (ACG) structure; a gas field and oil field respectively. Data have been made available by BP and the Shah Deniz and Azerbaijan International Oil Company (AIOC) partnership.

The South Caspian oil and gas fields are structural traps and are located in anticlines which have been uplifting since the late Pleistocene (see above). The source rock is the regionally extensive Oligocene – early Miocene Maikop Formation; a marine diatomacious shale with high total organic carbon content (~10%). The Pliocene – present-day high sedimentation rates (estimated at 1.6m /kry in Allen *et al.*, 2002) have produced a thick sedimentary succession above the Maikop Formation (12500 m), which exhibits a very low thermal gradient (14 – 16° / km). As a result the oil and gas windows lie at great depths of ~8 km and 13 – 14 km respectively (Belopolsky & Talwani, 2007). The Maikop shale has been producing hydrocarbons since the Pleistocene – present-day; hydrocarbon charging was contemporaneous with fold uplift and trap formation (Abrams & Narimanov, 1997). The reservoir interval consists of a stacked succession of Pliocene lacustrine fluvial sands and lake-marginal muds sourced mainly from the Palaeo Volga delta (Devlin *et al.*, 1999; Hinds *et al.*, 2004). Sands from the Palaeo Kura and Palaeo Amu Darya are also present, but are muddier and of poorer reservoir quality (Morton *et al.*, 2003). Natural oil seeps are common both onshore and offshore, and have lead to speculation that many of the structural closures are filled beyond their spill-point.

The Pleistocene succession studied in this thesis lies in the overburden and is not considered an exploration target offshore. Isolated fields have been reported around the basin perimeter that exploit Pleistocene, lake-marginal carbonates (Smith-Rouch, 2006) but no concrete data has been published on these, and these reservoirs are probably very small compared with those in the Pliocene. The Pleistocene succession contains several mass transport complexes (see chapter 4) and accumulations of gas hydrates deposits (Diaconescu & Knapp, 2000; Diaconescu *et al.*, 2001) that are considered as unconventional hydrocarbon plays in other basins (Mosher *et al.*, 2010), but these are not currently being investigated as such in the South Caspian Basin.

Mud volcanoes and gas hydrates

The South Caspian Basin contains many mud volcanoes, both onshore and offshore, which have erupted large volumes of shale and have been extensively studied (Ginsburg & Soloviev, 1994; Yusifov & Rabinowitz, 2004; Stewart & Davies, 2006; Roberts *et al.*, 2011a). Recent research has focussed on their structural configuration, evolution, and structural inheritance (Roberts *et al.*, 2010; Roberts *et al.*, 2011a; Roberts *et al.*, 2011b).

The mud is sourced from overpressured shales in the Oligocene – early Miocene Maikop formation 8000 – 13000 m below the surface. Its vertical migration is driven by buoyancy contrasts between the shale and its dense overburden, and is aided by disequilibrium compaction, and hydrocarbon maturation, tectonic compression and deep fluid migration (Ginsburg & Soloviev, 1994; Fowler *et al.*, 2000; Kopf *et al.*, 2003; Davies & Stewart, 2005; Stewart & Davies, 2006; Evans *et al.*, 2008). Mud migrates towards the surface along hydraulic fractures at depth (Davies & Stewart, 2005; Stewart & Davies, 2006) and volcano edifices are commonly clustered along the faulted hinges of buckle folds that surround the basin perimeter (Fowler *et al.*, 2000; Yusifov, 2004; Roberts *et al.*, 2011a). Although the location of mud volcanoes appears to be structurally controlled, isolated examples also exist that pre-date fold growth (Fowler *et al.*, 2000; Yusifov & Rabinowitz, 2004), showing that mud volcanism also initiated in non-folded areas.

The Caspian mud volcanoes are of particular interest to hydrocarbon exploration as many oil fields onshore are located in close proximity to them (Devlin *et al.*, 1999; Dimitrov, 2002; Planke *et al.*, 2003). Mud volcano systems indicate hydrocarbon maturation in the source rock and have even been suggested to function as hydrocarbon migration pathways (Katz *et al.*, 2000; Dimitrov, 2002; Moscardelli & Wood, 2008). However they are typically a problem for hydrocarbon exploration, as they degrade reservoir quality and pose a drilling hazard (Fowler *et al.*, 2000; Stewart & Davies, 2006; Tingay *et al.*, 2008). In addition to this the South Caspian mud volcanoes have (speculatively) emplaced large volumes of gas hydrates in the shallow seabed, which are a potential future energy resource (Ginsburg & Soloviev, 1994; Diaconescu & Knapp, 2000; Diaconescu, 2002).

Climatic cyclicity and controls

Water level in the internally drained Caspian Sea is governed by a balance between riverine runoff and evaporation (Kaplin & Selivanov, 1995). Several rivers empty into the lake from the surrounding mountain ranges, but the majority of hydraulic inflow is generated by the Volga river, the drainage area of which, extends over much of western Russia (Kaplin & Selivanov, 1995). Riverine runoff is governed by wet – dry climatic cycles, whilst evaporation is primarily controlled by warm – cool cycles (Jones & Simmons, 1996; Kosarev, 2005).

Lacustrine settings are extremely sensitive to changes in climate (Carroll & Bohacs, 1999), and the Caspian Sea, with the largest evaporation budget of any Quaternary lake, and a high sedimentation rate, is of great interest to research into both current and palaeoclimatic changes (Panin, 2005). Complete, margin-scale stratigraphic sequences commonly take between 100.000 years (in the Pleistocene – present) and 1 – 2 million years (in older formations) to accumulate in marine settings (Van Wagoner *et al.*, 1988), but in the South Caspian Basin, margin scale sequences are deposited at timescales, an order of magnitude shorter, allowing for high resolution sequence stratigraphy (Abreu *et al.*, 2000; Kroonenberg *et al.*, 2000).

The Caspian water level has fluctuated rapidly, and at much larger ranges than in comparable marine settings. Cycles spanning five orders of magnitude (65 years – 1 million years) have been recognised in the Miocene – Holocene series (Juhász *et al.*, 1997; Kroonenberg *et al.*, 1997; Mamedov, 1997; Rychagov, 1997; Ulomov *et al.*, 1999; Nummedal *et al.*, 2000; Zubakov, 2001; Kosarev, 2005; Svitoch & Yanina, 2007; Amirov, 2008; van Baak, 2010). Milankovic scale lake-level changes have been identified, occurring at similar ages to glacio-eustatic trends but the precise mechanisms that governed them are not fully clear; lake-level change may have been coincident (Jones & Simmons, 1996), out of phase (Kroonenberg *et al.*, 1997; van Baak, 2010) or independent (Zubakov, 2001) of global eustacy. The debate is hampered by a poor age control in the Pleistocene – Holocene sequence where only a few radiometrically dated samples exist, which are difficult to verify (discussed in Mitchell & Westaway, 1999), whilst magnetostratigraphic studies have produced conflicting interpretations (Discussed in chapters 3 and 5). A regional bio-chronostratigraphy has been defined (e.g.Ghenea, 1970; Popov, 1970; Jones & Simmons, 1996; Zubakov, 2001; Osipova, 2009); however, the Caspian Sea has generally been separated from the world's oceans since the Messinian, and much of its fauna is locally endemic, which complicates correlation of biostratigraphy with global climatic events (Jones & Simmons, 1996).

1.5. SYNTECTONIC FOLD BURIAL

Origin and significance of growth strata

Once topography in a sedimentary basin is modified by tectonically-driven, vertical motion of a fold or fault block, the combined processes of burial and erosion simultaneously reduce the scarp to a horizontal regional datum. 'Growth strata' (or 'syntectonic strata') represent the sedimentary packages that infill the relief created by the deformed 'pretectonic strata', and develop in all tectonic settings containing coeval sedimentation and deformation (Burbank *et al.*, 1996). Growth strata are themselves progressively deformed and incorporated into the tectonic structures forming wedge-shaped packages which thin towards the point of maximum uplift or minimum subsidence. They have long been recognised in the field (Riba, 1976), but only since the availability of seismic data, has it been possible to research their vertical architecture and stacking patterns in detail (e.g. Suppe *et al.*, 1992).

Established controls on growth strata architecture

The processes which control growth strata architecture are complex, though several have been observed in field and seismic data (e.g. Anadón *et al.*, 1986; Gawthorpe *et al.*, 2000; Castelltort *et al.*, 2003; Aschoff & Schmitt, 2008) and their generation has been modelled using sandbox and computer methods (e.g. Salvini & Storti, 2002; Patton, 2004; Strayer *et al.*, 2004).

The primary control on deposition is 'base level'. In subaqueous settings this is defined as sea level, though in reality it is probably wave base, whilst in aerially exposed, terrestrial settings, base level is the regional height of the sedimentary fill. Above base level there is non-deposition and erosion, and below base level there is sedimentation (Suppe *et al.*, 1992; Butler & Lickorish, 1997). For appreciable growth strata to develop, a structure must be located below base level, avoiding erosion, for an extended period (Salvini & Storti, 2002). If a relative base level drops occurs, either by falling relative water levels, or by an increased tectonic uplift, both syn-and pre-tectonic strata are eroded, leaving a characteristic angular unconformity along the fold's crest (e.g. Ford *et al.*, 1997; Patton, 2004).

A second control is the kinematic evolution of the structure itself. As a fold grows, the behaviour and movement of its limbs and axial surfaces, tilt, truncate and deform the syntectonic strata; this results in two, distinctive, and kinematically separate end-member models: folds that deform above a low-friction detachment layer (décollement folds and buckle folds), and folds underlain by and driven by vertical motion of a fault, (fault bend folds and fault tip folds). Each end member contains characteristic growth strata stacking patterns (Figure 1.2). As décollement- and buckle folds grow, their limbs are progressively steepened, and their fold axial plane remains fixed resulting in a fanning, down-section steepening stacking pattern in their growth strata wedge (Shaw *et al.*, 2004). Fault-bend, and fault-tip folds grow primarily by the migration of kink bands (Ramsay, 1967; Suppe, 1983; Suppe *et al.*, 1992; Mitra, 2003). Growth strata architecture along these structures consists of packages of parallel-dipping horizons contained within 'growth triangles' (Shaw *et al.*, 2004).

A third control is the depositional environment which determines the sedimentary processes transporting material to the structure (Castelltort *et al.*, 2004). 'Dynamic sedimentation' develops in areas of high sediment input; strata are laid down along horizontal beds which infill and reduce topography, whilst 'non-dynamic' sedimentation is created by pelagic fallout that drapes topography, neither reducing nor amplifying it. Studies using growth strata architecture are only possible in dynamic environments; syntectonic non-dynamic sedimentary packages are indistinguishable from pre-tectonic strata.

A fourth control, is the ratio between sedimentation rate, and vertical movement of the fold; the burial/uplift ratio (Storti & Poblet, 1997).The relative magnitudes of the two competing processes, occurring below base level, determine whether the fold is buried (burial>uplift), or whether the growth strata wedge remains adjacent to the fold hinge (forming an 'off-structure wedge') with the fold axis remaining as a topographic high (burial<uplift). Variations between burial rate and uplift produce characteristic stacking patterns: If burial and uplift are in equilibrium, then the growth strata form an 'apical wedge'; in section-view successive sedimentary beds pinch out at the fold crest in a fanning, down-section steepening geometry. The lateral edge of strata pinch-out (a point, in cross-section) remains constant though time and no material is accreted above the fold hinge. If burial>uplift, horizons progressively 'onlap' the fold limb and travel towards the fold hinge, eventually 'overlapping' and covering the entire structure. In the 'overlap wedge' strata are not truncated, and material accumulates above the fold hinge. If the burial rate is lower than the uplift rate the fold crest becomes exposed and strata show an onlap trend that travels away from the fold crest, termed 'rotative offlap' (Riba, 1976; Anadón *et al.*, 1986; Verges *et al.*, 1996; Ford *et al.*, 1997). This is often accompanied by an elevation of the fold crest above base level and erosion (Figure 1.3).

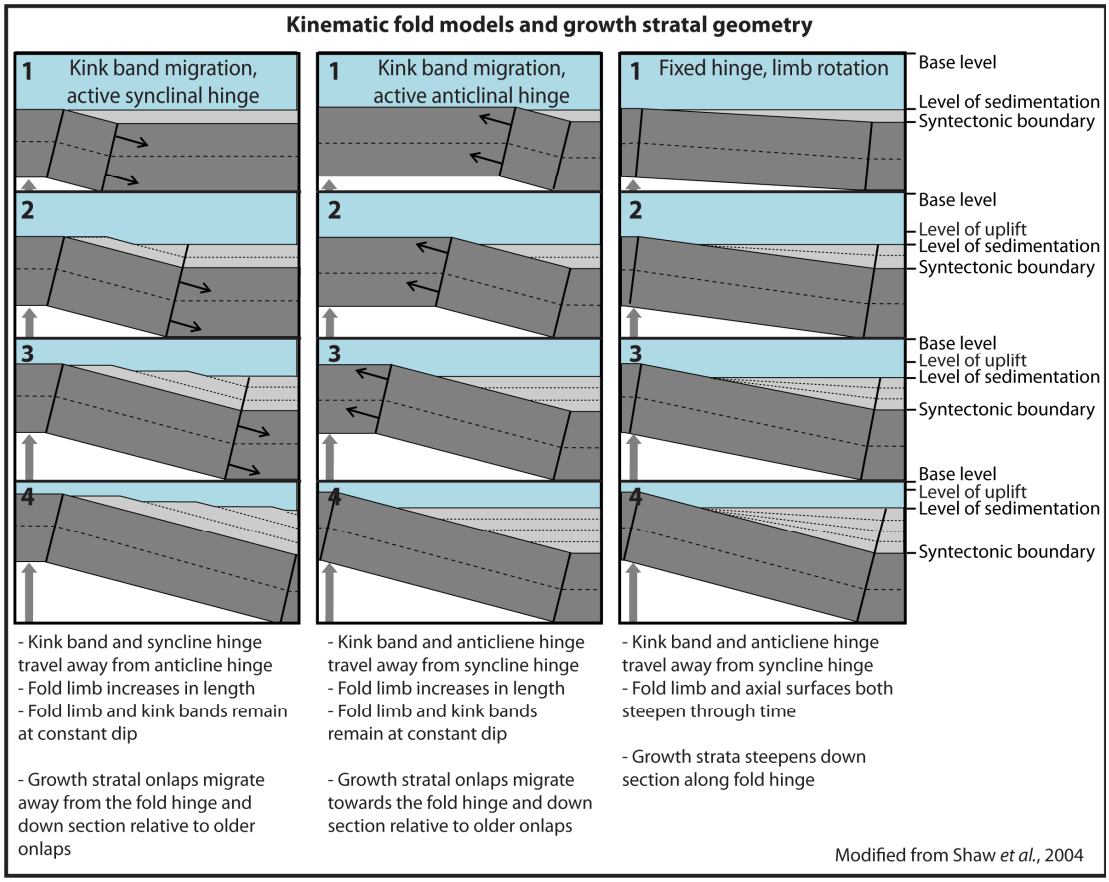

Figure 1.2 Stacking patterns of growth strata along kinematically different fold types. This figure is repeated in chapter 2

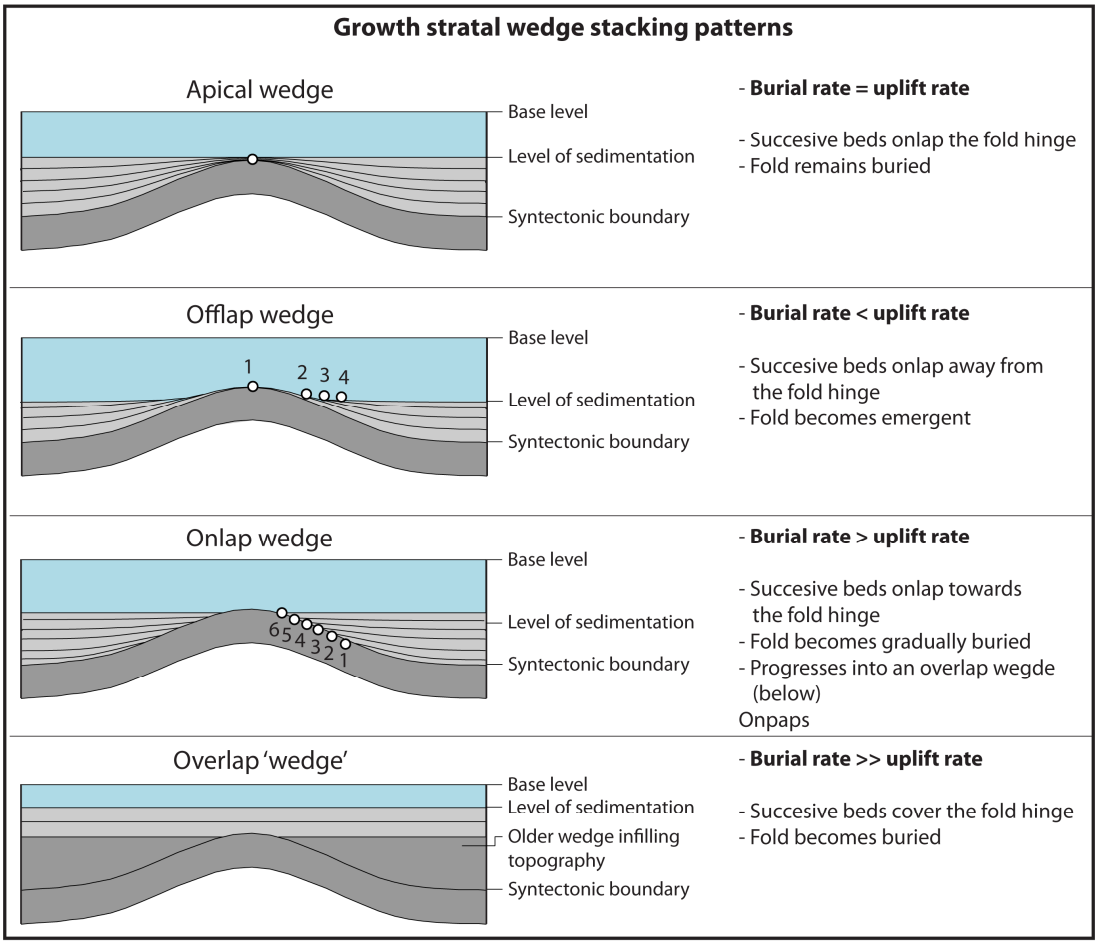

Figure 1.3 Stacking patterns and locations of growth strata terminations along buckle folds deforming at different burial/uplift ratios. This figure is repeated in chapter 2

2. Climatically forced progressive unconformities in folds

2.1. INTRODUCTION

Aims and overview

The syntectonic deposition of 'growth strata' (Suppe *et al.*, 1992) along geological folds is an important sedimentary process: crucial information regarding a structure's timing (Butler & Lickorish, 1997) and kinematic evolution (Erslev, 1991; Suppe *et al.*, 1992; Hardy & Poblet, 1994; Poblet & Stuart, 1995; Verges *et al.*, 1996; Shaw *et al.*, 2004) are recorded in the architecture of successive sedimentary packages which can also be used to understand other geological processes such as basin-wide structural evolution (Schneider *et al.*, 1996; Ghiglione & Ramos, 2005), structural controls on sedimentation (Burbank *et al.*, 1996; Poblet *et al.*, 1997; Storti & Poblet, 1997; Gawthorpe *et al.*, 2000) and the presence of hydrocarbon traps (Mitra, 1990; Shaw *et al.*, 2004). These studies often assume a sedimentary model where tectonically induced topography is completely buried by sediment and in which the fold is the dominant control on growth strata architecture (e.g. Hardy *et al.*, 1996), recently however the effects of sedimentary processes which complicate growth architecture have been highlighted and the magnitude of tectonics' impact has been questioned (Castelltort *et al.*, 2004; Pochat *et al.*, 2009).

This study investigates using regionally extensive seismic data whether climatically-driven sedimentation is a fundamental control on growth strata architecture. It presents seismic data from several folds within the South Caspian Basin (Figure 2.1a) and has four principal aims: [1] to document the growth strata and seismic scale unconformities along two anticlines of a similar age in the study area [2] to investigate whether both anticlines developed synchronously or individually, identifying regional and local episodes of deformation and sedimentation in their growth strata successions [3] to document the seismic stratigraphy of the north-western margin of the South Caspian Basin around Azerbaijan [4] to investigate whether significant events in the fold's growth strata correlate to stratigraphic events in the basin's history.

The South Caspian Basin is the ideal location to examine this process; the basin cover is deformed into numerous large anticlines and one of the world's largest sedimentation rates has recorded a high-resolution archive of structural movement (Devlin *et al.*, 1999). The study area is therefore an ideal natural laboratory to study the combined effects of uplift and climate on growth strata. The study's methodology is widely applicable to folds in other basins and carries implications for conventional interpretations of fold growth strata architecture. In addition to this, the study is of regional interest as it documents the stratigraphy and tectono-sedimentary interplay of the South Caspian Basin during the Late Pliocene and Pleistocene period.

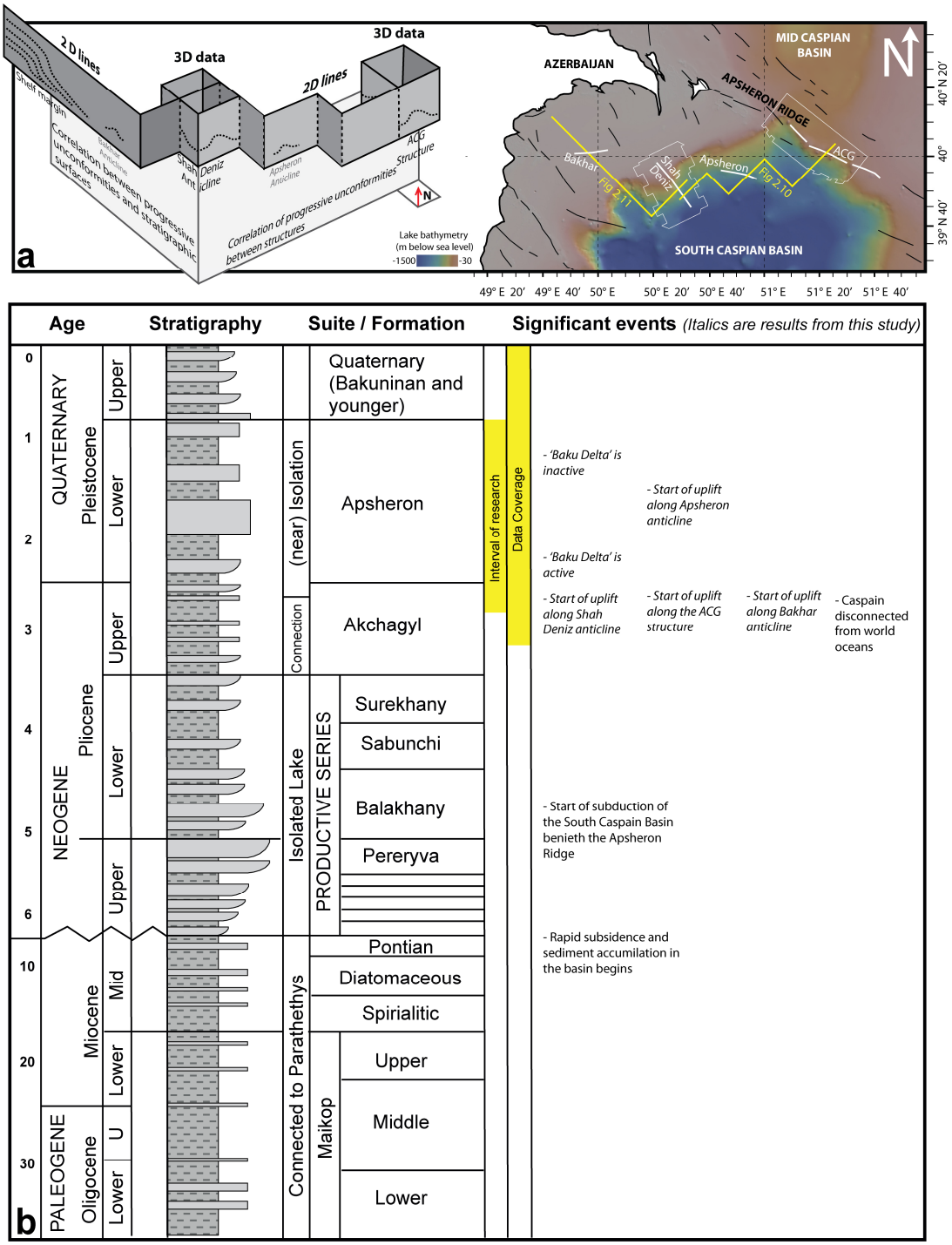

Figure 2.1. [a] Cartoon showing configuration and location of seismic data. Bathymetry and structure map of the study area. Fold traces are shown in black and white, locations of figures are shown in yellow. Fold locations modified from Jackson *et al.*, (2002), bathymetry map from Hall (2002) and GeoMapApp (2011) [b] Stratigraphic log showing main geological formations (locally termed 'suites'), and significant events in the basin's history. Modified from Devlin *et al.*, (1999).

Growth strata

Definition of growth strata

'Growth strata' (or 'syntectonic strata') represent the sedimentary packages that infill the relief created by deformed 'pretectonic strata'. Once topography in a sedimentary depocentre is modified by tectonically-driven, vertical motion of a fold or fault block, the combined processes of burial and erosion simultaneously reduce the scarp to a horizontal regional datum. Growth strata are themselves progressively deformed and incorporated into the tectonic structures forming wedge shaped packages which thin towards the point of maximum uplift or minimum subsidence. Growth strata occur in all tectonic settings where sedimentation and deformation were coeval, they have long been recognised in the field (Riba, 1976), including in this study's field area (Figure 2.2) but only since the availability of seismic data, has it been possible to research their vertical architecture and stacking patterns in detail (e.g. Suppe *et al.*, 1992).

Established controls on growth strata architecture

The processes which control growth strata architecture are complex, several have been observed in field and seismic data (e.g. Anadón *et al.*, 1986; Gawthorpe *et al.*, 2000; Castelltort *et al.*, 2003) and their generation has been modelled using sandbox and computer methods (e.g. Salvini & Storti, 2002; Patton, 2004; Strayer *et al.*, 2004). The primary control on deposition is 'base level', commonly either defined as sea level (though in reality it is probably wave base), or the regional height of the sedimentary fill (along terrestrial structures). Above base level there is non deposition and erosion, and below base level there is sedimentation (Suppe *et al.*, 1992; Butler & Lickorish, 1997).

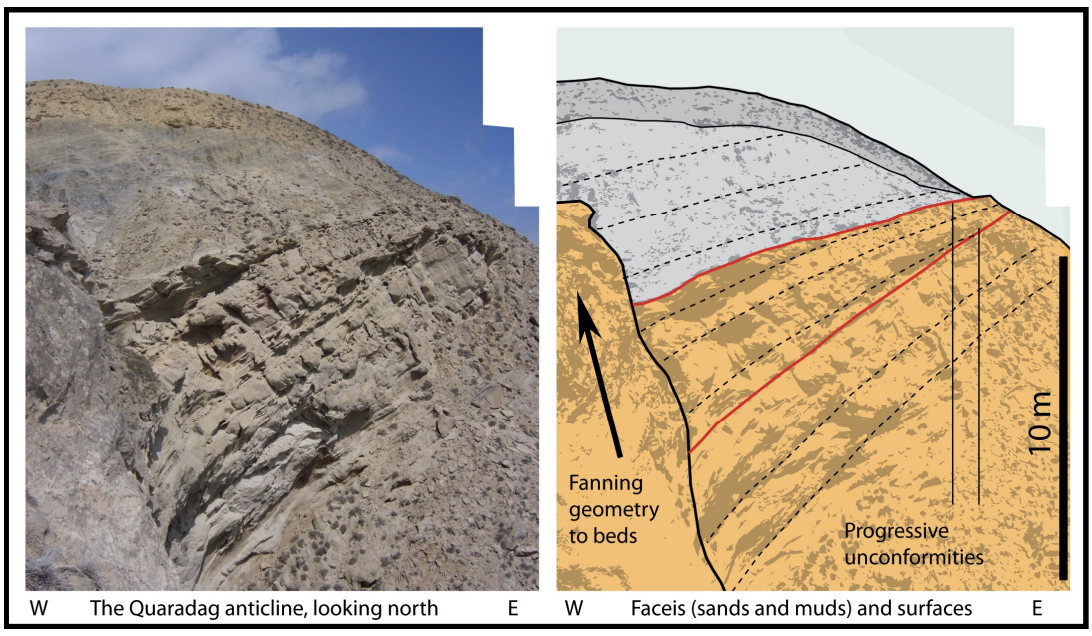

Figure 2.2. Unconformities observed in Apsheron Formation syntectonic growth strata along the Quaradag anticline (described in detail in chapter 3). Bedding dips steepen down-section in a fanning geometry. Location of photo mosaic is approximately: 40°15'28.06"N, 49°31'21.57"E, looking towards the north.

For appreciable growth strata to develop, the structure must be located below base level (Salvini & Storti, 2002). Base level drops create characteristic unconformities within growth strata packages (e.g. Ford *et al.*, 1997) which are described in more detail below.

A second control is the kinematic evolution of the structure itself. As a fold grows, the behaviour and movement of its limbs and axial surfaces, tilt, truncate and deform the syntectonic strata. This study describes growth strata along compressive folds, two principal end-members of these exist: folds which deform above a low friction detachment layer (décollement folds and buckle folds), which develop with the fold axis remaining static, and limbs progressively steepening and folds underlain by and driven by vertical motion of a fault, (fold bend folds and fault tip folds) which grow primarily by the migration of kink bands (Ramsay, 1967; Suppe, 1983; Suppe *et al.*, 1992; Mitra, 2003). Both end members can be identified based on their growth strata architecture; strata along limb rotation folds show a fanning pattern which becomes steeper with increasing depth, whereas inclined strata along kink band folds consists of packages of identically dipping horizons contained within a 'growth triangle' (Figure 2.3) (Shaw *et al.*, 2004).

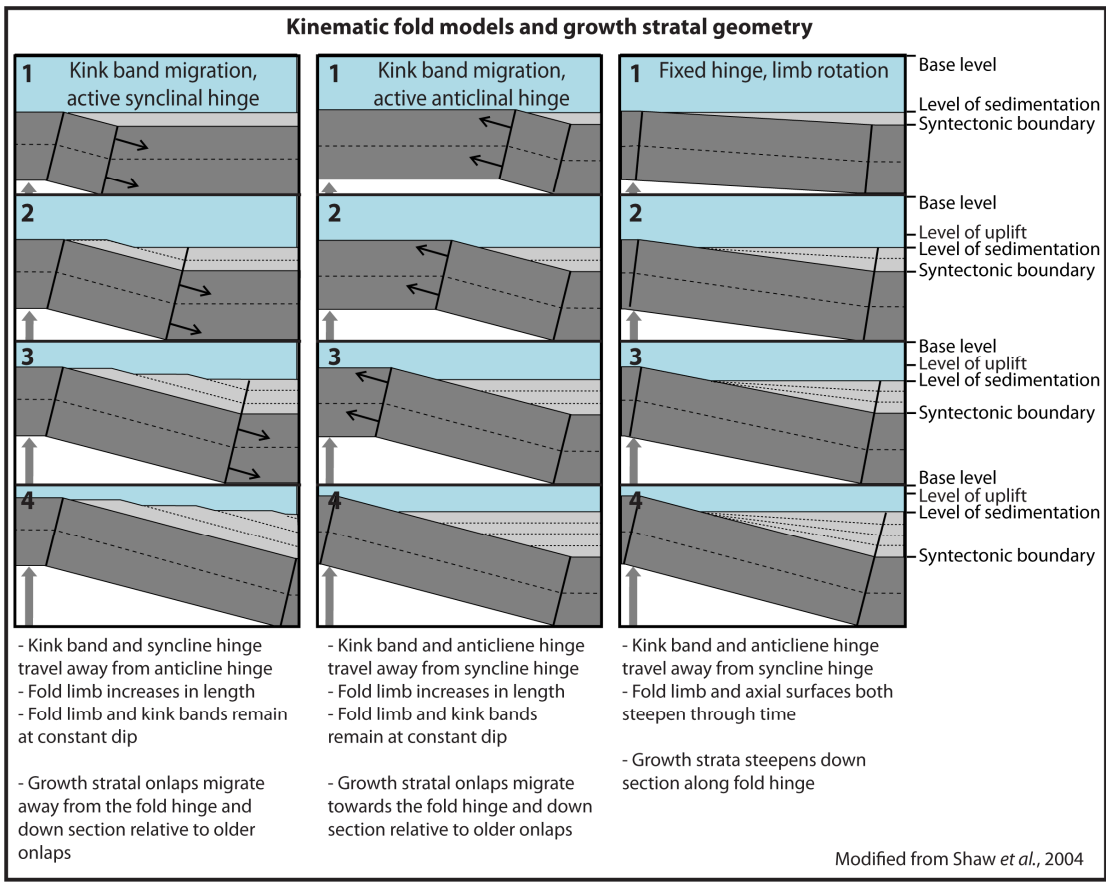

Figure 2.3. Stacking patterns of growth strata along kinematically different fold types.

A third control is the depositional environment which determines the sedimentary processes transporting material to the structure (Castelltort *et al.*, 2004). 'Dynamic sedimentation' develops in areas of high sediment input; strata are laid down along horizontal beds which infill and reduce topography, whilst 'non-dynamic' sedimentation is created by pelagic fallout that drapes topography, neither reducing nor amplifying it. Studies using growth strata architecture are only possible in dynamic environments; syntectonic non-dynamic sedimentary packages are indistinguishable from pretectonic strata.

A fourth control, and the focus of this chapter, is the ratio between sedimentation rate, and vertical movement of the fold; the burial/uplift ratio (Storti & Poblet, 1997).The relative magnitudes of the two competing processes, occurring below base level, determine if the fold is buried (burial>uplift), or if the growth strata wedge remains adjacent to the fold hinge (forming an 'off structure wedge') with the fold axis remaining as a topographic high (burial<uplift). Variations between burial rate and uplift produce characteristic stacking patterns: If burial and uplift are in equilibrium, then the growth strata form an 'apical wedge'; in section view successive sedimentary beds pinch out at the fold crest in a fanning , down section steepening geometry. The point of pinch-out remains constant though time and no material is accreted above the fold hinge. If burial>uplift, horizons progressively 'onlap' the fold limb and travel towards the fold hinge, eventually 'overlapping' and covering the entire structure. In the 'overlap wedge' strata are not truncated, and material accumulates above the fold hinge. If the burial rate lower than the uplift rate the fold crest becomes exposed and strata show an onlap trend that travels away from the fold crest, termed 'rotative offlap' (Riba, 1976; Anadón *et al.*, 1986; Verges *et al.*, 1996; Ford *et al.*, 1997). This is often accompanied with an elevation of the fold crest above base level and erosion (Figure 2.4).

Progressive unconformities and their origins

Angular unconformities that bound packages of growth strata are only present along anticline crests; further off-structure strata gradually become conformable. These localised angular discordances are termed 'progressive unconformities' (Birot, 1937. In Riba, 1976). Two geometries of progressive unconformity exist, 'onlap unconformities' and a 'truncation unconformities' each with different causal mechanisms (Figure 2.5), either by [1] the lowering of base level and erosion of the fold crest (Castelltort *et al.*, 2004), [2] by retrogradational stacking patterns caused by kink band growth kinematics (Suppe *et al.*, 1992), or [3] by uplift outpacing burial shifting sedimentation away from the fold (Riba, 1976; Anadón *et al.*, 1986; Storti & Poblet, 1997).

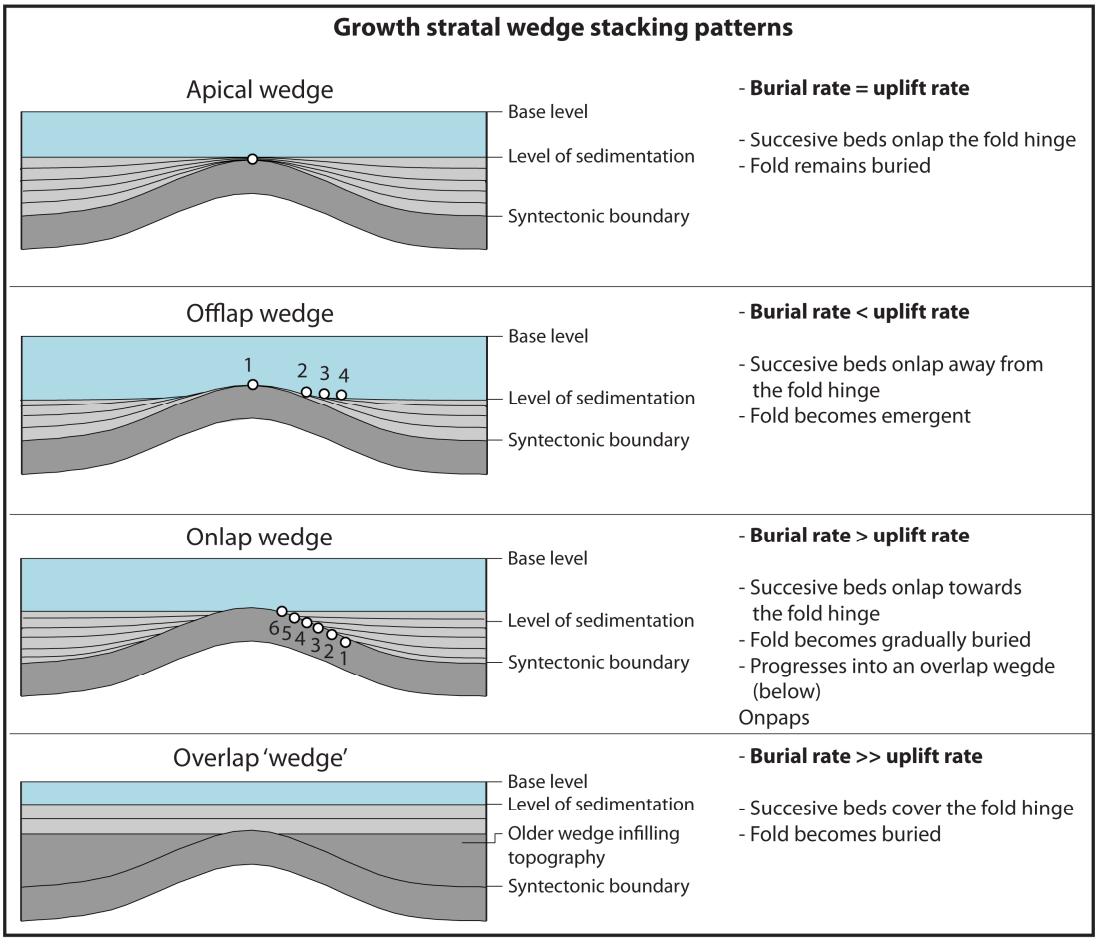

Figure 2.4. Stacking patterns and locations of growth strata terminations along buckle folds deforming at different burial/uplift ratios.

Geological setting

The South Caspian Basin, the southernmost portion of the present-day Caspian Sea, lies within the Arabia – Eurasia collision zone and behaves as an aseismic block, encircled by active orogens (Allen *et al.*, 2003). Convergent tectonic plate motions are accommodated by compression and strike slip in the Zagros, Alborz and Caucasus Mountains, and the subduction of the South Caspian Basin beneath the Mid Caspian Basin along an incipient accretionary prism, the 'Apsheron Ridge' (Jackson *et al.*, 2002; Allen *et al.*, 2003; Allen *et al.*, 2004; Guest *et al.*, 2007b; Tatar *et al.*, 2007; Hollingsworth *et al.*, 2008). The basin probably formed as a back arc basin, north of the Tethys Ocean, although the age of its formation is disputed with estimates covering the Jurassic to the Palaeogene, whilst further disagreement exists regarding the nature of its basement, which is commonly interpreted as unusually thick oceanic crust (Mangino & Priestley, 1998), which may extend only partially along the basin (Green *et al.*, 2009).

A combination of high subsidence rates, high sediment supply from rising mountain ranges and the focussing of rivers into the basin, has resulted in one of the thickest sedimentary successions in the world; Pliocene – Quaternary strata are up to 10 km thick (Inan *et al.*, 1997; Nadirov *et al.*, 1997; Allen *et al.*, 2002; Knapp *et al.*, 2004; Egan *et al.*, 2009; Green *et al.*, 2009). This study focuses on the upper Pliocene to Mid Pleistocene sedimentary succession, which is approximately 3000 m thick (Figure 2.1). The succession follows a broadly regressive trend containing several large scale transgressions (Jones & Simmons, 1996; Kroonenberg *et al.*, 1997) and is dominated by lacustrine mud with shallower interbedded silt and sand becoming significant from the base of the Quaternary onwards (Devlin *et al.*, 1999) (Figure 2.1b). Regional seismic lines show Pleistocene-present-day sedimentation at the basin margins characterised by several large clinoform deposits (Abdullayev, 2000; Fowler *et al.*, 2000; Hoogendoorn *et al.*, 2005; Abreu & Nummedal; Kalani *et al.*, 2008). The Shelf edge delta that is presented in this study may be from the Palaeo Kura, (Abreu & Nummedal) but it is located much further northwards than the current mouth of the Kura (Figure 2.1a). Either this indicates an avulsion of the Kura Delta to the South since the Holocene, a fact not documented in the exiting scientific literature (Inan *et al.*, 1997; Rychagov, 1997; Hoogendoorn *et al.*, 2005) or potentially the delta was deposited by a now extinct river such as the Alanzani. The delta is referred to as the Baku delta throughout the rest of this study due to its unknown origins and its location close to Azerbaijan's capital city.

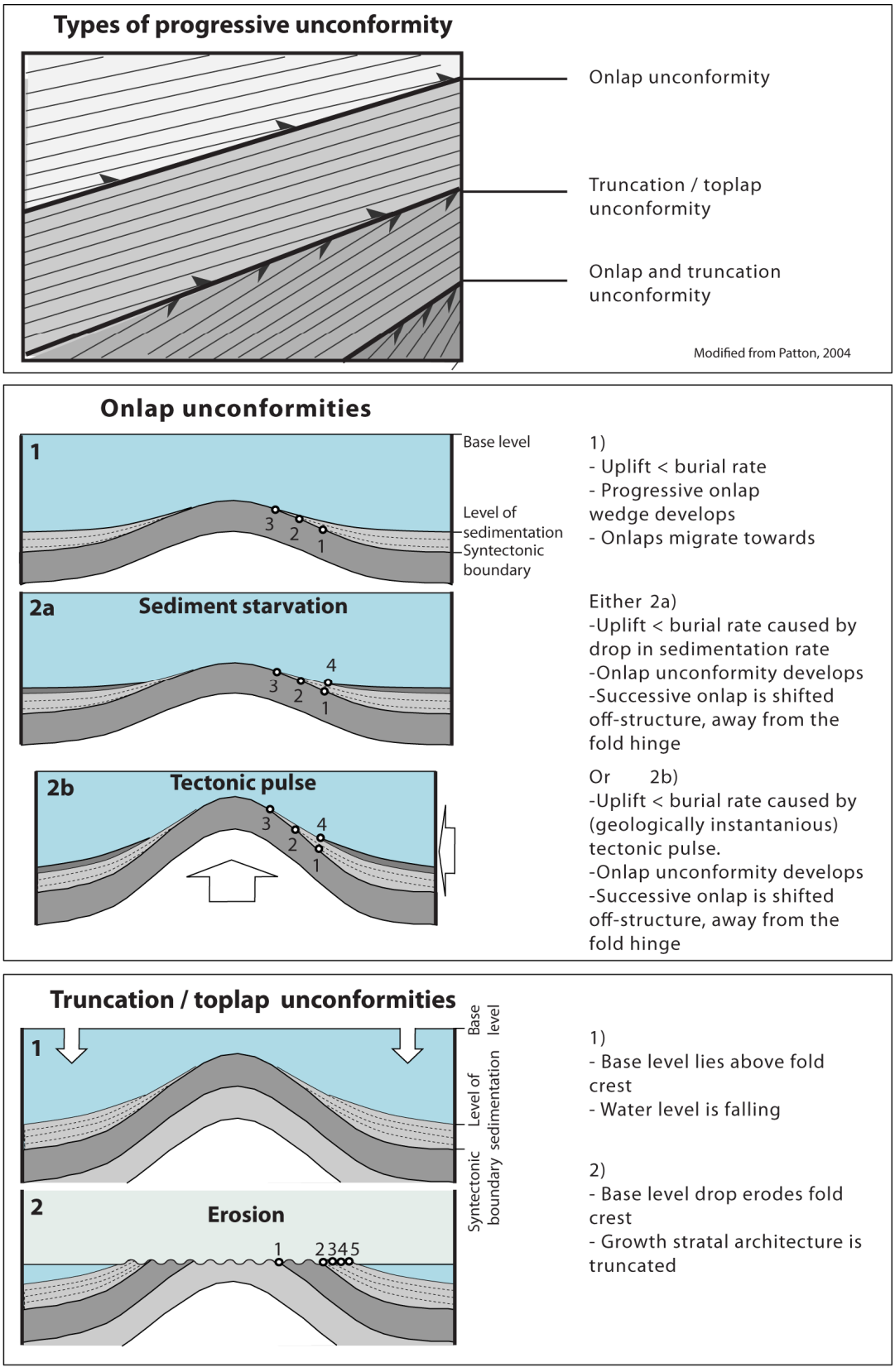

Figure 2.5. Different types of progressive unconformities and their generation mechanisms.

The South Caspian lake bed is extensively folded (Figure 2.1a). Sediment was deposited syntectonically along large anticlines which remain active today (Jackson *et al.*, 2002). Folds associated with the compressive margins are detached on overpressured Oligo – Miocene mud which escape to the surface via numerous mud volcanoes (Devlin *et al.*, 1999; Fowler *et al.*, 2000; Knapp *et al.*, 2004; Howie *et al.*, 2005; Stewart & Davies, 2006; Green *et al.*, 2009). Many of the anticlines host hydrocarbons from a regional Oligocene – Pliocene play (Devlin *et al.*, 1999; Katz *et al.*, 2000). This study presents seismic data from two folds in the Azeri portion of the South Caspian Basin: the Azeri Chirag Gunashli (ACG) structure and the Shah Deniz Anticline. The ACG structure lies along the Apsheron Ridge, the Shah Deniz anticline lies to the south, adjacent and tangential to the basin's western margin (Figure 2.1a). Two smaller, younger fold structures are also contained within the data, the Apsheron anticline, and the Bakhar anticline. Uplift of the folds started, in the Late Pleistocene (Devlin *et al.*, 1999; Fowler *et al.*, 2000), whilst onshore, folding started as early as the latest Miocene (Souque *et al.*, 2010). The folds have all been located basinwards of the shelf margin, (at least partially) below base level throughout their tectonic history (Abreu & Nummedal; British Petroleum, 2010).

The Caspian 'Sea' has been periodically connected to the world's oceans via the Black and Aral Seas, however since the Pleistocene it has largely been isolated from the world's ocean systems forming the world's largest endoheric lake (Jones & Simmons, 1996; Kroonenberg *et al.*, 1997). Terminology in this study reflects this; 'lake level', rather than 'sea level', is used and 'lake bed' rather than 'seabed'.

Study rationale

The study attempts to disentangle the combined effects of fold kinematics burial/uplift and climate change on a syntectonic sedimentary succession. The interval of study (defined in the methods section) runs from the late Pleistocene – mid Pliocene, a high-resolution sedimentary record of uplift approximately 3000 m thick and 1.5 – 2 Ma old. The Caspian Sea has been an internally drained basin and disconnected from the world's oceans throughout this period with sedimentation rates governed by variations in continental runoff from the adjacent mountain ranges, driven by periods of climatic aridity and evaporation (Jones & Simmons, 1996; Zubakov, 2001; van Baak, 2010). Sediment and water reached the lake though the same network of rivers, and palaeo lake level and palaeo sedimentation rates were probably closely linked. The Caspian lake level has rapidly fluctuated at large scales during the Pliocene to present period —currently lake level changes two orders of magnitude faster than global eustatic rise— (Jones & Simmons, 1996; Kroonenberg *et al.*, 1997; Zubakov, 2001), implying a varying sediment flux during this interval.

This study investigates the theory that that variation in the regional climate has affected runoff and perturbed the burial/uplift ratio along structures at several points in time and has been the main cause of progressive unconformities in the fold growth strata successions. If this is the case then most progressive unconformities should be regionally synchronous, and should also show a significant correlation to the lake level history. To ascertain this, the project identifies, at the seismic scale, all the progressive unconformities within two folds' syntectonic successions, mapping their correlative conformities over a regional seismic line connecting the two structures, and subsequently also onto the north-western basin margin where they are integrated with a seismic sequence stratigraphic model. The population of growth strata unconformities can be classified into regionally extensive or regionally unique end members which can subsequently be integrated with a regional seismic stratigraphic model (Figure 2.6).

2.2. DATA AND METHODS

Seismic data

This study uses two, three dimensional (3D) seismic cubes, which are situated around the Shah Deniz and ACG structures, and a dogleg grid of two-dimensional (2D) vertical seismic sections which connects both 3D data, and which extends onto the north-western shelf margin of the basin (Figure 2.1a). In addition to the seismic data, well picks were provided by BP for the top and base Apsheron suite. It is not clear how these picks have been ascertained, or if any biostratigraphic, radiogenic, magnetostratigraphic or sedimentological control has been applied to them.

The two 3D seismic data cover an area of approximately 1000 km^2 each. Processing steps include f-k filtering, depth conversion and automatic gain control (see Liu & Goulty, 1999; Brown, 2004). The data are displayed in normal polarity (an increase in acoustic impedance is a red-black-red reflection loop). Inline spacing in the ACG and Shah Deniz surveys is 12.5m. The average vertical resolution (quarter of the wavelength) is 20 m in both surveys in the interval of interest (approximately 0 – 4000 m), although resolution decreases with depth. Howie et al., (2005) provide further detail on the data processing of the surveys used in this study.

The 2D seismic data have been selected from a regional grid shot by Caspian Geophysical JV (Abdullayev, 2000). It extends for a distance of 90.5 km and 129 km respectively. Not all processing steps are known (data is proprietary) but the data have been time-migrated and seismic artefacts such as lake bed multiples have been removed. Line diagrams and interpretations of the 2D data are presented, which have been produced in a graphics program using an auto trace tool. The data are displayed in two way time. The average wavelength in the interval of interest is 13.5 milliseconds (one way time). Using a crude depth conversion (made by comparing the 2D seismic sections with the depth converted seismic volumes along adjacent dip sections from the Shah Deniz and ACG structures) the interval of interest is approximately 3000 m thick, and the estimated vertical resolution is 15 m.

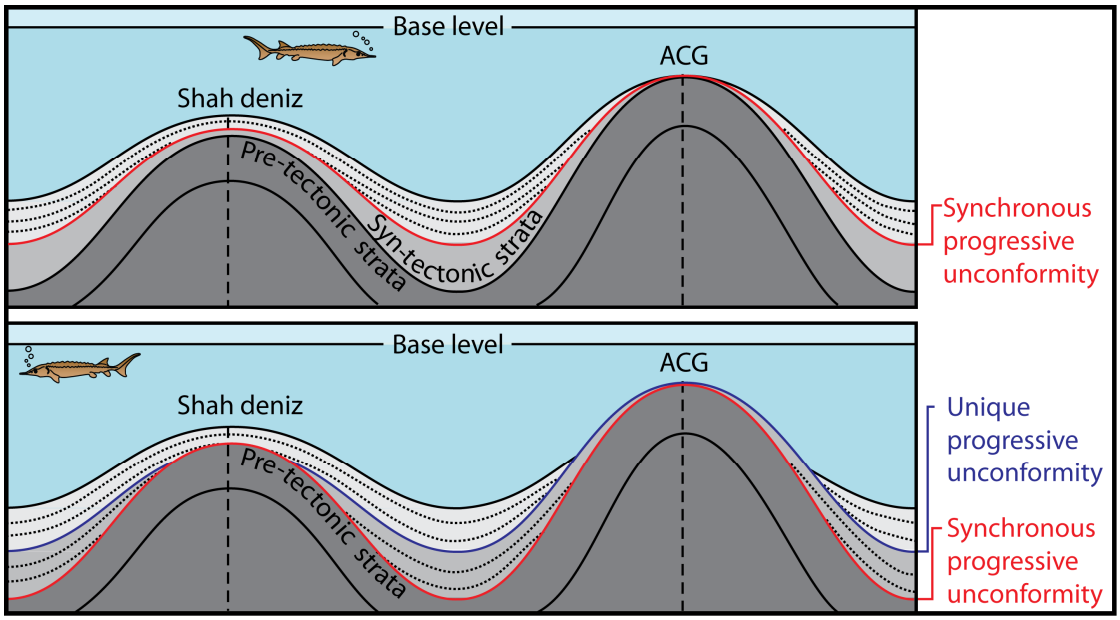

Figure 2.6. Correlated progressive unconformities between folds. Unconformities are either unique to a fold, probably driven by localised tectonic activity, or regionally synchronous, driven by a basin-wide process.

Interpretation strategy

Two key horizon types were interpreted in vertical seismic sections: [1] the reflection separating pre- and syntectonic strata, the 'syntectonic boundary' designates the lower limit of the interval of interest. Pretectonic horizons run parallel to lower reflections ('tram lining') and do not contain truncations and onlaps. [2] 'progressive unconformities' lie above the syntectonic boundary, and are identified by vertically adjacent reflections which are truncated against the surface.

Several geological processes complicate the growth strata pile and introduce noise into the data. Extensive submarine slope failures are common in the Pliocene – present succession (See chapter 4), which have remobilised and destroyed the much of the original growth strata architecture (e.g. Heinio & Davies, 2006; Morley, 2009). Mud volcanoes are common along both anticlines and deposit extensive (100 – 2000 m wide, <100 m thick) mudflows in downslope-tapering sediment packages that complicate the growth strata architecture (Fowler *et al.*, 2000; Davies & Stewart, 2005). Crestal collapse faulting (e.g. Morley, 2007) along both fold hinges also complicates and destroys reflections (Devlin *et al.*, 1999). In addition to this, the Shah Deniz anticline lies tangential to the South Caspian Basin margin, where a delta has partially prograded over the structure (Fowler *et al.*, 2000). Deltaic foreset sedimentation complicates growth strata geometries, depositing off-structure-thinning, tapered units (Gawthorpe & Hardy, 2002).

The seismic sections used in this study were chosen to mitigate these effects. However, a large portion of the stratigraphy along both anticlines has been remobilised by mass wasting, and is unsuitable. This study's regional grid of 2D seismic data avoids many of the lower (Upper Pleistocene and Pliocene) mass transport complexes and intersects the structures near to their centres. Progressive unconformities were identified along this grid using onlapping reflections, and correlated between both structures along the regional 2D line.

A second regional 2D line runs from the Shah Deniz anticline towards a clinoform complex located along the basin margin. The line was analysed using seismic stratigraphy techniques (Vail *et al.*, 1977; Van Wagoner *et al.*, 1988). Seismic stratigraphy was developed in marine environments, but its concepts have been successfully applied to non-marine systems (e.g. Mullins *et al.*, 1996), whilst seismic stratigraphic investigations have been carried out in the Caspian Sea previously (Abdullayev, 2000; Hoogendoorn *et al.*, 2005; Abreu & Nummedal; Kalani *et al.*, 2008). The three primary controls on facies and sedimentary architecture: water level, sediment supply and accommodation space, all operate along lacustrine margins (Scholz, 2002) though they differ from marine equivalents as relative water level is not primarily driven by eustacy and thermal expansion, but by the balance of evaporation and river input into the lake. The maximum possible lake level is governed by the topography of the continent surrounding the lake margin, the spill point (Carroll & Bohacs, 1999). In the Caspian Sea this is the Manysch strait, which lies approximately 20 m higher than the present-day lake level, and which connected the Caspian with the Black and Mediterranean seas during palaeo high-stands (Zubakov, 2001). A second major difference is sedimentation rate which is typically much higher in lacustrine settings (Carroll & Bohacs, 1999; Scholz, 2002). A seismic scale sequence takes 1 – 2 million years to accumulate in a marine setting, but can be deposited in Milankovic timescales (10.000 – 400.000 years) in lacustrine environments (Scholz, 1995; Scholz, 2002).

Seismic sequences, system tracts and palaeo lake level fluctuations were interpreted based on patterns of onlaps and the position of the palaeoshelf break through time; a basinwards shift in onlaps is interpreted as a regression, and a shoreward shift in onlaps indicates a transgression(Vail *et al.*, 1977). Several sequence stratigraphic models exist which differ in where they place the significant boundaries in the relative sea level curve (discussed in Catuneanu *et al.*, 2009), This study uses the Society for Sedimentary Geology (SEPM) sea level curve (Figure 2.7), which is suitable for clastic systems (Coe, 2003; Kendall, 2003) The maximum flooding surface and sequence boundary lie at points along the relative water level curve where flooding reaches its maximum rate of change, rather than at maxima or minima. Sequence boundaries were identified based on onlaps and downlaps onto a surface by shallower reflections, whereas maximum flooding surfaces were identified by downlaps (Figure 2.7). In addition to this, two more relevant surfaces were identified: the ‘basal surface of maximum regression’, a downlap surface, and the ‘transgressive surface’, a downlap surface which itself onlaps older reflections.

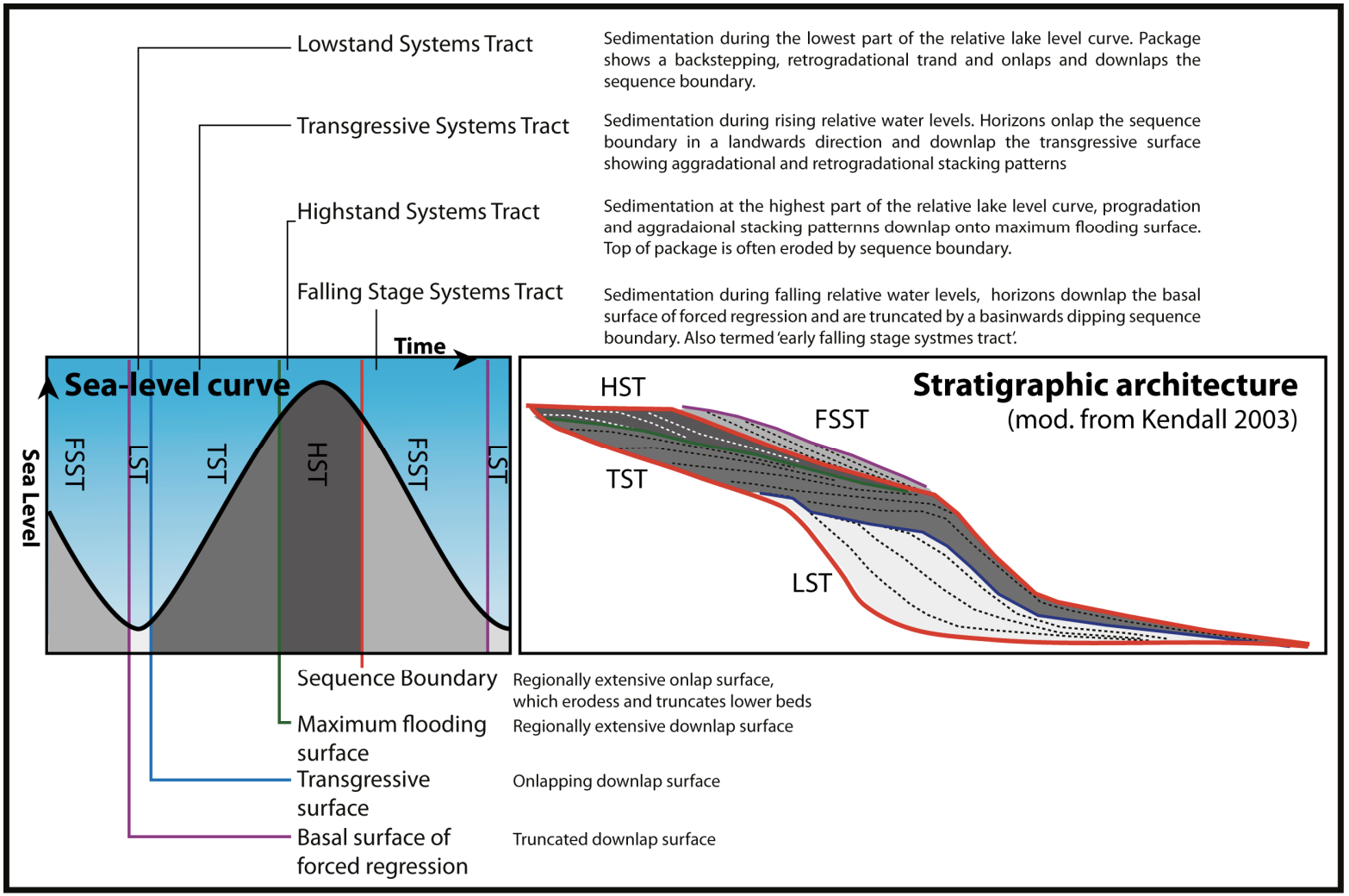

Figure 2.7. Idealised lake level curve and sequence stratigraphy, adapted from Kendall (2003). An idealised sequence is shown with all systems tracts and significant surfaces.

2.3. RESULTS

Observations

Style of growth strata packages along the ACG and Shah Deniz structures in 3D seismic data

Dip lines taken through 3D seismic data display growth strata from the ACG and Shah Deniz structures. Along the Shah Deniz fold the 3D data capture the entire growth strata succession from the anticline hinge to the syncline trough, however along the ACG fold the 3D surveys lateral extent is limited only a small amount of the succession is visible. The growth strata along both structures comprises several wedge shaped reflection packages, which show a fanning geometry. Wedges internally consist of up-section shallowing, stacked, onlapping and overlapping reflections bound by progressive unconformities. A single 'toplap unconformity' is identified along the Shah Deniz fold, though progressive unconformities are typically 'onlap unconformities' (Figure 2.8). The magnitude of off-structure lateral shift of reflections above successive onlap unconformities reduces through time, onlaps show a gradual trend towards the fold hinge up-section.

Using the 3D seismic data a loop around the Shah Deniz fold was constructed, correlating the progressive unconformities either side of the fold (Figure 2.9). Unconformities occur synchronously along each side of the fold, no unconformity is unique to a single flank. A similar loop could not be constructed for the ACG structure as the survey is too small and does not extend far enough away from the fold hinge to allow a the construction of a loop; this study therefore only analysis the south-west flank of the ACG structure. This is also a geologically valid compromise, the sedimentary regime is markedly different on either side of the ACG structure, as the Apsheron ridge, the subduction zone between the South- and Mid Caspian Basins forms a topographic threshold which separates the sedimentary systems of the Volga delta to the north, and Kura and Amu Darya deltas to the south (Kuprin, 2002).

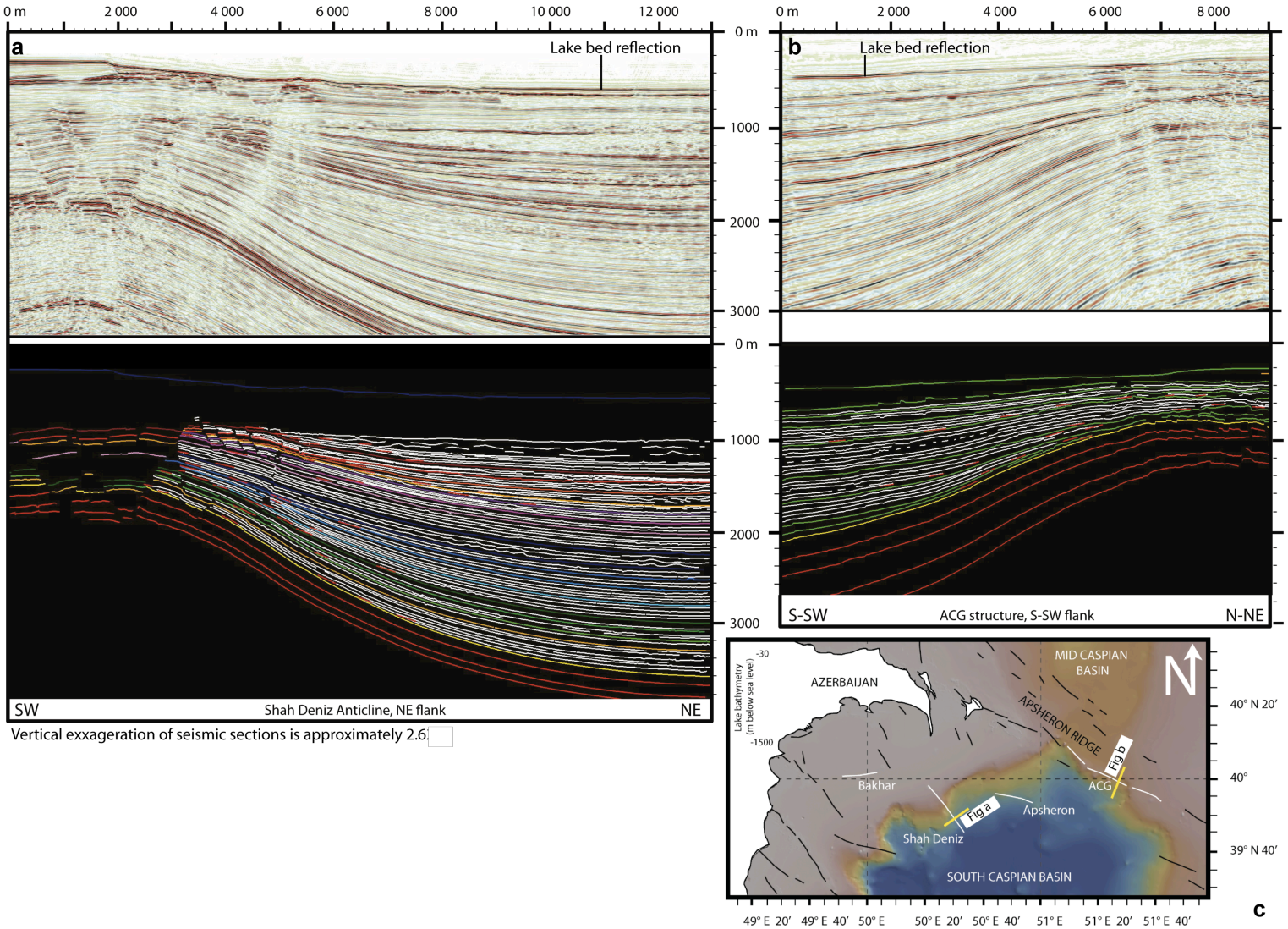

Vertical exxageration of seismic sections is approximately 2.6.

Figure 2.8. Seismic sections taken through individual flanks of the Shah Deniz [a] and ACG [b] anticlines. In the interpretation panel below each seismic section, onlapping reflections are shown as white lines. Onlaps are shown as red dashed. Progressive unconformities are multi-coloured. Pretectonic strata are coloured red. *To be printed on A3 landscape oriented paper*

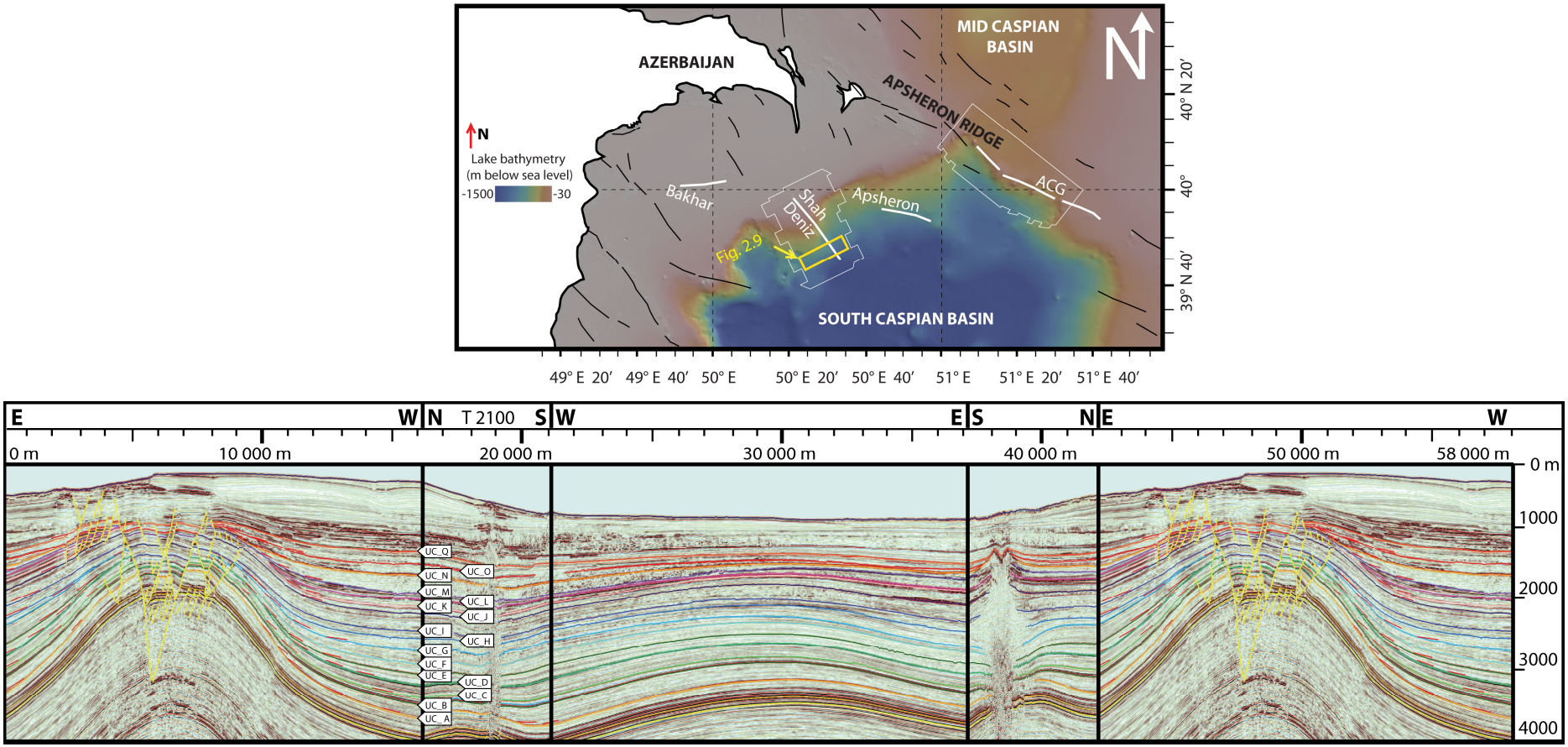

Figure 2.9. Vertically exaggerated (x 2.5) seismic section, arranged into a correlation loop (from left to right: dip section – strike section – dip section – strike section – dip section) around the Shah Deniz anticline. Progressive unconformities (multi coloured) are correlated around the anticline crest using a loop which intersects less deformed areas. The upper map shows the location of the loop, the yellow arrow shows the start of the loop. *To be printed on A3 landscape oriented paper*

Description of regional seismic line between the ACG and Shah Deniz structures

A composite regional seismic section (Figure 2.10a) trends approximately south-west – north-east, between the Shah Deniz anticline and the ACG structure (Figure 2.10b). A third structure, the Apsheron anticline, is situated in between the two larger folds. The syntectonic boundary between growth strata and pretectonic strata is the same high amplitude positive reflection along both the ACG and Shah Deniz structures whereas the Apsheron Anticline contains much younger (post Apsheronian time) growth strata. Its syntectonic boundary is not identified, and lies above the interval of study. The pretectonic datum, the level at which pretectonic strata are undeformed by the folds (McClay, 1992) for the Shah Deniz and ACG structures is estimated to lie at approximately 3800 ms (2wt). The height of the uplifted pretectonic strata along the fold hinge relative to this datum differs between each fold (Figure 2.10a); strata along the ACG structure is uplifted by 3300 ms (2wt), and the Shah Deniz structure is uplifted by 2200 ms (2wt).

The 2D seismic lines extend further off structure along the ACG anticline and show more progressive unconformities than are visible in the 3D data. The interval of interest contains 18 progressive unconformities between the north-eastern flank of the Shah Deniz anticline and the south-western flank of the ACG structure. These are named ‘Unconformity A’ to ‘Unconformity Q’ (Figure 2.10a). Of the 17 progressive unconformities, 14 are firmly correctable between both structures; mass transport complexes obscure the correlation for the rest of the data. Most unconformities (14/17) are synchronous between folds, a few (3/12) appear unique to a single fold (Figure 2.10, Table 2.2).

Shelf margin seismic stratigraphy

A composite regional seismic section (Figure 2.1a) trends approximately south east – north-west, extending from the north-western margin of the South Caspian Basin to the Shah Deniz anticline (Figure 2.11b). An additional fold, the Bakhar anticline, is also imaged along the section. The reflection separating pre- and syntectonic strata lies slightly deeper along the Shah Deniz anticline than the Bakhar anticline which only contains a very thin layer of syntectonic strata.

In total, 20 onlap/downlap surfaces are identified, which are used to define 12 sequences (detailed descriptions and interpretations are shown in Table 2.1, and Figure 2.11b). The seismic section can be further subdivided into three larger units named Ms-1 to Ms-3 based on the stacking patterns of the reflections within each unit (Figure 2.12).

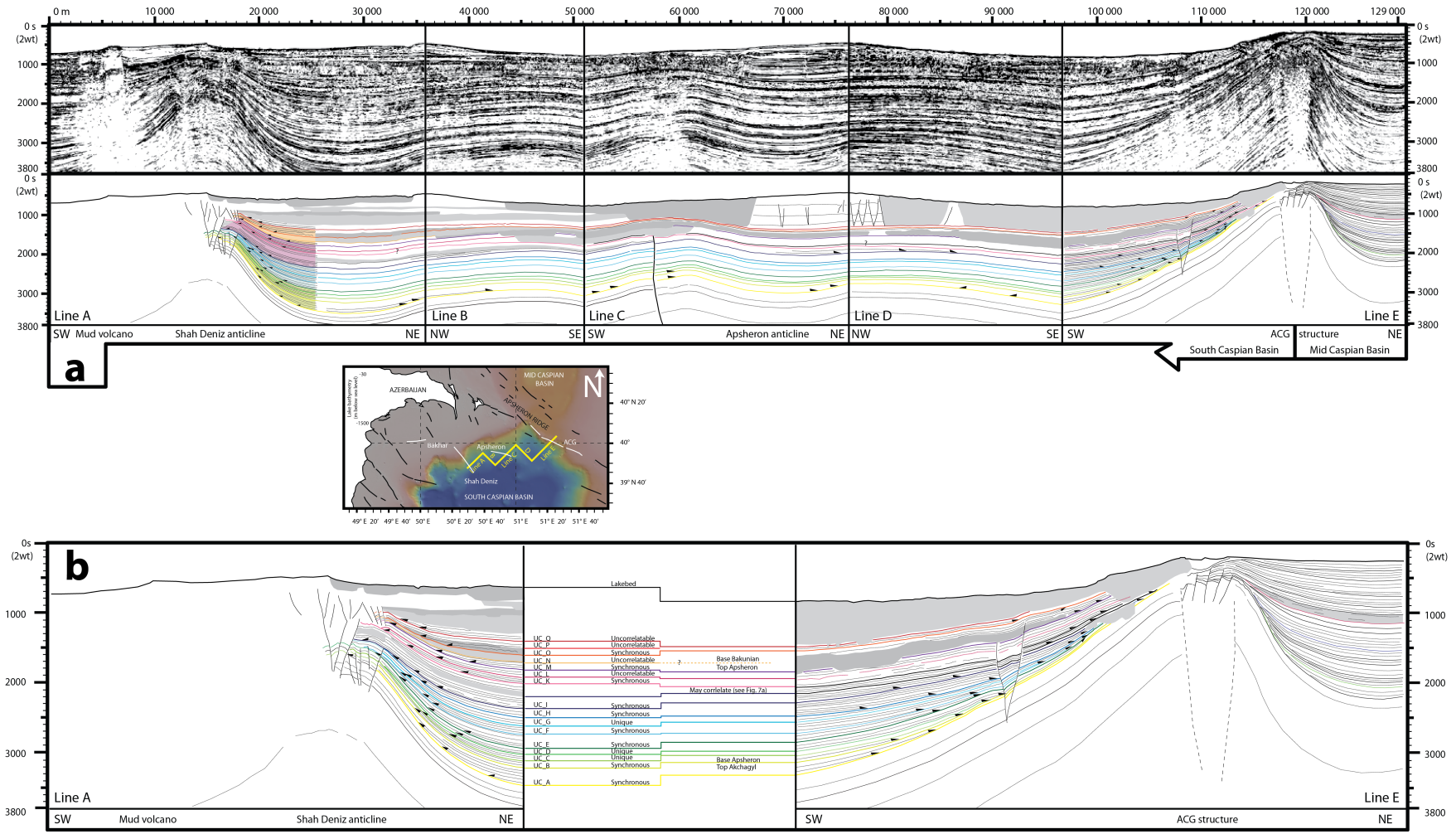

Figure 2.10 Correlated progressive unconformities between the Shah Deniz and ACG structures. [a] Line drawing of 2D seismic section, with progressive unconformities and onlapping reflections (black triangles). [b] close-up of onlapping reflections against each fold flank. Reflections are between folds and are either unique, synchronous or truncated by mass transport deposits. Vertical exaggeration is estimated as ~2.5x. *To be printed on A3 landscape oriented paper*

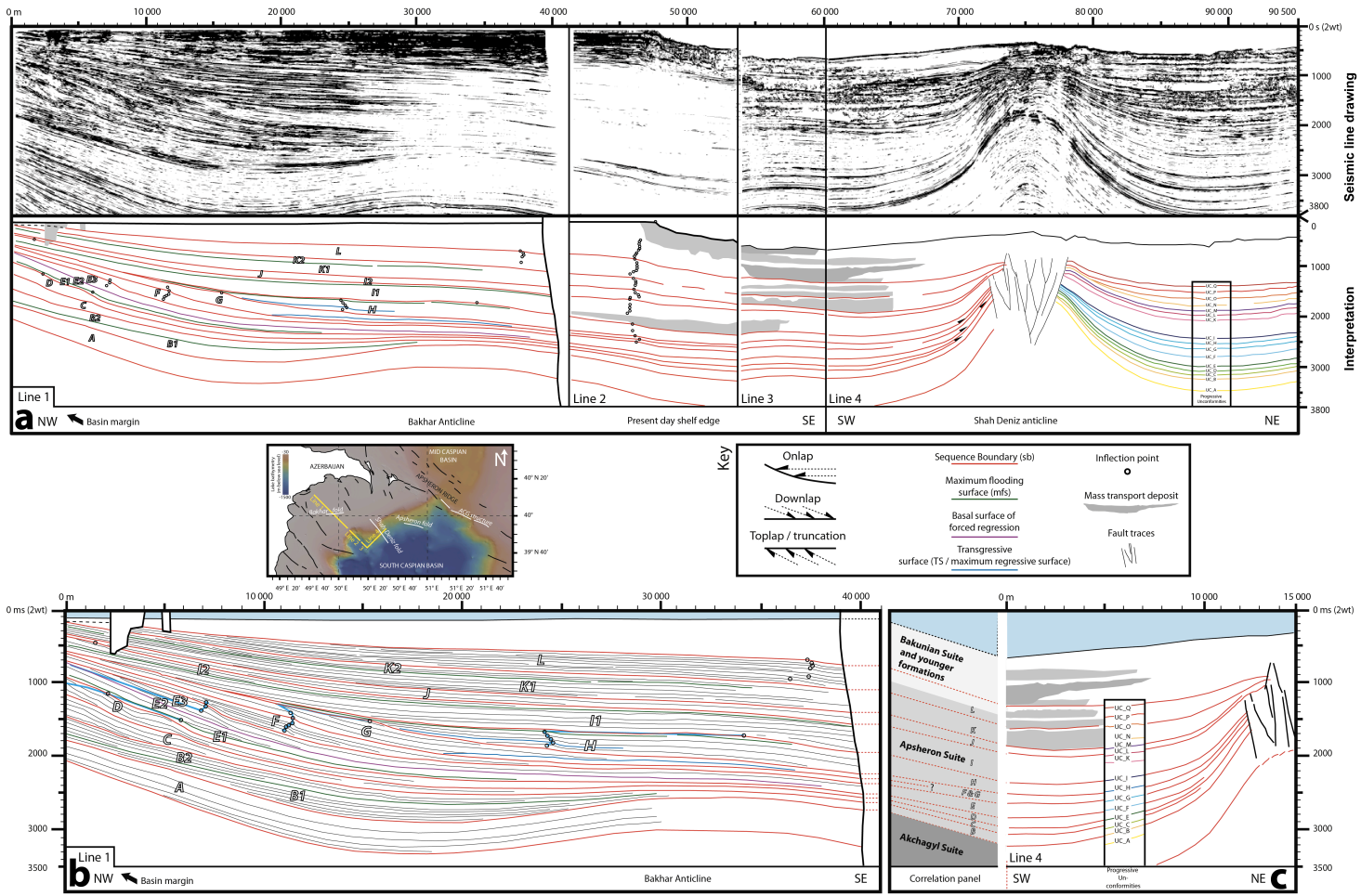

Figure 2.11 2D seismic section correlating the NW shelf margin of the South Caspian Basin, with the Shah Deniz anticline. [a] location of all sequence boundaries and maximum flooding surfaces, mapped onto the SW flank of the Shah Deniz anticline. Progressive unconformities are interpreted along the NE flank. [b] Detailed view of sequence boundaries on line 1, showing onlaps and downlaps of reflections contained with the sequence boundaries. Inflection points, locations of the palaeoshelf break, are indicated by black circles, and their motion paths are highlighted in blue. [c] Correlation between sequence boundaries and progressive unconformities along the SW flank of the Shah Deniz structure. Seismic sections are displayed in two way time and are vertically exaggerated by approximately 2.5x. *To be printed on A3 landscape oriented paper*

Package	Description	Interpretation	Stratigraphic unit	
A	450 ms Low to moderate amplitude reflections, trending parallel and onlapping the basin margin, showing progressive basinwards stepping of onlaps	Stratal package is pre-tectonic relative to the Shah Deniz and Bakhar anticlines. However, a small amount of tectonic thinning may exist in the very top of the package Horizontal , onlapping sedimentation infills accomodation space around the Bakhar and Shah Deniz anticlines. Basinward trend of onlaps indicates lake level rise	Transgressive systems tract	Sequence A
B1	300 ms thick package of moderate amplitude reflections, trending parralel and onlapping the basin margin, Bakhar anticline and Shah Deniz anticline. Basinward trend of onlaps at basin margin. Package also onlaps along the Bakhar and Shah Deniz anticlines.	Lake level drop intially shifted sedimentaition, and onlaps, basinwards. Thereafterwards, sediment filled the accomodation space, onlapping to the NW. Sedimentation was syn-tectonic w.r.t Bakhar and Shah Deniz Anticlines, onlapping both structures along progressive unconformities	Transgressive systems tract	Sequence B
B2	200 ms thick package of low to moderate amplitude reflections, which dip shallowly to the SE (basinwards). Package is wedge shaped, thinning strongly to the SE. Reflections downlap package B1.	B2 is the oldest of 7 sedimentary wedges with a triangular, clinoform geometry (B-E). Inlcined, basinward dipping (SE), clinoform foresets shallow to subhorizontal bottomsets. Topsets are not visible in the data, but probably lie to the NW. B2 has a progradational, aggradational stacking pattern; accomodation space was available, whilst sedimentation was renewed to the SE after an initial NW shift. B2 represents the highstand systems tract of sequence B, and has prograded over a maximum flooding (down lap) surface.	Highstand systems tract	
C	300 ms thick package of moderate amplitude reflections, which dip steeply to the SE (basinwards), shallowing to the SE. Package is wedge shaped, thinning strongly to the SE to 100 ms. Reflections downlap package B2.	Triangular shape of package C is interpreted as clinoform foresets and bottomsets.The downlapping of refelctions from package C on top of B, indicates sedimentation shifted intially to the NW (shore-wards), probably as a result of increased lake level, before prograding to the SE. Downlap surface separeting packages B and C is interpreted as sequece boundary.		
D	200 ms thick package of low to high amplitude reflections, which dip to the SE (basinwards). Package is wedge shaped, thinning strongly to the SE. Reflections downlap package C. A inflection point is present on the bounding reflection (shown with a circle), which is high amplitude. Older, inclined reflections are truncated by this bounding surface.	Package D, similar to package C, forms the frontal portion of a clinoform package. Truncated reflections within the package indicate a forced regression (sea level lowering, accompanied by erosion) of the wedge, showing sediment progradation but little or no aggradation. he inflection point of the bounding reflection represents the location of the palaeo shelf margin.	Entire sequence	Sequence D
E1	150 ms thick package of low amplitude reflections, which dip to the SE (basinwards). Package is wedge shaped, thinning strongly to the SE and also to the NW (landwards). Reflections overlie package C and may downlap it, but this is not visible on the data. An inflection is present on the bounding reflection (indicated by a circle).	Package E1 forms the base of a fourth sedimentary wedge. Basinwards stepping of the rollover point (the palaeo basin margin) w.r.t. package D, and thinning of the package landwards (NW) interpreted as a low relative lake level, which forced a progradation of the basin margin, with no accomodation space generation or aggradation above the former basin margin. Package E1 is condensed, but the package probably contains both the lowstand wedge and the transgressive systems tracts. The boundary between the two is not seimically visible.	Lowstand and transgressive systems tracts	Sequence E
E2	200 ms thick package of low amplitude reflections, which dip to the SE (basinwards). Package is wedge shaped, thinning to the SE Reflections overlie and downlap package E1, and are vertically truncated at the top of the package.	E2 lies in the middle of the fourth sedimentary wedge. The wedge shows progradation of the clinoforms which downlap onto the maximum flooding surface. Truncated reflections show erosion from a subsequent lake level drop	Highstand systems tract	
E3	100 ms thick package of moderate amplitude reflections, which dip to the SE (basinwards). Package is wedge shaped, thinning to the SE Reflections overlie and downlap package E2, and are vertically truncated at the top of the package.	Package E3 lies at the top of the fourth sedimentary wedge. E2 shows progradation of the clinoforms which downlap onto the maximum flooding surface. Truncated reflections show a forced regression or erosion surface, caused by a lake level drop. Downlap surface is the 'basal surface of forced regression'	Falling stage systems tract	
F	200 ms thick package of moderate to high amplitude reflections, which dip to the SE (basinwards). Package is wedge shaped, thinning to the SE Reflections olap, overlie and downlap package E3, and are vertically truncated at the top of the package. A thin horizontal downlap surface is just visible at seismic resolution, at the base of the wedge, to the SE.	Package F forms a fifth clinoform wedge. Several systems tracts are probably contained within the wedge, but are at the limit of seismic resolution. The horizontal downlap surface onto which higher reflections downlap, forms the regressive wedge of the lowstand systems tract. Relatively low lake levels and sedimentation resulted in minimal aggradation, an a basinward shift in onlaps. The rest of the wedge consists of the transgressive and hughstand systmes tracts, the landward stepping onlaps indicate a lake level rise. A maximum flooding surface, seperating the highstand and transgressive systems tracts is not identified.	Entire sequence	Sequence F
G	300 ms thick package of moderate to high amplitude reflections, which dip to the SE (basinwards). Similar to package D, or E, it also contains a horizontal onlapping reflection at it's base, however inclined reflections are truncated at thier tops along an inclined surface.	Package G forms the sixth clinoform wedge. Similar to package F, several systems tracts are contained within the package, but are benieth seismic resolution. At the regressive wedge of the lowstand systems tract, low lake levels and sedimentation rates produced minimal aggradation, and caused a basinward shift in onlaps. The rest of package G consists of the transgressive and hughstand systmes tracts. Landward (NW) stepping onlaps indicate an increased accomodation space (lake level rise). The truncation of the inclined reflections is caused by an erosional surface, which has destroyed most of the aggradational componant of package G and also some of package E.	Entire sequence	Sequence G
H	300 ms thick package of moderate amplitude reflections, which lie subhorizontally, and onlap package G, whilst progressively steepening to the SE (basinwards) to downlap package G. Reflections taper basinwards and show a shallow, and convex-upwards sigmoidal geometry. Package H shows significant aggradation whilst reflection infelction points (indicated by cicrcles) show initial basinwards (SE) progradation, then landwards retrogradation.	Package H forms a seventh clinoform wedge, although it is exceptionally low angle compared to packages C-G. Several systems tracts are contained within the package, but are at the limit of seismic resolution. A lowstand prograding wedge is indicated by successive prograding rollover points. These are overlain by a strongly aggradational, retrogradational series of reflections, indicating a lake level rise, increased accomodation space and a landwards shift of sedimentation. The reflection seperating the two trends (only partially visible) is interpreted as the transgressive surface seperating the lowstand and transgressive systems tracts. The upper bounding reflection of package H also truncates reflections below it, further to the NW, within package G. This reflection is interpreted as a ravienment surface created during the transgression prior to the depostion of package H. A highstand systems tract is not immediately clear, but may be extremely thin, represented by the uppermost reflection in package H, which tapers landwards and basinwards, possibly downlapping a reflection. However this is not fully seismically resolvable.	Entire sequence	Sequence H
I1	350 ms thick package of moderate to high amplitude reflections, which lie horizontally, and onlap package H. A subtle inflection point is observed to the SE which shows niether pro- or retrogradation through time. The package is wedge shaped, thickening towards the SE (basinwards), then tapering, whilst onlapping and overlapping the Shah Deniz anticline. Reflections at the base of the package are disrupted and chaotic. The package shows significant aggradation and landward stepping of onlaps, whilst upper reflections are laterally truncated.	Package I1 is significant as it marks the cessession of signoidal clinoform sedimentary architecture along the basin margin, and a new depositional style consisting of laterally extensive horizontal and subhorizontal reflections showing high amounts of aggradation (similar to Package A). This change in geometry could indicate the termination or avulsion of the shelf edge delta, or a change in the ratio between accomodation space and sedimentation rate, resulting in high rates of progradation (discussed in the interpretation section). The base of the package has been remobilised by a submarine slope failure and is a mass transport deposit. This may also account for the extremely thin highstand sytems tract of package H (see above), which may have been eroded by the slope failure. The basinward shift of onlaps relative to package H indicates a relative lake level drop, but the lowstand systems tract architecture has apparently been destroyed by the submarine failure. The subsequent landward stepping of onlaps, combined with a high aggradation, and minor, basinwards lateral terminations of the upper most reflections, all indicate a significant increase in accomodation spcae (lake level rise), which was infilled by landward migrating (NW) of onlapping sediments.	Lowstand and transgressive systems tracts	Sequence I
I2	150 ms thick package of low to moderate amplitude reflections, which dip shallowly to the SE (basinwards) and downlap package I1. Refelections show truncations against the upper bounding surface of the package, no onlaps are observed. A subtle inflection point is observed to the SE on line 2 which shows minor progradation. Package I2 is shallowly wedge shaped, tapering and thinning to the SE whilst onlapping the Shah Deniz anticline.	Package I2 downlaps onto I1, and shows prograding sedimentation, with little agradation. Sediment outpaced accomodation space generation and prograded into the basin. The downlap surface between I1 and I2 represents a maximum flooding surface. Truncated reflections at the top of package I2 may represent extremely shallow toplaps or a forced regression. The subtle inflection point at teh top of package I2 (circle) may represent a basin margin rollover point, however this would not lie down-dip of the clinoform foresets, and is therefore probably another sedimetary feature.	Highstand systems tract	
J	200 ms thick package of moderate to high amplitude, subhorizontal reflections, which onlap and downlap package H1. Successive onlaps step to the NW (landwards). The same sublte inflection point which is also seen in packages H and I is also present in package J and shows minor progradation	Onlaps step basinwards at the start of package J, indicating an inital basinwards shift of sedimentation (lake level fall), possibly coinciding with minor erosion and truncation of sequence I's highstand systems tract. Subsequent landward migration of the onlaps indicates a lake level rise	Entire sequence	Sequence J
K1	200 ms thick package of moderate to high amplitude, subhorizontal reflections, which onlap package J. Successive onlaps step to the NW (landwards). The same sublte inflection point of packages I and J-H is present which shows minor progradation (visible on line 2). The package is wedge shaped, tapering and thinning to the SE and onlaps the Shah Deniz anticline. to the E.	Onlaps step basinwards at the start of package K1, indicating an inital lake level drop. Subsequent landward migration of the onlaps indicates a lake level rise. Interpreted as transgressive systems tract.	Transgressive systems tract	Sequence K
K2	100 ms thin package of moderate to high amplitude, reflections, which downlap package K1, and at the most NW portion of line 1, are vertically truncated against package L above it. The NW portion of the line shows Inclined reflections within package K2, that shallow to subhorizontal attitudes towards the SE (basinwards).	Shallow downlaps indicate a decreasing accomodation space relative to sedimentation rate, and the progradation of sediment basinwards. Reflections downlap onto the maximum flooding surface seperating packages K1 and K2.	Highstand systems tract	
L	200 ms thick package of moderate to high amplitude, reflections which onlap and downlap package K2. The reflection seperating both packages is relatively high amplitude. Reflections shallow from gently inclined to to subhorizontal towards the SE (basinwards). A shallow inflection point is present towards the SE portion of line 1. A subtle inflection point is observed to the SE on line 2 which shows minor progradation. The package is wedge shaped, tapering and thinning to the SE whilst onlapping the Shah Deniz anticline.	Basinward stepping of onlaps at teh base of package L indicate an intital lake level fall, however, subsequent reflections show and aggradational stacking pattern indicating a large increase in accomodation space, driven by a relative lake level rise. The inflection points within package L show both progradational-aggradational and solely-aggradational trends, implying that sedimentation intially outpaced accomodation space generation, but later kept pace with it.	Entire sequence	Sequence L

TIME

Uplift along the Bakhar anticline

Uplift along the Shah Deniz anticline

Table 2.1 Detailed descriptions and interpretations of each sequence and systems tract along the seismic line of figure 2.9. *To be printed on A3 landscape oriented paper*

Interpretations

Growth strata architecture and progressive unconformities

The angular discordance between onlapping seismic reflections onto the fold limbs and progressive unconformities shows that on a seismic scale, sedimentation was 'dynamic' infilling topographic lows, rather than 'non dynamic'; pelagic drape (e.g. Castelltort *et al.*, 2004). The down-section steepening of growth strata reflections suggests the folds are buckle folds which grew with a component of limb rotation (e.g. Hardy & Poblet, 1994) as opposed to kink band migration (Suppe *et al.*, 1992). Volumetrically, most of the syntectonic succession along both the ACG and Shah Deniz structures was deposited beneath sedimentary base level, during periods where sedimentation outpaced uplift, indicated by onlapping horizons that successively migrated towards the fold hinge (e.g. Doglioni & Prosser, 1997; Shaw *et al.*, 2004).

Periods in time where uplift rate outpaced burial rate occur over a single seismic reflection and were regionally extensive events; most developed synchronously between the widely separated (85 km) ACG and Shah Deniz folds (Figure 2.10, Table 2.1). Both folds uplifted at varying rates indicated by the height of the pretectonic strata at the crest compared with the pretectonic datum (which lies at 4000 ms 2wt depth); the ACG structure (uplifted by 3500 ms 2wt, compared with the pre-tectonic datum,) uplifted comparatively faster than the Shah Deniz fold (uplifted by 2500 ms 2wt over the same time interval), yet both were synchronously affected by relative sedimentation drops.

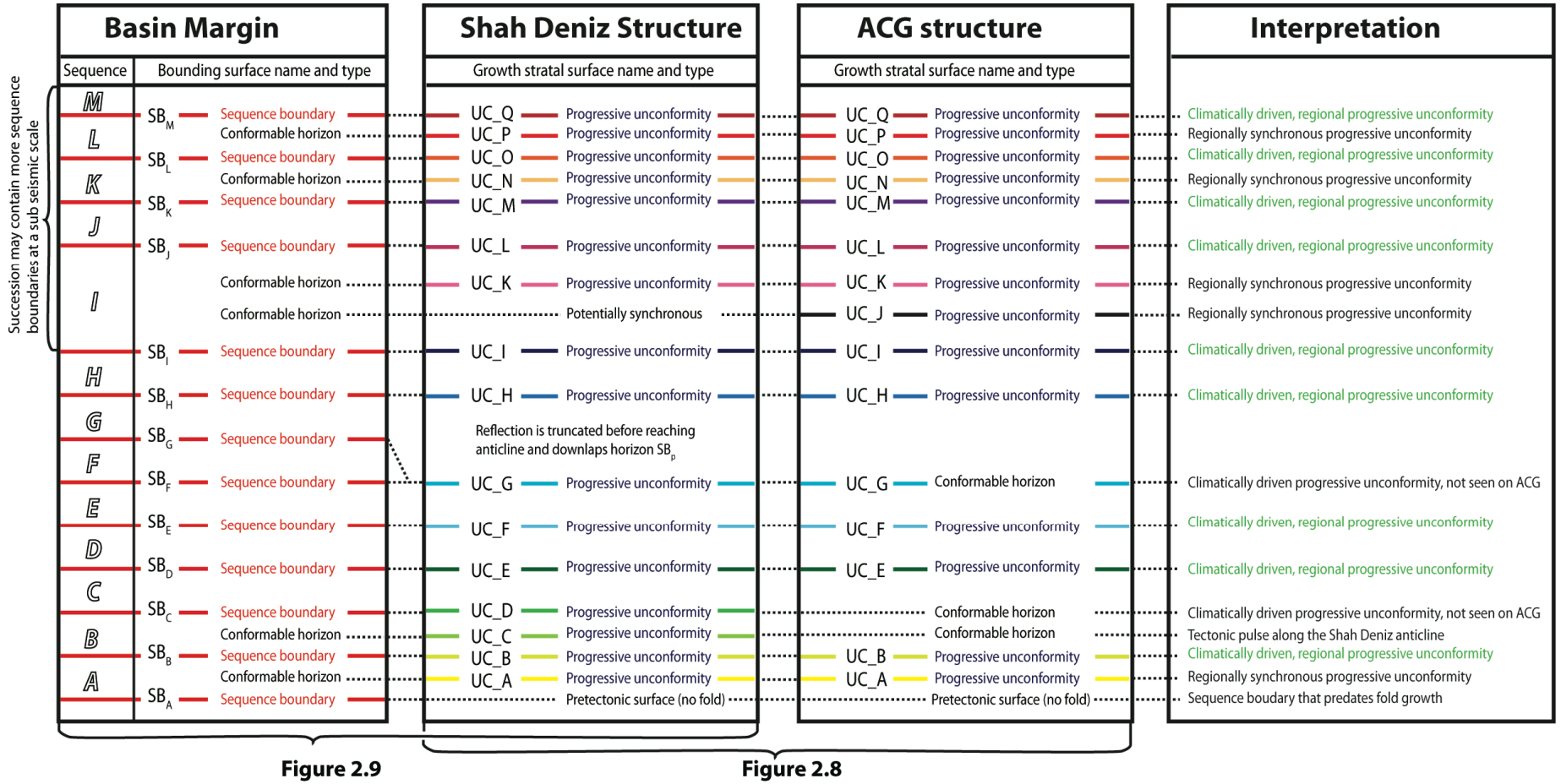

Table 2.2. Correlation chart. Progressive unconformities are correlated between folds and stratigraphically significant surfaces along the basin margin

Shelf margin seismic stratigraphy

The interval of study along the shelf margin consists of 12 (third order) seismic sequences (S_A – S_B). Several individual maximum flooding surfaces and sequence tracts are also identified (Table 2.2). Transgressive and high-stand sequence tracts form aggrading, prograding horizontally onlapping, and prograding, downlapping wedge packages (e.g Keighley *et al.*, 2003). High seismic amplitudes around the inflection points of sequence indicate the presence of sands and more proximal facies at the palaeo slope breaks (Abdullayev, pers. comm. 2010). Low-stand and falling stage systems tracts form laterally extensive, high amplitude condensed sections, sometimes developing thin (1 seismic reflection, or 15 – 25m thick), low-stand wedges. Similar sedimentary styles are observed along the opposite margin of the basin (Abdullayev, 2000), where the lateral continuity of the condensed horizons is similarly extensive, whilst falling stage and low-stand systems tracts from Pliocene strata exposed onshore show similar changes in sedimentation rate (Nummedal *et al.*, 2000).

This study's sequence stratigraphic interpretation is comparable to a previously published interpretation from the western South Caspian Basin Margin (Abreu & Nummedal, 2007). However this study uses differently dated 'seismic picks' to place the interpretation into its regional context, and these date the Caspian stratigraphic units approximately one million years younger than the published line. This is explored in more detail in Appendix 1 and carries implications for interpretations later in this thesis (Chapter 3).

The seismic line is further subdivided into 3 larger megasequences (Ms_1 – Ms_3) based on their architectural style (Figure 2.12). Megasequence Ms_1 (sequences S_A to S_B) is dated as Akchagylian (late Pliocene) at its top, its base is undated. It is characterised by subhorizontal onlapping reflections. Similar seismic facies reported along the eastern basin margin show a rapid increase in accommodation space and relatively static sedimentation rates, caused by accelerated basin subsidence (Abdullayev, 2000). The age of the unit corresponds to the Akchagyl flood which connected the Caspian Sea to the Black, and Mediterranean Seas; a potential cause of the increased accommodation space. The basin margin lay further to the north-west during this period, the subhorizontal architecture therefore could also indicate pelagic offshore sedimentation, contrasting with more proximal environments observed above it in megasequence Ms_2.

Megasequence Ms_2 (sequences S_C – S_H), is dated as Apsheronian (base Pleistocene – mid Pleistocene). The reflection stacking pattern resembles a conventional shelf break margin and consists of sigmoidal reflections, the shelf and basin slope, deposited along a shelf edge delta. The 5 initial sequences show both a prograding and aggrading shelf edge trajectory, and are followed by a single prograding wedge. The South Caspian was separated from the world's oceans during this period and sedimentation was lacustrine, close to the margins of the lake (Jones & Simmons, 1996; Abdullayev, 2000). Clinoforms indicate that sedimentation was outpacing accommodation space generation causing the shelf edge to prograde substantially into the basin interior. Relative lake level followed a regressive trend, with 6 smaller lake level cycles contained within it. A water depth of between 200 – 400 m is estimated from clinoform heights (the vertical distance between bottom-sets and top-sets, measured normal to the regional dip).

Megasequence Ms_3 (sequences $S_I - S_L$) is dated as Bakunian (mid Pleistocene) at its base, but its upper age is not known. Similar to megasequence Ms_1, it consists of subhorizontal reflections, which thicken to the south east. The stacking pattern indicates an increase in accommodation space generation and the end of the Baku Delta clinoform complex. The landward stepping of onlaps by almost 40 km relative to those in Ms_2, indicate that this coincided with a large lake level rise, probably the Bakunian transgression (Kroonenberg *et al.*, 1997). A broad transgressive or regressive trend is not apparent from the data, however at least 4 smaller sequences are observed from basinwards stepping onlaps (Scholz, 2002).

Correlation of sequence boundaries with progressive unconformities

The seismic reflections representing condensed falling stage, low-stand systems tracts and sequence boundaries are commonly synchronous with the correlative conformities of progressive unconformities (Figure 2.11c, Table 2.2). The majority of progressive unconformities within the growth strata successions of the ACG and Shah Deniz anticlines occurred during periods of relative lake level fall.

There is a good correlation between sequence boundaries and progressive unconformities in megasequences Ms_1 and Ms_2, though throughout Ms_3 more progressive unconformities than sequence boundaries are identified. This may be due to the sedimentary style in this interval, which is predominantly subhorizontal and where sequence boundaries may be difficult to identify at seismic resolution (Kroonenberg *et al.*, 1997). In sequence S_I, a comparatively thick sequence, two anomalously high amplitude reflections are observed, which are not visibly onlap or downlap surfaces, but nevertheless may represent condensed deposits of falling stage and low-stand systems tracts. These could speculatively be interpreted as sequence boundaries and correlated with unconformities Uc_J and Uc_K though more data would be needed to ascertain this fully.

Comparing megasequences with larger growth strata packages shows only partial trends. The boundary between megasequences Ms_1 and Ms_2 lies close to that reflection separating growth strata packages separated by unconformity UC-C, but they do not correlate perfectly (Figure 2.12). Although sedimentary style changes significantly along the basin margin between Ms_1 and Ms_2, the sedimentation style around the Shah Deniz and ACG fold remains similar. The boundary between Ms_2 and Ms_3 is significant however; the sedimentary style changes around the Shah Deniz anticline along the megasequence boundary, from closely spaced onlap wedges, to a thick succession of onlapping and overlapping packages, sedimentation rate clearly outpaced fold uplift during the deposition of sequence S_I. This coincides with a large transgressive unit, megasequence Ms_2, and the secession of progradation from the palaeo Baku delta. Either sedimentation rate increased dramatically during sequence S_I or fold growth slowed, only to recommence again during the sequences $S_J - S_L$. No additional well picks are available to test this, which would allow for estimates of sedimentation rate. Correlating sequence S_I onto the ACG fold is equally unsuccessful, a large mass transport deposit has remobilised much of the package.

2.4. DISCUSSION

Progressive unconformities are generated by reductions in the burial/uplift ratio along a fold, which is destabilised by either tectonic or climatic processes (Storti & Poblet, 1997). Below the main arguments that support a climatic control on the South Caspian progressive unconformities are summarised and implications for sedimentation, and the kinematic evolution are discussed.

Climatic forcing and progressive unconformity generation

Three main observations favour a climatic control on progressive unconformity development. The majority of unconformities are regionally synchronous and laterally extensive horizons, indicating that the events that generated them operated at a (basin) wide scale. Additionally, most of the unconformities are correlated with stratigraphically significant surfaces along an unfolded portion of the basin margin, which indicates a regional change in sedimentation during their development. Although a precise timescale for the South Caspian stratigraphy does not exist and some of the unconformities could not be correlated between structures, the 15 – 16 , synchronous progressive unconformities over a time period of approximately 1.5 million years are *the same order of magnitude* as 100.000 year eccentricity Milankovic cycles (Table 2.3) and which is the dominant climatic control on the global Pleistocene geological record (Ruddiman, 2006) and which would be expected in a climatically sensitive, lacustrine succession (Fischer & Bottjer, 1991; Scholz, 2002; Keighley *et al.*, 2003). However it is stressed that this extrapolation is speculative. It is explored in more detail in chapter 5.

If the progressive unconformities were primarily generated by localised tectonic uplift along the folds, there would be little correlation between structures individually and the basin margin stratigraphy. The folds lie along an accretionary prism and would be expected to develop at separated intervals (Davis *et al.*, 1983; Hardy *et al.*, 1996). If the area deformed via regionally synchronous and extensive tectonic pulses, it also seems unlikely that the Apsheron structure, the smaller fold that lies between the ACG structure and the Shah Deniz anticline, would have remained comparatively inactive for such a long period (Figure 2.10). The repetition rate of progressive unconformities at Milankovic *order* timescales, the regional extent of the surfaces, and the correlation between unconformities and sequence boundaries all point towards a climatic rather than tectonic control.

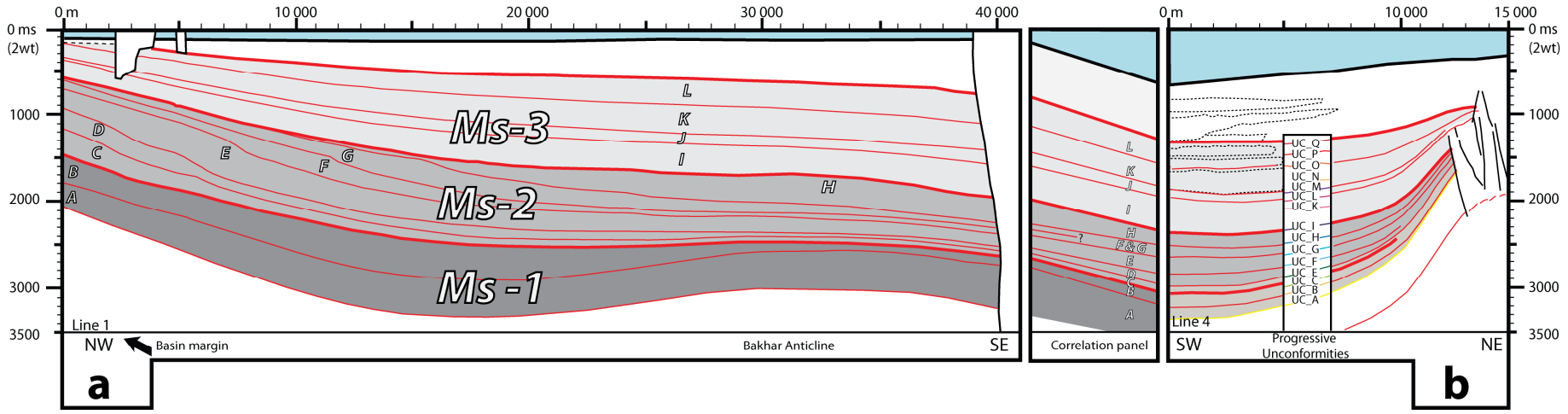

Figure 2.12. Large scale seismic megasequences (Ms-1 to MS-3) comprised of sequences (A to L). Megasequence boundaries are highlighted in thick red. Vertical exaggeration is estimated as ~2.5x. *To be printed on A3 landscape oriented paper*

Sedimentary process	**Observed in**		**Occurrence**	
	Data	Location	Age range	Amount
Stratigraphic mega sequences	Regional 2D seismic lines	Basin margin and interior	Latest Akchagyl-undetermined, post Apsheronian	**3**
Stratigraphic sequences	Regional 2D seismic lines	Basin margin	Latest Akchagyl-undetermined, post Apsheronian	**13**
			Apsheron Formation only	**11**
Synchronous progressive unconformities	Regional 2D seismic lines	Basin interior	Latest Akchagyl-undetermined, post Apsheronian	**15**
			Apsheron Formation	**12 or 13**

Apsheron Formation, age estimates			
Publication	From (Mya)	To (Mya)	timespan (My)
Jones & Simmon 1996 (max), Allen et al., 2002	1.6	0.7	0.9
Van Baak 2010 (min estimate)	1.8	0.9	0.9
Devlin *et al.,* 1999	1.85	0.7	1.15
Van Baak 2010 (max estimate)	2	0.9	1.1
Fowler et al., 1999 (min estimate)	2.28	1.04	1.24
Fowler et al., 1999 (max estimate)	2.47	0.97	1.5

Expected orbital cycles within the Apsheron formation			
Axial precession	Obliquity	Eccentricity	
23,000 years Cycles	41,000 years Cycles	100,000 years Cycles	400,000 years Cycles
39.1	22.0	9	2.25
39.1	22.0	9	2.25
50.0	28.0	11.5	2.875
47.8	26.8	11	2.75
53.9	30.2	12.4	3.1
65.2	36.6	15	3.75

Expected orbital cycles, Apsheron-Present			
Axial precession	Obliquity	Eccentricity	
23,000 years Cycles	41,000 years Cycles	100,000 years Cycles	400,000 years Cycles
69.6	39.0	16	4
78.3	43.9	18	4.5
80.4	45.1	18.5	4.625
87.0	48.8	20	5
99.1	55.6	22.8	5.7
107.4	60.2	24.7	6.175

Sedimentary process	**Observed in**	
	Data	Location
Stratigraphic mega sequences	Regional seismic lines	Basin margin and interior
Stratigraphic sequences	Regional seismic lines	Basin margin
Progressive unconformities	Regional seismic lines	Basin interior

Climatic characteristics			
Repetative?	Eavenly spaced?	Regionally synchronous?	Climate is known to affect this sedimentary process
yes	yes	Yes	yes
yes	yes	Yes	yes
yes	yes	Yes	yes

Interpretation	
Climatic?	Closest orbital cycle
unproven	400,000 year eccentricity
likely	100,000 year eccentricity
likely	100,000 year eccentricity

Table 2.3 Comparison chart of repetitive events observed in this study (top), published ages of the Pleistocene South Caspian succession (middle) , and possible Milankovic cyclicity (bottom)

Sedimentation rates and climatic controls during relative lake level cycles

Sequence boundaries are generated at the start of relative water level falls, (Kendall, 2003), which are indicated along the South Caspian shelf margin by abrupt basinwards shifts of reflection onlaps and the lowering of the level of sedimentation (e.g Vail *et al.*, 1977). Low-stand wedges and fans (e.g. Posamentier & Vail, 1988) are rare along the shelf margin, and where present, only consist of single seismic reflections (Figure 2.11), implying that sedimentation rates during relative lake level falls were comparatively low. Similarly, the high seismic amplitudes of the sequence boundaries are interpreted as condensed sections formed during periods of sedimentation hiatuses (Abdullayev, 2000), well-lithified hard-grounds which are comparatively dense, resulting in large impedance contrasts and high seismic amplitudes (Weimer, 1990).

When integrated with sequence stratigraphy, the fold growth strata stacking patterns serve as a record of sedimentation rate; if sedimentation remained high during lake level falls, the sequence boundaries would not be coincident with progressive unconformities. A gradual lowering of the sedimentation rate would be indicated by progressive offlap stacking patterns (Figure 2.4b) and non-correlation of the two surfaces (e.g. Ford *et al.*, 1997). However, the off structure migrations of onlaps, and the development of sequence boundaries occur synchronously over the vertical height of one seismic reflection (approximately 25m). This study interprets a cyclical fluctuation in the palaeo sedimentation rate, which was high during periods of lake level transgression (uplift/burial>1, onlaps migrated towards the fold crest), but which dropped during lake level regressions resulting in a prolonged sedimentary hiatus. During this time a condensed bed was deposited and the fold crest was uplifted above the level of sedimentation (uplift/burial <1, onlaps shift off structure along a single reflection).

The sedimentation rate can be used to evaluate climatic controls on the relative lake level which, in an internally drained basin is governed by the combined, independent processes of tectonics and climate, expressed as subsidence versus evaporation and riverine runoff (Talbot & Allen, 1996). Theoretically, climatically driven lake levels fall during periods of either, relatively low river input (dry climate), relatively high evaporation (warm climate), or both (warm and dry climate) (Carroll & Bohacs, 1999; Keighley *et al.*, 2003). The exact mechanism that governs the South Caspian lake level is uncertain, and lake level falls have been 'correlated' with both cold (Jones & Simmons, 1996; Zubakov, 2001) and warm periods (Krijgsman *et al.*, 2010; van Baak, 2010) using a poorly dated stratigraphic record (Kroonenberg *et al.*, 2000), which is discussed in chapter 5. Transgressions along marine margins are driven by ice sheet melting and thermal expansion, which commonly operate independently of the sediment influx along the basin margin (Posamentier & Vail, 1988). However in lacustrine settings, water and sediment enter the basin via the same river network. In the South Caspian Basin relative lake level falls occurred during periods of low sediment input and low river activity, whilst transgressions occurred during high river activity. This suggests that river input rather than evaporation was the dominant control on relative lake level, and that lake level regressions occurred during hot and dry climates (Table 2.4).

Kinematic evolution and sedimentary controls on fold growth

The folds in this study are classified as 'buckle folds' (or 'detachment folds') that grew kinematically via progressive limb rotation along a detachment surface, whilst the hinge remained static (Mitra, 2003). This agrees with previous interpretations, that identify the Miocene Maikop suite as the detachment layer (Devlin *et al.*, 1999; Fowler *et al.*, 2000; Howie *et al.*, 2005). Further kinematic inferences can be drawn from the progressive unconformities within the growth strata succession.

Folds are interpreted to grow either episodically via a series of tectonic bursts or gradually with only very slow changes in deformation rate. Each interpretation carries implications for the rheology, kinematics and amount of underlying fault control on the fold (Butler & Lickorish, 1997). They also imply different generation mechanisms for progressive unconformities. In the tectonic pulse model progressive unconformities are created by episodic slip along underlying faults or episodic compression events, which periodically uplift the fold crest above the level of sedimentation shifting later onlaps off structure (e.g. Anadón *et al.*, 1986; Ford *et al.*, 1997; Masaferro *et al.*, 2002; Ghiglione & Ramos, 2005; Soleimany *et al.*, 2011). Alternatively, in gradual fold growth models, unconformities are created by sedimentary 'starvations' driven by either reduced continental runoff or rising water levels and shoreline retro-gradation, both of which reduce the burial rate along the fold allowing it to become topographically elevated above the level of sedimentation (e.g. Butler & Lickorish, 1997; Castelltort *et al.*, 2003; Castelltort *et al.*, 2004).

Most models which interpret tectonic pulses assume a constant sedimentation rate, large enough to completely cover all topography (termed 'fill to the top sedimentation' or 'ideal differential aggadation'), additionally they rely on dating spikes from bio- or magnetostratigraphy in the growth strata record. In certain settings this sedimentary model is unrealistic, particularly in distal environments, where pelagic rainout blankets both positive and negative topography (Castelltort et al., 2004) whilst age data taken from the fold hinge can be low resolution, and are susceptible to erosion and periods of non deposition (McCaig & McClelland, 1992; Butler & Lickorish, 1997). As a result, the idealised signal that would delineate between both kinematic end-members (Figure 2.13) is often aliased (e.g. Masaferro et al., 2002). This study avoids these pitfalls by regionally correlating the progressive unconformities, and shows that in the majority of cases, these were generated by sedimentary processes (discussed above) Individual unconformities caused by isolated tectonic pulses do exist, but these are comparatively rare (Table 2.2). This is consistent with a gradual and continuous fold growth model. Recent studies in other basins have also come to similar conclusions; structural processes which are repetitive and which reoccur on Milankovic order time-scales (10,000 – 400,000 years) are rarely tectonically driven (Castelltort et al., 2003; Castelltort et al., 2004; Pochat et al., 2009). In fact, episodic, strongly repetitive kinematic behaviour along folds is only concretely observed on timescales of 1000 years or less (Tapponnier et al., 2001).

When viewed at a seismic resolution and over Milankovic order time scales, the South Caspian fold growth is gradual and constant; however long term (million year scale) changes can be interpreted, which sedimentary processes may have influenced. The magnitude of lateral onlap shifts along progressive unconformities reduces over time (Figure 2.10) indicating a gradual reduction of the fold uplift rate relative to the sedimentation rate. This effect is more pronounced along the Shah Deniz anticline than along the ACG structure despite both structures being the same age (Figure 2.10, Table 2.2) and emplaced in the same tectonic regime (Jackson *et al.*, 2002). In addition to this the Shah Deniz fold has uplifted by far less than the ACG structure (2500 ms 2wt, compared with 3500 ms 2wt), and is blanketed by a far greater thickness of sediment above its hinge

(Figure 2.10). An explanation for this may lie in the relative proximity of each structure to sedimentary sources; the Shah Deniz anticline lies in the depocenter of the 'Baku Delta' (Figure 2.1a) whilst the ACG structure is buried only by very distal sediments —from the Baku, Palaeo Kura and Amu Darya deltas on its southern limb, and Palaeo Volga delta on its northern limb (Kuprin, 2002; Abreu & Nummedal). The increased uplift rate of the ACG structure can initially be explained by its distal position in the incipient accretionary wedge; compressive structures closer to the subduction zone typically undergo higher amounts of strain than (younger) structures in the foreland (Davis *et al.*, 1983). However this behaviour was conceivably enhanced by sedimentary processes; higher sedimentation rates around the Shah Deniz anticline would increase gravitational loading and friction along its basal detachment, inhibiting its lateral and vertical growth (e.g. Storti & McClay, 1995; Hardy *et al.*, 1998; Strayer *et al.*, 2004), whilst a higher proportion of sand in the Shah Deniz stratigraphy offers more flexural resistance, limiting its topographic elevation (Finch *et al.*, 2003). Sedimentary processes can therefore prime the development of a structure and influence it during its growth on longer timescales as well.

Climatic conditions during lake level falls			
Cold and dry	Low runoff, low evaporation, lowered lake level	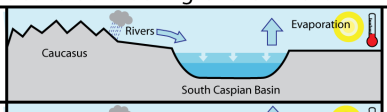	Possible in the South Caspian Basin. Lake level falls are associated with lower sedimentation rates, interpreted as reduced river activty
Hot and dry	Low runoff, high evaporation, lowered lake levels	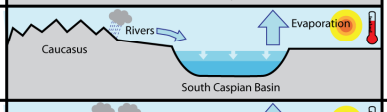	
Hot and wet	High runoff, but evaporation exceeds this and lake level is lowered	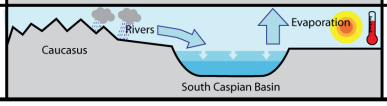	Unlikley in South Caspian Basin, lake level falls are not associated with significant sedimentation.

	Model A Lake level follows global sea level trend		**Model B** Lake level opposes global sea level trend	
Global eustacy	Glaciation	Deglaciation	Glaciation	Deglaciation
Climatherm	'Cold' (arid)	'Warm' (humid)	'Cold'	'Warm'
Caspian lake level	Fall	Rise	Rise	Fall
Mechanism	Cool climate freezes rivers, reducing runoff into lake. Riverine runoff reduces at higher rate that reduction in evaporation (which also falls due to cooling). Lake level falls.	Rivers are rejuvinated during interglacials, runoff increases at higher rate than evaporation increase. Lake level rises.	Rivers flowing northwards, away from the Capsian, into the Arctic Sea are blocked by ice sheet. Ponded rivers form glacial lakes along ice sheet margin which overflow and spill southwards into the Caspian Sea. Lake level rises	Less water enters the Capsian as northward flowing river network is re-established. Higher temperatures also increase evaporation. Both contributeing to lake level lowering.

Table 2.4. Hypothetical climatic conditions during lake level fluctuations (top), and a summary of the two opposing climatic models that have been proposed for the South Caspian Basin (bottom)

2.5. CONCLUSIONS

This study described and analysed several regionally extensive seismic sections which transect the western shelf margin of the South Caspian Basin and several large folds which lie in its interior. The syntectonic sedimentary 'growth strata' deposited along the folds flanks contain numerous angular disconformities; 'progressive unconformities'. By mapping these over a regionally extensive area two opposing models of tectonic and climatic controls on their generation were tested.

The results of this study show that progressive unconformities commonly develop synchronously between folds, over a regionally extensive area. The unconformities appear at regular, repetitive, potentially Milankovic scale, intervals in the growth strata succession and many can be correlated with stratigraphic sequence boundaries along the basin margin. Therefore a climatic control on the generation of progressive unconformities is concluded.

The South Caspian folds are buckle anticlines which grew via limb rotation at a gradually uplifting constant or slowly changing rate. During uplift they were buried by sediment which was supplied by rivers draining into the basin at varying rates. Progressive unconformities developed during falling stage- and low-stand systems tracts, corresponding to climatically dry periods of low river activity and sedimentary hiatuses in the South Caspian Basin. Sedimentation may have also played a role in blanketing and suppressing fold growth over million year timescales.

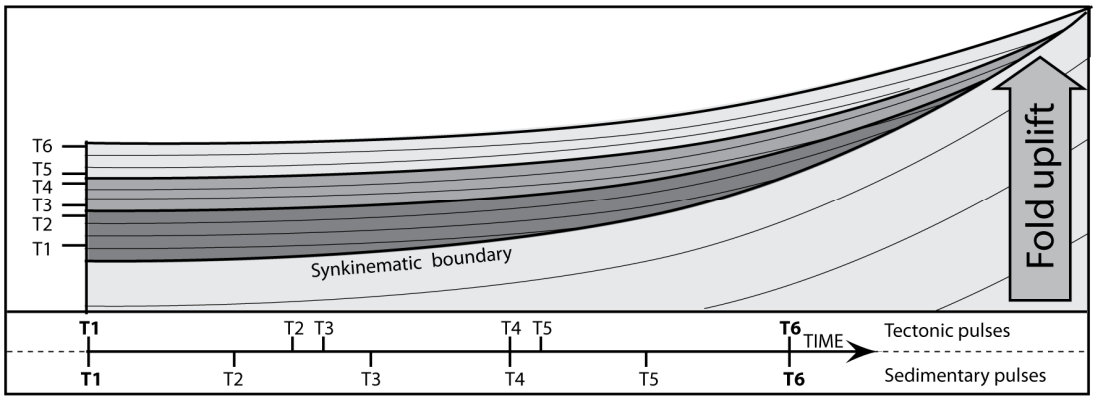

Figure 2.13. Growth strata wedge showing vertical position of time picks, and idealised age distributions for episodic and constant fold growth scenarios

3. Sedimentology of the Apsheron Formation

3.1. INTRODUCTION

Aims and objectives

The South Caspian Basin is an exceptionally large, lacustrine basin, which is filled by over 20 km of Mesozoic and Tertiary sediments. The sedimentary cover is deformed into several large folds, many of which host, world-class oil and gas fields from a regionally extensive play. The basin's current tectonic, sedimentary, and hydrological configuration dates from the earliest Pleistocene (Gelasian) when it became separated from the world's oceans. The oldest sedimentary formation documenting this period is regionally named the 'Apsheron Suite'.

Water levels in endoheric lacustrine settings oscillate more frequently and at higher magnitudes than comparable marine settings, and are not directly affected by changes in eustacy (Carroll & Bohacs, 1999). This, combined with exceptionally rapid sedimentation rates (estimated at ~1.7 m / Kyr in Allen *et al.*, 2002) and compressive tectonics (Jackson *et al.*, 2002), have produced a high resolution, syntectonic sedimentary record. The Apsheron Formation is therefore an ideal dataset to study the interplay of sedimentation, fold growth and climate change at the field scale. The formation is of further interest as it forms part of the growth sequence covering the main regional hydrocarbon reservoirs and traps, recording their structural development (Devlin *et al.*, 1999; Buryakovsky *et al.*, 2001a). Despite this, no field studies documenting the sedimentology of the Apsheron Formation sedimentology have been published.

This study presents new sedimentological data from Lower – Middle Pleistocene deposits of the Apsheron Formation from the north-western margin of the South Caspian Basin around Azerbaijan. The study presents graphic logs and outcrop observations which document the sedimentary processes and palaeoenvironments preserved within the Apsheron Formation.

The aims of this study are as follows: [1] to document the Apsheron Formation lithofacies and facies associations, [2] to interpret the range of depositional environments present in the formation, [3] to integrate the results into a depositional model and the wider regional geological context and [4] to assess the relative roles of climate and tectonics in the Apsheron Formation sediments.

Geological setting

The South Caspian Basin encompasses the southern portion of the present Caspian Sea (Figure 3.1). The basin is structurally complex; the Oligocene – present-day sedimentary succession is extensively folded along the basin's northern and western margins (Figure 3.1b), both of which are undergoing compression (Jackson *et al.*, 2002; Knapp *et al.*, 2004; Stewart & Davies, 2006). The deformation and folding in the basin interior are an eastwards continuation of the collision occurring along the Greater Caucasus, which sits in the wider structural regime of the Arabia – Eurasia convergence (Jackson *et al.*, 2002; Allen *et al.*, 2004). The basin has subsided rapidly since the Miocene and this, combined with abundant sediment supply fed from adjacent mountain ranges and large, regionally extensive river systems has contributed to a rapidly deposited exceptionally thick (20km) sedimentary succession (Allen *et al.*, 2002; Green *et al.*, 2009). Folding initiated in the basin interior during the latest Pliocene (Devlin *et al.*, 1999; Fowler *et al.*, 2000) and may have started as early as the latest Miocene along the basin's western margin (Souque *et al.*, 2010). The Pleistocene Apsheron Formation was deposited in active syncline mini basins within the folded cover sequence. Several of these folds are exposed along the coastline of Azerbaijan and have been eroded along their crests, exposing 100 m-scale outcrops of Apsheron Formation stratigraphy along remnant fold flanks (Figure 3.1d).

Rocks from the Apsheron Formation —named after Azerbaijan's Apsheron Peninsula— crop out around the entire perimeter of the Caspian Sea. The formation is described in Iran and in the Aral Sea, and an equivalent formation exists in the Black Sea Basin (the Gurian Formation) (Jones & Simmons, 1996; Svitoch, 2010b). The Apsheron Formation lies stratigraphically above the Late Pliocene – Lower Pleistocene Akchagyl Formation, a quasi-marine flooding event that connected the Aral, Caspian, Black and Mediterranean seas (Degens & Paluska, 1979; Jones & Simmons, 1996). It lies below the Bakunian Formation, which coincides with a major transgression and connection between the Caspian and Black Seas (Popov *et al.*, 2006; Svitoch, 2010a). Regional terminology subdivides the Late Pliocene, and Early Pleistocene into the Akchagylian, Apsheronian and Bakuninan Stages. Locally each stage's corresponding sedimentary successions is termed a 'Suite' however this thesis refers to these units *sensu lato* as 'formations' (Figure 3.1a).

During the Akchagylian, rising Mediterranean waters from the west encroached and flooded the lake via the Black Sea, establishing a marine connection (Jones & Simmons, 1996). This ended at the start of the Apsheronian, apparently due to increased rates of basin subsidence which increased accommodation space and lowered water levels (Nikiforova, 2004; van Baak, 2010). Since then the Caspian Sea has predominantly been, an endoheric, brackish lake, similar to today's (inferred from environmentally sensitive ostracods and pollen in Jones & Simmons, 1996; Nikiforova, 2004). There were intermittent, possibly marine connections via the Black Sea during the Pleistocene but these were short-lived (Jones & Simmons, 1996; Zubakov, 2001). Lake level in the internally drained South Caspian basin has been determined by the balance between continental runoff —primarily from the Volga river— and atmospheric evaporation (Degens & Paluska, 1979). The palaeo-Volga delta lay as far south as the South Caspian Basin during the Miocene (Hinds *et al.*, 2004), but was migrating northwards towards its current position, during the Apsheronian. Four other deltas were active during this period: the Palaeo Kura (Abreu & Nummedal, 2007), the Palaeo Amu Dayra (Abdullayev, 2000), the Palaeo Danube (Degens & Paluska, 1979) and an unnamed river, draining off the Caucasus, the delta of which is described in regional seismic lines (see chapter 2).

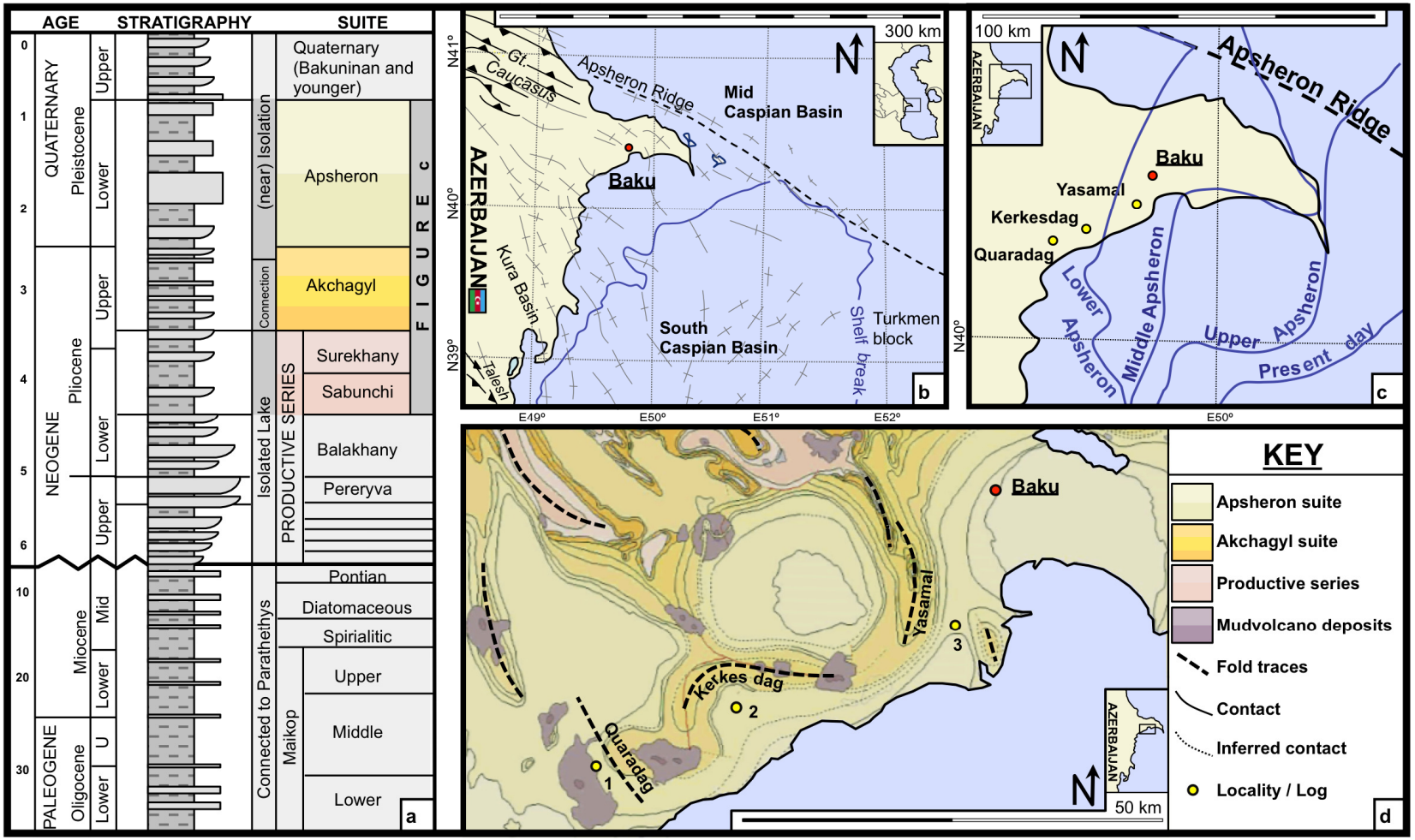

Figure 3.1 Geological outline. [a] Stratigraphic log , showing ages and sedimentary 'suites' (formations) modified from Devlin et al., (1999). [b] Structural map of Azerbaijan region showing fold traces, and location of the Apsheron Ridge. Modified from Allen et al., (2002) [c] estimations of the location of the Apsheronian palaeoshelf break, modified from Grant (2010 , pers. comm.). [d] Geological map of the study area (modified from Geospatial Research Limited, 2008 and reproduced with permission from BP), showing Apsheron, Akchagyl and Productive Formations and traces of the main folds in the area.

The Apsheron Formation is lithologically similar to the younger Bakunian, and older Akchagyl Formations, but is distinguishable by its fossil assemblage (Kuprin, 2002). The Apsheron Formation is interpreted as representing a high-stand deposit following a major transgression in the Akchagylian (Abdullayev, 2000). The Apsheron Formation forms an extensive 1200 m thick package, measured both on 3D depth-converted seismic (chapter 2) and in published borehole data (Abreu & Nummendal 2007) . It is characterised by a major transgression just below its base and is overlain by a shallow regressive trend (Jones & Simmons, 1996; Abreu & Nummedal, 2007; Torres, 2007). Maps of the Apsheronian palaeoshelf break (British Petroleum, 2010\ unpublished internal report), show a similar progradational trend (Figure 3.1c). Sedimentation at the basin margin is characterised by thick, progradational clinoform complexes, which downlap on to condensed Akchagyl Formation high-stand deposits (see chapter 2).

The age of the Apsheron Formation is disputed. Akchagyl and Apsheron Formation rocks contain depth-diagnostic ostracods, molluscs and diatoms and, combined with volcanic ash band dating at the base of the Akchagyl Formation and magnetostratigraphy, have been matched to global sea level curves to give an age estimate (Figure 3.2). Early estimates place the base of the Apsheron Formation at 1.6 Ma, the top at 0.9 Ma with intraformational ash bands at 0.96 Ma (Jones & Simmons, 1996; Kroonenberg *et al.*, 1997; Devlin *et al.*, 1999). Recent studies advocate a longer duration for the formation; van Baak (2010) uses magnetostratigraphic data to place the base at between 1.8 – 2.3 Ma and the top at 0.9 Ma. Other researchers place the base Apsheronian coincident with the base of the modern Pleistocene (base Galasian, see Gibbard *et al.*, 2010), at 2.58 Ma, running to 0.8 Ma. This corresponds to northern hemisphere glaciations and global sea level fall, which presumably was the mechanism that separated the Caspian from the world's oceans after the Akchagyl formation floods (Richards, 2010, pers. comm).

Previously published fieldwork from Azerbaijan focuses on the palaeo-Volga delta which was situated over the Apsheron Peninsula during the Pliocene, and which deposited the reservoir rocks for the region's prolific hydrocarbon system (Abdullaev *et al.*, 1998; Reynolds *et al.*, 1998; Hinds *et al.*, 2004; Vincent *et al.*, 2005; Vincent *et al.*, 2010). Hydrocarbons are also reported within deposits of the Apsheron Formation, with reservoir and seal components present (Buryakovsky *et al.*, 2001b; Smith-Rouch, 2006) though few specific details on the plays are published and the Apsheron is not generally considered a target.

Apsheron Formation outcrops are described in papers focusing on other geological aspects of the area (e.g. Zubakov, 2001; Allen *et al.*, 2003; Svitoch & Yanina, 2007; Torres, 2007; Souque *et al.*, 2010) and it has been described in studies of regional seismic stratigraphy (Abdullayev, 2000; Abreu & Nummedal, 2007). Recent work has focussed on dating the Apsheron Formation and the correlation of transgressions with glacial and interglacial episodes (van Baak, 2010). However, this chapter represents the first detailed, process-based sedimentological interpretation of the formation.

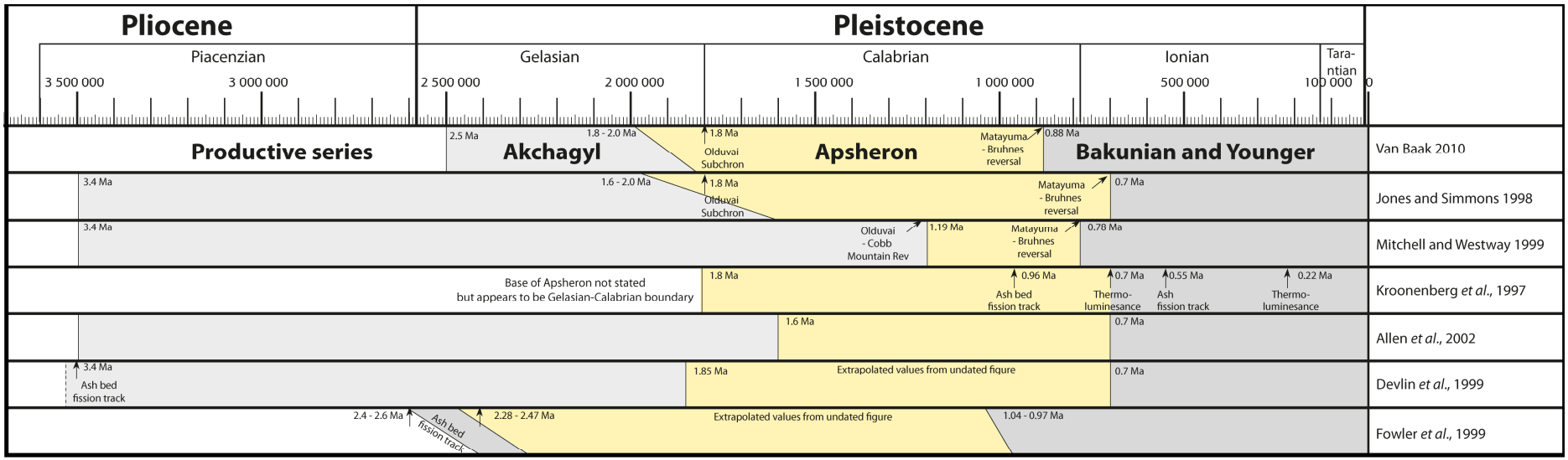

Bakunian and younger Formations	Ash fission track, within formation (0.55 Ma) Thermoluminescance at boundary (0.7 Ma)
Apsheron Formation	Ash fission track (0.96 Ma) Magnetic reversal, near top of formation (0.88 Ma) Magnetic reversal within the formation (1.8 Ma)
Akchagyl Formation	Ash fission track near base (2.4 - 2.6 Ma) Ash fission track, near base (3.4 Ma)

Figure 3.2. Summary of published age estimates and dating methods for the Pleistocene South Caspian Stratigraphy

3.2. METHODOLOGY

Sedimentary data were recorded in graphic logs from three field localities (Figure 3.1d, Figure 3.3). Gamma ray emissions from the outcrop in situ were recorded using a handheld gamma-ray spectrometer (Appendix 2). A Munsell chart (Goddard *et al.*, 1995) was used to describe rock colour, (Appendix 3). The steep hillsides are weathered and do not offer continuous exposure so holes and trenches were excavated to access the bedrock at 1m intervals. Further analysis of the field outcrops was undertaken using satellite and 25m grid DEM data in Google Earth.

3.3. RESULTS

The results are organised into three sections. First the lithofacies are presented, ordered from low, to high energy processes. Secondly, facies associations are described and their depositional environments are interpreted, these are ordered from deep to shallow water environments. Finally this study describes the field scale stacking patterns and places the Apsheron Formation in a sequence stratigraphic context.

Lithofacies

The Apsheron Formation consists of extensive successions of muds and silts, capped by sands and coquinas (bioclastic limestone consisting go shell fragments) divided into twelve lithofacies. These are described, interpreted and summarised in Table 3.1.

Facies associations and depositional environments

This study identifies 4 facies associations that include four depositional environments: FA1 Offshore and offshore transition muds, FA2 shoreface sands, FA3 shoreface submarine fan deposits, and FA 4 coastal storm beds (Figure 3.4). These are described in detail in the sections below. Graphic logs along wide Apsheron formation exposures along the Kerkesdag and Quaradag anticlines, and locations of type logs are shown in Figure 3.5.

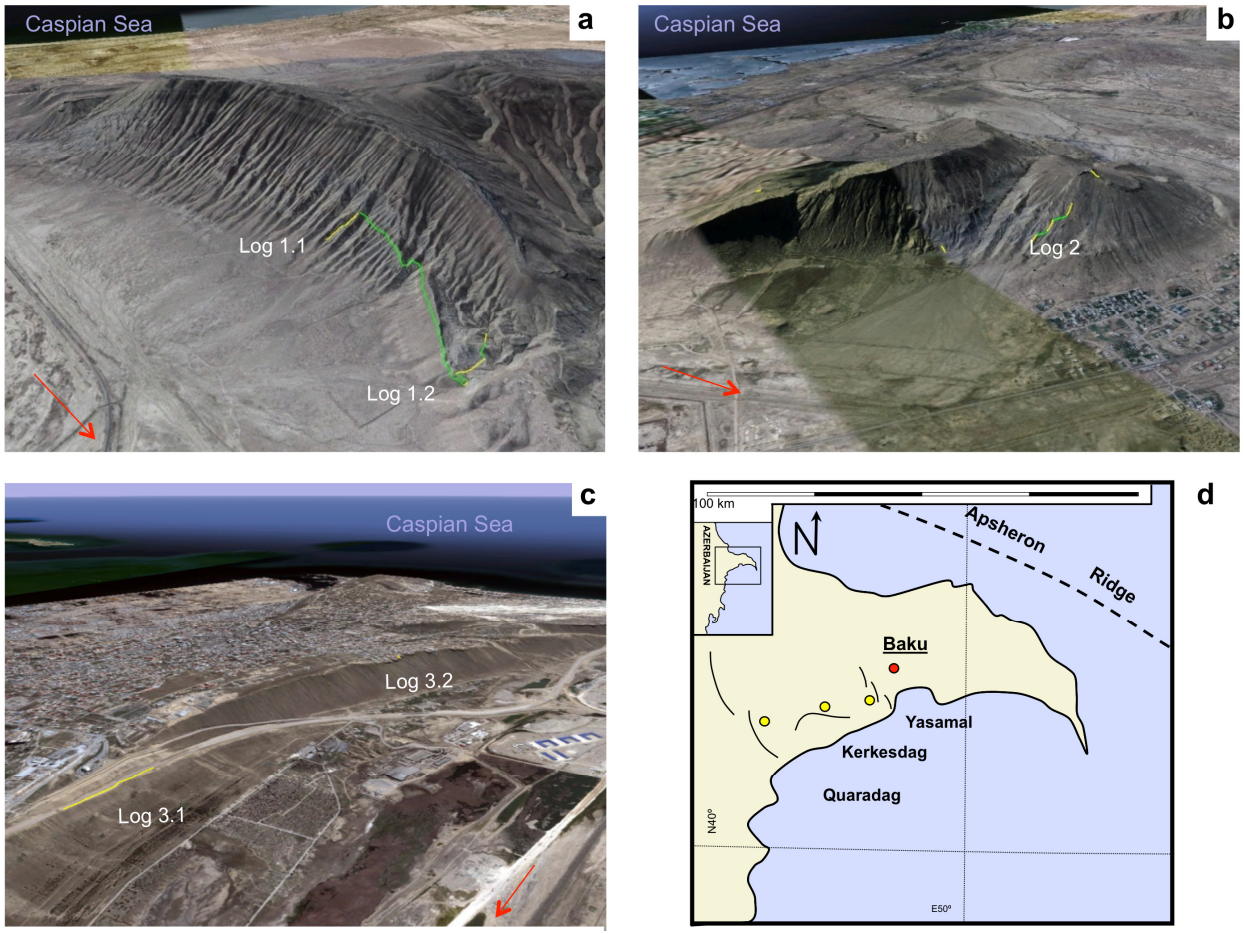

Figure 3.3 Field localities and log traces, (yellow), separated along marker beds (green); [a] Quaradag anticline, [b] Kerkesdag Anticline, [c] Yasamal Anticline. North arrows (in black) and position of Caspian Sea marked on images. Satellite imagery and elevation data from GeoEye, TerraMatics and DigitalGlobe (2011). GPS coordinates of logs are shown in figure 3.5.

FA	Code	Name	Thickness	Description	Interpretation
FA1	M_B	Bedded Mudstone	Individual beds 10-20cm, bedded in successions up to 75m thick	Blue-grey to dark grey mudstone. Internal lamination is absent but facies is planar horizontally bedded on a cm scale, with flat top and basal contacts. Bedding is picked out by discontinuous lenses of orange silt (Figs. 7 a and b). Beds form thick, laterally extensive, successions. M_B contains sporadic clusters of rusty spots and blebs (Fig. 7 c) which are interpreted as burrow motteling. Gastropods and thick walled bivalves in life position are present in isolation (Fig. 7 d) and in clustered lenses (Fig. 7 e). Bioturbation is seen in ferric stained, horizontal grazing traces (Figs. 7 d, 7 f and 7 g) and is also evident from disrupted silt lenses. M_B also contains rare fossilised wood (Fig. 7 h). Rare contorted and folded isolated laminations (Fig. 7 i)	Fine grainsize and lack of any non-horizontal lamination imply low energy suspension settling. lack of mm scale lamination could reflect continous sedimentation, or destruction of lamanie by bioturbation or bottom water currents. Laterally discontinuous silt lenses deposited by weak bottom currents. Dark grey, fossil poor muds containing narrow horizontal grazing traces and continuous silt lenses were deposited under low oxygen, dysaerobic conditions. Lighter coloured muds containing shell clusters and disrupted (bioturbated) silt horizons are interpreted as more aerobic, perhaps elevated sections of the lakebed that protruded into the oxic zone. Inclined depositional surface indicated by cm scale slumping
FA1	M_{FL}	Faint laminated mudstone	10-50 cm	Light and dark grey mudstone. very similar to M_B but muddy sections are faintly laminated showing mm scale colour banding (Fig. 8 a). grainsize changes are not visible in hand specimin. M_{LF} lies betwwn M_B and M_{St} facies along a gradational contact (Fig. 8 b).	Low energy suspension setteling. M_{LF} muds are essentially the same as M_B muds, but with an intact primary depositional fabric. This is explained by a faster sedimentation rate which prohibited extensive bioturbation.
FA1	M_{St}	Silt laminated mudstone	Individual beds 10 - 50cm, bedded in successions up to 50 m thick	Silty mudstone, banded in a pattern of greys browns and greens. (Figs. 8 c and 8 d). Well laminated on a cm scale and bedded with planer bottom contatcs and planer or erosive upper contacts. Laminatios are silty and sandy. Low angle undulose laminations erode and incise older fabric. (Fig. 8 e). M_{St} further contains isolated cm thick silt and sand beds (Fig. 8 f) and isolated sandy (current) ripples (Fig. 8 g). Bivalve shells in life position, similar to those found in M_B are common but gastropods are absent. Trace fossils include sub-horizontal grazing traces, U-shaped dwelling burrows (Fig. 8 h), and bivalve resting traces (Fig. 8 g).	Suspension setteling of muds and planer silt laminations combined with bottom water currents producing mm scale erosion and ripples and emplacing cm thick beds of sand and silt. U-shaped dwelling burrows indicate higher levels of oxygen than M_B or M_{FL}.
FA1	Tf_A	Ash tuff	10 - 50cm, found in lamina-tions in overlying muds for another 50cm	Light grey, fine grained poorly consolidated ash tuff. Internal lamination is absent. Facies is bedded in laterally extensive planer beds with abrupt basal contacts and gradational upper contacts (Fig. 9 a). Thicker beds are contorted by 0.5m scale dewatering structres (Fig. 9 b). Orange staining affects the uper parts of the beds (Fig. 9 c). Fossils and are absent.	Suspension setteling of ash in low energy, subaqueous setting. Rapid and sudden influx of ash outpaces background sedimentation of muds. Subsequent waning of ash fallout results in a gradational laminated contact with overlying muds.
FA1	Cq_M	Coquina with muddy matrix	5 -20cm	Dark brown or dark grey muddy coquina. Consisting of poorly sorted gravel (<1.5cm) and coarse angular shell valves and fragments within a muddy matrix (<25%). Bed bases are sharp and sub planer with shallow erosive scours (Fig 9 d). Shell fragments pick out clear horizontal banding, some of which show normal grading. (Fig. 9 e). mm sized muddy nodules, possibly trace fossils, and shell valves are commonly stained ferric orange.	Waning shell size and shell valve fragmentation imply shells do not represent a life assemblage but were emplaced by a depositional process. Poor sorting indicates rapid deposition. Muddy matrix interpreted as reworked low energy deposits. Ferric staining to muds and shells indicate oxidation of the substrate
FA1 & 3	Cq_{Sn}	Coquina with sandy matrix	Individual beds 20-50 cm, bedded in successions of up to 4m thick	Buff brown coquina. Similar in hand specimen to Cq_c but lacking the carbonate matrix and <10% mud grade particles in the matrix. Bedded in laterally extensive horizontal laminated units with erosive, undulating bases containing rip up clasts of lower lithologies (Fig 9 f), or preserved in dune cross stratified units lining the base of troughs (Fig. 9 g) Laterally extensive beds show very coarse grained shell valves and fragments at base, fining upwards to sand grade particles (80%) (Fig. 9 h), lamination, and rippled silts (Fig 9 f). Cq_{Sn} in troughs only contain oscillatory cm scale sorting/nts (Fig. 9 i).	Facies deposited by two processes: Planer laminated, graded beds emplaced by erosive, high energy turbid flows; Bouma sequence A-D recognised in outcrop (Fig. 9 f). Waning energy at the top of the beds allowed ripples, planar lamination and trace fossils to develop. Trough cross bedded units are emplaced by wave action into dunes. Potentially these are formed by (wave) reworked turbid deposits.
FA2	St_o	Wavy bedded Sands and Silts with oscillating grainsize	Individual beds 10 - 50cm, bedded in successions at least 10 m thick	Light buff and brown heterolithic silts and very fine, muddy sandstone (greywacke) arranged into cm scale planer beds and lenses with wavy contacts displaying flaser and lenticular laminations (Fig. 12 a). Isolated muddy sand bodies are present in cross bedded horizons and concave, erosive lenses, 10-20cm thick (Fig. 12 b). Sn_{Sp} contains both symmetric, structureless and asymmetric, cross bedded ripples. Bivalves, and gastropodsis are rare bue the facies is rich in vertical trace fossils which mix silt and sand laminations (Fig. 12 c). Sn_{Sp} displays varying degrees of competency. It is easily chipped with a rock hammer but several beds are lithified by nodular carbonate concretions.	Repetitive waning flows in a moderate energy subaqueous setting. Pervasive wave and current ripples Abundant vertical burrows and pale colour indicate periods of relatively high oxygen levels. Concave sand lenses represent shallow channels that have been distorted by differential compaction. Post depositional migration of calcium rich fluids selectively through connected sand bodies created the nodular horizons.
FA2	Sn_M	Muddy sandstone	I20-50 cm	Brown medium grained sandstone with a muddy matrix (<5%). Commonly found within channel fill sediments (see FA4) in m scale planar, low angle cross beds, with undulose bases and flat tops (Fig 12 d), but also in adjacent strata in isolated lenses (Fig. 12 b, within Sn_O). Faint cross lamiantion, flaser lamination and ripples are present. Shells in life position are absent but may contain vertical burrows. Most beds are easily chipped with a rock hammer but isolated sections are lithified into a nodular carbonate and these are very well lithified.	Deposited by channel flows into a variety of channels. Flaser lamination and ripples could be (partially) wave generated.
FA3	Sn_O	Sands showing oscillatory grading	Individual beds <5cm, bedded in successions of 1-4m thick	Grey to tan, sandstone with a wide variety of grainsizes of shell- and lithic fragments. Successive cm scale normally graded sets of sand grade particles are capped with planer and rippled sets of silt grade particles producing a pattern of oscillatory grading which contains a broadly fining upwards trend (Fig 12 e). The facies is deposited along erosive and planer bases filling 50cm deep scours, onlapping adjacent strata (Fig. 12 f and is eroded and overlain by coarse beds of SnCS (Fig. 12 g). Sn_O contains ripples in the finer graind sets and rare cross bedded gravelly beds, (Figs. 12 e and 12 h). Many of the ripple crests are eroded, preserving only the troughs, these are sometimes filled with coarse sand and shell debris or comprise of lenticular sandy lenses between muddy silt. Both symmetric and asymmetric ripples are present, internal laminations of which are poorly preserved, though some show faint bidirectional upbuilding. Fossils and trace fossils are absent.	Deposition under fluctuating, pulsating energy conditions; coarser material is deposited in subcritical flow, which wanes allowing ripples to develop in fine grained supercritical flows. cm scale cross bedding created by current ripple migration. Relatively fine grained sets bound by erosive bed contacs at top and base, show that the deposition of Sn_O occurred during relatively low energy periods and had only a moderate preservation potential.
FA3	Sn_{MD}	Sandstone with muddy drapes	30-70 cm	Grey or brown sandstone. Grain size is moderately sorted, commonly containing very coarse particles at the bed base whic fine upwards. The facies is arranged into low angle and bi-directional dune cross bedded, or swaley cross bedded, cross laminated units with concave bases and flat tops. (Figs. 15 a, b and c). Towards the top of the beds muddy laminations are thickest containing shallow gutters and ripples which weather proud of the outcrop (Fig. 15 d and e). Mud poor sections display liesegang staining (Fig. 15 f).	Deposition along erosional surfaces as lunate dunes under fluctuating high energy and slack water. Silt-sand laminations are often associated with tidal packages, but this is not applicable here as the Apsheroninan Caspian had no appreciable tidal range. The muddy drapes are interpreted as packages deposited by wind generated tides.
FA3 & 4	Sn_{CS}	Coarse, shelly sandstone	20-100 cm	Buff brown coarse sandstone. Similar in composition to Cq_{Sn} but grains are sand particle sized. Beds have erosive basal contact (Fig. 15 g) and both flat and undulose tops. Angular rip up clasts of the underlying lithology, large (cm scale) shell fragmments and small dewatering structures lie along the bed base (Fig. 7g). Beds show faint, trough, and dune cross bedding (Fig. 15 h). Weathering picks out rare, vertical structures, possible trace fossils (15 i)	Facies is mature varient of Cq_{Sn} and deposited by two processes: Planer laminated, graded beds emplaced by erosive, high energy turbid flows; Bouma sequence A-D recognised in outcrop. Waning energy at the top of the beds allowed ripples, planar lamination and trace fossils to develop. Trough cross bedded units are emplaced by wave action into dunes. Potentially these are formed by (wave) reworked turbid deposits.
FA2 & 4	Cq_C	Coquina with carbonate matrix	50-150 cm, bedded in succes-sions of up to 30 m thick	Buff brown, very coarse grained biocalstic limestone composed of shell fragments and valves (40%) in a crystalline carbonate matrix (35%). Rounded mudstone pebbles and other lithic fragments (<5%) form a gravelly lag along the bed base and are present in smaller amounts higher in the beds. Most shells are dissoved away leaving empty casts (Fig 18 a). Cq_C is classified as a 'skeletal grainstone' (Dunham), 'biosparite' (Folk), and is described in this study as a 'coquina'. Bedded in thick, m-scale units with wide erosive bases and either flat or undulose tops. Beds are laterally extensive over a km scale, but smaller m width scale beds are also present in channel fills. Channel coquinas contain a distinctive pink and black mottleing (Fig. 18 b). Clasts are generally poorly sorted but more sorted sections show faint, cm scale planar and cross lamination (Fig. 18 c, d and e). Rare 10cm scale trough cross and planer lamination is observed in weathered sec tions (Fig 18 f). Carious weathering of the rock reveals vertical tubular structures, interpreted as burrows (Fig. 18 e).	Particle size and sorting indicates deposition a very high energy environment. Units of poor sorting and misaligned shell valves are dumped rapidly in high energy event that wanes to a pulsating subcritical flow, producing successive laminations of coarse and fine grained shelly sands. Subsequent diagenisis has created nodular calcitic concretions and stained channel coquinas with magnesium. Undersaturated pore waters have dissolved away aragonite shell valves which have remained voids resulting in a large mouldic porosity.

Table 3.1 Lithofacies descriptions from the Apsheron Formation *To be printed on A3 landscape oriented paper*

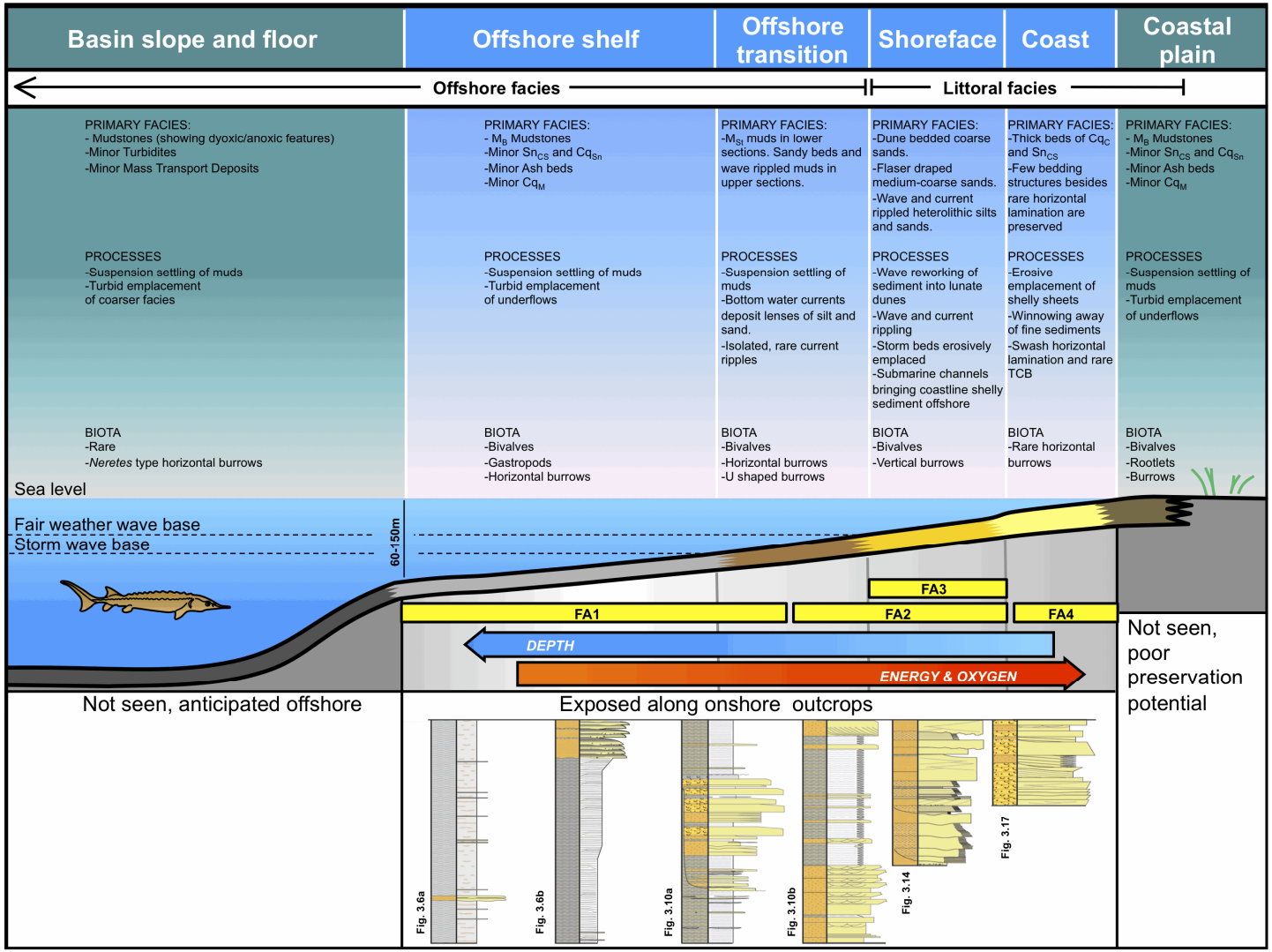

Figure 3.4 Summary and lateral relationships of facies associations and depositional environments.

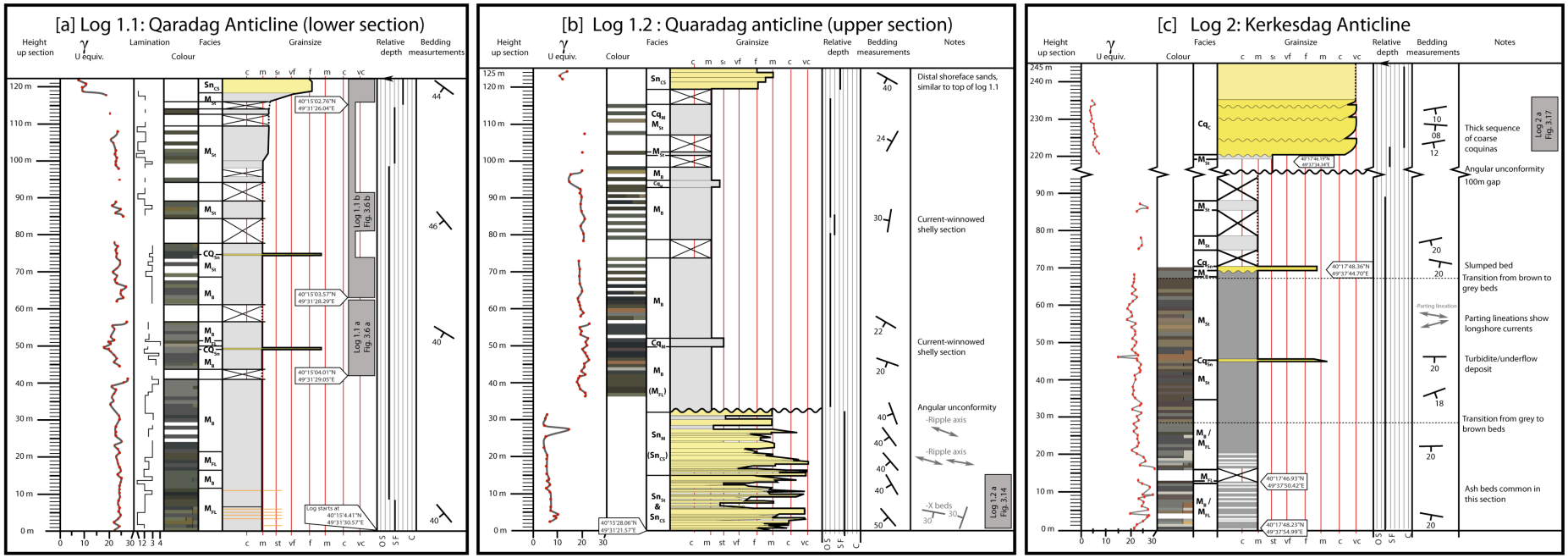

Figure 3.5 Vertically extensive logs taken along the Quaradag and Kerkesdag anticlines, incorporating facies, colour and bulk gamma ray data, and showing interpretation of relative depths [a] Log 1.1: lower portion of Quaradag, also contains lamination data which was ultimately not used in the study. [b] Log 1.2: upper portion of Quaradag. [c] Log 2: Kerkesdag . *To be printed on A3 landscape oriented paper*

FA1: (MB, MLF, Mst, SnCS, TfA, CqSn, CqM) Offshore shelf muds and silts

DESCRIPTION: FA1 typifies the majority of the Apsheron succession. It continues uninterrupted for 300 m along the Kerkesdag anticline (Figure 3.5a, Figure 3.6a) and is also found in shorter, 50 m – 100 m thick sections along the Quaradag and Yasamal Anticlines (Figure 3.6b). Where its base is exposed it onlaps coarse grained FA2 type lithofacies along an angular unconformity (Figure 3.5b).

Extensive outcrops of FA1 associations show a grey-brown colour banding on a 50 m-scale (Figure 3.6 a and b), which corresponds to sections of either M_B and M_{FL} mudstones (grey), or M_{St} silty mudstones (brown). Planar-bedded M_B muds, and finely laminated M_{FL} mudstones are relatively monotonous in hand specimen; mm-scale bands of orange silt, and vague <mm planar muddy laminations are the only widespread bedding structures, and these are often disrupted. (Table 3.1, Figure 3.7 a, Figure 3.8 a – i, and Figure 3.9 a – c). Several sections of M_B lack any discernable bedding structures at all. M_{St} is browner in colour than M_B and M_{FL} mudstones and is more complex. It contains two adjacent types of laminations; <mm lenses of silt, and <mm fluctuations of mud colour. M_{St} laminations are arranged into <mm shallow bedding structures, scours and mm-scale isolated ripples (Table 3.1, Figure 3.7 b, and Figure 3.9 c – i).

The FA1 mudstone successions also contain rare interbeds of other lithofacies. Laterally extensive (>50 m), beds of course grained, graded Cq_{Sn} coquinas, and Sn_{CS} sandstones, 10 – 30 cm thick, overlie the mudstones along shallow erosive basal contacts. Several of these coarser beds are disaggregated and contorted in disharmonic folds (Figure 3.8 i). Muddier Cq_M coquinas are organised into cm-scale planer beds of shell fragments and muds (Figure 3.10 d and e). A third type of interbed is fine grained, planar based, pale grey, T_{FA} beds (1 – 20 cm thick). These occur sporadically in groups of beds. Pale<mm laminations are observed in M_{FL} lithofacies above these ash beds (Figure 3.10 a). The largest ash bed is over 20cm thick and is contorted by dewatering structures reaching 50 cm in height (Figure 3.10 b).

FA1 contains both trace fossils and body fossils (Table 3.1 and Figure 3.8 c – g). These have not been identified but are photographed and archived (Appendix 5). The most common trace fossil is seen in the M_B and M_{FL} muds and comprises short (5 – 20 mm), meandering muddy burrows that run bedding-parallel. It probably represents a Cruziana-type ichnofacies (Frey and Pemberton, 1984). Silt filled U-shaped burrows are observed in M_{St} facies (Figure 3.9 h). Bivalves are widespread and intact articulated valves are found in all types of mudstone. Bivalve fossils are commonly isolated, though clusters of valves and shell fragments are also seen in M_B muds (Figure 3.8 e). Gastropods are present in places in the facies association.

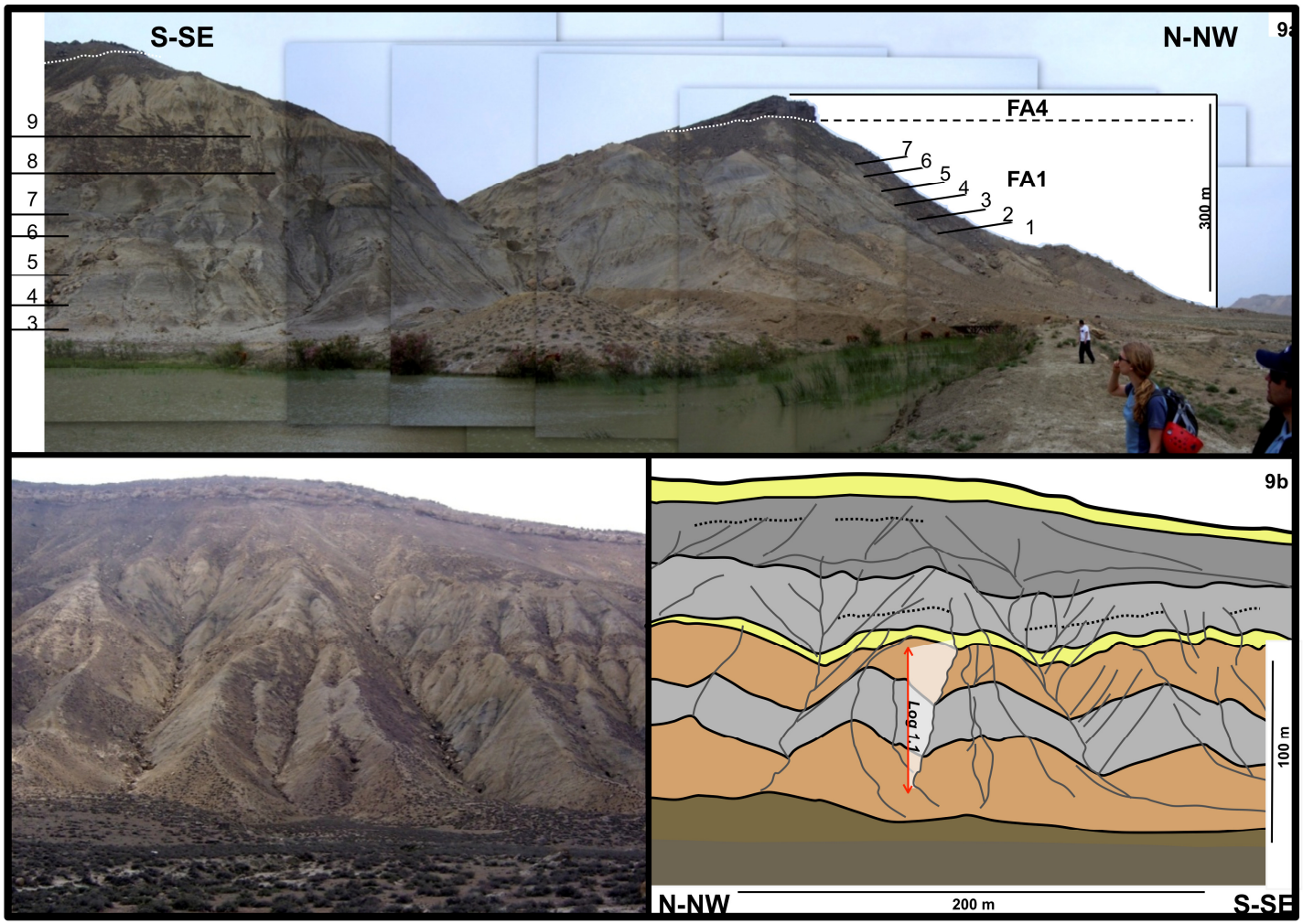

Figure 3.6. Field photos of FA1 outcrops: [a] Photomontage of the Kerkesdag anticline, showing thick FA1 succession, displaying coloured banding (1 – 9). [b] Quaradag anticline, showing coloured banding, picked out in the adjacent cartoon. Approximate location of number '1' on figure a is: 40°17'48.23"N 49°37'54.99"E. Base of gully on figure b is: 40°15'4.41"N, 49°31'30.57"E

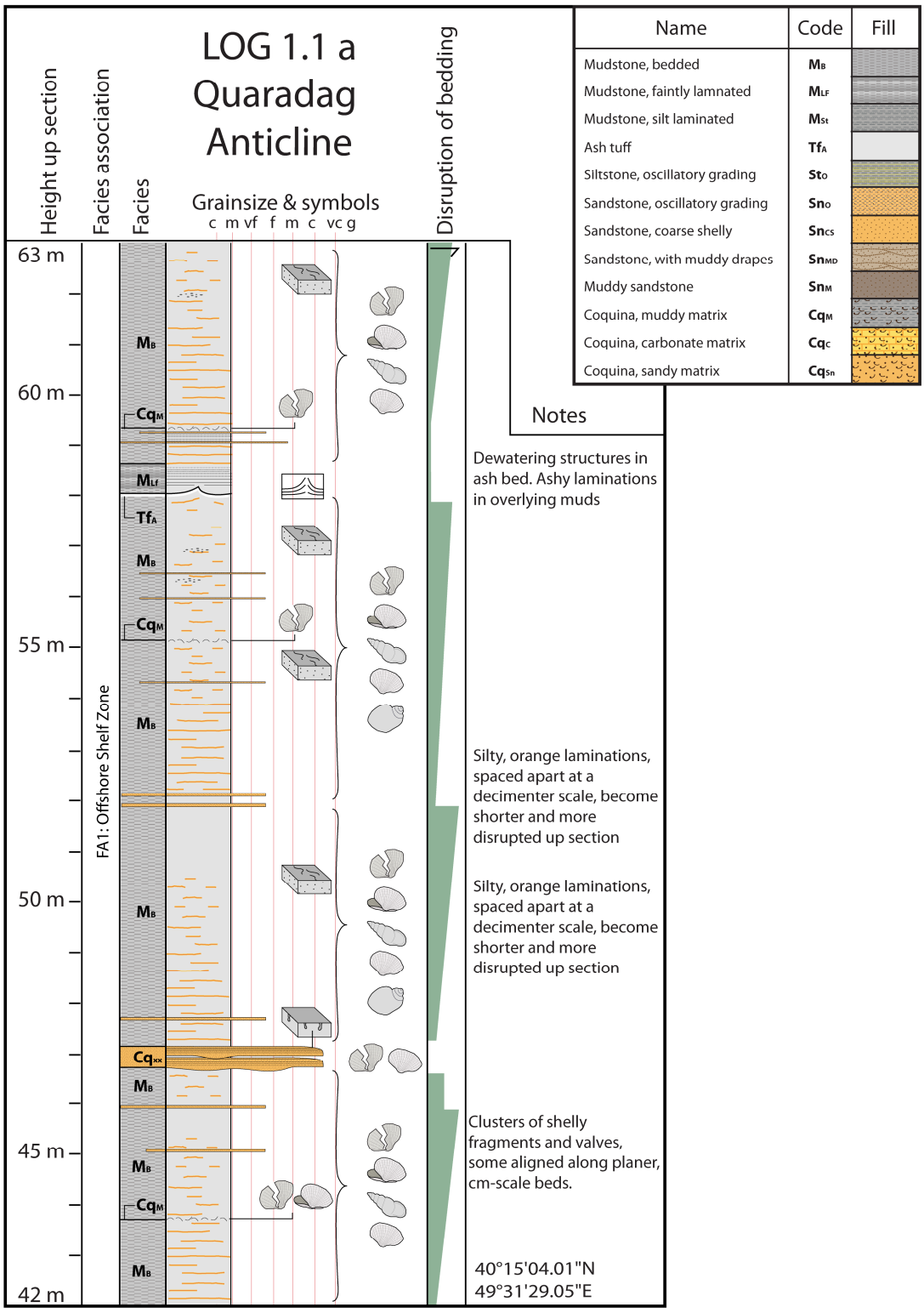

Figure 3.7 [a]. see next page for description

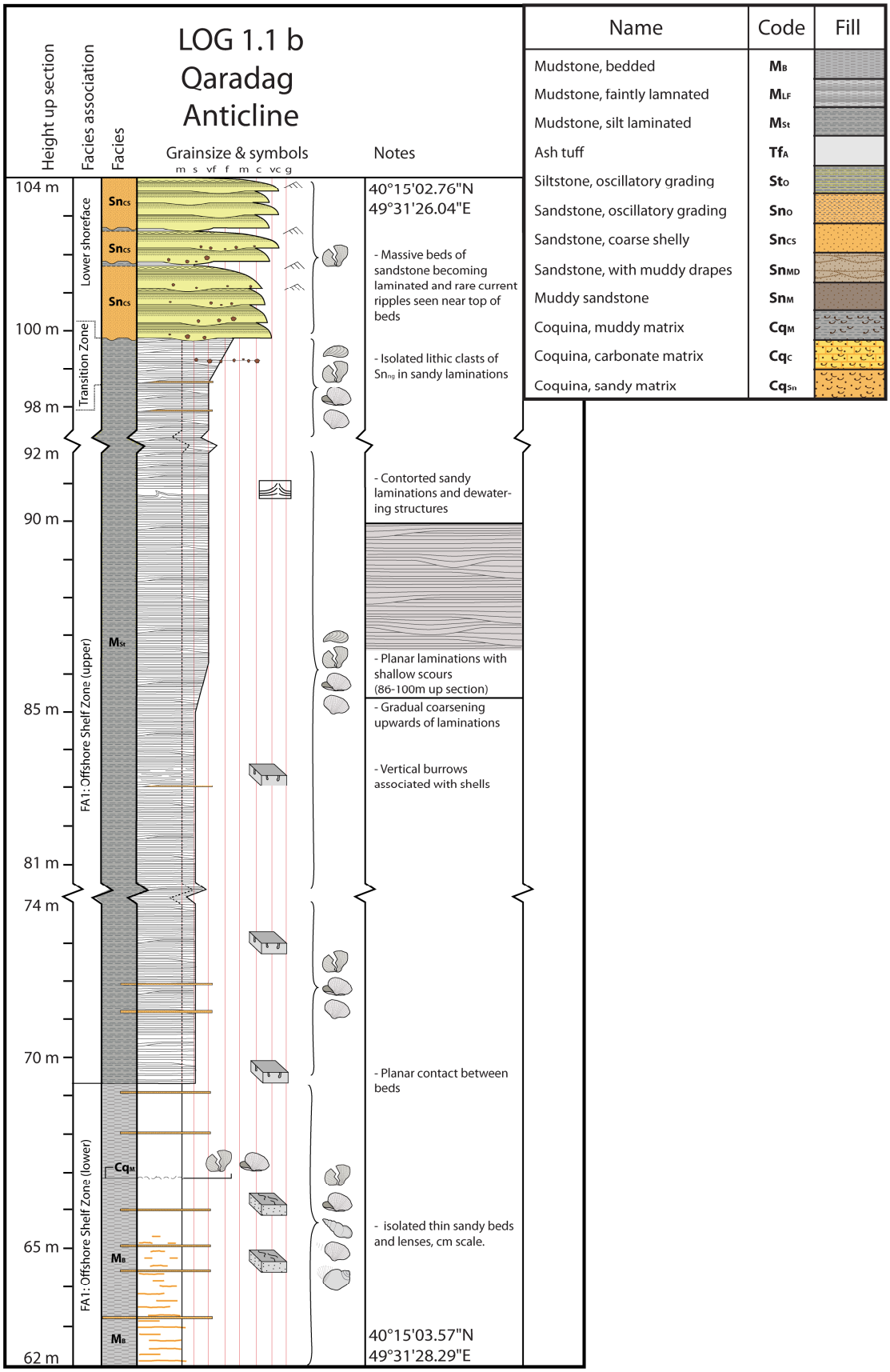

Figure 3.7. Representative logs of facies association FA 1: [a] (previous page) showing low energy offshore self (FA1a), and [b] high energy offshore shelf. Top of log contains turbidite beds from facies association FA2

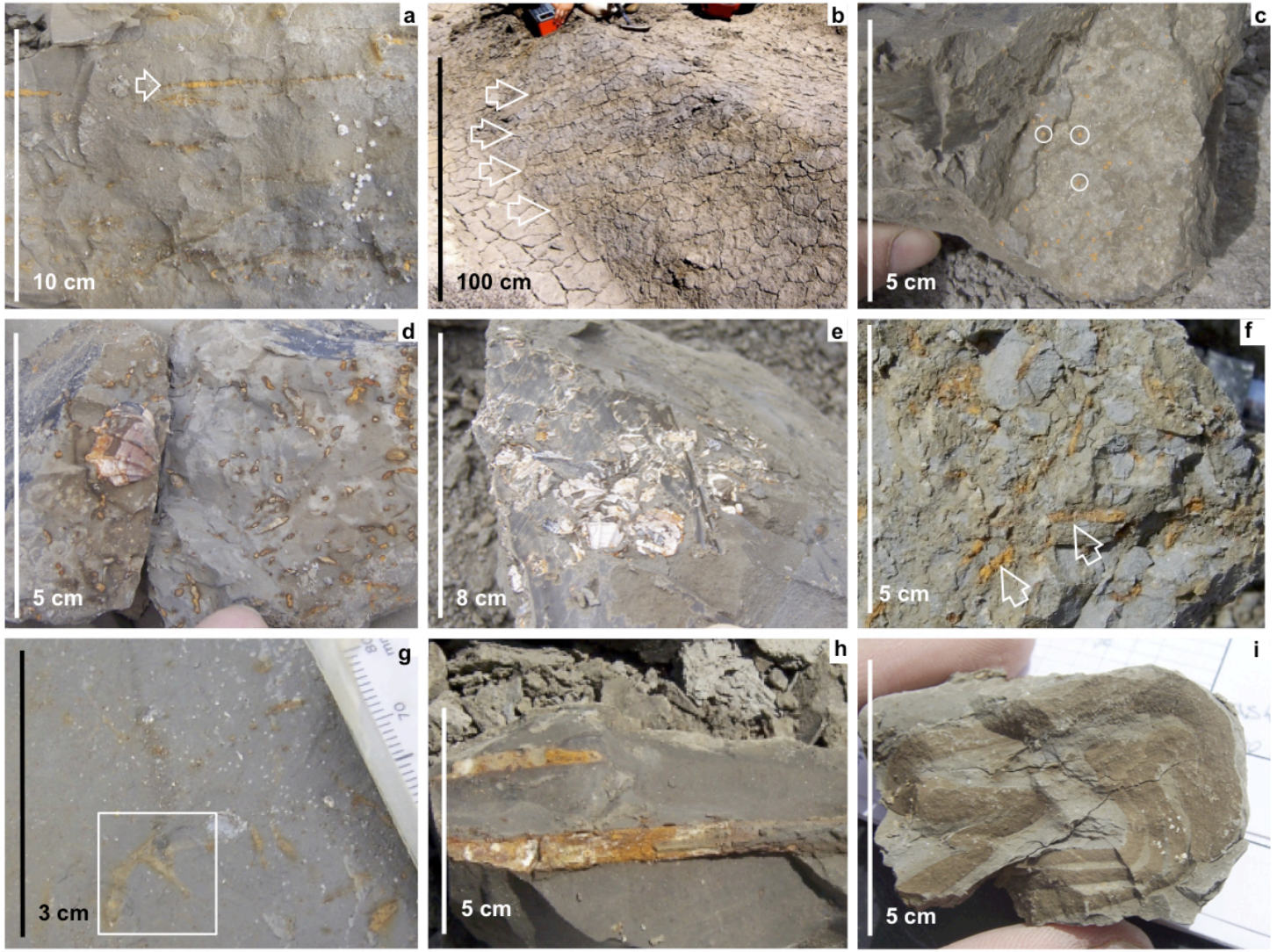

Figure 3.8. Field photos of FA1 facies: [a] Ferric stained silt bands pick out cm-scale bedding in M_B muds. [b] Silt banding and cm-scale bedding more apparent in weathered outcrop. [c] Silt stained blebs, possibly trace fossils in M_B. [d] Thick ribbed bivalve and horizontal traces in M_B. [e] Isolated clusters of shell valves in M_B. [f] Anastomosing, horizontal trace fossils in M_B. [g] Branching horizontal trace fossils in M_B. [h] Fossilised wood in M_B. [i] Contorted folded lamination in M_B

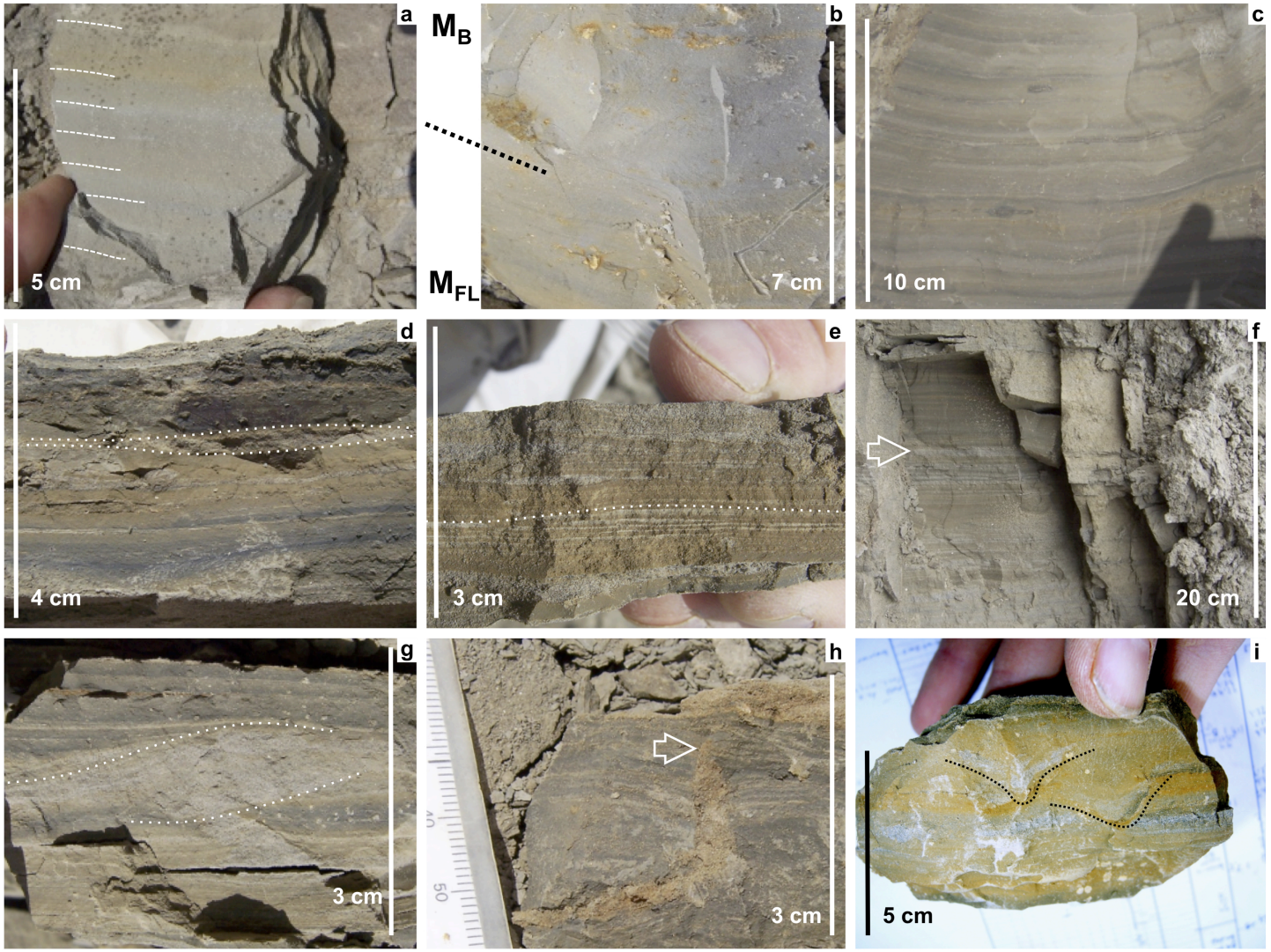

Figure 3.9. Field photos of FA1 facies: [a] faint, graded laminations in M_{FL}. [b] Graded contact between M_B and M_{FL}. [c] well developed colouration lamination in M_{St}. [d] close up of M_{St}, showing silt lenses (dashed lines) and cm-scale colour changes between muds. [e] Undulating silt laminations, truncating lower fabric along white dotted line. [f] cm-scale sand beds in M_{St}. [g] cross laminated concave-upwards sandy bedding structures in M_{St}, interpreted as isolated ripples. [h] J, or U shaped burrow in M_{St}, below sandy horizon, visible at top of photograph, and filled with sand. [i] Convex-upwards structures in M_{St}, interpreted as bivalve resting traces

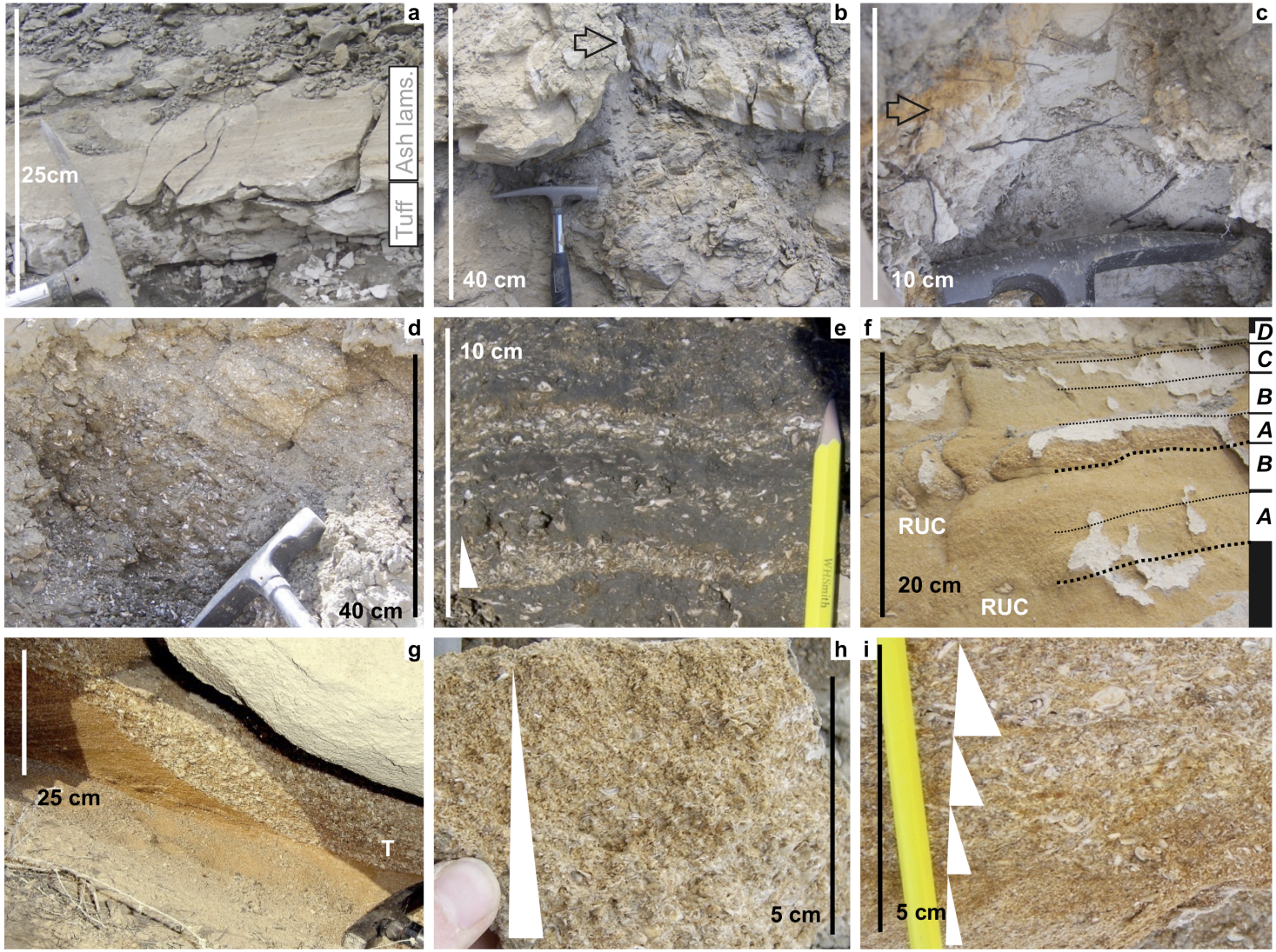

Figure 3.10. Field photos of FA1, FA2 and FA3 type facies: [a] Layer of ash tuff at base of photograph, with laminations of ash in overlying MFL facies. [b] Convoluted bedding in Tf_A ash bed, interpreted as dewatering flame structure. Arrow shows tip of flame structure [c] Iron staining to top of ash bed. [d] Shell valves and fragments (white specks seen in photo) in Cq_M facies. [e] close up of shelly bands some show grading (band nearest base of photo, shown with white triangle). [f] Beds of Cq_{Sn} showing rip up clasts at bed base (RUC), and grading into laminated sand grade particles, and laminated silts. Interpreted as Bouma sequences A – D. [g] Cq_{Sn} in trough cross bedded unit, confined to a single trough (T). [h] Graded isolated bed of Cq_{Sn}. Grading shown by white triangle [i] Cq_{Sn} showing moderate sorting, cm-scale lamination and grading.

INTERPRETATION: FA1 was deposited below storm wave base along the offshore zone of the basin shelf. This study defines two sub environments of FA1: the 'lower offshore shelf' and the shallower, higher energy 'upper offshore shelf' based on bedding structures grain size (Martel & Gibling, 1991). Suspension settling of mud produced finely laminated, vertically extensive successions of mudstones along the lower offshore shelf. Bedding structures in structureless MB muds may have been destroyed or altered by bioturbation or weak reworking of the palaeolake bed by bottom water currents. Thin lenses of silt and fine sands with shallow scours and isolated mm-scale ripples in upper offshore shelf muds indicate weak bottom water currents travelling from more proximal areas, possibly distal turbidites (O´Brien & Kemp, 1996; Collinson et al., 2006).

Volcanic events intermittently deposited beds of Tf_A ash along the lower offshore shelf. The lack of mud in the ash bands, and the presence of dewatering structures both indicate that these were deposited rapidly in dumping events. Ash particles continued to rain out of the water column upon the resumption of muddy background sedimentation. Preservation of the fragile ash beds indicates an environment that was pervasively low energy. Occasional higher energy events are also observed however. Shell valves in Cq_M lithofacies indicate winnowing currents (Martel & Gibling, 1991), beds of graded S_{fu} sands indicate deposition from turbidity currents, and disharmonically folded, disaggregated beds of Cq_M show slope failure and slumping. These beds may have been deposited by storm processes such as storm surges which remobilised sands and shelly material from the nearshore (Norris, 1986; Tucker, 1990), transporting them in dense turbid underflow currents over the shelf (Cheel & Leckie, 1993), and bottom-touching storm waves, which cause liquefaction of the lake bed in shallower areas of the shelf and generate slope failures and slumps further downslope (Walker, 1984).

Rhythmic, mm-scale coloured muddy laminations in upper offshore shelf M_{St} muds may relate to microscopic grainsize fluctuations (Collinson *et al.*, 2006) or in dark–light coloured sections, organic carbon content (Hosterman & Whitlow, 1980). These potentially represent 'varves'; seasonal sedimentation variations common to many lacustrine settings. The darker laminations were laid down during summer sedimentation in a thermally stratified, low-oxygen lake, and lighter bands during winter cooling and mixing (Schulz *et al.*, 1996; Talbot & Allen, 1996). A varve interpretation is speculative however, as no chronological evidence exists that each lamination represents an annual layer. The absence of similar colour changes in lower offshore shelf M_B lithofacies is explained either by constantly low oxygen levels at that depth which did not fluctuate enough to change redox conditions, bioturbation destroying original laminations, or by sedimentation remaining constant during deposition.

Thick-shelled bivalves in life position and Cruziana-type trace fossils indicates that the environment was oxic, or at least dysoxic, even along the lower offshore shelf (Frey & Pemberton, 1984). Ferric laminations alongside darker muds suggest that the silts and muds that settled out to form the laminations were oxygenated before deposition along the shelf. Death assemblages of shells in Cq_M are present near the base of the succession and may represent transgressive lags.

Arguably the interpretation of the offshore shelf is ambiguous, as similar lithologies are present in deep basin interiors, and are also observed in cored sections of the modern Caspian Basin centre (Kosarev, 2005). However, silt laminations, the presence of thick shelled bivalves in life position and Cruziana ichnofacies, are all consistent with a shelf environment interpretation which is further supported by previous work on the location of the Apsheronian offlap break position (Grant, Pers. Comm (2011), Figure 3.1 b).

FA2: (St, Sn_{st}, Cq_c, Sn_m) Offshore transition zone

DESCRIPTION: facies association FA2 outcrops along a road cutting on the northern flank of the Yasamal anticline (Figure 3.12 a). Its upper and lower contacts are not observed, but the weathering character of the surrounding area, and small outcrops along the road indicate that it lies between successions of FA1 muds.

FA2 consists of St_o sand and siltstone lithofacies, stratified in planar, wavy beds with rare cross laminated, flat based, convex-upwards lenses of Sn_M sandstone (Figure 3.13 a – c). The facies is bioturbated by vertical Skolithos burrows. Beds trend planar horizontal, turning to inclined dipping SSE towards the present-day Caspian shoreline (Figure 3.11 a). The sands and silts are laterally truncated , and incised by a channel, one margin of which is exposed, and which is at least 10 m thick (Figure 3.11 c). The channel fill comprises an assortment of Sn_M muddy sandstones (Figure 3.13 d), and well cemented Cq_C shelly gravel (Figure 3.19 b). Strata exhibit m-scale cross bedding with an apparent dip of 20 – 10 degrees to the NNW. These accrete laterally away from the channel margin and the current Caspian coastline (Figure 3.11 c). The shell beds display a distinctive pattern of cross cutting red and dark grey mottling (Figure 3.19 b). The channel is overlain by further St_o silts and sands.

INTERPRETATION: FA2 represents a transition zone, near storm-weather base, between the upper offshore shelf and the lower shoreface. The outcrop of FA2 also contains a submarine channel (Figure 3.11 c). The key observation supporting this transition zone environment are the abundance of muds together with wavy laminated sands, interpreted as wave generated structures (Hampson, 2010).

The depositional energy in the transition zone was much higher than along the offshore shelf, indicated by coarser facies, small bedforms and Skolithos burrows. However, wave energy was periodically low enough for silt preservation suggesting deposition below fair-weather wave base. Fluctuations between muds and sands suggest a steady fluctuation of hydraulic energy with repeated bedload deposition from storm waves or currents followed by periods of slack water and suspension settling (Martel & Gibling, 1991).

Isolated, convex-upwards sand lenses may represent shallow crevasse splays fed from the main channel. The channel itself is filled with lags of shelly Cq_c facies, interpreted as reworked upper shoreface lithofacies (see FA4) from more distal environments. Several of the coquinas show trough cross bedding, indicating reworking of the material into submarine dunes or mega ripples similar to those seen in FA3. The lateral accretion of coquina and hash at the channel margin, shows the channel was migrating with a northwards component over the shelf. The Apsheronian shelf break is oriented NNE – SSW (Figure 3.1 c) so the channel may have been oriented semi-parallel to the shelf margin at the Stonepay outcrop. Thickening-upwards of the channel fill, and the appearance of dunes higher in the succession, suggests a gradual shallowing; The channel may have been incising the shelf during a lake level fall.

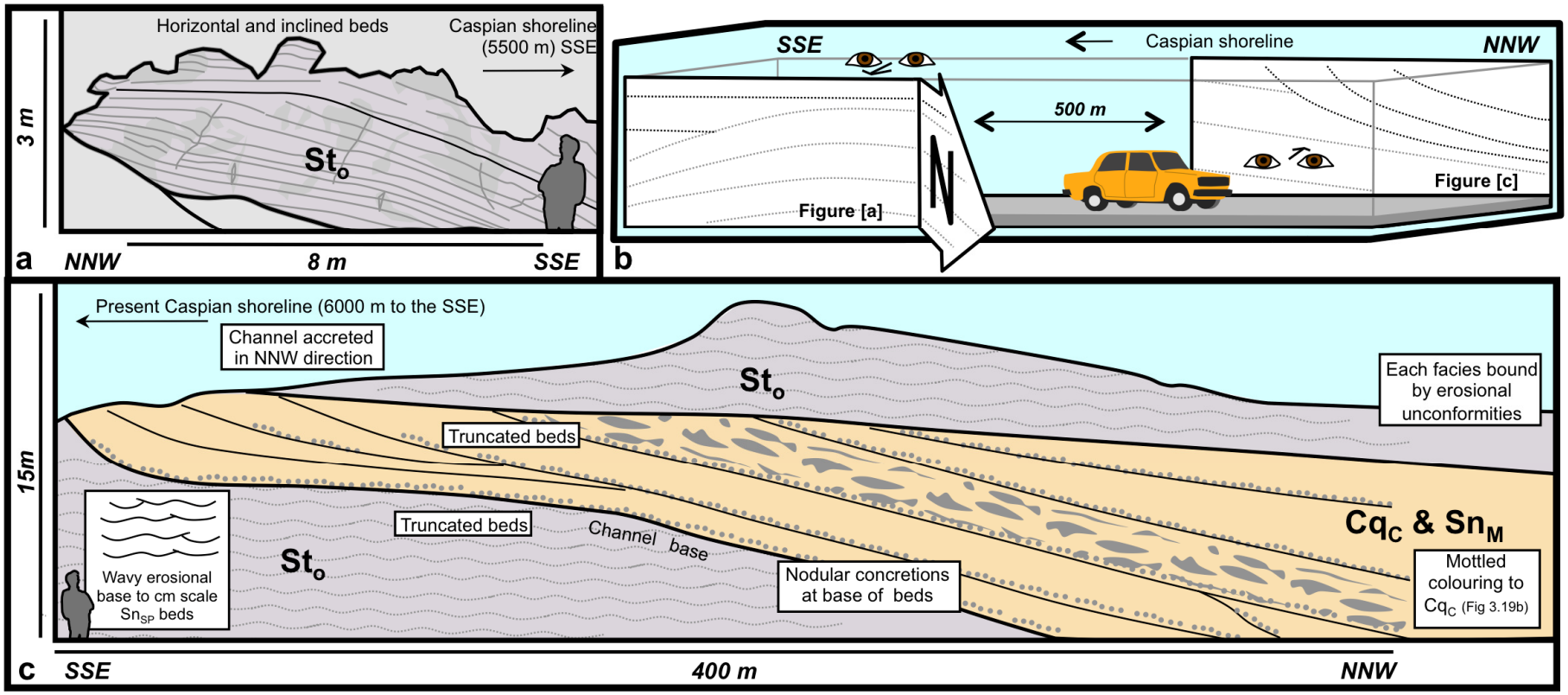

Figure 3.11 Sketches of outcrops along the Stonepay roadcutting. [a] partial exposure of St_O silts and sands arranged into horizontal topsets and inclined foresets. [b] location sketch of the two outcrops along the roadcutting. Note that figure a is viewed looking towards the W – SW, and figure b looking towards the E – NE [c] inclined St_O muds and silts incised by large channel filled with shelly Cq_C gravels and Sn_M sands. Metre-scale crossbeds migrate away from the Caspian shoreline. Location of roadcutting is 40°21'28.50"N, 49°47'46.72"E

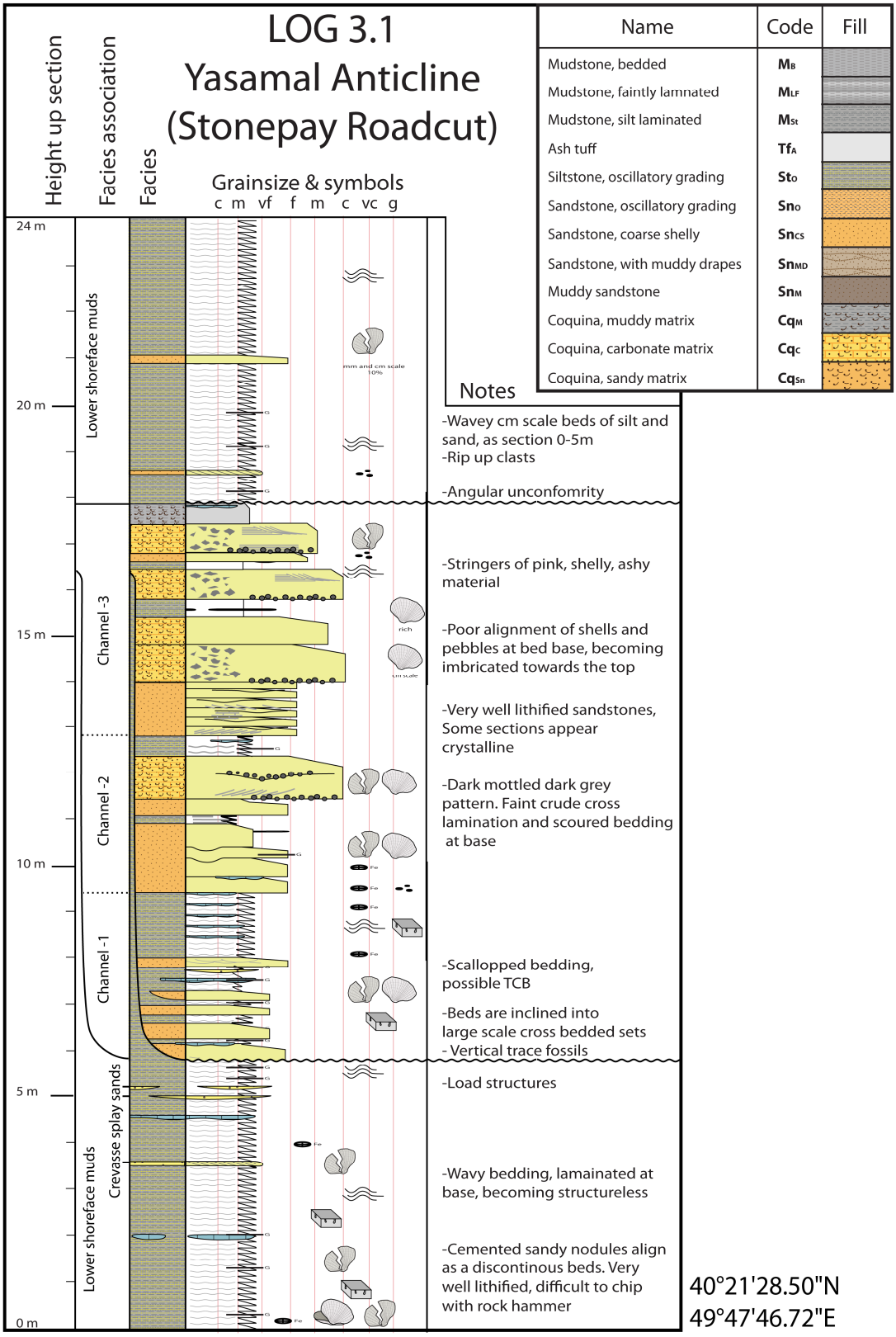

[a] (Caption on following page)

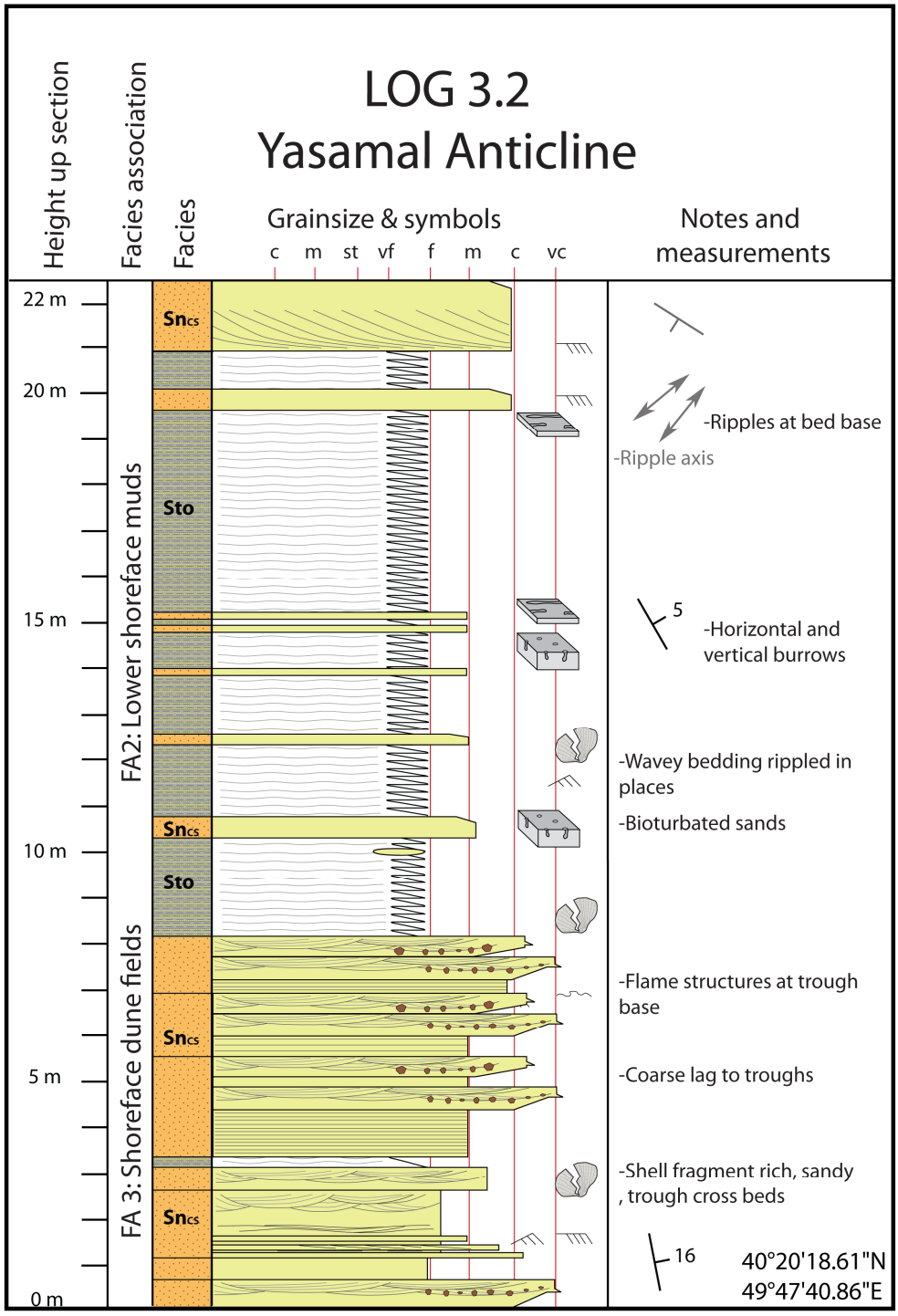

Name	Code	Fill	Name	Code	Fill
Mudstone, bedded	M_B		Sandstone, coarse shelly	Sn_{CS}	
Mudstone, faintly lamnated	M_{LF}		Sandstone, with muddy drapes	Sn_{MD}	
Mudstone, silt laminated	M_{St}		Muddy sandstone	Sn_M	
Ash tuff	Tf_A		Coquina, muddy matrix	Cq_M	
Siltstone, oscillatory grading	St_O		Coquina, carbonate matrix	Cq_C	
Sandstone, oscillatory grading	Sn_O		Coquina, sandy matrix	Cq_{Sn}	

Figure 3.12. Type logs of FA2: Lower shoreface. [a] log 3.1 showing lower shoreface silts and sands, and a submarine channel. [b] log 3.2 showing lower shoreface silts and FA3 type (upper shoreface), trough cross bedded shelly sands

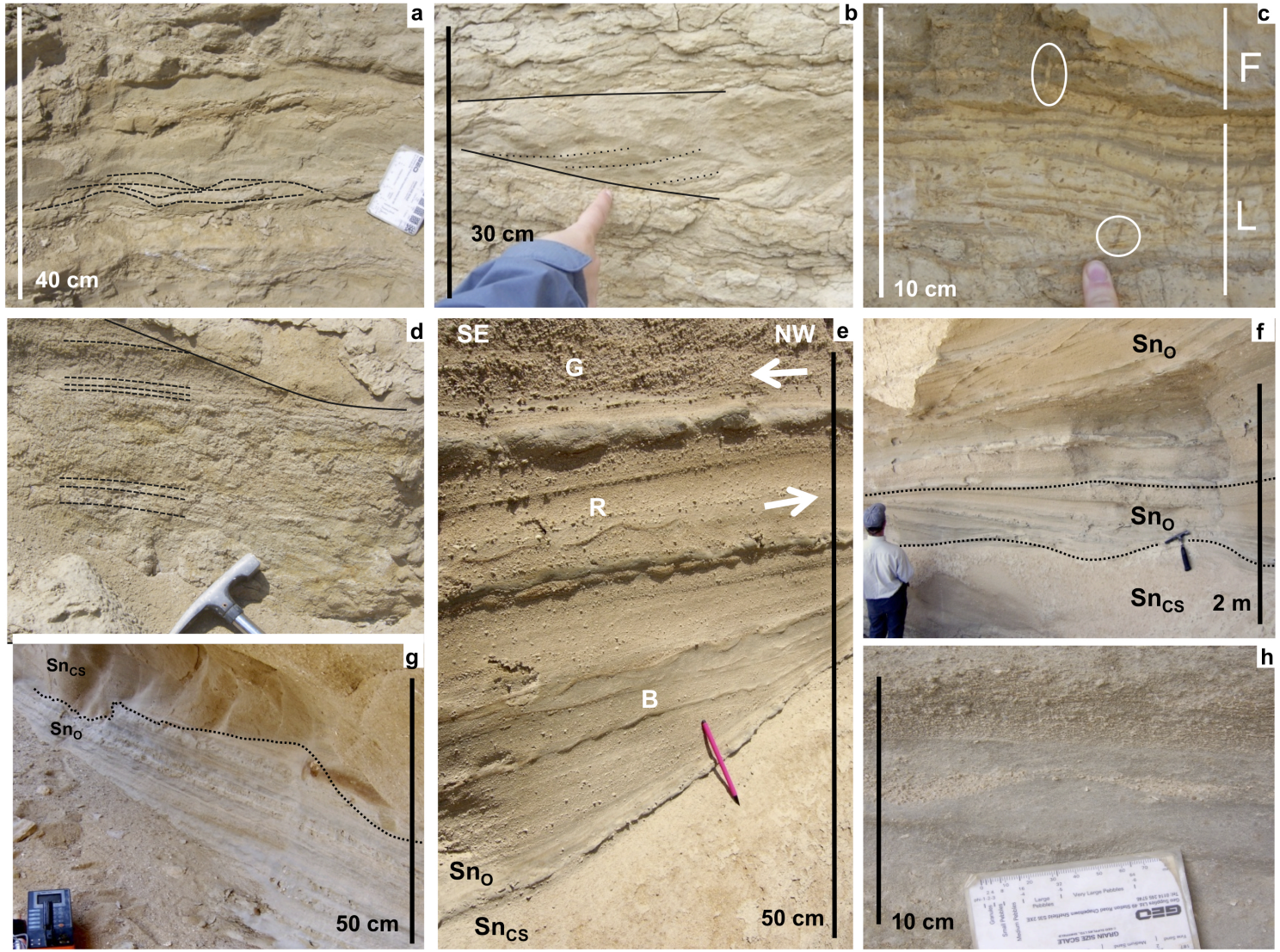

Figure 3.13 Field photos of Fa2 and FA3 type facies: [a] Wavy heterolithic bedding in StO facies. [b] Cross bedded, convex structure in SnO. [c] Vertical trace fossils in flaser (F) and lenticular (L) bedding, in SnO. [d] Muddy sandstone SnM, showing faint horizontal lamination. [e] graded sets of SnO, containing abundant ripples, and rare, cross laminated gravels (G). Ripples show bidirectional up-building at (B). Apparent palaeocurrent directions (white arrows) estimated from ripple asymmetry and cross lamination. [f] Beds of SnO overlying SnCS over an undulating contact. Contacts between SnO are also undulose and erosive. [g] SnCS overlying SnO facies over an angular and erosive contact. [h] muddy climbing ripple, ripple trough is filled with coarser shell fragments.

FA3: (Sn_{CS}, Sn_{MD}, Sn_{O}, Cq_{Sn}) Lower to mid shoreface

DESCRIPTION: FA3 outcrops along the Westerly tip of the Quaradag anticline and along the Yasamal anticline. The facies association outcrops along laterally extensive (200 m) exposures and reaches 25m in thickness (Figure 3.15), thinning towards the current Caspian coastline, where it grades laterally into muddy, FA1 type, facies. FA3 overlies FA1 facies associations above a wavy erosional contact and is overlain by a return to FA1 type lithofacies along an angular (progressive) unconformity (Figure 3.5b, Figure 3.14).

The lower part of FA3 consists of graded beds of S_{CS} containing angular rip up clasts of mudstone and siltstone. Massive beds of shelly Sn_{CS} show erosive bases and undulose top surfaces with depressions 1m deep and several metres wide, which are onlapped by planar bedded and rippled Sn_{O} sandstones (Figure 3.13 e). Symmetrical ripples showing bidirectional upbuilding, and inclined ripples are both observed within Sn_{O} beds. Ripple axis, where exposed, are oriented approximately N – S, and ripple inclinations show apparent vergence both to the NW (landwards) and the SE (basinwards). The Sn_{O} sandstones are themselves partially eroded and are draped by further Sn_{O} lithofacies (Figure 3.13 f). Thick beds of Sn_{CS} overlie Sn_{O} sands unconformably along jagged erosional profiles (Figure 3.13 g) and pass-upwards into Sn_{MD} muddy sandstones (Figure 3.16 a). Sn_{M} and Sn_{CS} sands are dune cross bedded, which in places is modified by vertical burrows, ripples and shallow gutters (Figure 3.16 a, d, e, and h). Towards the top of the association shallowly dipping, finely cross laminated sandy beds that dip to the NW (landwards), are interbedded with coarse trough-cross stratified shelly beds, separated by thin beds of rippled silts. Grainsize is especially coarse and poorly sorted at the top of the unit. No intact shelly fossils are observed in life position, but valves and shell fragments are occasionally present in lags at the base of some beds.

Figure 3.14. Photomontage showing stacked FA3 type (shoreface) facies, overlain by FA1 type (offshore shelf) facies over an angular unconformity, interpreted as a growth strata boundary. Taken at Quaradag Anticline, approximately 30meters SE of GPS waypoint 40°15'28.06"N, 49°31'21.57"E

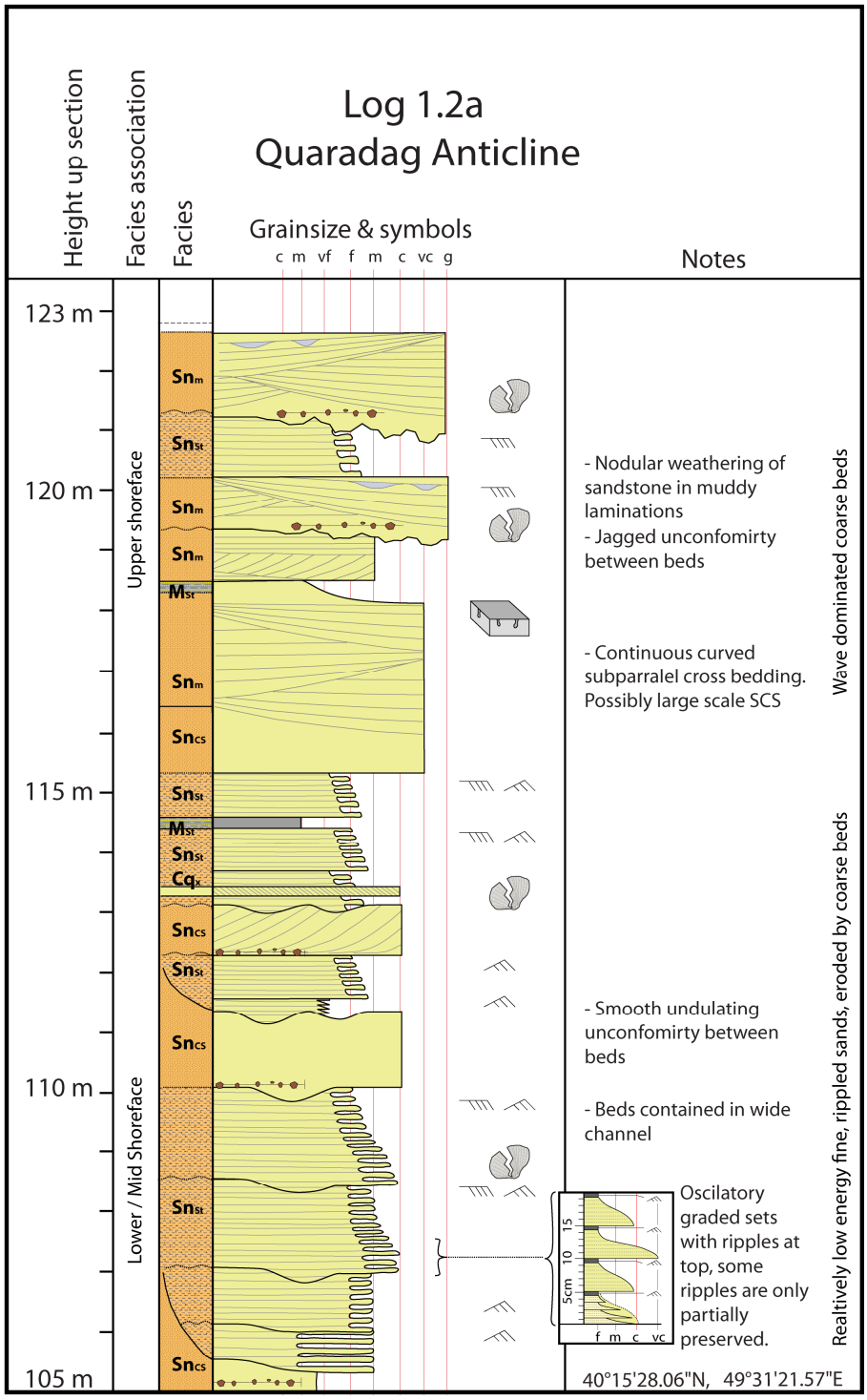

Name	Code	Fill	Name	Code	Fill
Mudstone, bedded	M_B		Sandstone, coarse shelly	Sn_{CS}	
Mudstone, faintly lamnated	M_{LF}		Sandstone, with muddy drapes	Sn_{MD}	
Mudstone, silt laminated	M_{St}		Muddy sandstone	Sn_M	
Ash tuff	Tf_A		Coquina, muddy matrix	Cq_M	
Siltstone, oscillatory grading	St_O		Coquina, carbonate matrix	Cq_C	
Sandstone, oscillatory grading	Sn_O		Coquina, sandy matrix	Cq_{Sn}	

Figure 3.15 Type log of facies association FA3: Shoreface. From the westerly tip of the Quaradag Anticline

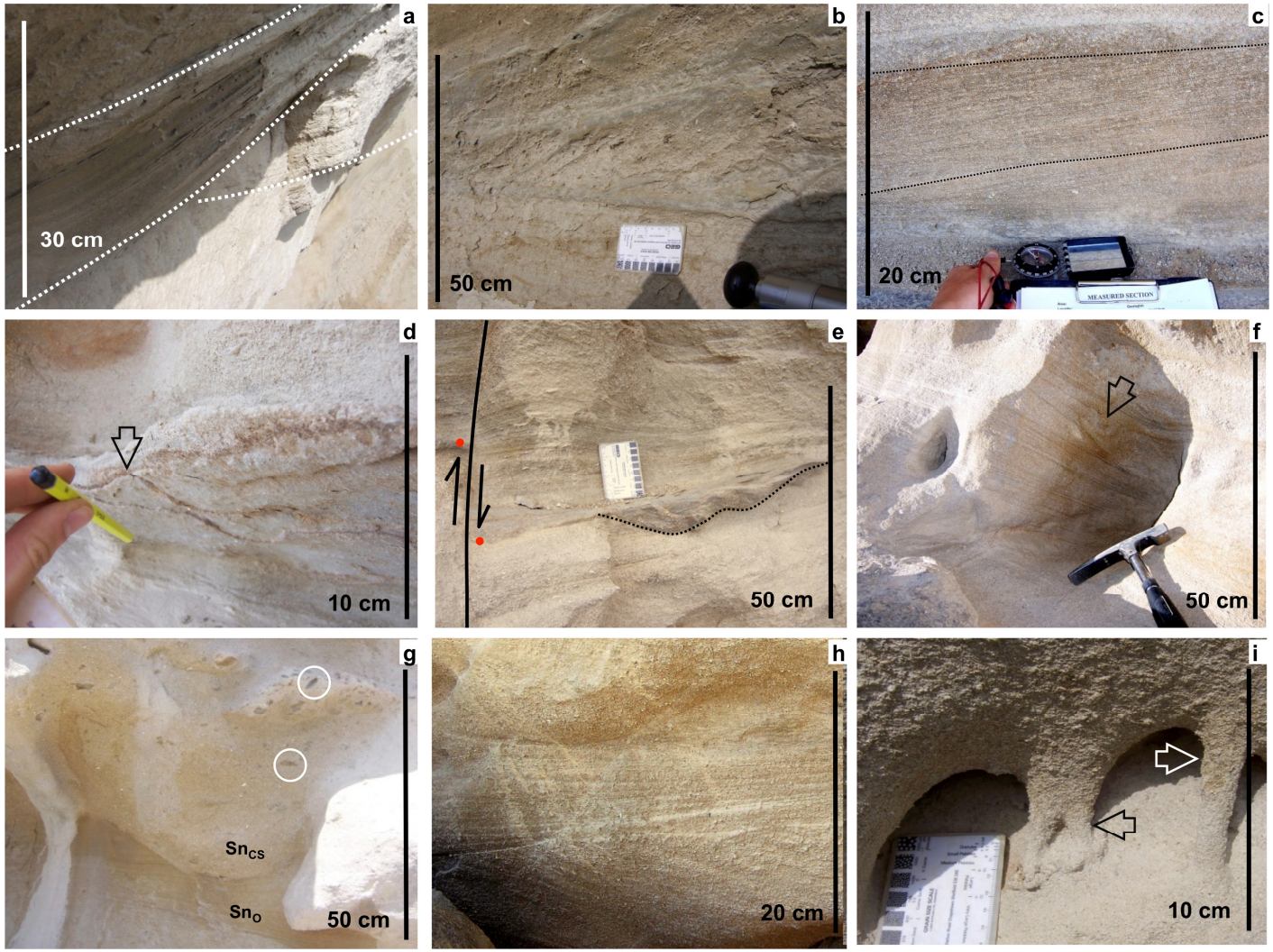

Figure 3.16. Field photos of FA3 type facies: [a] scalloped bedding, dune scale trough cross bedding, or hummocky cross stratification, in SnMD sands. [b] cm-scale cross bedding in SnMD sandstone. [c] mm-scale cross bedding in SnMD showing reactivation surfaces (dotted lines). [d] Muddy ripple crests in SnMD. [e] Muddy gutters in SnMD, outcrop is faulted and offset by 10cm to the right of the photo (red dots show marker bed). [f] Liesegang rings in SnMD. [g] Rip up clasts in poorly sorted massive bed of SnCS, overlying SnO along undulose erosive contact. 2 have been circled, many more are seen on photo. [h] Trough cross bedding in SnCS. Note angular discordance of the laminations in the lower half of the photo. [i] Cylindrical structures weathered out of SnCS, interpreted as vertical trace fossils.

INTERPRETATION: FA3 is interpreted as a lower shoreface environment containing a small number of offshore transition zone beds. It was deposited above both storm and fair-weather wave base. Sedimentary observations that support this interpretation include the coarse grainsize, wave ripples, dune cross stratification and Skolithos-type trace fossils. The graphic log of the type locality shows a gradual coarsening-upwards, shallowing-upwards trend from the offshore transition zone environment at its base to a shoreface, breaker zone environment at its top (Figure 3.15).

In the lower part of the facies association the rippled sands and silts are interpreted as fair-weather sedimentation consisting of tractional flows of coarse and fine sands containing wave and longshore current generated ripples. These are interbedded with m-scale beds of Sn_{CS}, characterised by poor sorting, angular rip up clasts and erosive bases interpreted as rapid emplacement during storm conditions (Tucker, 1990). Erosive events are recorded several times in FA3 suggesting that at times hydraulic energy was very high. The undulose tops of these massive sand beds may represent wave processes, or rip channel bases incised by offshore-directed storm surge currents (Cheel & Leckie, 1993).

The upper part of FA3 is coarser grained and characterised by extensive submarine dune-cross bedding of Sn_{CS} and Sn_{MD} sands. It is interpreted as the mid-shoreface build-up zone (Tucker, 1990). Fine grained Sn_O beds are absent, suggesting energy conditions were too high for their preservation. Rip up clasts at the base of the dunes indicate dune emplacement and basal erosion were either synchronous or that Sn_{CS} (storm) beds were later reworked into dunes. Fine scale muddy drapes exist within the Sn_M sandstones that commonly indicate high-frequency tidal packages (e.g. Nio & Yang, 1991). However, there is an absence of (detectable) tides in the lacustrine Caspian 'sea', so these muddy drapes may represent variations in storm intensity or longshore currents (e.g. Hampson, 2010).

The 'dune cross bedding' observed in Sn_M and Sn_{CS} facies may be poorly preserved/developed swaley cross stratification (Dott Jr & Bourgeois, 1982). These bedforms are commonly interpreted as storm deposits from a mixed, wave and current-generated flow, and can occur in both deep and shallow water environments (Cheel & Leckie, 1993). In this context they are interpreted as storm deposits that remained preserved between storm and fair-weather wave base.

FA4: (Cq_c, Sn_m, St) Upper shoreface and foreshore

DESCRIPTION: FA4 outcrops along the north and south summits of the Kerkesdag anticline in laterally extensive sheets (400 – 1500 m in a SE — basinwards — direction). Its total thickness is unknown but outcrops measure 25 – 30 m in height. The base of FA4 overlies FA1 muds above an angular unconformity. It is overlain by further FA1 muds, though this contact is not exposed.

The lower section of FA4 consists of several 30 – 50 cm, beds of massive Cq_c containing gravel clasts and basal pebble lags (Figure 3.17, Figure 3.18). Beds are commonly massive and weather into a smooth surface, however occasional cm-scale horizontal lamination and basinwards-migrating, shallow cross bedding are faintly visible in fresh outcrop (Figure 3.19 c, e). The basal beds of Cq_C are overlain above an undulating unconformity by steeper dipping interbedded Sn_{CS} and Cq_c facies (Figure 3.17 and Figure 3.19 d). These beds contain occasional ripples at bed tops of finer sands and scalloped, convex-downwards bedforms that are picked out by carious weathering and interpreted as either trough cross bedding, or shallow channels, (Figure 3.17, Figure 3.19 f).

INTERPRETATION: FA4 represents upper shoreface – foreshore deposits. Key observations supporting this are the abundant coarse grainsize, thick beds, and rare cm-scale horizontal laminations. Downlapping beds and coarsening-upwards packages show a shallowing-upwards trend through the facies association.

Shell-rich lithofacies similar to FA4 are found in a variety of coastal and shelf environments from foreshore to shelf edge (Norris, 1986; Tucker, 1990; Riggs *et al.*, 1995). Bed thickness, sediment grain size and vertical abundance all increase with decreasing water depth (Norris, 1986); FA4 is therefore interpreted as the upper shoreface-foreshore zone. Wave swash (directed to the south-east) is indicated by basin wards-oriented planar cross bedding in the finer grained beds. Trough-cross bedding developed in slightly lower energy conditions as a result of bidirectional longshore currents. metre scale beds of coarsening-upwards massive Cq_C are similar to nearshore coastal bars reported along the present-day Caspian shoreline and which extend for hundreds of metres from the shoreline (Kroonenberg *et al.*, 2000). However, the modern examples of Cq_C form seaward boundaries to muddy lagoons and no lagoonal lithofacies are observed in FA3, presumably due to lack of preservation potential in the high energy environment. Thickening and coarsening-upwards of individual beds, combined with the arrangement of the facies association into downlapping foresets, all suggest a gradual shallowing-upwards trend.

The shell beds extend laterally across a wide area (400 – 1500 m normal to the shoreline), and are only 30 – 50 m thick, shelly lithofacies therefore probably extend over a wide range of depositional environments to deeper areas in addition to being accumulated as storm lag deposits along the shoreface (e.g. Riggs et al., 1995). Shelly FA4 lithofacies are assumed to amalgamate or transition to sandier FA3 type lithofacies at some point (e.g. Norris, 1986) but this is not observed in these outcrops.

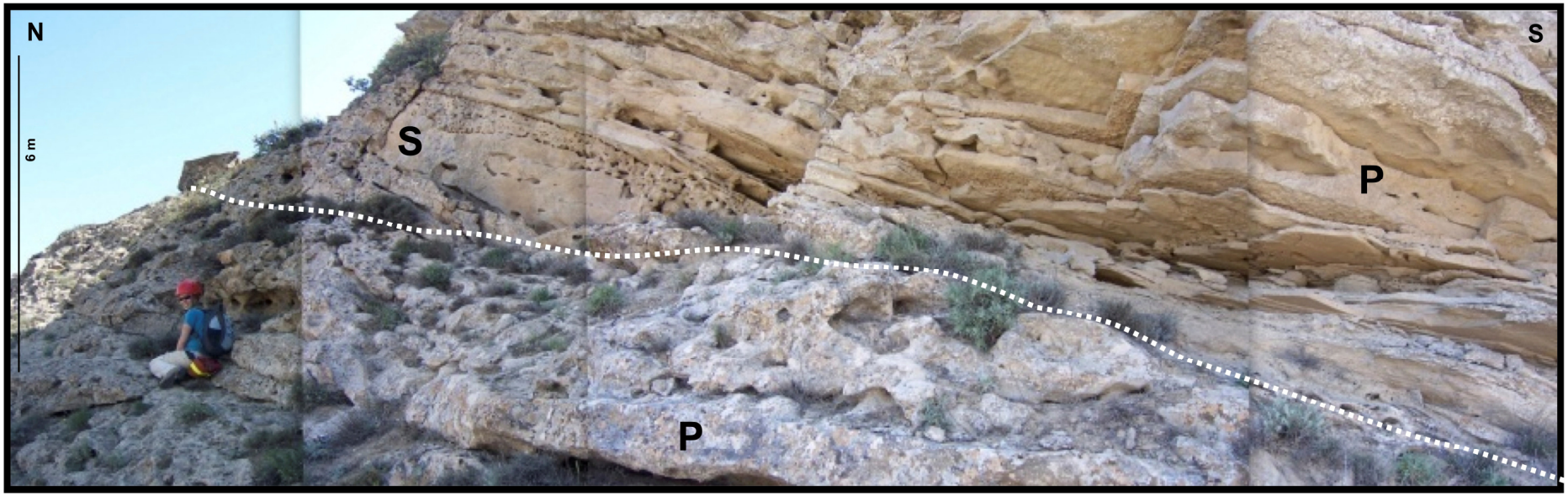

Figure 3.17 Photomontage showing FA4 type (high energy, coastal) facies, exposed along the northern tip of the Kerkesdag Anticline. Photo is annotated with an angular unconformity (dotted line), scalloped (S) and planer (P) bedding. Photo is taken at base of Log 2a, at 40°17'46.19"N, 49°37'34.34"E.

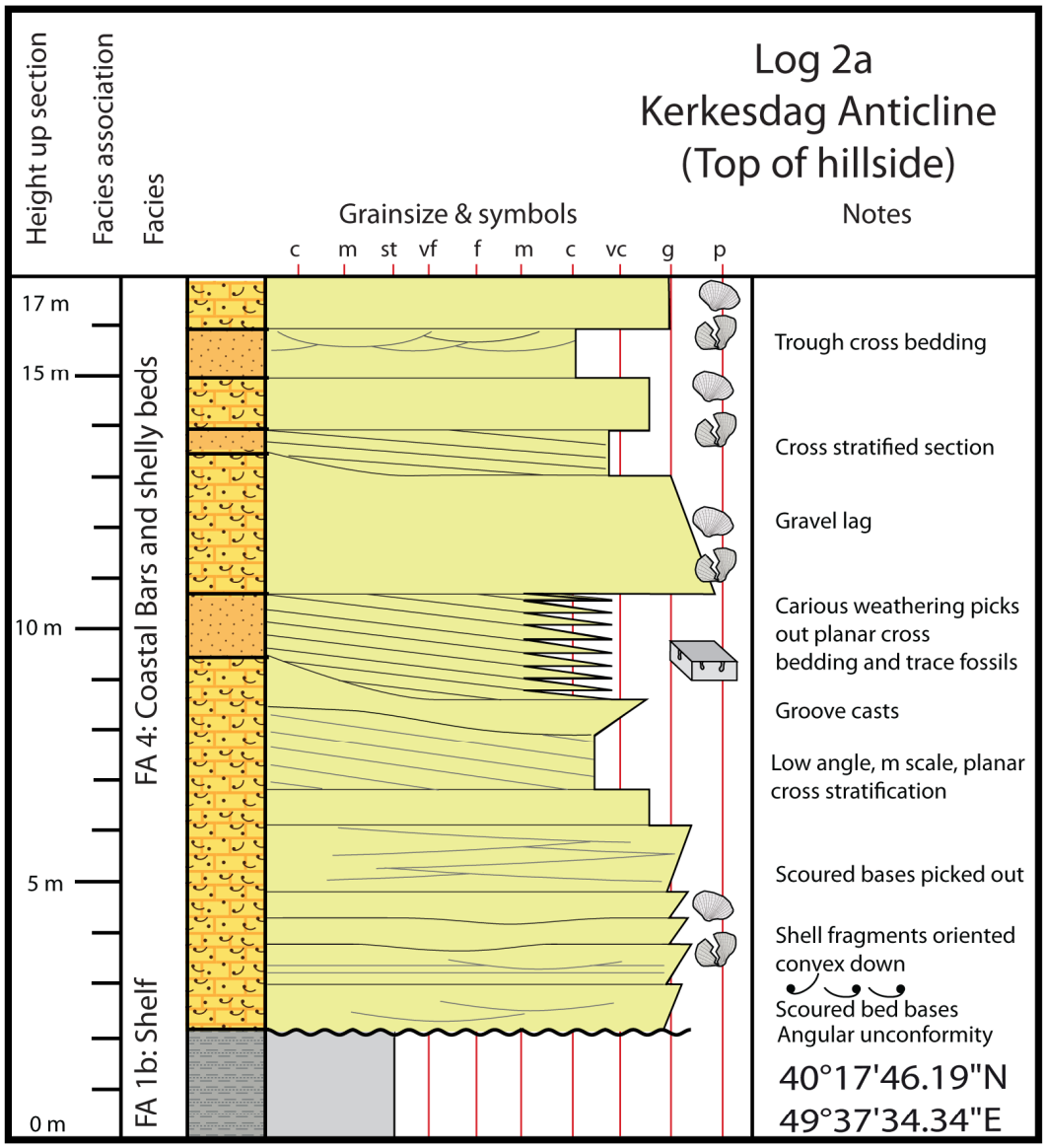

Name	Code	Fill	Name	Code	Fill
Mudstone, bedded	M_B		Sandstone, coarse shelly	Sn_{CS}	
Mudstone, faintly lamnated	M_{LF}		Sandstone, with muddy drapes	Sn_{MD}	
Mudstone, silt laminated	M_{St}		Muddy sandstone	Sn_M	
Ash tuff	Tf_A		Coquina, muddy matrix	Cq_M	
Siltstone, oscillatory grading	St_O		Coquina, carbonate matrix	Cq_C	
Sandstone, oscillatory grading	Sn_O		Coquina, sandy matrix	Cq_{Sn}	

Figure 3.18 Type log of facies association FA4.

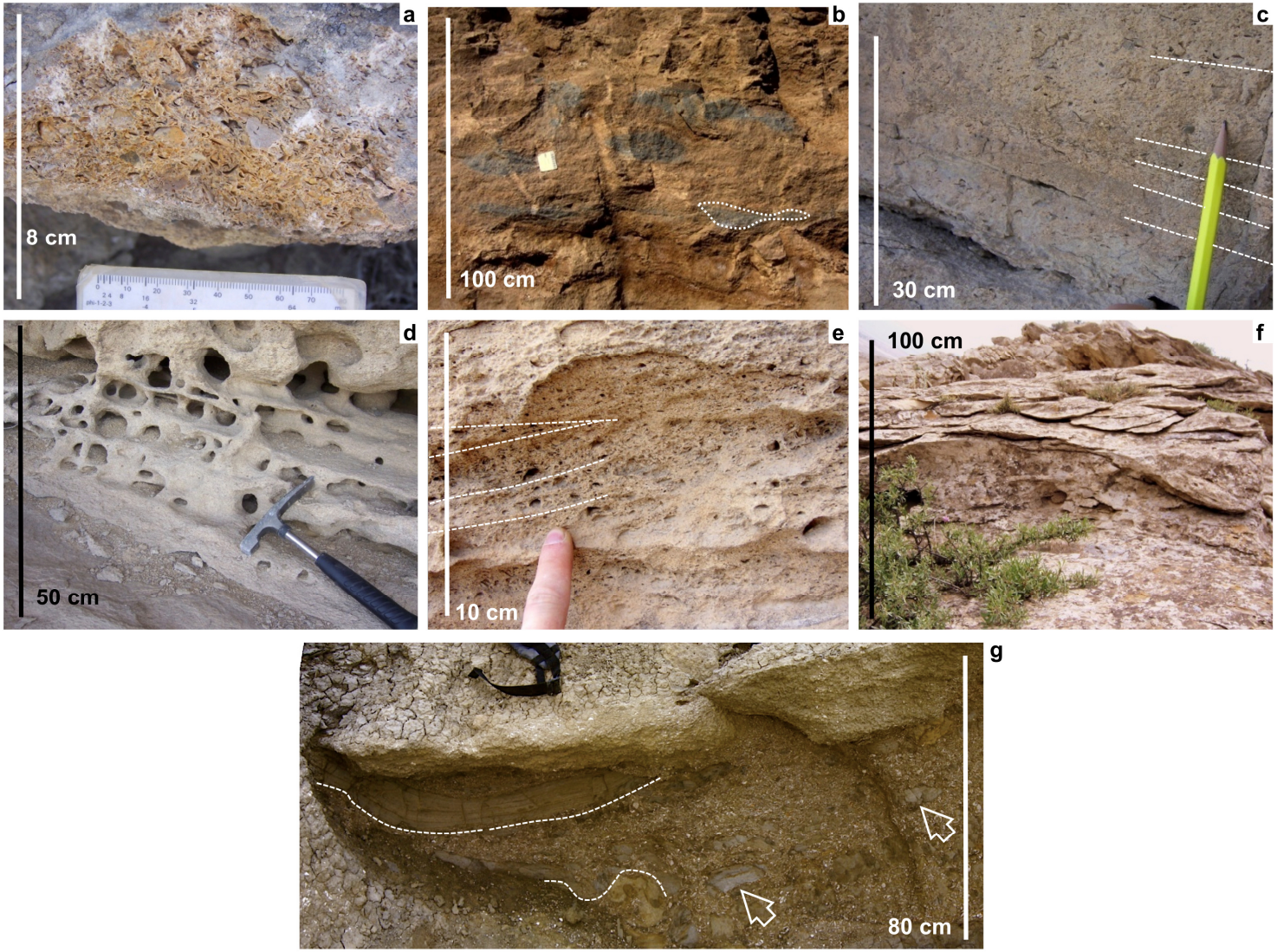

Figure 3.19. Field photos of FA4 and minor FA1 and FA2 type facies: [a] Close up of CqC, coquina, predominantly consisting of carbonate matrix, which shows aragonite dissolution moulds of bivalve fragments. [b] dark grey mottling to CqC (picked out by white dotted line). [c] Faint horizontal lamination in CqC. [d] Horizontal lamination in SnCS and CqC, carious weathering picks out vertical structures, interpreted as burrows. [e] faint cross lamination in CqC. [f] Trough cross bedding in CqC picked out by weathering. [g] Muddy contorted Cq_M coquina FA1 interbed. The bed is disharmonically folded (dashed lines) and contains blocky layers of mudstone within it (arrows).

Stacking patterns, lateral correlation of logs and lake level fluctuations

Marker beds of coarse sands and coquinas (FA3 & FA4 facies associations) —referred to simply as 'sand beds', below— were mapped out over the folds and the wider study area with the aid of GoogleEarth satellite imagery (Figure 3.20 a – c). Coarse logs were constructed down each fold flank which record the approximate thickness of FA1 facies associations and the relative locations of the sandy marker beds (Figure 3.20 d). Correlations between shorter graphic logs from each hillside (e.g. Figure 3.5) were made by comparing facies association stacking patterns and marker beds from the hillside exposures (Figure 3.20 a – c, Figure 3.22).

DESCRIPTION: the majority of the roughly 500 m of stratigraphy exposed along the Quaradag anticline consists of offshore muds. It contains 5 sand marker beds. The oldest two sand beds are restricted to the northern tip of the fold and pass southwards (basinwards) into FA1 muds. (Figure 3.20 a). Two younger sand beds form a cap rock across the top of the hillside, and are separated from the lower sands by 130 m of muds, and from each other by between 20 – 50 m. Their full lateral extent is not visible but they extend at least 1700 m further to the south (basinwards) than the lower two. A fifth sand bed, is exposed at the southern tip of the anticline.

The Kerkesdag anticline shows a similar pattern (Figure 3.20 b), consisting mostly of FA1 muds. A sand bed of FA4 type lithofacies lies across the northern peak of the hillside along an angular unconformity. It dips to the south, and transitions laterally into FA1 muds to the South (shorewards). Large segments of the sand body lie out of *situ* along the northern tip of the anticline (shown in green on Figure 3.20 b). Another 100 m of mud separates this sand bed from a further three sand beds lying over the southern peak, each individually separated by 30 – 50 m of mud. These are similarly tilted, but their lateral extent is not visible.

The Yasamal Anticline contains 8 sand bodies which are vertically separated by 30 – 50 m, and tilted towards the south (Figure 3.20 c). Satellite imagery (Figure 3.23) shows the beds passing laterally into FA1 muds to the North (basinwards), and the lateral terminations of the beds shifting to the south (basinwards).

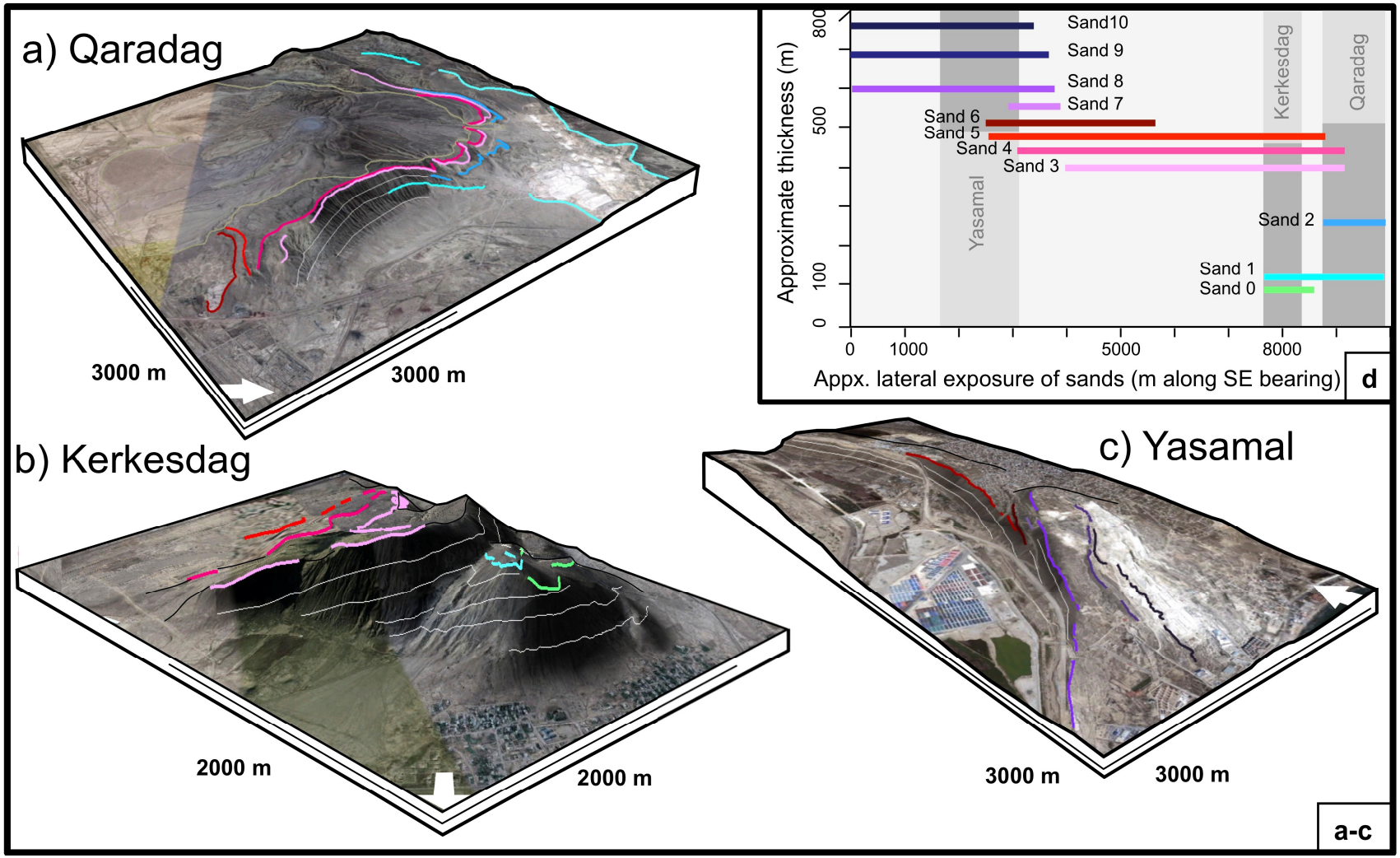

Figure 3.20 Projections of hillside exposures, annotated to show the relative position of sand beds (sections of FA3 and FA4 type facies). [a – c] perspective views over all three localities. Satellite imagery and elevation data property of GeoEye, TerraMatics and DigitalGlobe (2011). [d] Chart showing lateral position and relative height of each sand bed and hillside. *To be printed on A3 landscape oriented paper*

INTERPRETATION: The portion of the Apsheron Formation examined in this thesis is broadly divided into a 'deep lake' section and a 'shallow lake' section. Mud-dominated FA1 facies from the offshore shelf lie at base of the succession, whilst a higher abundance of coarser shelly and sandy FA3 and FA4 lithofacies (shallower, coastal environments) characterise its upper part (a).

The formation can be further subdivided into 'sequences': relatively conformable successions of genetically related strata, bound by unconformities and their correlative conformities. Each sequence consists of several shorter 'parasequences': conformable packages of genetically linked strata bound by abrupt flooding surfaces following the terminology outlined in Van Wagoner *et al*., (1988) and Catuneanu *et al*., (2009). The sandy marker beds used to construct the correlation panel of Figure 3.22 are comprised of relatively shallow water facies associations (Figure 3.4) which lie between relatively deep water FA1 facies. These sandy marker beds are therefore interpreted —in the 'deep lake' section of the Apsheron Formation at least— as low-stand systems tract deposits (Figure 3.21).

This interpretation is markedly different to the Productive Series. Productive Series which have the opposite correspondence to palaeo lake levels than this study proposes for the Apsheron Formation. The Productive Series are interpreted as fluvial floodplain deposits; sandstones represent humid periods of high runoff and high lake levels, whilst mudstones in the productive series represent low river activity and arid lake low-stands (Hinds *et al.*, 2004). However, Productive Series muds are crucially different to those in the Apsheron Formation as they contain desiccation cracks and rootlets, indicating low water levels and subarial exposure (Hinds *et al.*, 2004). A deep water depositional environment interpretation of the Apsheron Formation muds is supported by [1] extensive vertical and lateral continuity of mud units, [2] marine molluscs and trace fossils, [3] preservation of fragile laminations and ash beds.

Three sand beds from the lower 'deep lake' section of the Apsheron Formation, which are exposed along the Kerkesdag and Quaradag anticlines (sand bed 1, 2 and 3) denote the stratigraphic position of 3 low-stand systems tracts and their associated stratigraphic sequences (sequence 1, 2 and 3). The first sand bed (sand bed 1) is deposited on top of FA1 muds over an angular unconformity. This indicates that there was erosion of uplifting, or tilted beds along the Kerkesdag Anticline prior to the sand's deposition. Sand bed 1 is therefore interpreted to have been deposited during the early stages of lake level rise (Figure 3.23), similar to present-day coquina terraces along the Caspian coast (Kroonenberg *et al.*, 2000).

Sand bed 2, associated with low-stand 2 is only present along the Quaradag anticline and is absent along the Kerkesdag anticline. Kerkesdag lies at a more distal palaeo location (further to the south east), than Quaradag, and the absence of low-stand sands is interpreted to reflect a deep palaeoenvironment which remained mud-prone both before and during low-stand 2 (Figure 3.20). The regression of sequence 2 is therefore interpreted as smaller in magnitude than the regression of sequence 1.

Sand bed 3 represents a significantly larger magnitude low-stand. It extends over a much larger lateral area towards the coast than the previous two sand beds (Figure 3.20 d) and indicates a basinwards shift of the shoreline and the largest magnitude lake level drop observed in the formation.

The sand beds in the upper section of the Apsheron Formation repeat at a shorter vertical spacing (20 – 40 m) than in the lower half of the formation (100 m) Figure 3.22). This change in sedimentary style is interpreted as an effect of low relative water levels, which followed the major regression of sequence 3. The sedimentary environments during this 'shallow lake' section of the formation are interpreted to have been close to storm and fair-weather wave base, such that low amplitude, high-frequency changes in the South Caspian lake level curve — parasequences— were sufficient to alter the sedimentary regime from muddy suspension settling processes to sandy wave and storm dominated processes. The parasequences step basinwards (Figure 3.20) and become thinner up section Figure 3.22) indicating further progradation of the basin margin, shallowing of the lake level, and reduction of accommodation space.

Within this upper Apsheron Formation 'shallow lake' section, a low-stand and transgressive systems tract is speculatively interpreted around a 60 m thick mud section, which divides this section into two further sequences (sequences 4 and 5 in Figure 3.22).

Parasequences did not alter sedimentation in the same way in the lower 'deep lake' section of the Apsheron Formation because this deep-water palaeo environment was relatively insensitive to low amplitude lake level changes. However, parasequences may be represented by the 50 m-scale colour banding, observed the in FA1 muds (Figure 3.6), which reflect alternating energy conditions and therefore possibly subtle lake level changes. The gamma ray logs collected through the Quaradag and Kerkesdag anticlines also show fluctuations at a similar scale Figure 3.22 a) which may be indicative of up-section changes in fine grained lithic content, and organic matter preservation (e.g. Schmoker, 1981), and ultimately related to fluctuating palaeolake level.

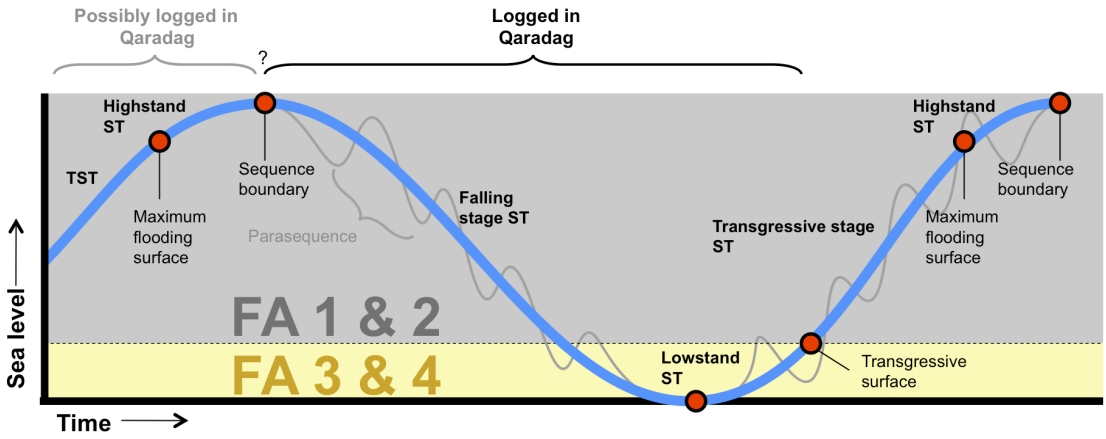

Figure 3.21 Relationship between facies associations and relative lake level. Blue line shows the lake level curve associated with sequences, the grey line shows fluctuating parasequences. Systems tracts are abbreviated to 'ST'.

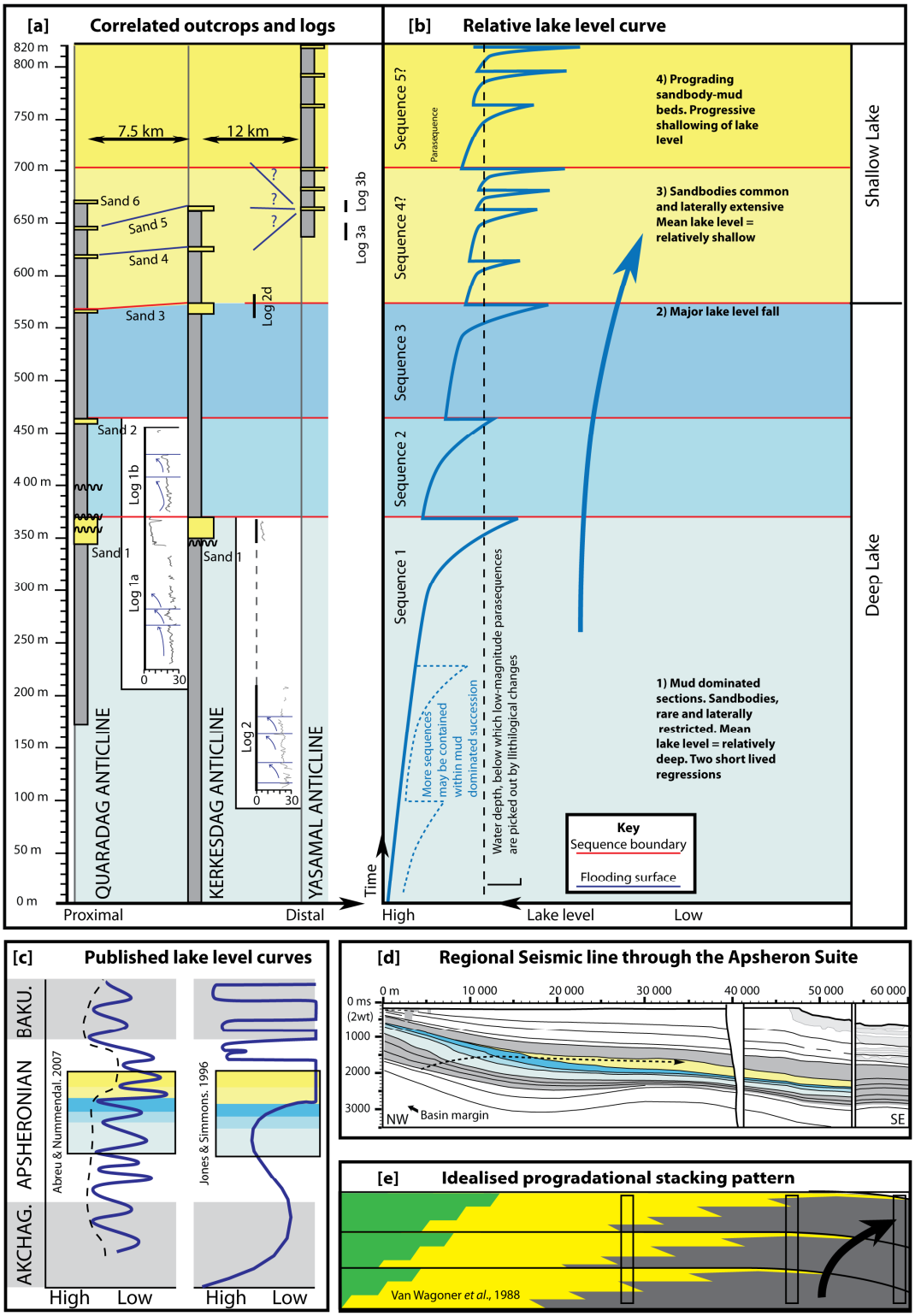

Figure 3.22 Summary of field data and interpretations. [a] All sedimentary logs, in relative stratigraphic order, showing correlated sand bodies. [b] Constructed relative lake level curve, based on depositional environments (Figure 3.4) and lateral extent and position of sand bodies (Figure 3.20). [c] Published lake level curves from Jones and Simmons (1996) and Abreu and Nummendal (2007), matched to this study's constructed relative lake level curve. [d] Seismic stratigraphy along the South Caspian Basin margin (chapter 2), a large regression is also observed in the seismic data, coloured in yellow. [e] idealised progradational parasequence stacking patterns from Van Wagoner *et al.*, (1988). Colour changes represent, terrestrial, proximal and distal sediments.

3.4. DISCUSSION

Correlation with regional lake level curves and dating of outcrops

Two published lake level curves exist for the Apsheronian constructed from environmentally sensitive biota (locations unknown, from Jones & Simmons, 1996). and seismic stratigraphy along the Kura palaeo delta (Abreu & Nummedal, 2007). The Abreu and Nummendal (2007) curve has been modified in this study based on evidence discussed in chapter 2 (Appendix 1). The seismic stratigraphy derived curve is higher resolution, yet both curves show a broad transgressive trend throughout the Apsheronian and a large magnitude lake level drop in the upper half of the formation. This trend also agrees with the basinwards migration (south-eastwards) of the Apsheronian palaeo offlap break (Figure 3.1 c) and the overall shallowing trend identified in the outcrops Figure 3.22 b). A correlation can therefore be proposed between the onshore outcrops and the published curves; each indicates a period of regression followed by low relative lake levels during the middle Apsheronian. Absolute dating of the outcrops using these data is impossible however, as both published curves disagree on the age of the Apsheronian, and don't conform to the most recent age range estimates (see chapter 1).

Age dating is a problem throughout much of the Caspian Pliocene-Holocene succession and this study highlights possibilities for further research. The nearest dating 'spikes' come from ash bands taken from the Akchagyl Formation which are dated 3.4 Ma (Devlin *et al.*, 1999) and the upper part of the Apsheron Formation, Dated at 0.96Ma (Kroonenberg *et al.*, 1997). The Precise nature of the dating is obscure and the original reference is not published. Informally, the base of the Apsheronian is distinguished from the lithologically similar, older Akchagyl Formation by the absence of ash bands (Mark Allen, pers. comm. 2008). However, the Apsheron Formation clearly contains abundant ash throughout. The possibility exists therefore for detailed tephachronological dating of the formation (e.g. Westgate & Briggs, 1980) which would elucidate the existing dating problems. Another source of dating could come from mollusc biostratigraphy, which has been defined for the Pleistocene Paratethys (Nikiforova, 2004; Osipova, 2009).

Climatic controls on sedimentology

The Caspian Sea has a long history of frequent and high magnitude water level fluctuations (Kroonenberg *et al.*, 1997). Pre-Apsheronian transgressions were a mixture of wet dry – cycles (Hinds *et al.*, 2004) and eustacy. However, since the Apsheronian the Caspian 'Sea' has been an internally drained basin, unconnected to the world's oceans, with lake level primarily governed by the balance between continental runoff and evaporation (Degens & Paluska, 1979). Endoheric depositional systems such as this are highly sensitive to climatic forcing (Fischer & Bottjer, 1991), and Milankovic scale cyclicity has been reported in younger Caspian sediments (Kroonenberg *et al.*, 1997). Evidence for climatic controls is therefore anticipated in field outcrops of the Apsheron Formation.

The exact mechanism of climatic control on Caspian lake level is disputed: Jones and Simmons (1996) present two opposing models, based on pollen data, and magneto-stratigraphy, which are expanded upon by Van Baak (2010) (Table 3.2). Apsheronian and later lake levels fluctuated at similar rates to contemporary eustatic records (e.g. Zachos *et al.*, 2001), but it is unclear whether the arid – humid cycles were coincident with the global eustatic sea level curve. This study does not provide evidence to support one theory over another, but favours a model where river runoff and lake level are highest during interglacial periods. Such systems have been documented in other endoheric lakes (e.g. Benson & Thompson, 1987; Juhász *et al.*, 1997) and has been argued for in chapter 2. The ultimate model relies on a robust age control, which is claimed by proponents of both models (Mamedov, 1997; van Baak, 2010) but is notably poor in the Para-Tethys Plio – Pleistocene stratigraphy.

Onshore exposures of the Apsheron Formation form, in their entirety, a progradational, shallowing-upwards succession greater than 850 m thick (Figure 3.22). An identical trend at a similar scales is visible in offshore seismic data (Abdullayev, 2000; Abreu & Nummedal, 2007; Kalani *et al.*, 2008) and from palaeo environmentally sensitive ostracod data (Jones & Simmons, 1996). One proposed explanation for this shallowing trend through the Apsheron Formation is that regional tectonics lowered and opened a waterway to the east of the Caspian Sea, the 'Manych Strait' which prgressively drained the Caspian Lake into the topographically lower Black Sea (Kroonenberg *et al.*, 1997; Zubakov, 2001 27; Nikiforova, 2004). The evidence that this waterway was active or present during the Pleistocene is disputed however, as the Manysch area was tectonically uplifting during this period (Mamedov, 1997). Alternatively the observed trend is interpreted as a gradual climatic shift from wetter to dryer conditions as the lake slowly shrank; this is based on pollen palaeoclimate interpretations which show a gradual cooling trend through the Apsheron Formation (Nikiforova, 2004).

Climatic controls on the Apsheron Formation at outcrop scale may be inferred from a repetitive colour pattern, 50 m thick, of successive dark (greys and greens) and light (browns and oranges) beds of mudstones. The Kerkesdag anticline, the longest record of banded muds in this study area, contains 13 of these bands (Figure 3.6).

	Model A Lake level follows global sea level trend		**Model B** Lake level opposes global sea level trend	
Global eustacy	Glaciation	Deglaciation	Glaciation	Deglaciation
Climatherm	'Cold' (arid)	'Warm' (humid)	'Cold'	'Warm'
Caspian lake level	Fall	Rise	Rise	Fall
Mechanism	Cool climate freezes rivers, reducing runoff into lake. Riverine runoff reduces at higher rate that reduction in evaporation (which also falls due to cooling). Lake level falls.	Rivers are rejuvinated during interglacials, runoff increases at higher rate than evaporation increase. Lake level rises.	Rivers flowing northwards, away from the Capsian, into the Arctic Sea are blocked by ice sheet. Ponded rivers form glacial lakes along ice sheet margin which overflow and spill southwards into the Caspian Sea. Lake level rises	Less water enters the Capsian as northward flowing river network is re-established. Higher temperatures also increase evaporation. Both contributeing to lake level lowering.

Table 3.2 Opposing climate models that have been proposed for the Caspian Sea

The cyclical nature of the mud colour changes is suggestive of a climatic link (Scholz, 2002; Tucker, 2003). The colour of mudstone is determined by its composition, depositional environment diagenesis, and chemical composition (Hosterman & Whitlow, 1980; Potter *et al.*, 1980; König *et al.*, 1997). The ratio of iron in its oxidised and reduced state (Fe^{3+}/ Fe^{2+}) is the primary variable determining whether mudstones are shades of red/brown (high) or green/grey (low) irrespective of iron content (McBride, 1974). The amount of organic carbon is also important; reddish mudstones contain lower amounts of organic carbon than greys or blacks (Grim, 1951; McBride, 1974; Hosterman & Whitlow, 1980; Potter *et al.*, 1980). Both redox state, and the amount of organic carbon are related to oxygen levels of the depositional environment —determined by water depth, lake bed topography, sedimentation rate, water movement and bacterial action (Grim, 1951) — and in rare cases by the primary composition of the sediment (Potter *et al.*, 1980).

Sediment deposited along the NW South Caspian Basin margin was transported throughout the Apsheronian, by the long-lived Kura- and 'Baku' palaeodeltas, (Hoogendoorn *et al.*, 2005; Abreu & Nummedal, 2007) draining from the Lesser Caucasus Mountains (Morton *et al.*, 2003). These deltas remained active throughout the lower-middle Apsheronian (Chapter 2), so the colour banding observed along Apsheron Formation outcrops is unlikely to represent repetative and cyclical changes in the sediment source or primary composition.

This study suggests a climatic control mechanism which involves periodic water column stratification and mixing, primarily determined by the temperature of the water entering the lake (e.g. Reading & Collinson, 1996). During climatically warm periods, warmer, less dense runoff entered the lake creating a thermally stratified water column and reducing conditions along the palaeolake bed. This would have resulted in sedimentation of green (chlorite and glauconite) and dark grey (preserved organic carbon) mudstones. During cooler periods, colder surface runoff waters mixed with bottom waters more readily resulting in oxidising lake bed conditions and orange or yellow shaded mudstones (haematite and goethite).

The Apsheron Formation represents a time period of between 0.9 and 1.78 million years in it's entirely (Figure 3.2). Any age estimate of the successions examined in this study without a magnetostratigraphic, biostratigraphic or geochemical control is extremely speculative. However if one uses published lake level curves (Jones & Simmons, 1996; Abreu & Nummedal, 2007) then approximately half of the Apsheron Formation thickness has been mapped in the 850 metres of sediment exposed onshore. If the mud-colour cycle is climatically and orbitally forced, then a Milankovic *scale* frequency of 41.000 years, corresponding to changes in the earth's precession (Zachos *et al.*, 2001) is certainly not implausible, and matches well with where the outcrops are placed in the overall Apsheronian succession (Figure 3.23, Table 3.3)

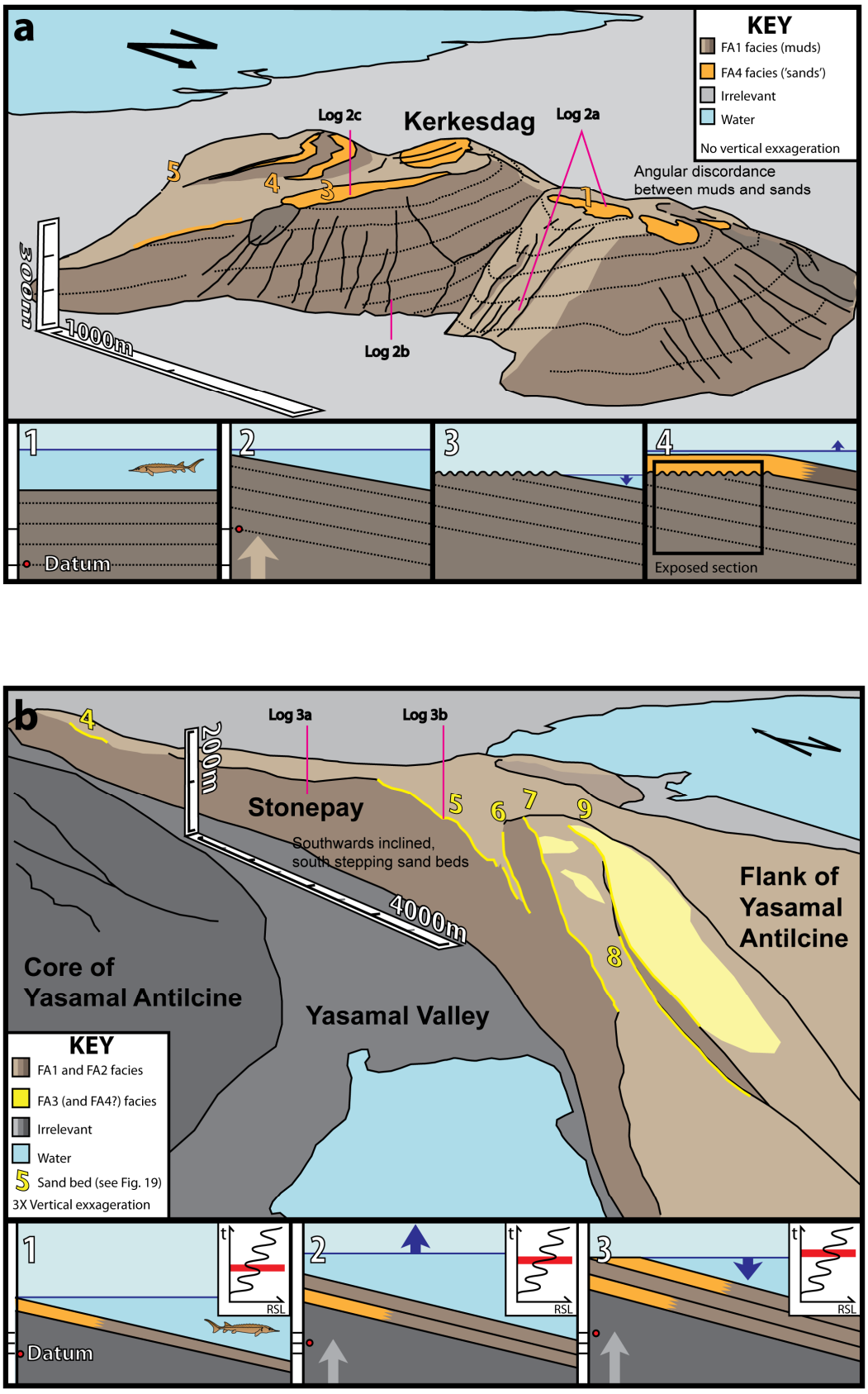

Figure 3.23 Two types of stacking pattern related to differing interactions between depocentre uplift and relative lake level changes

Sedimentary process	Observed in		Occurrence		
	Data	Location	Age range	Amount	notes
Sand - Mud successions	Outcrop and sattelite data	Basin margin, shelf	Intra - Apsheron Formation, extensive	14	5 seen in outcrop, extrapolated to 14 over entire Apsheron Formation
Brown-Grey mud couplets	Outcrop data	Basin margin, shelf	Intra - Apsheron Formation, limited	34	50 m frequency observed in outcrop, extrapolated to 34 over entire formation

Apsheron Formation, age estimates			
Publication	From (Mya)	To (Mya)	timespan (My)
Jones & Simmon 1996 (max), Allen et al., 2002	1.6	0.7	0.9
Van Baak 2010 (min estimate)	1.8	0.9	0.9
Devlin *et al.*, 1999	1.85	0.7	1.15
Van Baak 2010 (max estimate)	2	0.9	1.1
Fowler *et al.*, 1999 (min estimate)	2.28	1.04	1.24
Fowler *et al.*, 1999 (max estimate)	2.47	0.97	1.5

Expected orbital cycles within the Apsheron formation			
Axial precession 23,000 years Cycles	Obliquity 41,000 years Cycles	Eccentricity 100,000 years Cycles	Eccentricity 400,000 years Cycles
39.1	22.0	9	2.25
39.1	22.0	9	2.25
50.0	28.0	11.5	2.875
47.8	26.8	11	2.75
53.9	**30.2**	**12.4**	3.1
65.2	**36.6**	**15**	3.75

Expected orbital cycles, Apsheron-Present			
Axial precession 23,000 years Cycles	Obliquity 41,000 years Cycles	Eccentricity 100,000 years Cycles	Eccentricity 400,000 years Cycles
69.6	39.0	16	4
78.3	43.9	18	4.5
80.4	45.1	18.5	4.625
100.0	48.8	20	5
99.1	55.6	22.8	5.7
107.4	60.2	24.7	6.175

Sedimentary process	Observed in	
	Data	Location
Sand - Mud successions	Outcrop and sattelite data	Basin margin, shelf
Brown-Grey mud couplets	Outcrop data	Basin margin, shelf

Climatic characteristics			
Repetative?	Eavenly spaced?	Regionally synchronous?	Climate is known to affect this sedimentary process
yes	yes	?	?
yes	yes	?	?

Interpretation	
Climatic?	Closest orbital cycle
likely	41,000 year obliquity
likely	100,000 year eccentricity

Table 3.3 Comparison chart of repetitive events observed in this study (top), published ages of the Pleistocene South Caspian succession (middle) , and possible Milankovic cyclicity (bottom)

Tectonic controls on sedimentation

Folding driven by the compression and subduction of the South Caspian Basin (Jackson *et al.*, 2002) was initiated prior to the Apsheron Formation and accompanied its deposition. Offshore syntectonic strata are dated as Akchagylian – present-day (Devlin *et al.*, 1999 and chapter 2) and even older estimates are reported onshore (Souque *et al.*, 2010). Controls of the active folding on sedimentation at the field scale are therefore anticipated.

Previous studies in tectono-stratigraphically comparable settings summarise these effects:

1) Fold growth influences the geometry of syntectonic strata packages creating progressive onlap wedges which thin towards the fold hinge, and contain progressively steepening beds. These effects become more obvious towards the fold hinge (Castelltort *et al.*, 2003).

2) Fold activity modifies and generates locally driven 'autogenic' sedimentary processes (Hampson, 2010). The fold forms a topographical barrier to sediment transport and deflects palaeo currents from wave and wind generated currents to hinge-parallel orientations (Burbank *et al.*, 1996; Morley, 2009), whilst at a seismic scale, fold growth and limb steepening promotes large scale sediment remobilisation and removal via slope failure (Heinio & Davies, 2006).

3) Fold activity locally alters relative base level, exerting a control on, depositional environments, lithofacies and stratigraphy. Lateral and vertical lithofacies changes show a bias towards shallower palaeo environments along fold flanks and hinges (Castelltort *et al.*, 2003) and above angular 'progressive unconformities' (see chapter 2) caused by fold uplift (Gawthorpe & Hardy, 2002). Increased fold activity generates 'tectonically enhanced forced regressions' —sequence boundaries driven by local base level reduction and coincident with regional tilting events (Gawthorpe *et al.*, 2000). Reduction of accommodation space by fold amplification results in progressively thinner sequences (Castelltort *et al.*, 2003).

Evidence for tectonic controls in the Apsheron Formation is limited. In the lower portion of the formation, along the Kerkesdag and Quaradag anticlines, wedged strata are observed (Figure 3.14) but persistent, repetitive down-section steepening of bedding (e.g. Gawthorpe & Hardy, 2002) is not (Figure 3.5). Fold hinges are oriented normal and oblique to the E,SE – W,NW trending coastline (Figure 3.1 d), but show little evidence of deflecting sediment pathways; structurally corrected palaeocurrent data shows predominantly shore parallel orientations (Figure 3.5, Figure 3.12, Appendix 5) implying unrestricted flow over the fold crests. An apparent 'tectonically enhanced forced regression' (e.g. Gawthorpe *et al.*, 2000) , lies along the Kerkesdag anticline; shallow water lithofacies overlie an angular unconformity (a, Figure 3.23a). However, correlated sandy beds from the adjacent Quaradag anticline lie conformably over deeper facies associations, even lying beneath a younger progressive unconformity, not above it (a), indicating that along the Kerkesdag anticline lake level fell prior to tilting and that the change in lithofacies was not tectonically forced. Both tilting events are overlain by a thick pile (100 – 200 m) of offshore muds Figure 3.22 a, and b), demonstrating that fold uplift was comparatively small compared with the vertical range of lake level. A subsequent transgression outpaced and drowned both the uplifting folds.

At least in the lower half of the Apsheron Formation regressions were therefore probably not tectonically forced, but coincident with a climatically-driven lake level drop that merely amplified its effects around the Kerkesdag anticline, and completely outpaced the uplift along the Quaradag anticline. The anticlines uplifted relatively slowly compared with sedimentation rates and developed little surface expression. They may well have been similar to the current configuration of the Shah Deniz anticline (see chapters 2 and 4) (Fowler *et al.*, 2000), which lies close to the present basin margin clinoform complex, and is almost completely buried, as sedimentation rates are far greater than uplift along the fold (see chapter 4).

Higher in the Apsheron Formation, along beds of the Yasamal anticline there is a stronger case for tectonically forced or modified regression as successive sand bodies show a gradual progradational shifting of sedimentation to the south (basinwards), away from the fold hinge (Figure 3.23 b). This may show a climatically forced, progradational, regressive trend, but could also be driven, or at least modified, by growth of the Yasamal Anticline which was actively uplifting during the Apsheronian (Allen, pers. comm. 2010). The sediment packages become thinner up section suggesting a progressive reduction of accommodation space, either resulting from progressively falling lake levels or the uplifting lake margin.

Summary: Fold growth vs. climate forcing

Tectonic and climatic processes are identified in Apsheron Formation outcrops. Climatic signals are interpreted from 25 – 50 m-scale colour banding in FA1 dominated successions. In the lower half of the formation, tectonic effects are subdued suggesting that the Apsheronian sedimentation rate was much higher than fold uplift rates. The effect of folding on the Apsheron Formation was limited to post-depositional tilting of older beds. Higher in the formation, programing parasequences may be part of a tectonically enhanced regression, but clear evidence to support this is limited. The anticline was active during this time, but bedding appears conformable and does not show clear growth strata architecture. In summary, fold uplift was probably only a minor control on Apsheron Formation sedimentation, a shallowing trend onto which cyclical climate driven fluctuations are superimposed are interpreted as climatically driven.

3.5. CONCLUSIONS

The Apsheron Formation represents a series of depositional environments ranging from the coastal zone to offshore shelf. Sedimentation of offshore muds was dominated by suspension settling with minor reworking by bottom water currents. Proximal sandy and shelly lithofacies show wave and storm dominated nearshore depositional processes.

A gradual shallowing-upwards trend is interpreted in the Apsheron Formation. A regionally important regression separates the formation into a 'deep lake' offshore mud dominated section, and 'shallow lake', nearshore section characterised by extensive beds of coarser proximal facies. Lithofacies fluctuate on a 25 – 50 m-scale between coarse grained and muddy units.

Although the Apsheron Formation was deposited alongside during growing folds, this process evidently influenced sedimentation relatively little compared with many folded sedimentary basins elsewhere in the world. This is explained by high burial rates along the NW margin of the South Caspian Basin which outpaced uplift rates along the folds. Climate change was a far more influential control of sedimentation. Sequence boundaries were apparently climatically controlled, with no tectonically forced regressions. Further climatic controls suggesting 41.000 year Milankovic frequencies are interpreted from 25 – 50 m-scale mudstone coloured banding, which are interpret as alternating cool and warm periods.

Further research on the Apsheron Formation should focus on absolute dating of volcanic biostratigraphic or magnetostratigraphic data. Only once that is achieved can the hypotheses suggested by this study regarding the age of the formation, Milankovic forcing and climatic mechanisms on sedimentation be tested.

4. Mass Transport Deposits in Fold Growth Strata

4.1. INTRODUCTION

Submarine landslides, commonly termed 'mass transport deposits', are a widespread and fundamental process in shaping and infilling sedimentary basins. They are important as they: a) are potential geo-hazards (Hampton *et al.*, 1996; Locat & Lee, 2002); b) transport significant amounts of sediment to offshore areas (Hjelstuen *et al.*, 2007; Talling *et al.*, 2007); c) induce possible global climate change mechanisms via gas hydrate disassociation (Maslin *et al.*, 2004); and; d) are a consideration for hydrocarbon exploration, creating both drilling problems (Barley, 1999; Weimer & Shipp, 2004) and unconventional types of hydrocarbon traps (Weimer & Shipp, 2004; Butler & Turner, 2010; Mosher *et al.*, 2010). As a result, there is a growing interest in understating their causal mechanisms and morphological characteristics, which is aided by increasingly sophisticated seismic imaging (Frey-Martinez *et al.*, 2005; Bull *et al.*, 2009).

This study uses three dimensional (3D) seismic data from the western margin of the South Caspian Basin (Figure 4.1a), where active tectonics, exceptionally high sedimentation rates, rapid water-level fluctuations and mud volcanism, all contribute to a complex setting. This study describes syndepositional structures from a series of mass transport deposits and use these to interpret processes that occurred during submarine slope failure and emplacement. The syndepositional structures show complex strain, and several have not been described in this context before. This study also considers the kinematics of the South Caspian mass transport deposits, showing the influence of changing local topography on their evolution and speculate as to their triggering mechanisms.

Seismic interpretation of the South Caspian mass transport deposits provides insights into a fundamental sedimentary process that has affected much of the thick Quaternary sedimentary succession. Additionally, the basin margin is the focus of extensive hydrocarbon exploration and production (Devlin *et al.*, 1999), which mass transport deposits have the potential to influence by modifying and eroding the cover sequence, creating regional unconformities and by potentially destabilising offshore infrastructure. It has also been suggested that they may pose drilling hazards due to their gas hydrate content (Diaconescu, 2002).

Submarine slope failures and mass transport deposits

Submarine slope failures occur when down slope directed shear stresses, acting along inclined planar surfaces such as bedding planes, exceed the shear strength of the slope (Varnes *et al.*, 1978). Once failure commences, material is translated downslope above a décollement surface, termed a 'basal shear surface', and continues until the balance between shear stress and shear strength is restored. Upon the initiation of failure, deformation radiates from a point source with compressive deformation of the moving mass progressing downslope and extensional deformation 'retrogressing' upslope (Farrell, 1984). The slope failure grows and increases in volume by the downslope accretion and upslope incorporation of slope material into the translated mass. Geological processes which promote subaqueous slope failure are extensively discussed in Varnes (1978) and Locat & Lee (2002) and summarised in Appendix 8. Slope failure is rarely triggered by a single process, but is preceded by one or more 'primers' that gradually reduce the ratio between slope strength and shear stress. The ultimate 'trigger', such as an earthquake, often remains elusive in the geological record (Varnes *et al.*, 1978; Davies & Clark, 2006).

Many different classification schemes exist for submarine slope failures (e.g. Carter, 1975; Varnes *et al.*, 1978; Nemec, 1990; Martinsen, 1994; Mulder & Cochonat, 1996; Weimer & Shipp, 2004; Frey-Martínez *et al.*, 2006; Moscardelli & Wood, 2008), and specific nomenclature often differs between studies. This paper uses the terms 'mass transport deposit' for the sediment package emplaced during a slope failure and 'mass transport complex' where multiple slope failures have coalesced into a larger unit (e.g. Gamberi *et al.*, 2011). The three terms 'slump', 'slide' and 'debris flow' describe individual sections of larger mass transport deposits or deposits, which display characteristic seismic facies and syndepositional structures (e.g. Moscardelli & Wood, 2008). Submarine slope failure differs from other gravity-driven sedimentary processes such as turbidity currents, as the remobilised strata deforms plastically or at least semi-plastically, during emplacement, whereas turbidity currents behave as a Newtonian fluid (Nemec, 1990).

A mass transport deposit can be arranged into idealised structural domains displaying characteristic kinematics and strain (Lewis, 1971; Bull *et al.*, 2009): an 'extensional domain' is located at the head of the failure containing predominantly extensional strain and a volume reduction relative to the stable slope, a 'translational domain' in the middle containing relatively undeformed strata, and a 'compressive domain' at the toe of the failure containing contractional strain and a height increase with respect to the stable slope. This tripartite scheme is idealised and breaks down at large scales; larger, mass transport complexes, consisting of several coalesced deposits, often display multiple (>3) domains (Martinsen, 1994; Gardner *et al.*, 1999), but it is nevertheless still a practical way of organising structures within a population of failures.

Geological setting

The South Caspian Basin, the southernmost portion of the present-day Caspian Sea, probably formed as a back arc basin, north of the Tethys Ocean, although the age of its formation is disputed with estimates covering the Jurassic to the Palaeogene, whilst further disagreement exists regarding the nature of its basement, which is commonly interpreted as oceanic crust (Vincent *et al.*, 2005). The basin lies within the Arabia – Eurasia collision zone, The South Caspian Basin behaves as an aseismic block, encircled by active orogens. The convergent tectonic plate motions are accommodated by compression and strike slip in the Zagros, Alborz and Caucasus Mountains, and the subduction of the South Caspian Basin beneath the Mid Caspian Basin along an incipient accretionary prism, the 'Apsheron Ridge' (Jackson *et al.*, 2002; Allen *et al.*, 2003; Allen *et al.*, 2004; Guest *et al.*, 2007b; Ballato *et al.*, 2008).

A combination of tectonic subsidence, high sediment supply from rising mountain ranges and the focussing of rivers into the basin, has resulted in one of the thickest sedimentary successions in the world; Pliocene – Quaternary strata are up to 10 km thick (Knapp *et al.*, 2004). This study focuses on the Pleistocene to present-day, lacustrine, sedimentary succession, which is approximately 3 km thick (Allen *et al.*, 2002). It follows a broadly regressive trend (Jones & Simmons, 1996) and is dominated by mud with shallower interbedded silt and sand becoming significant from the base of the Quaternary onwards (Devlin *et al.*, 1999) (Figure 4.1b). Regional seismic lines show Pleistocene – present-day sedimentation at the basin margins characterised by several large clinoform deposits (Abdullayev, 2000; Abreu & Nummedal, 2007).

Belts of folds associated with the compressive margins are detached on overpressured Oligo – Miocene mud (Figure 4.1b) which escape to the surface via numerous mud volcanoes (Fowler *et al.*, 2000; Stewart & Davies, 2006). Many of the anticlines host hydrocarbons from a regional Oligocene – Pliocene play (Devlin *et al.*, 1999; Katz *et al.*, 2000). This study presents seismic data from two folds in the Azeri portion of the South Caspian Basin: the Azeri Chirag Gunashli (ACG) structure and the Shah Deniz Anticline. The ACG structure lies along the Apsheron Ridge, the Shah Deniz anticline lies to the south, adjacent and tangential to the basin's western margin (Figs. 1a and c). A clinoform deposit has prograded over the Shah Deniz anticline, burying it and reducing its topographic expression on the lake bed. Both folds have been active since the Late Pliocene (Fowler *et al.*, 2000).

The Caspian 'Sea' has been periodically connected to the world's oceans via the Black and Aral seas, however since the Pleistocene it has largely been isolated from the world's ocean systems (Jones & Simmons, 1996), forming the world's largest endoheric lake. Terminology in this paper reflects this; 'lake level', rather than 'sea level', and 'lake bed' rather than 'seabed', is used.

4.2. DATA AND METHODS

Three dimensional (3D) seismic data provide one of the most effective methods of studying mass transport deposits as they sample deep into the subsurface, providing high spatial resolution and the ability to visualise both the external and internal volume of a deposit (Frey-Martinez *et al.*, 2005). This study uses two industry 3D seismic surveys, covering an area of approximately 1000 km2 each (Figure 4.1a). Processing steps include f-k filtering, depth conversion and automatic gain control (see Liu & Goulty, 1999; Brown, 2004). The data are displayed in normal polarity (an increase in acoustic impedance is a red – black – red reflection loop). Inline spacing in the ACG and Shah Deniz surveys is 12.5m. The average vertical resolution (quarter of the wavelength) is 20 m in both surveys in the interval of interest (approximately 0 – 2000 m), although resolution decreases with depth. Howie *et al*., (2005) provide further detail on the data processing of the surveys used in this study.

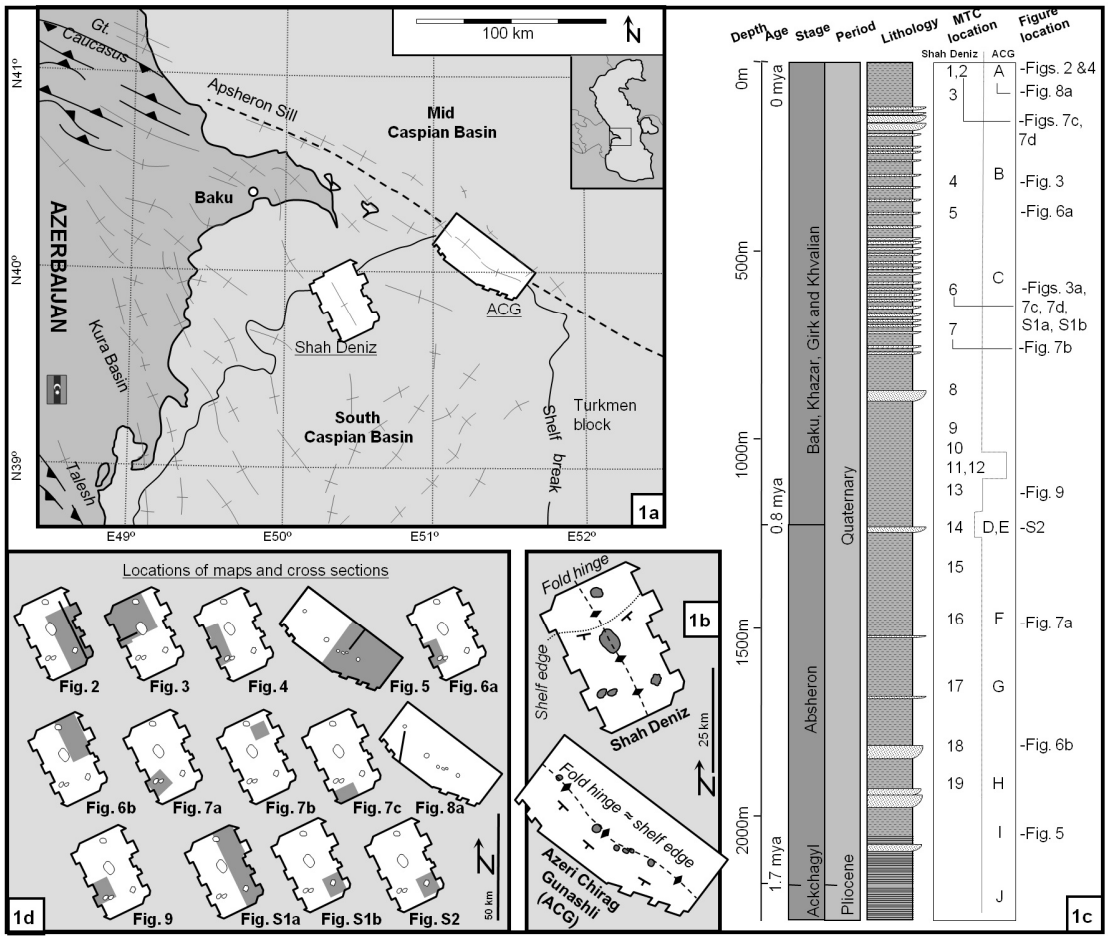

Figure 4.1 (1a) Structural elements of the study area and location of seismic surveys. Fold and fault traces adapted from (Jackson, J. et al., 2002). (1b) Outlines of the seismic surveys with the location of fold traces, basin margin and mud volcanoes shown. (1c) Lithological log of the interval of interest and stratigraphic position of mass transport deposits. (1d) Oriented outlines of both seismic surveys used in this study showing orientations of maps (grey shading) and seismic profiles (black lines).

On seismic profiles a mass transport deposit is identified by its characteristic facies: a rugose upper bounding surface located above discontinuous and low amplitude reflections (e.g. Posamentier & Kolla, 2003), although they can also contain seismic facies of higher amplitudes (e.g. Moscardelli & Wood, 2008). Once a mass transport deposit is identified it is imaged by mapping its lower and upper bounding reflections, termed the 'upper surface' (after Weimer & Shipp, 2004) and the 'basal shear surface' (after Varnes *et al.*, 1978) respectively.

In this study area, a mass transport deposit upper surface is commonly a high amplitude, positive reflection. It is laterally continuous over the mass transport deposit with an uneven, ridged morphology, especially around the downslope area. The basal shear surface is located at the underside of the unit, and is the first semi-continuous, planar reflection separating chaotic seismic facies of the mass transport deposit from the continuous planar reflections, or deeper mass transport deposits below it. Inclined, discontinuous reflections within the mass transport deposit terminate against the basal shear surface. The basal shear surface is an erosional surface that is generally parallel to reflections but cuts down through strata leaving a stepped ramp and flat type geometry . Material was translated down slope over the basal shear surface, which also acts as a detachment surface.

The internal structure of the mass transport deposit was imaged in three ways: a) windowed root mean square (RMS) amplitude extractions taken through the mass transport deposit, using the bounding surfaces (basal shear surface, or upper surface) as input horizons, or by b) 3D attribute-analysis (edge detection) of the seismic volume, and subsequent flattening and time-slicing through the mass transport deposit using a bounding surface, or an adjacent surface as a datum (e.g. Frey-Martinez *et al.*, 2005; Frey-Martínez *et al.*, 2006; Moscardelli & Wood, 2008; Gafeira *et al.*, 2010), and by c) dip magnitude maps taken along the basal shear surface (e.g. Posamentier & Kolla, 2003). Syndepositional structures within the mass transport deposits were best imaged close to the basal shear surface; they become less well imaged towards the top of the deposit.

Once the internal structures of the mass transport deposits were visualised and described, slope failure transport directions, and palaeoslope configurations were interpreted from the orientation of key kinematic indicators (e.g. Bull *et al.*, 2009).

The slope failure deposits in this study are named 'MTD' (Mass Transport Deposit) or 'MTC' (Mass Transport Complex) depending on their size and complexity, and numbered on the basis of their height relative to the current lake bed. Their stratigraphic locations are shown in Figure 4.1c.

4.3. RESULTS

A general description of the study area and a representative mass transport deposit is presented below. The mass transport deposit is organised into its three idealised domains (extensional, translational and compressive). Subsequently seismic examples of syndepositional structures taken from each domain are presented which form the focus of this paper. Finally the kinematic information that is obtained from these data is summarised and used to speculate on the origins and controls of the South Caspian mass transport deposits.

Structural setting

Along the Shah Deniz anticline, reflections between the lake bed and 800 m depth are planar to sigmoidal in cross-section due to the orientation of the fold relative to the basin margin clinoforms (Figure 4.1 Figure 4.2a). The present-day basin margin slope break (or 'rollover point'), the boundary between the shelf and slope, lies within the seismic data, and is identified in cross-section as the point where the lake bed reflection changes from subhorizontal angles to inclined, dipping 10° towards the basin interior (Figure 4.2a). Older basin margin slope breaks are visible in clinoforms in the 0 – 800 m depth range.

Of the 27 mass transport deposits identified along the anticline, the oldest are located within late Pliocene strata and the most recent are visible on the present-day lake bed. Many are so extensive, they are only partially imaged by the seismic data. Around the Shah Deniz anticline, the headwalls of the majority of the failures lie along the (palaeo) slope break, with lateral margins of many mass transport deposits running parallel to the fold hinge trace. Along the ACG structure, the mass transport deposits are volumetrically smaller and less numerous than at Shah Deniz. Most are imaged within the extents of the seismic volume. The mass transport deposits are elongate (up to 15 km long) with narrow (1.75 to 3 km wide) headwall areas located along the fold hinge. Their lateral margins run approximately parallel to the dip direction of the fold flanks.

The interval of interest is syntectonic with respect to both the folds: reflection packages wedge out towards the fold hinge and are themselves folded. In the strike direction of the fold flanks, reflections are planar and continuous, with the exception of the upper 800 m of the Shah Deniz survey where reflection geometries show the clinoform deposit present within it.

Two types of normal fault offset the interval of interest: 1) tightly spaced, oriented parallel to the fold hinge (Figure 4.2b) and, 2) radial, curved faults, emanating from mud volcano craters. When considered as neutral surface folds (Lisle, 1999), the interval of interest lies within the arc of net extension on both structures; the first group of faults is interpreted as being driven by flexure of the outer arc (Devlin *et al.*, 1999). The second group is more complex and interpreted as a product of the interfering stress fields of fold extension, basin subsidence and mud volcano growth.

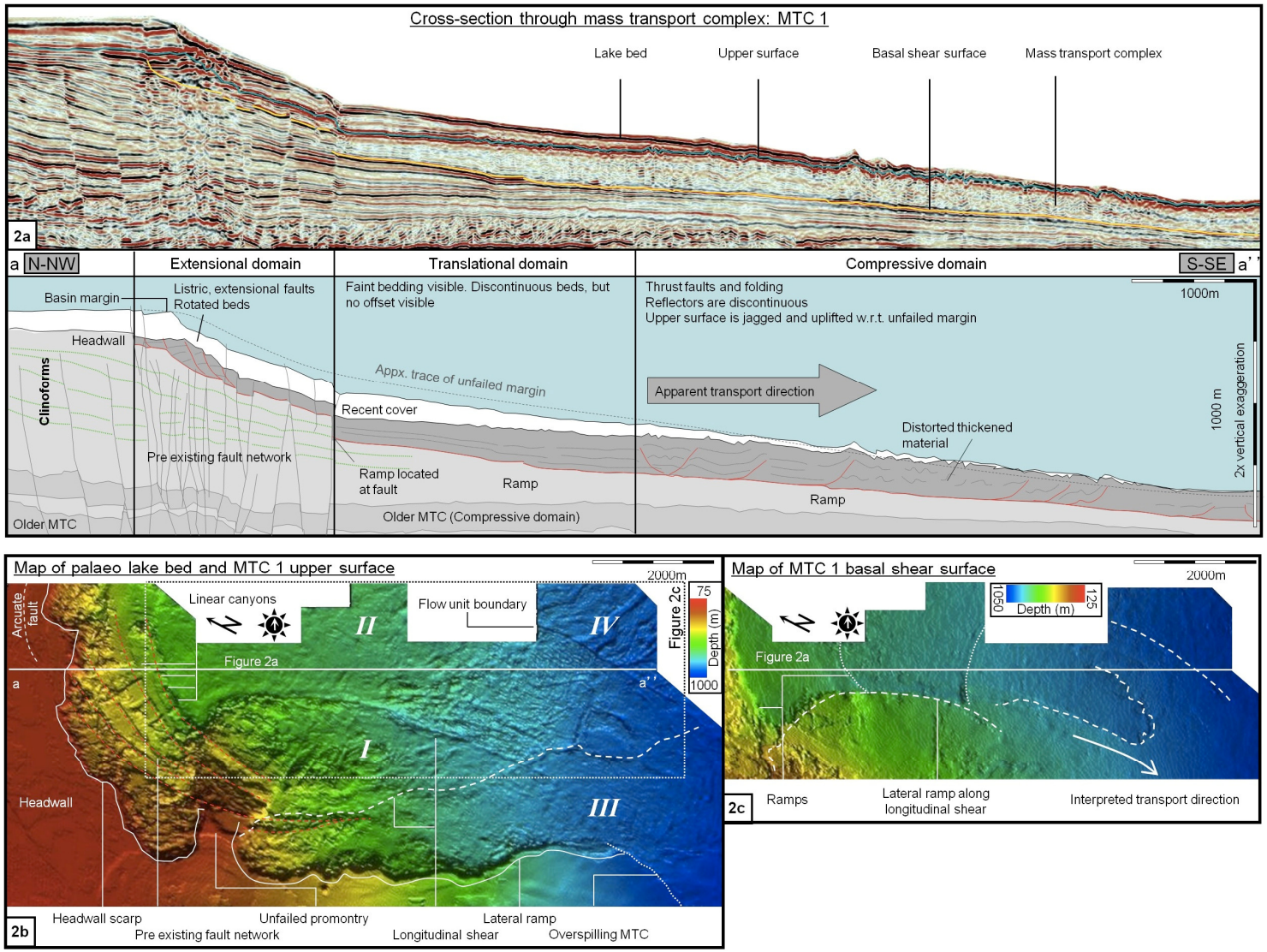

Figure 4.2 Domains of a representative mass transport deposit. [a] Vertically exaggerated (x 2) seismic section running down slope, showing major surfaces and characteristic syndepositional structures in each domain [b] Plan view of the palaeolake bed and mass transport deposit upper surface showing main components of a mass transport deposit. Cross-cutting flow units are numbered I – IV. Faint lineations are dashed white. Image is illuminated from the SW (2c) Shaded depth map of the mass transport deposit basal shear surface showing main components. Faint lineations have been dashed white. Image is illuminated from the SW. Images taken from mass transport deposit 1 from Shah Deniz. *To be printed on A3 landscape oriented paper*

Description of a representative mass transport deposit

Most of the mass transport deposits in the study area have a much larger aerial extent than the two 3D seismic surveys and are only partially imaged. However, portions of all three structural domains are imaged within the most recent deposit on the Shah Deniz Anticline, named 'MTC-1' (Mass Transport Complex -1), (Figure 4.2).

The upper surface of MTC-1 is a high amplitude, positive, continuous and irregular reflection, and its basal shear surface runs semi-parallel to bedding planes in a ramp and flat configuration (Figure 4.2a). Near the upslope margin of the deposit the basal shear surface curves-upwards towards the lake bed, truncating horizons and defining the upslope termination of the failure. The seismic package between the two bounding reflections is wedge-shaped along its length and thickens downslope (Figure 4.2a). The partial outline of the slope failure is visible on the mapped horizon of the upper surface reflection; there is a contrast in morphology and relative height between the smooth, elevated stable lake bed and the rough downthrown mass transport deposit. Its upper and western margins consist of a sinuous headwall scarp consisting of multiple lobes, and a straight, lateral scarp (Figure 4.2b).

MTC-1 contains three structural domains (Figure 4.2a). Its extensional domain reaches from the headwall scarp to the translational domain, the upper surface lies at a lower elevation than the adjacent lake bed in this domain, and the mass transport deposit itself is relatively thin (75 m compared with almost 200 m further downslope), deformed by extensional faults. The translational domain contains relatively undeformed strata and faint, low amplitude, semi continuous horizons. The upper surface is smooth and remains lower than the adjacent stable lake bed. The compressive domain is comparatively thick; the mass transport deposit upper surface is rugose and elevated with respect to the stable palaeolake bed. Much of the original depositional structure has been destroyed and the resulting seismic facies is typified by low amplitude, discontinuous, tilted and chaotic reflections. Faint thrust faults thicken the deposit and incline reflections (Figure 4.2a). The lower termination of this compressive domain, the toe, lies outside of these data.

Extensional domain syndepositional structures

Divergently oriented headwall scarp lobes

Description: The upper limit of a mass transport deposit is commonly a sinuous 'headwall' organised into several convex upslope scarps, 75 – 200 m high, separated by elongated promontories extending into the failure. Arcuate faults and curved, rotated blocks lie up-dip of the main scarp (Figure 4.2a and b). The upper surface lying within each headwall lobe is hummocky and irregular (Figure 4.2Figure 4.3a), underneath this, amplitude extractions and time slices reveal high amplitude, convex-upslope lineations, blocky segments 50 m across and en-echelon normal faults extending into the sides of the headwall scarp (Figure 4.3a). In cross-section the blocks correspond to coherent portions of the failed mass, which can be correlated with stable areas up-dip (Figure 4.3b).

The headwall lobes of several mass transport deposits along the Shah Deniz fold are oriented convex-up-dip along two, tangentially aligned slopes: one created by the basin margin, dipping to the SE, and another created by the fold limbs, dipping to the SW or NE either side of the fold hinge. These headwalls contain a sharp right

angle bend in the lateral margin and an increase the width of the mass transport deposit at the headwall (Figure 4.3a).

Interpretation: Convex-upslope headwall scarps are a common feature in mass transport deposits, often forming along a break in slope (Mazzanti & Blasio, 2010), The closely spaced, upslope concave lineations and structures along the headwalls are indicative of 'retrogression', the episodic growth of the extensional domain upslope during slope failure. Evacuated headwall lobes undercut and destabilised higher portions of the slope, which initiated a chain reaction of further collapses (Varnes *et al.*, 1978; Gardner *et al.*, 1999; Sawyer *et al.*, 2009). Arcuate faults, 'crown cracks' along the headwall of the most recent mass transport deposit on the Shah Deniz fold (Figure 4.2b) indicate that this process is still continuing (e.g Carter, 1975; Varnes *et al.*, 1978). Headwall lobes also grew in size laterally by normal, rotational faulting along the headwall scarp (Figure 4.3a and b), which detached large sections of the sidewall, as rafted blocks (Ilstad *et al.*, 2004).

The majority of the South Caspian mass transport deposits can be classified as 'slope-attached' (Moscardelli & Wood, 2008), on the basis of their cuspate scarp morphology, and the location of the headwalls along the basin margin. Minor 'detached' mass transport deposits, which display narrow and elongate headwall scarps and which are sourced from small local highs and mud volcanoes only constitute a small proportion of the total failed material.

Elaborate headwall scarp outlines on the Shah Deniz fold, which display tangentially oriented scarp lobes, are interpreted as deposit retrogressive failures, where an initial collapse, sourced along the basin margin, subsequently destabilised material inclined on minor adjacent slopes, promoting further, bidirectional growth of the failure (Figure 4.3d), This study refers to this process as 'divergent retrogression'.

Not all the mass transport deposits contain divergently oriented headwall lobes. Mass transport deposits containing narrower (≈1000 m wide) lobes contain relatively thick (≥150 m) amounts of sediment in their extensional domain (Figure 4.4) which presumably offered lateral support to adjacent slopes and prevented divergent retrogression from developing, whereas divergent (≈2500 m wide) scarps, were at one point, completely evacuated. This study therefore speculate that the presence and size of divergent lobes is not only controlled by the surrounding topography, but also by the efficiency of material evacuation in the extensional domain which creates accommodation space for further material to fail into.

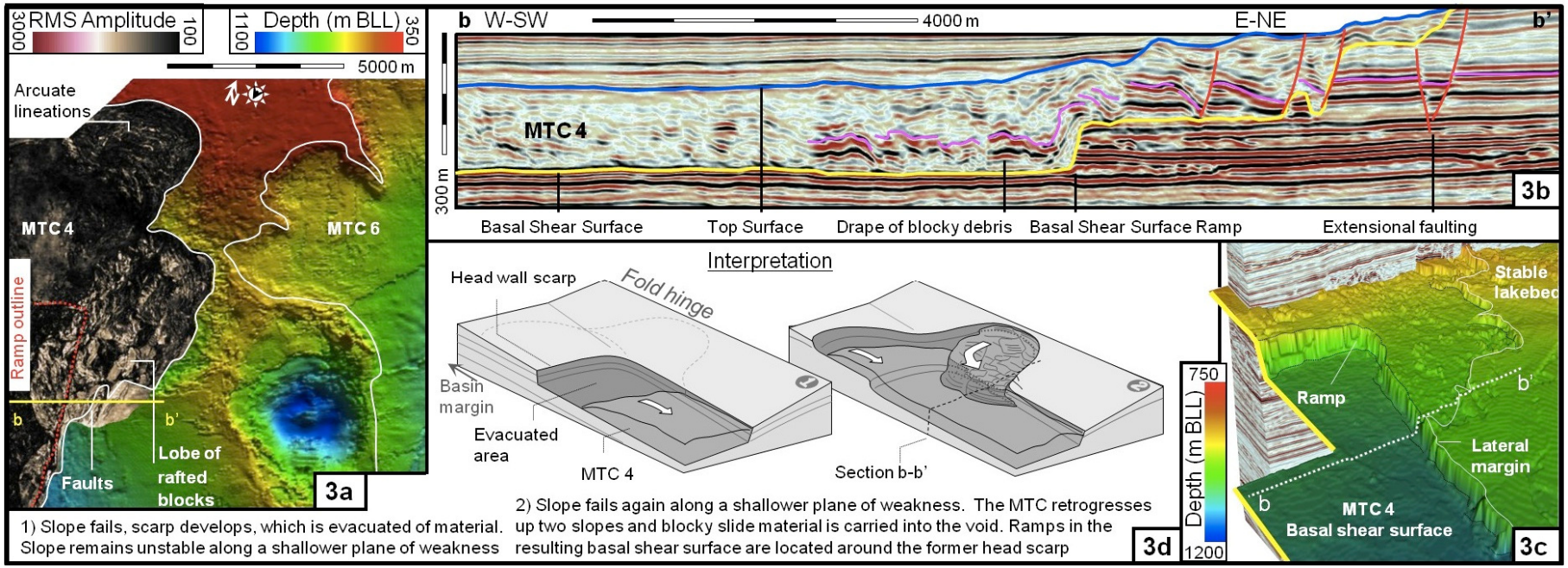

Figure 4.3 Divergently oriented headwall scarps [a] Composite depth map of a mass transport deposit upper surface, illuminated from the north. Convex upslope headwall scarp lobes are oriented 90 degrees away from the lateral margin. The left of the image is coloured with a root mean square (RMS) amplitude extraction. The extraction window is 30 m tall and taken 25 m beneath the upper surface. [b] Vertically exaggerated (x 5) seismic section through the deposit showing basal ramp and drape of material following the ramp outline, highlighted with a pink marker horizon. [c] Perspective view of the basal shear surface showing the outline of the ramp, The image is located at the edge of the seismic survey and contains a square gap of no data. [d] Interpretation; multiple, divergently retrogressive failures, translated material along two basal shear surfaces linked by ramps. The ramp from figure 3b is an older headwall scarp of an earlier failure. Images taken from deposits MTC-4 and MTC-6, along the Shah Deniz fold.

Basal shear surface ramps: fault controlled ramps, and palaeo headwall scarps

Description: Mass transport deposit basal shear surfaces run along multiple reflections which are located at different stratigraphic heights, linked by several ramps. Two types of ramp are observed in the extensional domain; The first type runs along multiple normal faults, which connect closely spaced, down-stepping segments of basal shear surface with each other. In plan view the fault traces form a curved fanning pattern which runs along the slope break and coalesces, turning by 90˚ to run parallel to the fold axis (Figure 4.2a and b). The basal shear surface is offset along ramps at the fault traces, but the vertical throw of the faults does not conform to the vertical offset of the basal shear surface (Figure 4.2a).

The second type of basal shear surface ramp shows no spatial correlation to underlying faults (Figure 4.3b). The ramp is 100 m tall and vertical in section view. In plan view it is curved, running parallel to both the mass transport deposit lateral ramp and headwall (Figure 4.3c). High amplitude, blocky material near the base of the deposit (described in the section above) remains semi-continuous above the curved ramp, forming a lobe of blocky material that drapes and follows the topography of the basal shear surface (Figure 4.3a and b).

Interpretation: Basal shear surface ramps are a common feature in mass transport deposits (Frey-Martínez *et al.*, 2006; Moscardelli *et al.*, 2006) though their formation mechanisms are not fully understood (discussed in Bull *et al.*, 2009) At least two modes of generation can be inferred for the examples observed in the extensional domain.

The disagreement between fault slip direction and basal shear surface offset along the first ramp type show that the ramps were not simply created by faulting and vertical offset of a basal shear surface, running along a single bedding plane, but rather that multiple beds acting as shear surfaces, were connected by ramps localised along the faults, which were vertical zones of weakness in the slope. The faults therefore either pre-date the emplacement of the mass transport deposit, or formed synchronously with it, no growth strata is preserved to determine which, as the fault blocks are eroded by the overlying mass transport deposit. If the latter is the case, it could imply a seismic trigger (e.g. Gee *et al.*, 2005) for the most recent slope failure along the Shah Deniz Anticline.

The second type of ramp is not fault controlled, its origin is determined from the drape of blocky material that overlies it. The drape structure shows there was accommodation space, allowing the blocky material to travel into a pre-existing void, the shape of which is outlined by the ramp. The void is interpreted as an earlier evacuated headwall scarp, created by a previous failure. The blocky drape was emplaced by a subsequent, divergently retrogressive failure along a shallower plane of weakness (Figure 4.3d).

Slope bound canyons and creep

Description: Steep-walled, linear canyons 50 m deep incise the basin slope, and continue for over five kilometres downslope; their full extent is not contained in the seismic data. The canyons emanate from several point sources along the slope break, and are absent above the basin slope. Strata alongside the canyons are disrupted and folded at low amplitudes. In map view the disturbed strata are organised into linear, 200 m wide ridges orientated normally to the canyon. No headwall scarps or other ruptures of the lake bed are visible (Figure 4.4). The canyons are contemporaneous with a larger mass transport deposit (MTC-1) located on the opposite side of the fold hinge, and described above (Figure 4.2), which also contains remnants of short, linear canyons of a similar width and spacing along its headwall scarp (Figure 4.2b).

Interpretation: The area of creep around the canyons represents mass movement which froze during its early stages and failed to develop into a slope failure. Slope bound canyons commonly develop during sea level falls (Posamentier & Vail, 1988; Field *et al.*, 1999), and a 100 m lake level drop is reported to have occurred at the same time as MTC-1 was emplaced (Amos *et al.*, 2008). Remnants of similar canyons along the headwall of a mass transport deposit on the adjacent fold flank imply that this process may have been a major primer or trigger to the most recent Caspian failure, though more research would be needed to determine this.

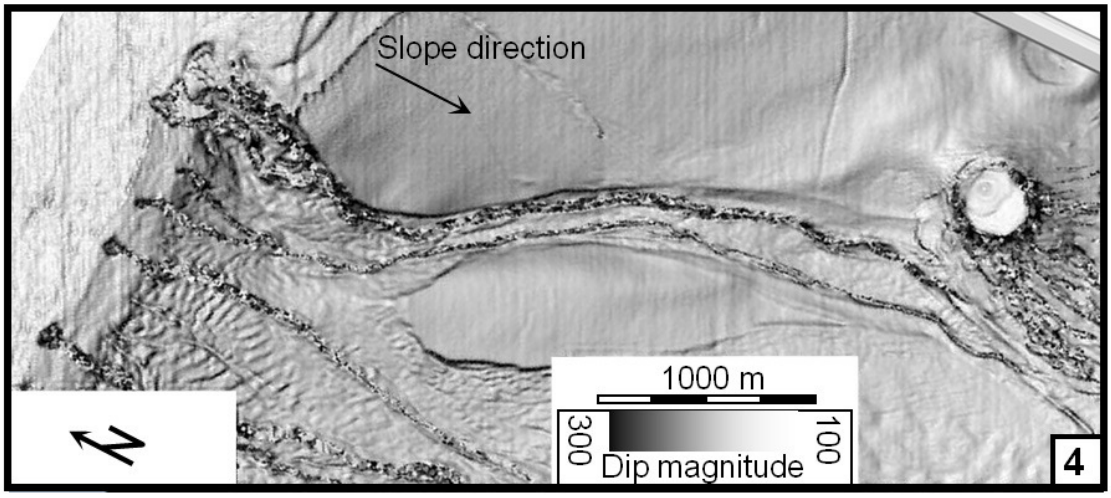

Figure 4.4 Headless canyons located along the shelf break. Dip magnitude map of a palaeolake bed. Dip magnitude is a dimensionless variable that picks out changes in slope along a seismic horizon. The shelf break runs approximately E – W to the left of the map. Material alongside the canyons is disrupted. A circular mud volcano edifice and its mudflow lie to the right of the image. The canyons are contemporaneous with the larger mass transport complex MTC-1 from the Shah Deniz anticline, shown on Figure 4.2.

Mass transport deposits lacking headwall scarps; 'whole wedge failures'

Description: Several mass transport deposits contain no seismically detectable scarp topography in their extensional domains. The upper surface forms part of a growth strata wedge, the reflections of which are laterally truncated onto the adjacent fold. Reflections within the deposit onlap the basal shear surface, which forms part of the fold flank and no scarp upslope of the failed material is detectable along section views. The point of truncation is located lower downslope towards the middle of the mass transport deposit and tapers-upwards towards the edges (Figure 4.5a and b).

Interpretation: The scarp morphology is unusual when compared with published examples of slope failures (e.g Moscardelli *et al.*, 2006) or more conventional mass transport deposits in the study area (e.g. Figure 4.2b, Figure 4.3a) which all display well-developed convex upslope, headwall scarps. The 'whole wedge' failures occur along growth strata wedges, on fold flanks that steepen up-dip and extend further upslope than the strata pinch outs (Figure 4.5 b). The area where no scarp exists was inherently unstable prior to failure; located along the steepest portion of the slope, subject to higher shear stresses and unsupported by cohesive material upslope (due to the wedge shape of the strata package). This study proposes that the entire growth wedge was translated downslope, possibly progressively by a succession of retrogressive failures, leaving an evacuated zone up-dip of the mass transport deposit (Figure 4.5 c). More conventional headwalls from other mass transport deposits in this study, are commonly located close to changes in slope angle, such as the basin margin slope break (Figure 4.2), and are composed of thick (>100 m) packages of sediment. Slope angle and sediment pinch-out are therefore likely controls on the location and style of up-dip termination of the mass transport deposits.

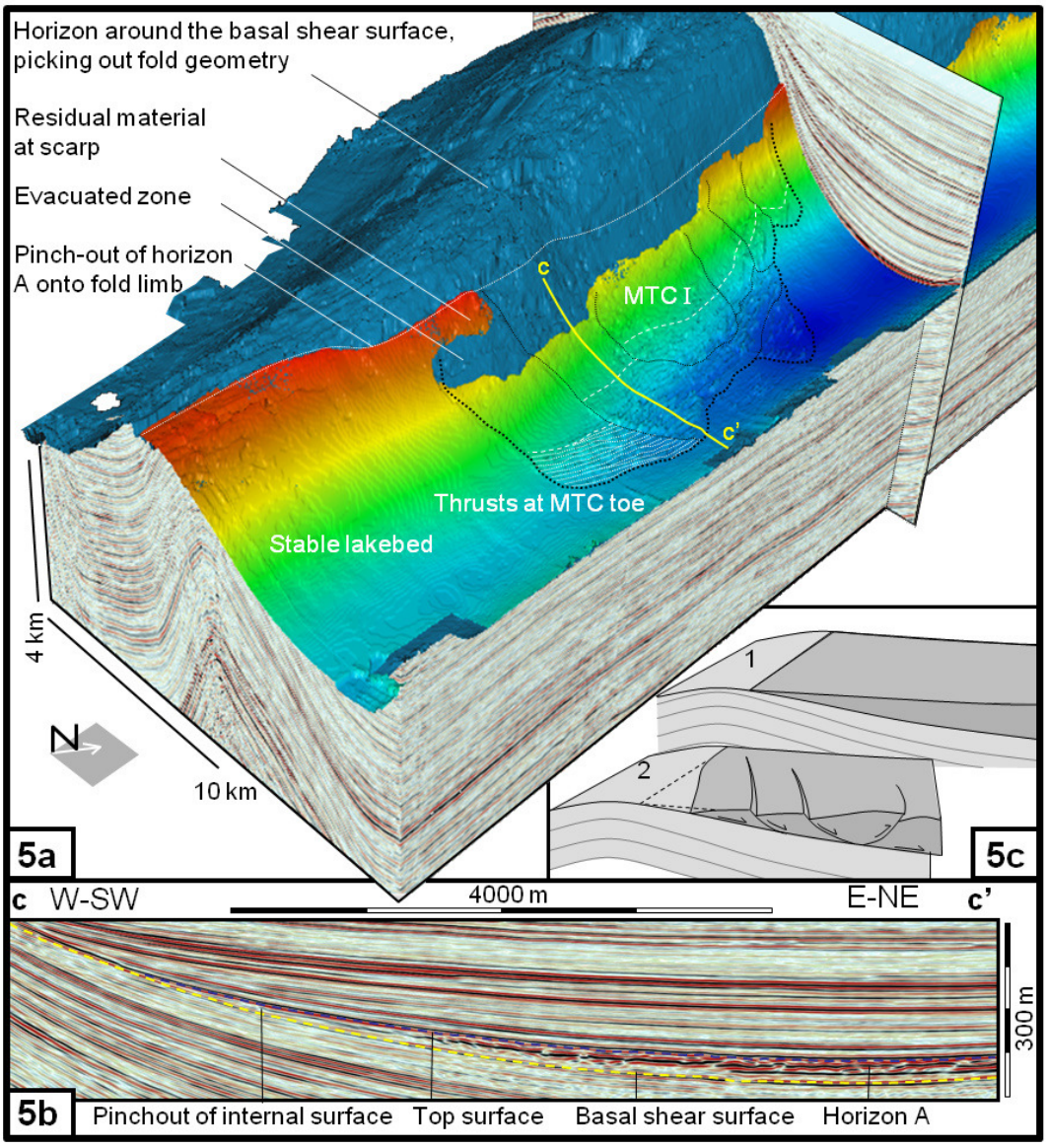

Figure 4.5 Mass transport deposit without a conventional headwall scarp. [a] 3D view of a mapped coherent reflection within the mass transport deposit (Horizon A) and a lower horizon, corresponding to the basal shear surface. Horizon A is coloured by depth , the basal shear surface is blue. Horizon A pinches out onto the basal shear surface, the location of pinch-out falls towards the centre of the mass transport deposit where material displacement is the greatest. [b] Vertically exaggerated (x 6) seismic section through the deposit, up-dip of the upper surface pinch out, no scarp is observed. [c] Interpretive cartoon showing evolution of the mass transport deposit, leaving no headwall scarp. Example taken from mass transport deposit 1, from the ACG structure.

Translational domain syndepositional structures

Flow units and basal shear surface lateral ramps

Description: Translational domains in the larger mass transport deposits appear monotonous when viewed from their upper surfaces, but amplitude extractions taken through the body of the deposit reveal they are composed of several smaller units, displaying internal fabrics of sinuous or chaotic patterns with convex downslope frontal margins (Figure 4.6). The boundaries between each unit correspond to gently curving, shallow (20 – 50 m) depressions and ridges in the upper surface (Figure 4.2b) and stratigraphic fluctuations of the basal shear surface connected by lateral ramps (Figure 4.2c).

Interpretation: Mass transport complexes consist of several mass transport deposits, separated by longitudinal shears (e.g. Prior *et al.*, 1984), which each developed episodically through several separated failures of varying relative flow rate and timing (Prior *et al.*, 1984; Frey-Martinez *et al.*, 2005). Slope failures with increasing erosive power incised lateral ramps into the basal shear surface which truncated and remobilised older mass transport deposits (Bull *et al.*, 2009). Cross-cutting relationships between individual mass transport deposits and basal shear surface ramps can be established to obtain a relative chronology of events (Figure 4.2c and Figure 4.6). These show the youngest units located furthest up-dip highlighting the retrogressive growth of the South Caspian mass transport complexes.

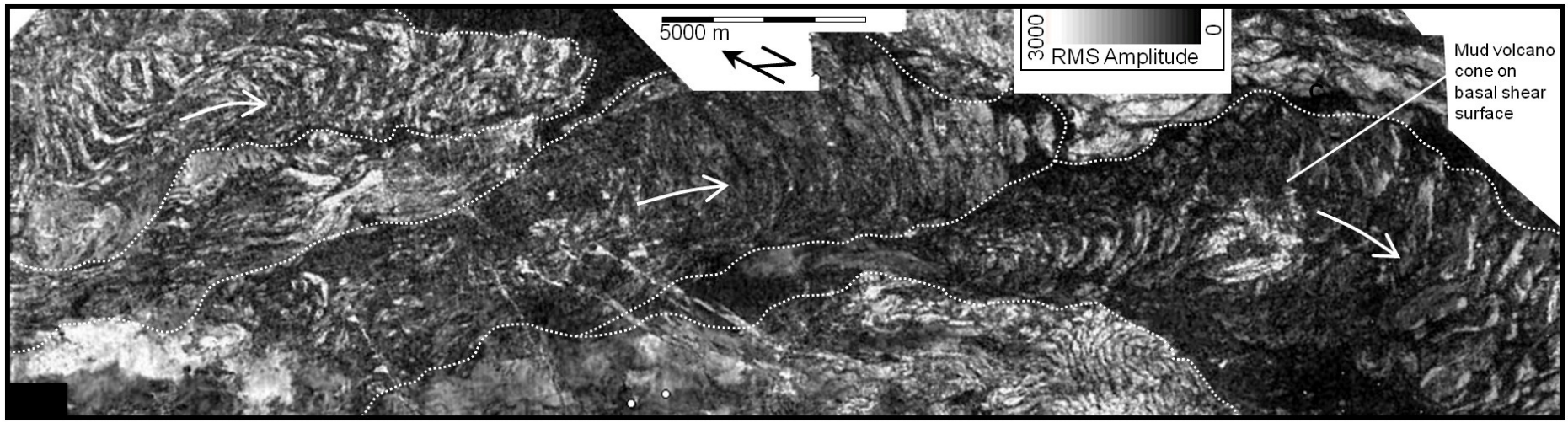

Figure 4.6 Individual mass transport deposits within a mass transport complex. Lateral shear zones and deposit frontal lobes are highlighted in dotted white, interpreted material transport directions are shown with white arrows. Amplitude extraction taken from mass transport deposit 6 on Shah Deniz, 30 m above the mass transport deposit basal shear surface, with an extraction window of 25 m.

Mud volcano interaction structures

Description: Numerous mud volcanoes are located along both folds (Figure 4.1b). Mass transport deposits located around mud volcanoes contain two distinctive structures in their translational domains: along basal shear surfaces, relic mud volcano edifices form elevated circular expressions 40 – 50 m tall (Figure 4.8a and b). Amplitude extractions taken through the overlying mass transport deposit show higher amplitudes around the volcanoes, and high amplitude triangular units located downslope of them (Figure 4.7 a, b). Mass transport deposit lateral ramps are curved and sigmoidal in plan view beside mud volcano edifices (Figure 4.8a). The deposit thickens up-dip of the mud volcano, extending beyond its lateral scarp and overlying the stable lake bed. Amplitude extractions reveal flow unit boundaries that follow the margin scarp curvature down-dip of the mud volcano.

Interpretation: The two structures show that mud volcanoes are comparatively stable portions of the slope which were relatively resistant to failure. The triangular zones represent material that was shielded from erosion by mud volcano topography. Besides being a useful kinematic indicator, these zones may form unconventional hydrocarbon traps (Moscardelli *et al.*, 2006). Similar patterns are reported in other mass transport deposits around obstacles such as remnant and translated blocks (Masson *et al.*, 1993; Bull *et al.*, 2009). The mud volcanoes formed rigid anisotropies which altered the advancement of the slope failures, creating layer-shortening features, (compression, thickening and emergence over the stable lake bed) and deflection of the lateral scarp around the volcanoes, analogous to transpressive 'restraining bends' in tectonic scale strike slip faults (Sylvester, 1988). The lateral extrusion of the mass transport deposit over the lake bed, required the internal energy in the translating material to overcome basal shear surface friction and its own weight, suggesting a rapid emplacement, or a low friction basal surface (Frey-Martínez *et al.*, 2006).

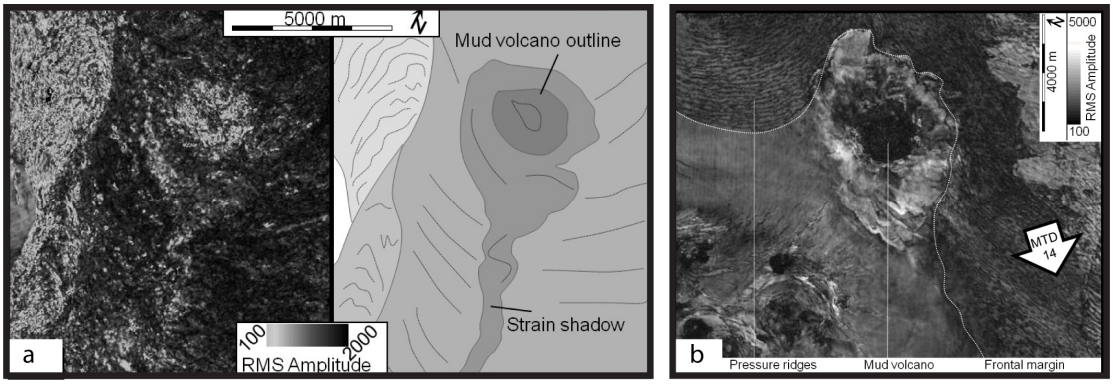

Figure 4.7 mud volcano interaction structures [a] Erosional shadow remnant. Root mean square (RMS) amplitude extraction taken through mass transport deposit 6 on Shah Deniz from 20 m above the basal shear surface with an extraction window of 30 m [b] Mass transport deposit frontal margin obstructed by a mud volcano crater. Low amplitude, concave downslope pressure ridges are visible in the mass transport deposit. Several more mud volcanoes (low amplitude, circular features) are shown to the bottom right of the image. Arrow shows the material transport direction. RMS Amplitude extraction taken from mass transport deposit MTD-14 on the Shah Deniz fold, 25m above the basal shear surface with a 25 m extraction window.

Basal shear surface grooves

Description: Several basal shear surfaces contain numerous gently curving, tightly spaced, shallow lineations, that persist for several kilometres, the longest extends for 9 km.(Figure 4.8b). In seismic profiles these features are below vertical resolution (< 20 m), but they are imaged on amplitude and dip magnitude maps taken along the surface.

Interpretation: Basal shear surfaces containing numerous tightly spaced grooves indicate the physical state of the overlying submarine landslide; they are created by rigid material incising the slope in semi-liquefied, blocky debris flows, rather than more plastic slides and slumps, and as a result contain far fewer thrust and fold structures such as those described in the previous section (Posamentier & Kolla, 2003; Gee *et al.*, 2005; Moscardelli *et al.*, 2006; Bull *et al.*, 2009). What determines the evolution of submarine slope failures into debris flows is unclear, but initial sediment density and energy transferred to the sediment are possible controls (Locat & Lee, 2002). The grooves persist over several kilometres providing kinematic indicators and a minimum transport distance of the debris flow (9 km). Incising blocks may have been destroyed or lifted out of the flow by hydrodynamic processes (e.g. Mohrig *et al.*, 1998; Gee *et al.*, 2005), so the transport distance is potentially much larger.

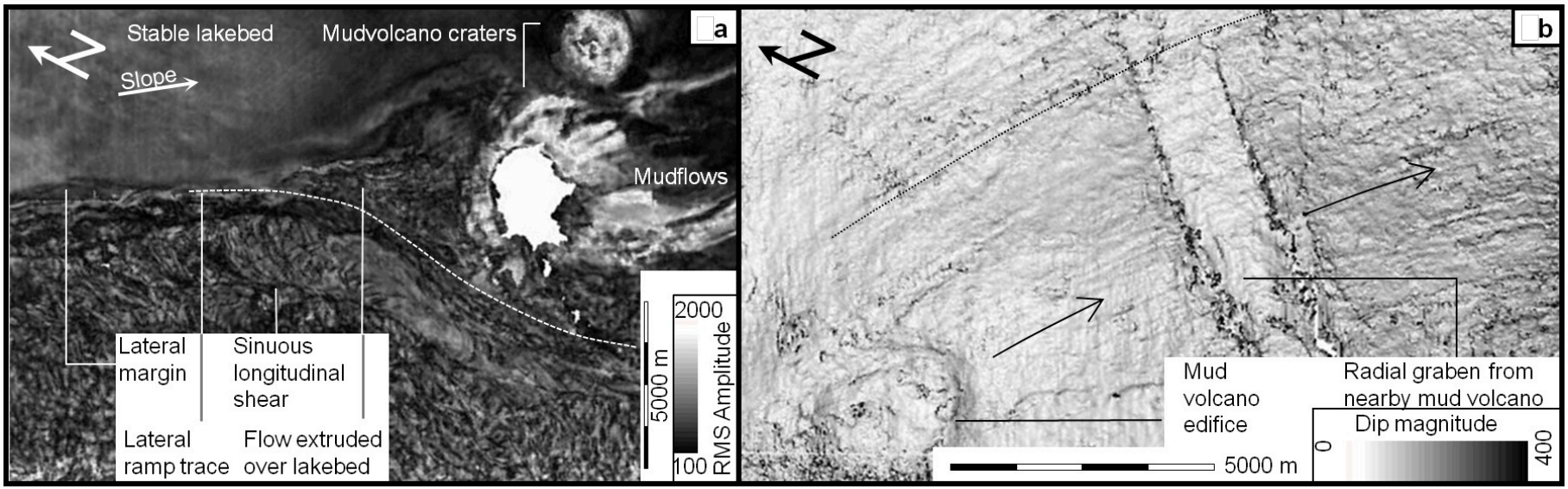

Figure 4.8 Translational domain structures. [a] Amplitude extraction taken though a mass transport deposit and the adjacent stable slope. The deposit contains sigmoidal lateral shear traces. Upslope of the mud volcano, the slope failure is extruded over the lake bed. Volcano mud flow orientations show slope dip direction. Amplitude extraction taken through mass transport deposit MTD-8 on Shah Deniz, 60 m above the basal shear surface with an extraction window of 30 m. [b] Dip magnitude map of a basal shear surface showing incised grooves, which show the material transport direction. The longest groove is 9 km long, providing a minimum transport distance. Taken from mass transport deposit MTD-18 on Shah Deniz.

Compressive domain syndepositional structures

In the compressive domain mass transport deposits reach up to 500 m in thickness, elevating upper surfaces by up to 100 m with respect to the adjacent lake bed. Mass transport deposits terminate downslope in a frontal ramp (not shown in Figure 4.2) where the basal shear surface curves-upwards, emerging onto the stable lake bed.

Segmented arcuate thrust networks

Description: Amplitude extractions and edge detection maps taken through mass transport deposits reveal the shape of lateral and downslope margins and strictures contained within the compressive domain. The shape of the downslope margin is varied: wide, convex downslope lobes (length / width = 0.5) contrast with elongate (length / width = 1.6) frontal margins, which show no appreciable widening with respect to the translational domain (Figure 4.9a and b).

Areas up-dip of the frontal margins often contain numerous, fine scale, tightly spaced, convex downslope lineations (25m across). In section view, these areas correspond to packages of highly discontinuous and tilted reflections which continue for 5 – 10 km before terminating against a frontal ramp. Rounded, high and low amplitude segments, which are relatively undeformed in section view, lie up-dip of the lineations (Figure 4.9a – c). The lineations commonly trend in a convex downslope pattern, aligned similarly to the frontal margin, but are sinuous and convex upslope around topographic highs e.g. mud volcanoes (Figure 4.7) and can display intricate patterns, where tightly spaced, curved lineations are contained within larger arcuate segments; segments become narrower and tighter upslope, and lineations within them trend similarly (Figure 4.9 a). Cross cutting relationships between segments can be seen, and packages of lineations correlated with each other. A particularly complex pattern is shown in Figure 4.9c, the partially imaged frontal lobe of a mass transport deposit (named MTC-6, along the Shah Deniz anticline). Tightly spaced lineations and an area of low amplitudes (marked LA on the figure) at the front of the failure are offset and contorted along a linear boundary.

Interpretation: Growth of the frontal area is driven by compression from material upslope and gravitational spreading of the thickened unit (Varnes *et al.*, 1978) Lateral, gravitational spreading widens the compressive domain with respect to the translational domain and the variety of frontal margin shapes may indicate varying magnitudes of this processes occurring between slope failures. This may be related to the amount of thickening that developed in the compressive domain, and the presence of obstacles inhibiting its frontal, downslope growth, such as slope angle reduction, or mud volcano edifices (Marques & Cobbold, 2002). The downslope configurations of the mass transport deposits in this study all terminate against a frontal ramp, and classifies these examples as frontally confined (Frey-Martínez *et al.*, 2006), meaning they did not develop enough internal energy to overrun their frontal ramps and spill on to the seabed. This could be due to the basal shear surfaces lying along relatively deep bedding planes, and predisposing the creation of thick deposits.

Tightly spaced, convex downslope lineations are a common structure on mass transport deposits, and are termed ‘pressure ridges’ (Varnes *et al.*, 1978; Prior *et al.*, 1984; Masson *et al.*, 1993), Where seismic resolution allows, the pressure ridges correlate with imbricate thrust and fold belts, visible in section view . Commonly though, the frontal domain is rather chaotic; presumably pressure ridges in those sections depict fold or thrust traces of structures below seismic resolution.

The pressure ridge sheets are truncated and offset by larger arcuate thrusts and longitudinal shears, which define crescent-shaped segments (Figure 4.10). The segments are less tightly convex downslope than upslope, reflecting a younging-downslope trend towards the failure toe, similar to the pressure ridges (Figure 4.9a). Cross-cutting relationships between the segments reveal an episodic strain history; smaller pressure ridges formed first, and were diachronously offset by larger faults. Analogous arcuate, segmented, patterns are found in 'salients': tectonic scale, thrust sheets (Twiss & Moores, 1992), and have been sandbox modelled by varying the motion path of thrust sheet, and the shape of the up-dip margin of the thrust sheet (Macedo & Marshak, 1999; Lickorish *et al.*, 2002). The convergence of the bounding thrusts and shears towards the eastern margin of the mass transport deposit (Figure 4.9a) suggests that in this case, the segmented pattern is probably created by a progressive rotation of the slope failure, which shifted its toe to the east. Kinematic analysis of the mass transport deposits also confirms that their motion paths are mostly non linear, and change along section.

The contorted pressure ridge network of the mass transport deposit (Figure 4.9c), is also segmented, but contains additional complexity in its seismic fabric. The mapped area lies within the toes of two consecutive mass transport complexes, which travelled in opposing directions along the same basal shear surface. As a result, the older mass transport deposit was truncated, deformed and offset along a longitudinal shear (Figure 4.9c). The basal shear surface evidently remained a weak plane in the slope after failure, and was reactivated after a considerable time period; the upper surfaces of each mass transport deposit are separated by over 500 m of sediment, estimated to represent 0.3 Mya of deposition (Figure 4.1b).

Thrust sheet geometry and throw distribution

Description: Compressive domain thrust sheets (identified above) extend for several kilometres (>5000 m) and reach between 100 – 400 m thickness. Within the most recent mass transport complex along the ACG structure (MTC – A), thrust fault hanging wall ramps are picked out in section view by coherent, high amplitude reflections (Figure 4.10a). The fault trace geometry is not consistent along the sheet; thrust planes change character and geometry down slope: displaying larger vertical throws (Figure 4.10b), steeper (greater) ramp angles with respect to the basal shear surface, and increasingly contorted fault hanging wall strata. The geometry of the thrust sheet also changes, becoming thicker downslope, whilst the basal shear surface steepens downslope away from the crest of the anticline.

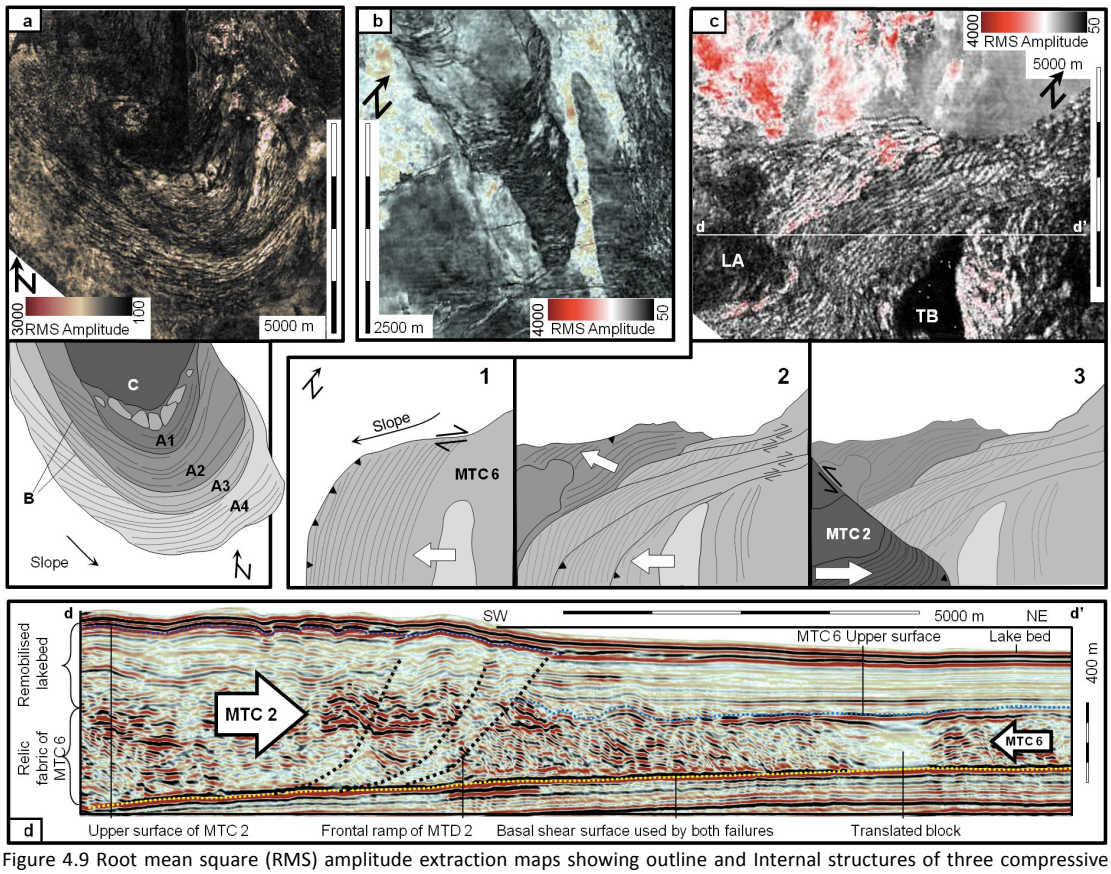

Figure 4.9 Root mean square (RMS) amplitude extraction maps showing outline and Internal structures of three compressive domains. [a] Wide frontal margin, containing fine-scale arcuate thrusts. The thrust sheet is segmented into four sections, A1 – 4, separated by flow unit boundaries B. Also present are translated blocks, C. [b] Elongate frontal margin displaying fault and fold traces at its tip. [c] Partially imaged compressive domain, containing a translated block, TB, and sinuous thrust lineations. Cartoon shows mass transport deposit evolution based on cross-cutting relationships of. [d] Vertically exaggerated (x 3) seismic section taken through the contorted compressive domain of Figure c. The highlighted area is offset by two mass transport complexes travelling in opposite directions. Figure 4.9 a,b, and c – d taken through mass transport deposits 16, 7, and 6, respectively, along the Shah Deniz anticline . All amplitude extractions are taken 30 m above the basal shear surface with a 25m window length.

Interpretation: The described fault geometries are not what are commonly observed in tectonic or sandbox scale thrust sheets (e.g. Davis *et al.*, 1983), which are commonly considered analogous to landslide compressive domains (Varnes *et al.*, 1978; Martinsen & Bakken, 1990; Schnellmann *et al.*, 2005; Butler & Turner, 2010). In an idealised thrust sheet, strain, fault geometry, and kinematics are governed by critical taper theory (Davis *et al.*, 1983), growing as a self-similar wedge which maintains a constant angle along its upper surface; thrusts grow at the tip of the sheet and propagate forwards, whilst strata is deformed and thickened internally at the head of the sheet. In section view along an idealised wedge, thrust faults show a decrease in angle and throw towards the toe, whilst strata are thicker elevated and more contorted towards the head; exactly the opposite trends of what is observed in the cross section of Figure 4.10a.

Some of our observations may be explained by geometric conditions along the sheet: firstly, the deformed strata were not initially bedded in a flat layer, but along a downslope thickening growth strata wedge; some of the thickness increase is therefore caused by the pre-tectonic geometry above the basal shear surface. Secondly, the increases in fault angle may be caused by a corresponding downslope increase in the basal shear surface tilt; thrust sheet fault angles increasing with décollement angle has been sandbox modelled in accretionary wedges, though not mechanically explained (Koyi & Vendeville, 2003).

We also suggest a kinematic explanation. The thrust sheet forms part of a mass transport deposit, which is contained within a much larger mass transport complex (Figure 4.1a). The thrust sheet may have initially formed within an isolated mass transport deposit, which was subsequently translated in its entirety by another, later mass movement extending further downslope. Similar extensional domains forming ahead of compressive domains are documented along other slopes (e.g. Martinsen, 1994; Gardner *et al.*, 1999; Lucente & Pini, 2003). Translation of the entire thrust sheet, may have reactivated steepened thrusts at its rear, resulting in extensional movement along its faults, and the up-dip fault plane shallowing and reduction of throw along section (Figure 4.10).

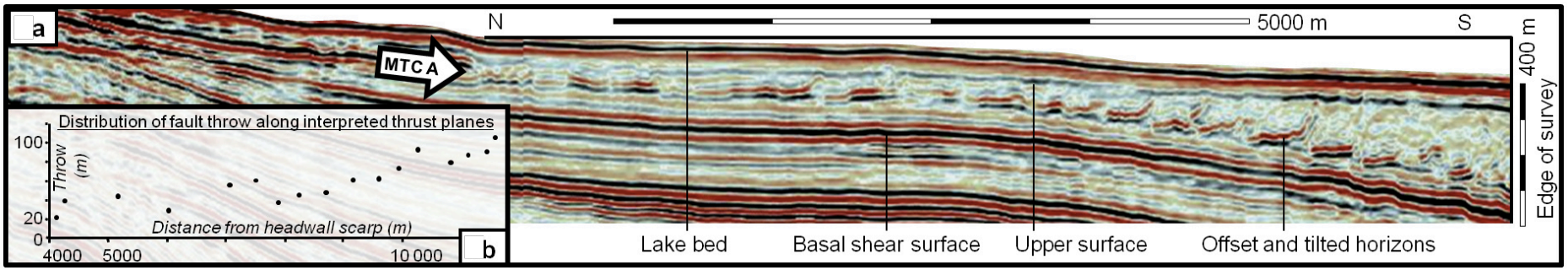

Figure 4.10 Compressive domain thrust belt. [a] Vertically exaggerated (x 6) seismic profile through a thrust sheet. Thrust hanging walls are picked out by tilted, moderate amplitude, negative (black – red – black) reflections. The section is oriented parallel to the material transport direction of the mass transport deposit (MTC-A, along the ACG structure), and is vertically exaggerated by a factor of 3. [b] Throw distribution of thrusts from Fig 8a. Throw along the thrusts increases downslope, though the toe of the failure lies off the extent of these data.

Compressive domain blocks and scours

Description: One compressive domain contains oblong scours 900 m wide and 30 – 50 m deep along the basal shear surface (Figure 4.11a). Sections through the mass transport deposit show high amplitude negative reflections forming convex-upwards, flat based structures, 125 m in height, located at the scour tips (Figure 4.11b). Reflection coherency is low within the mass transport deposit, but low amplitude inclined reflections lie within the mounds. The lobate outline of the failure is revealed by edge detection maps, which also shows faint pressure ridges (Figure 4.11c).

Interpretation: The high amplitude mounded features are rafted blocks of intact strata that were translated downslope and tilted as they were eroded away at their base (e.g. Masson *et al.*, 1993). Similar to grooves they are indicative of the rheology of the slope failure, and are associated with low cohesion debris flows, rather than brittle and plastically deforming slumps and slides (Posamentier & Kolla, 2003; Gee *et al.*, 2005; Moscardelli *et al.*, 2006; Bull *et al.*, 2009). Their axial orientation relative to the transport direction of the debris flow (interpreted from scour edge orientations, and faint convex downslope lineations) reflects their respective relative position in the flow; towards in the centre, where material transport is greatest and velocity gradient lowest, blocks are oriented normal to the flow direction, and alongside the edges they align to run parallel to it (Mazzanti & Blasio, 2010). The blocks were generated along the headwall scarp (e.g. Figure 4.3a) and transported to the debris flow toe by decreased basal friction during failure (Prior *et al.*, 1984; Mohrig *et al.*, 1998; Gee *et al.*, 2005), before grounding out of the flow during freezing of the deposit (Huvenne *et al.*, 2002).

Location and kinematics of the South Caspian slope failures

Description: Kinematic information (as discussed in Bull *et al.*, 2009). was interpreted in the extensional domain from convex upslope headwall scarp outlines and their associated structures, in the translational domain from convex downslope trends of flow unit fabrics, strain shadows and basal groove orientations, and in the compressive domain, from basal scours and the convex downslope orientation of pressure ridges (summarised in Appendix 8).

The data contains 27 mass transport deposits. Generally, compressive domains are sampled by our seismic data in older mass transport deposits, and extensional domains in the younger deposits. Along the Shah Deniz anticline, cuspate headwalls migrate basinwards over time, whilst the centre of the survey is less disrupted over time .

Kinematic indicators within the mass transport deposits show they broadly travelled in two directions: either down the basin margin, parallel to the fold hinge towards the basin interior, or perpendicular to the fold hinge and down the fold flanks (Figure 4.12a). A few anomalous examples travelled obliquely to these trends, towards the fold hinges. Within a single mass transport deposit flow directions were non-uniform, this is especially obvious around the Shah Deniz structure. Mass transport deposits meandered and turned right angle bends around the tip of the Shah Deniz anticline; the inflection point changed throughout time, stepping gradually basinwards (Figure 4.12b).

Interpretation: The location of the mass transport deposits, and kinematic indicators contained within them show the topographic evolution of the South Caspian Basin margin, especially around The Shah Deniz anticline. The basinwards migration of 'slope bound', cuspate headwall scarps correlates with the Pleistocene progradation of the western South Caspian Basin margin (Abreu & Nummedal, 2007), whereas knick points of mass transport deposits which were deflected around the fold tip, and migrated basinwards through time, show the uplift of the fold (Fowler *et al.*, 2000) and the lengthening of the fold hinge (Figure 4.12b). Both the sedimentary growth of the basin margin, and uplift of the anticline created slopes within the Shah Deniz area. As these two slopes are tangentially oriented, the predominant flow direction of mass transport deposits in the survey reflects the relative magnitude of each slope-forming process. Kinematic indicators show that the majority of the failures emanated from the basin margin, in a direction parallel to the fold hinge (e.g. Figure 4.2). The role of the Shah Deniz fold in destabilising the basin margin by over steepening (e.g. Heinio & Davies, 2009) is therefore interpreted to have been relatively small, with the fold topography largely subdued by high basin-margin sedimentation rates (see chapter 3). The fold did however influence the evolution of the mass transport deposits by pinning the lateral development of the mass transport deposits' translational and compressional domains (Figure 4.12b) and creating divergent headwall scarps (e.g. Figure 4.3). Generation of slope failures along the basin margin, combined with fold controlled, lateral pinning created two, long-lived, alternating, sediment transport corridors on either side of the Shah Deniz anticline along which material was translated from the shelf edge towards the basin interior (e.g. Gee *et al.*, 2005; Moscardelli & Wood, 2008).

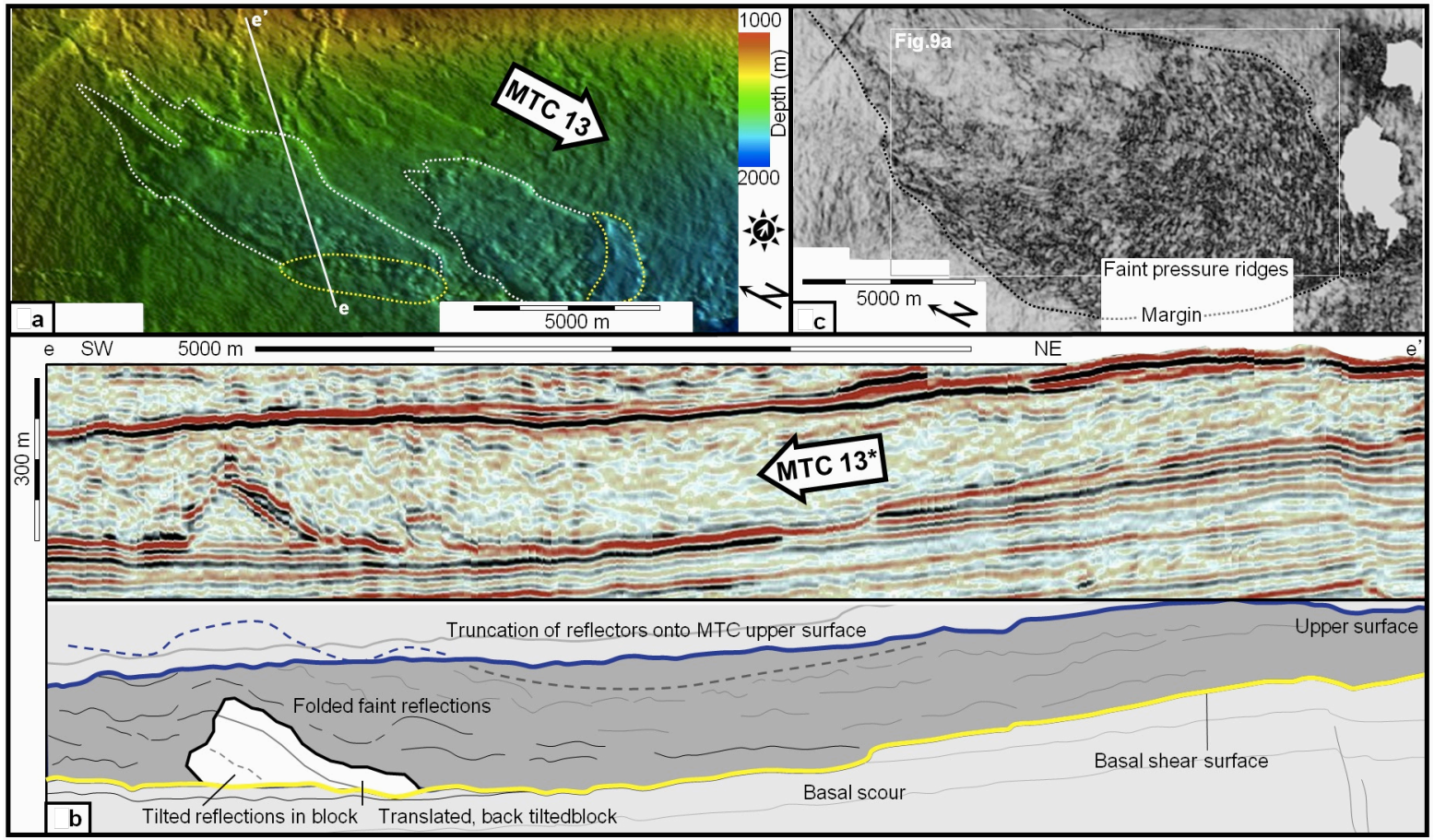

Figure 4.11 Translated blocks and basal shear surface scours. [a] Shaded depth map of the basal shear surface showing wide basal scours. Outlines of translated blocks shown in yellow, interpreted flow direction shown with arrow. Surface is illuminated from the west. [b] Vertically exaggerated (x 6) seismic profile through the block and scour, transport direction is apparent as seismic section is oriented oblique to scours. [c] Horizontal slice taken through a flattened attribute analysed volume. The example is taken from mass transport deposit MTC-13 along the Shah Deniz fold. The seismic volume has been processed with an edge detection algorithm and flattened along the mass transport deposit basal shear surface. The depth slice is taken 25 m above that surface.

4.4. DISCUSSION AND CONCLUSIONS

Seismic mapping reveals much about the structure and kinematics of the 27 Pliocene – present-day mass transport deposits and deposits, imaged along the South Caspian Basin Margin. The range of syndepositional structures described in this study (Figure 4.13). The key interpretations from this study are presented and discussed below:

Morphology and kinematics of the South Caspian mass transport deposits

1) Mass transport deposits along the western margin of the South Caspian Basin, range from 10,000 to 50,000 m in lateral extent, but as most are not fully contained within the data, they are potentially much larger. Several deposits are accumulated into larger mass transport complexes, the largest of which lies along the present-day lake bed.

2) Mass transport deposits are sourced from two locations: The basin slope, and the flanks of anticlines. The basin slope is the source area for the majority of the failures. Anticlines control the development of the mass transport deposits by destabilising upslope areas of the mass transport deposits and restricting their lateral extent creating long-lived sediment transportation corridors that evolve over time as the folds grow.

3) The mass transport deposits can be split into a tripartite division consisting of an ‘extensional domain’ at the head, a ‘translational domain’ in the middle and a ‘compressive domain’ at the toe.

4) Most mass transport deposit extensional domains display elaborate, convex upslope headwall scarps and extensional faults at their margins, and contain blocky debris. Their headwall morphology classifies them as ‘slope-bound’. Exceptions exist which have no headwall scarp at all, which this study terms ‘whole wedge failures’.

5) The basal shear surfaces of the mass transport deposits run along multiple bedding planes, connected by lateral and tangential ramps. The basal shear surface is laterally terminated along headwall, lateral and frontal ramps. Lateral and frontal ramp traces meander around mud volcanoes, which form obstacles to the slope failures.

6) Compressive domains are deformed by extensive thrust and fold sheets, and terminate against a frontal ramp. They are classified as ‘frontally confined’.

7) Many of the mass transport complexes contain syndepositional structures indicative of episodic failure; ramps along the headwall show successive retrogression along vertically shallowing basal shear surfaces; lateral ramps along the basal share surface show multiple slope failures exhibiting varying degrees of erosion; and frontal domains show evolving kinematics, basal shear surface reactivation, and potentially changes between compressive and extensional strain. The mass transport deposits evolved over time and did not fail instantaneously.

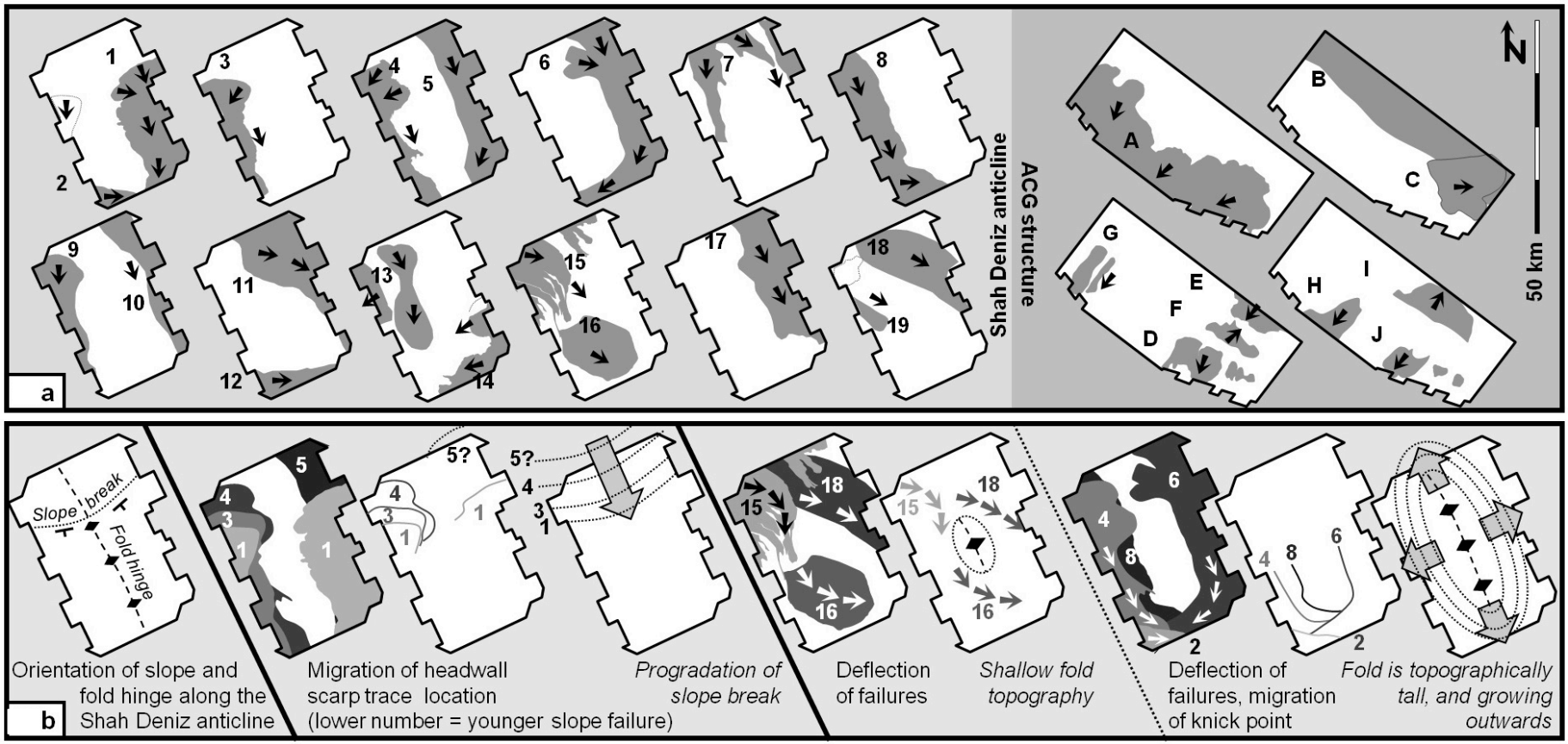

Figure 4.12 Location and outlines of mass transport deposits in the study area. [a] Outlines of the seismic survey and mass transport deposits outlines. Arrows show sediment transport directions interpreted from kinematic indicators. [b] Interpretations regarding basin margin progradation and fold hinge growth, drawn from selected mass transport deposit outlines.

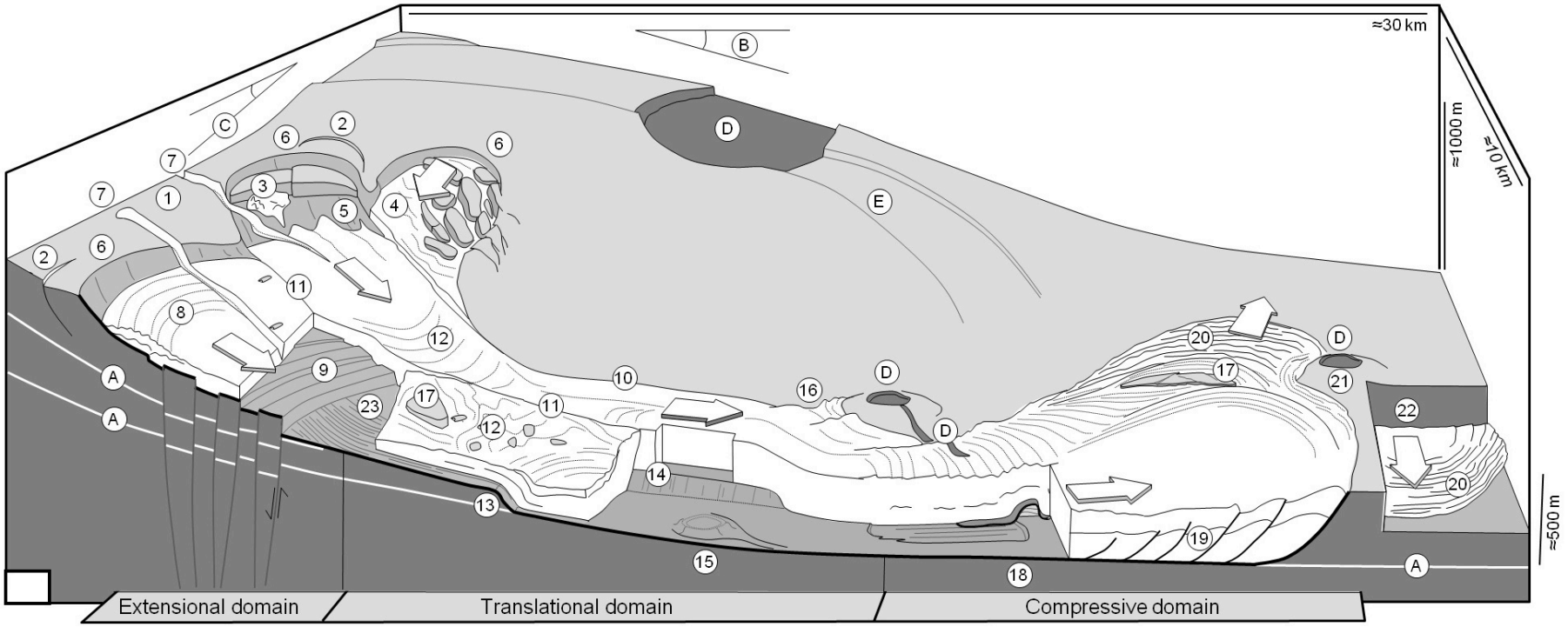

Figure 4.13 Cartoon of a Caspian mass transport deposit and a summary of all the syndepositional features contained within it relative to each structural domain. Broad white arrows show material transport directions. Modified from Bull & Cartwright (2009) and Prior et al., (1984). Key: (A) Layers of weakness. (B) Slope created by basin margin. (C) Slope created by fold uplift (D) Mud volcano crater. (E) Curved grabens emanating from mud volcano centre. Extensional domain (1) Headwall scarp (2) Crown cracks. (3) rotated blocks and residual debris (4) rafted blocks and sidewall fragmentation. (5) detached portion of the flow exposing evacuated basal shear surface. (6) arcuate scarps, showing divergent convex upslope orientations towards the fold flank and basin slope. (7) Headless canyons incising the headwall. (8) convex upslope lineations. (9) Normal ramps and flats in the basal shear surface located around fault traces. Translational domain (10) lateral margin (11) longitudinal shear zone. (12) Flow fabrics, convex downslope, and chaotic. (13) Normal ramp, with coherent drape of mass transport deposit facies. (14) Lateral ramp. (15) elongate strain shadow behind obstacle (16) restraining bend in the lateral margin. (17) Translated blocks Compressive domain (18) Blocks and basal shear surface scours. (19) Thrust sheet. (20) Pressure ridges. (21) Obstacle at mass transport deposit toe modifying frontal morphology. (22) Older mass transport deposit travelling along the old layer of weakness. (23) basal shear surface grooves.

Novel structures

This study describes several novel, unreported features: 1) divergently oriented mass transport deposit headwall lobes 2) the absence of a traditional headwall scarp in failed growth strata packages —which this study terms 'whole wedge failure'— 3) restraining bends in the lateral margin, and 4) an increase in throw along thrust faults towards the mass transport deposit toe (Figure 4.13).

Many of the elaborate extensional and translational domain structures relate to the configuration of the slopes on which they formed; the South Caspian Basin margin consists of multiple, obliquely oriented slopes, undergoing rapid sedimentation and tectonic uplift, and contains abundant mud volcanoes which controlled the development of the divergent headwall lobe orientations (Figure 4.3) and lateral margin restraining bends (Figure 4.8b), whilst wedge-tip failure (Figure 4.5 c) is generated along tectonically driven, strata wedges. Such structures are therefore probably exclusive to tectonically active margins, and analogues feature may be present in similar settings such as northern South America (Ratzov *et al.*, 2007), and offshore Trinidad (Moscardelli *et al.*, 2006).

The compressive domain contains several intricate structures. New insights regarding the evolution of this domain in 'frontally confined' landslides, have been highlighted by Frey-Martinez et al., (2006) and traditional evolutionary models (e.g. Farrell, 1984) questioned. Our interpretations show that this region evolves in a complex, episodic fashion, exhibiting changing kinematics, and potentially even alternating between compression and extension.

The 'whole wedge failures' described in this study may impact hydrocarbon exploration in the region; they lie above the reservoir interval, and erode 100 m-scale, regionally extensive, disconformities, which could affect predictions regarding stratigraphy prior to drilling (e.g. Heinio & Davies, 2009; Butler & McCaffrey, 2010). It is therefore essential to carefully map mass transport deposits occurring in growth strata in three dimensions, particularly as these unconformities are difficult to detect in vertical seismic sections (Figure 4.5 b).

Geological controls on the unstable South Caspian Basin margin

Several geological processes are known to destabilise submarine slopes (discussed in Frey-Martinez *et al.*, 2005), several of which are present in the study area; high sedimentation rates (Nadirov *et al.*, 1997; Allen *et al.*, 2002), active seismicity, with magnitudes of >6 (Jackson *et al.*, 2002), large and rapid lake level fluctuations (Kroonenberg *et al.*, 1997), and gas hydrates accumulations (Diaconescu & Knapp, 2000; Diaconescu *et al.*, 2001) all operate along the western South Caspian Basin margin. As slopes are progressively weakened by several 'primer' processes, the final triggers that combined to destabilise each of the slope failures are practically impossible to deduce and may even have been relatively low magnitude events (Varnes *et al.*, 1978; Davies & Clark, 2006).

Multiple syndepositional features within the most recent mass transport complex margin demonstrate this; the headwall scarp along the Shah Deniz Anticline lies along fault traces which were active before and potentially during, its emplacement implying a seismic trigger (e.g. Gee *et al.*, 2005). However, evidence for slope destabilisation by (low-stand) canyon erosion (e.g. McHugh *et al.*, 2002) also exists on adjacent, contemporaneous slopes, whilst previous work suggests the same complex was triggered by gas hydrate disassociation (Diaconescu & Knapp, 2000; Diaconescu *et al.*, 2001; Diaconescu, 2002). The multitude of processes which are present in this single mass transport complex demonstrates how unlikely it is that a single trigger should be sought for each separate deposit; rather, individual portions of the mass transport complex failed episodically and were each conceivably destabilised by different triggers which operated simultaneously along the basin margin.

By examining the population of mass transport deposits as a whole however, longer term, basin-scale processes which contributed to a regime of instability can be interpreted. The sedimentary succession examined in this study is dominated by mass transport deposits, however no major failures beneath the Pliocene – Pleistocene boundary are encountered (Figure 4.3) and neither do published regional seismic lines (Abdullayev, 2000; Abreu & Nummedal, 2007). Pliocene and older slopes in the study area were apparently stable, with conditions changing in the basin after the Pliocene. The Pleistocene epoch is as a falling stage systems tract, and sedimentation around the basin margin is characterised by the development of thick, progradational clinoform complexes (Abdullayev, 2000; Abreu & Nummedal, 2007). Slope breaks along the clinoforms are shown to be the primary locations along which failures are generated (Figure 4.12a) and are known sites of rapid burial, overpressure generation and slope instability (Dugan & Stigall, 2010; Urgeles *et al.*, 2010). The base of the Pleistocene also coincides with a change in the regional tectonic regime: the initiation of an accretionary wedge and fold train along the Apsheron Ridge (Devlin *et al.*, 1999): the incipient subduction zone between the South, and Mid Caspian Basins (Allen *et al.*, 2002). This event generated regional subsidence and seismic activity, steepened slopes, and potentially elevated pore fluid pressures in areas close to the subduction zone.

5. Discussion, Summary and Conclusions

5.1. DISCUSSION

The principal research aim of this thesis was stated in chapter 1:

Is it possible to identify climatic signals and autogenic sedimentary processes within fold growth strata, and if so, how do these control syn-tectonic sedimentation and growth strata architecture?

This question is readdressed below and its relevance and impact is evaluated. The geological processes described in this thesis are then reviewed, and a summary of interpreted orbital climatic signals is presented. Subsequently this chapter outlines suggestions for further work.

Climatic and tectonic controls on growth strata development

A primary observation of climatic forcing in sedimentary successions is a strongly cyclical, vertically pervasive stacking pattern (e.g. Scholz, 2002; Tucker, 2003), which is observed at several scales in this thesis. These include; [1] progressive unconformities (chapter 2), [2] slope failures (chapter 4), [3] coloured bands in mud prone successions (chapter 3), and [4] mud – sand couplets in less mud-prone successions (chapter 3). In addition to these, this thesis also describes the seismic stratigraphy along the basin margin, which identifies fourth and fifth-orderdepositional cycles. All these processes are potentially climatically driven, but many of them took place within fold mini-basins that were actively deforming. Therefore the effects of tectonics, specifically fold uplift, must be addressed before climatic forcing can be considered. The following sections discuss the relative influences of tectonics and climate on the sedimentary processes mentioned above.

Variations in burial/uplift ratio and progressive unconformities

In chapter 2, the separation of fold uplift and climate change was addressed by correlating seismic reflections of progressive unconformities over regionally separated structures and the basin margin. Progressive unconformities develop in fold growth strata due to variations in burial/uplift ratio (Storti & Poblet, 1997), driven either by fold uplift rate (tectonic pulses), or burial rate (sedimentary pulses). The distinction between the two competing processes is difficult to make along an individual fold, and progressive unconformities are sometimes cursorily assumed to be driven by tectonics (Masaferro *et al.*, 2002).

The key observation made in this study was that many progressive unconformities in the South Caspian Basin, developed synchronously, not only around separated structures, but at the same time as (seismically detectable) sequence boundaries along the basin margin. The unconformity surfaces were initiated over regionally extensive, (perhaps even basin-wide) areas, at times of relative water-level falls. This process can be concisely explained without needing to appeal to tectonics, by fluctuations in sedimentation supply, which in this study area, an enclosed lacustrine basin, occurred at the same time as relative water-level fluctuations. The study suggests a model of climatically influenced fold growth strata, whereby wet and dry periods in catchment areas surrounding the basin repetitively altered the amount of riverine water and sediment flowing into it. Fold uplift rates apparently remained constant, or at least changed only slowly. Several uncorrelated unconformities also exist in the data however, which were probably caused by localised strain across individual folds.

Conversely if the synchronous unconformities of chapter 2 were explained by tectonic pulsing, this would imply that both folds as well as the western basin margin were repeatedly uplifted simultaneously. The study's two folds are separated by a considerable distance (85 km) and are part of separate, strain-partitioned, structural regions of the basin. The ACG structure is located within the Apsheron Ridge accretionary prism —driven by a northwards component of motion and subduction of the South Caspian Plate—, whereas the Shah Deniz fold lies in a fold train that curves to the west (Green *et al.*, 2009) —apparently part of deformation associated with the West Caspian Fault, accommodating the South Caspian Basin's westwards component of motion (Allen *et al.*, 2003). A third fold, the Apsheron Anticline (also part of the Apsheron Ridge), lies between Shah Deniz and ACG structure, and has experienced periods of no structural activity and uplift, despite containing early growth strata of a similar age. Because of the differing kinematic origins and non-uniform growth histories of folds in the area, this thesis concludes that there is no evidence for widespread, simultaneous, tectonic pulses.

A progressive unconformity was also observed in the field along the Quaradag anticline (Figure 3.14). In this example the unconformity lies above a facies association change from shallow water low-stand sand beds to deep water lithofacies. This observation supports the model of coincident timing of progressive unconformities with lake level falls —observed from folds in the basin interior— and suggests this also operated along the basin shelf. However, lateral correlations between the Quaradag and Kerkesdag anticlines, reveal complexity; the low-stand sand at Quaradag Figure 3.22 a) was deposited *before* the progressive unconformity, but the equivalent deposit around Kerkesdag was deposited *after* tilting and erosion. This may be due to variations in the fold activity — altering the burial/uplift rate— between both structures.

In summary: progressive unconformities form common components of South Caspian Basin fold growth strata architecture. Most progressive unconformities were probably climatically controlled and initiated at times of relatively low sediment supply and falling relative water levels. Fold growth rate remains a crucial factor in determining the sensitivity of the growth strata to climate-induced unconformities.

Slope failure and mass transport deposits

Ancient landslide deposits (mass transport complexes) within the growth strata of the Shah Deniz and ACG structures occur repetitively in the sedimentary succession, but understanding their tectonic and climatic controls is challenging. Landslides are generated by a range of autogenic, climatic and tectonic processes, many of which probably operate synchronously on a slope (Appendix 6). Identifying the triggers and exact timings of *palaeo* landslides is especially complex as data coverage is poor, and important geological information is often eroded away during the event or by later slope failures. In addition to this, using a regional correlation between both structures to identify the effects of fold uplift on the data —as used in chapter 2— is flawed, as both folds and slope systems are subject to separate primers and triggers and are unlikely to have been identically and simultaneously unstable. A (climatic) slope destabilisation of the Shah Deniz anticline, may not necessarily result in regionally synchronous landslide event along the ACG structure. Fully establishing the climatic and tectonic controls on the landslides is therefore challenging and speculative at best.

Despite this uncertainty, the question of 'tectonics versus climate' was at least partially addressed in chapter 4. Tectonics destabilises slopes in two ways; fold amplification steepens slopes, *priming* them for later failure, and fault seismicity can *trigger* landslides via a variety of mechanisms (Varnes *et al.*, 1978; Hampton *et al.*, 1996). Seismic mapping of the mass transport complexes in this study area showed several examples where fold growth, and slope steepening along fold flanks was not a major primer; around the Shah Deniz Anticline most failures did not nucleate along fold flanks, but were instead sourced along an adjacent, tangentially oriented slope formed by basin margin clinoform foresets. At the time of these failures, rapid sedimentation from an adjacent delta, (named the 'Baku Delta' in Chapter 2), minimised the influence of the underlying fold on slope topography and stability. Instead, rapid sedimentation was itself a probable primer that weakened slopes, causing steepening, sediment loading, and overpressure generation through disequilibrium compaction (e.g. Osborne & Swarbrick, 1997). The slope destabilisation caused by the Baku Delta is localised to the north-western basin margin, and is not present around the distally located ACG structure, which contains fewer, and generally smaller, mass transport deposits (Figure 1, and Table 2). At this location, many of the smaller landslides may well have been primed by fold uplift and steepening although there are also extensive (estimated at above 3500 km^2 in area, and several hundred metres thick) and regionally synchronous mass transport deposits, such as at the present-day lake bed, that may have been initiated by a larger, basin-wide process, as yet undefined. Whilst the study addressed priming mechanisms of the South Caspian landslides, their ultimate *triggers* still remain unknown. Climatic forcing or fault activity are both plausible triggers for each landslide.

Field scale cyclicity; mud colouration and deep – shallow cycles

Field outcrops of the Apsheron Formation around the Quaradag and Kerkesdag folds, described in chapter 3, show repetitive sediment stacking patterns which are superimposed onto a overall trend of coarsening-upwards and shallowing-upwards. In the upper (shallower) portion of the formation, tops of parasequences are defined by extensive beds of sand and bioclastic limestone every 100 – 150 m, and in the shallowest sections, every 10 – 40 m, whilst in mud-dominated (deeper) sections of the formation, rock colour alternates between brown and grey shades of mud at approximately 50 m intervals.

The mudstone – sandstone facies changes reflect cyclical fluctuations of relative water level, whereas a model of wet – dry climate cycles that altered redox conditions along the lake bed is postulated to explain the colour banding in the mudstones. Redox conditions in the Apsheron palaeoenvironments may have been altered by fluctuations in lake level, or fluctuating episodes of river activity and thermal water column stratification (e.g. Reading & Collinson, 1996).

Relative water level in the basin is driven by a combination of climatic and tectonic controls, which are not always separable. The underlying reason for the long scale, overall shallowing trend in the Apsheronian is unknown and requires further research (discussed below). However, for the higher frequency oscillations, the relative roles of both controls can be speculatively addressed. Observations and inferences from chapter 2 suggest tectonic pulses were of minor influence on the sedimentary environment (discussed above). Apsheron Formation palaeocurrent data, although sparse, shows that fold topography did not deflect sediment pathways and that the topographic expression of the two anticlines was negligible. The present-day configuration of the Shah Deniz fold, may form an analogue to the Apsheronian Kerkesdag and Quaradag folds. It is located in a similar position, up-dip of the basin margin shelf break and is largely buried under a thick sedimentary succession, which thins towards more distal areas. If this is an accurate analogue, then the Kerkesdag and Quaradag folds were topographically insignificant, and the Apsheron Formation sedimentary fluctuations were non-tectonic, climatic events.

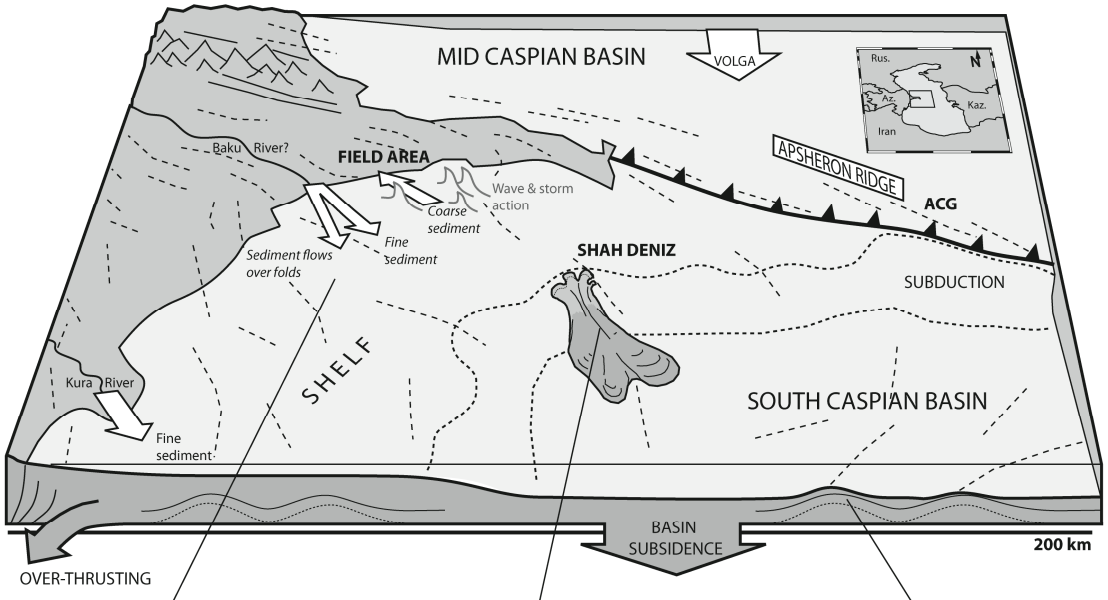

Shelf sedimentation

- Apsheron formation is mud-prone. Suspension settling of laminated fine grained sediment.
- Sediment is sourced from the Caucasus, transported to shelf via river systems.
- Bi-directional sediment flux: fine grained sediment is sourced from onshore, but course grained sediment is transported from distal to proximal areas.
- Apsheron Suite shows a fluctuating lake level within an overall shallowing-upwards trend.

Tectonic controls

-Large scale basin margin uplift may contribute to or amplify the global shallowing trend.
-Localised fold growth is of little influence; sedimentation rate outpaces fold uplift and lake level fluctuations are of a larger magnitudes than tectonic uplifts.

Climatic controls

- Drying of climate is the likely driver to the shallowing upwards trend seen in the formation.
- Offshore shelf conditions change cyclically, potentially at Milankovic frequences (41.000

Mass wasting

- (Palaeo) shelf margin is a gravitationally unstable area.
- Large volumes of sediment are transported from the shelf edge and from fold flanks to distal areas by submarine slope failures

Tectonic controls

- Sediment routing pathways controlled by fold topography.
- Upslope development of slope failure is influenced by fold location.
- Minor failures are sourced on inclined fold flanks.
- Earthquakes are potential landslide triggers.

Climatic controls

- Slope failures are sourced along shelf break, defined by sedimentary architecture., in turn this is controlled by climate.
- Sedimentation rate is key primer to slope instability.
- There may be a link between changes in lake level and timing of slope failures, though this has not be conclusiuvely established.

Offshore fold growth and burial

- Antilcines are buried during thier growth.
- Folds uplift in a smooth and gradual manner, however sediment supply fluctuates by cyclical pulses.
- The 'growth strata' succession contains several unconformities, which are regionally extensive and synchronous with stratigraphic events.

Tectonic controls

- Fold growth is driven by the subduction and thrusting of the South Caspian crust beneith the Mid Caspian Basin and Caucasus; part of the wider, compressive tectonic regime of the Arabia-Eurasia Collision
- Tectonic pulses along individual folds can produce (rare) stratigraphic unconformties in the growth stratal succession.
- 'Buckle type' fold kinematics produce down section fanning geometries to the growth stratal succession.

Climatic controls

- Lake level and sediment supply are closely linked; lake level rises (transgressions) correspond to periods of increased sedimentation and fold burial, wheras lake level falls (regressions) correspond to sedimentary starvations and fold crest emergence.

Figure 5.1 Summary diagram of sedimentary and tectonic processes of the South Caspian Basin

Milankovic frequency of repetitive sedimentary processes

Earth's orbital geometry perpetually changes through time along repetitive 'Milankovic cycles; variations in earth's Precession, Obliquity and Eccentricity, which operate on 23,000 – 400,000 year timescales. These variations affect the earth's climate by altering the distribution and amount of solar insolation. Orbital variations are visible throughout the Cenozoic geological record, often oscillating around other trends, driven by changes such as tectonics, and global atmospheric composition (Zachos *et al.*, 2001). Milankovic cyclicity has been observed in other lacustrine basins, which are typically climatically sensitive environments (e.g. Carroll & Bohacs, 1999; Keighley *et al.*, 2003; Prokopenko *et al.*, 2006) and is anticipated in the tectono-sedimentary processes described in the sections above.

Accumulating and tabulating the occurrence of all the sedimentary processes described in this thesis is a preliminary attempt at addressing orbital forcing on the Pleistocene South Caspian Basin (Table 5.1). This is challenging as age data in the Pleistocene stratigraphy are rare and significant disagreement exists between published estimates (Figure 5.2). In addition to this, several data are only partially sampled, so a comparison between different records involves considerable extrapolation. Nevertheless there appears to be broad agreement of observations between seismic and field data, and Orbital forcing can at least be tentatively suggested, if not fully proven.

Milankovic scale repetitions are most apparent if the analysis uses the age ranges from two published estimates: Christiaan van Baak's thesis (2010) based on magnetostratigraphy, and Fowler *et al*., (2000) based on BP proprietary data. Both of these estimates place the Apsheron and Akchagyl formations within the Pleistocene (Figure 5.2), which agrees with palynological data (Richards *et al.*, 2012), however both estimates ignores each other's (unpublished) ash band dates that place the top of the Apsheron Formation near 0.96 Ma, and the base of the section as near 2.28 Ma (Kroonenberg *et al.*, 1997; Fowler *et al.*, 2000). Clearly there are still uncertainties surrounding the absolute dates of the Apsheron Formation; the length estimates of which range between 0.9 million years to 1.5 million years. If the longest age range estimates are used, couplets of mud facies colour bands (Figure 3.6) repeat at a rate approximating 41,000 year obliquity cycles, whilst fourth-ordersedimentary sequences, observed in onshore field outcrops, and offshore in seismic data, are consistent with 100,000 year eccentricity cycles. The fourth-ordersequences are by extension, also coincident with progressive unconformities along fold crests. However, some processes do not appear orbitally forced; the frequency of slope failures remains elusive for instance, and seismic scale, mega-sequences described in chapter 2, do not correspond with any predicted Milankovic frequency. The latter may well reflect periods of varying basement subsidence, driven by tectonics (Degens & Paluska, 1979; Allen *et al.*, 2002) or thermal-isostatic processes (Egan *et al.*, 2009; Green *et al.*, 2009).

Sedimentary process	Observed in		Occurrence		
	Data	Location	Age range	Amount	notes
Stratigraphic mega sequences	Regional 2D seismic lines	Basin margin and interior	Latest Akchagyl-undetermined, post Apsheronian	3	
Stratigraphic sequences	Regional 2D seismic lines	Basin margin	Latest Akchagyl-undetermined, post Apsheronian	13	
			Apsheron Formation only	11	
Synchronous progressive unconformities	Regional 2D seismic lines	Basin interior	Latest Akchagyl-undetermined, post Apsheronian	15	
			Apsheron Formation	12 or 13	
Mass transport complexes	Shah Deniz Fold, 3D seismic	Basin margin and interior	Akchagyl Formation - present day	17 or 18	
			Apsheron Formation only	6	
	ACG structure, 3D seismic	Basin interior	Akchagyl Formation - present day	10	
			Apsheron Formation only	7	
Sand - Mud successions	Outcrop and sattelite data	Basin margin, shelf	Intra - Apsheron Formation, extensive	14	5 seen in outcrop, extrapolated to 14 over entire Apsheron Formation
Brown-Grey mud couplets	Outcrop data	Basin margin, shelf	Intra - Apsheron Formation, limited	34	50 m frequency observed in outcrop, extrapolated to 34 over entire formation

Apsheron Formation, age estimates				Expected orbital cycles within the Apsheron formation				Expected orbital cycles, Apsheron-Present			
Publication	From (Mya)	To (Mya)	timespan (My)	Axial precession 23,000 years Cycles	Obliquity 41,000 years Cycles	Eccentricity 100,000 years Cycles	Eccentricity 400,000 years Cycles	Axial precession 23,000 years Cycles	Obliquity 41,000 years Cycles	Eccentricity 100,000 years Cycles	Eccentricity 400,000 years Cycles
Jones & Simmon 1996 (max), Allen et al., 2002	1.6	0.7	0.9	39.1	22.0	9	2.25	69.6	39.0	16	4
Van Baak 2010 (min estimate)	1.8	0.9	0.9	39.1	22.0	9	2.25	78.3	43.9	18	4.5
Devlin *et al.*, 1999	1.85	0.7	1.15	50.0	28.0	**11.5**	2.875	80.4	45.1	18.5	4.625
Van Baak 2010 (max estimate)	2	0.9	1.1	47.8	26.8	**11**	2.75	100.0	48.8	20	5
Fowler *et al.*, 1999 (min estimate)	2.28	1.04	1.24	53.9	**30.2**	**12.4**	3.1	99.1	55.6	22.8	5.7
Fowler *et al.*, 1999 (max estimate)	2.47	0.97	1.5	65.2	**36.6**	**15**	3.75	107.4	60.2	24.7	6.175

Sedimentary process	Observed in		Climatic characteristics				Interpretation	
	Data	Location	Repetative?	Evenly spaced?	Regionally synchronous?	Climate is known to affect this sedimentary process	Climatic?	Closest orbital cycle
Stratigraphic mega sequences	Regional seismic lines	Basin margin and interior	yes	yes	Yes	yes	unproven	400,000 year eccentricity
Stratigraphic sequences	Regional seismic lines	Basin margin	yes	yes	Yes	yes	likely	100,000 year eccentricity
Progressive unconformities	Regional seismic lines	Basin interior	yes	yes	Yes	yes	likely	100,000 year eccentricity
Mass transport complexes	3D seismic	Basin margin and interior	yes	partially	?	?	unkown	
Sand - Mud successions	Outcrop and sattelite data	Basin margin, shelf	yes	yes	?	?	likely	41,000 year obliquity
Brown-Grey mud couplets	Outcrop data	Basin margin, shelf	yes	yes	?	?	likely	100,000 year eccentricity

Table 5.1 Comparison chart of repetitive events observed in this study (top), published ages of the Pleistocene South Caspian succession (middle) , and possible Milankovic cyclicity (bottom) *This table should ideally be printed on A3 paper*

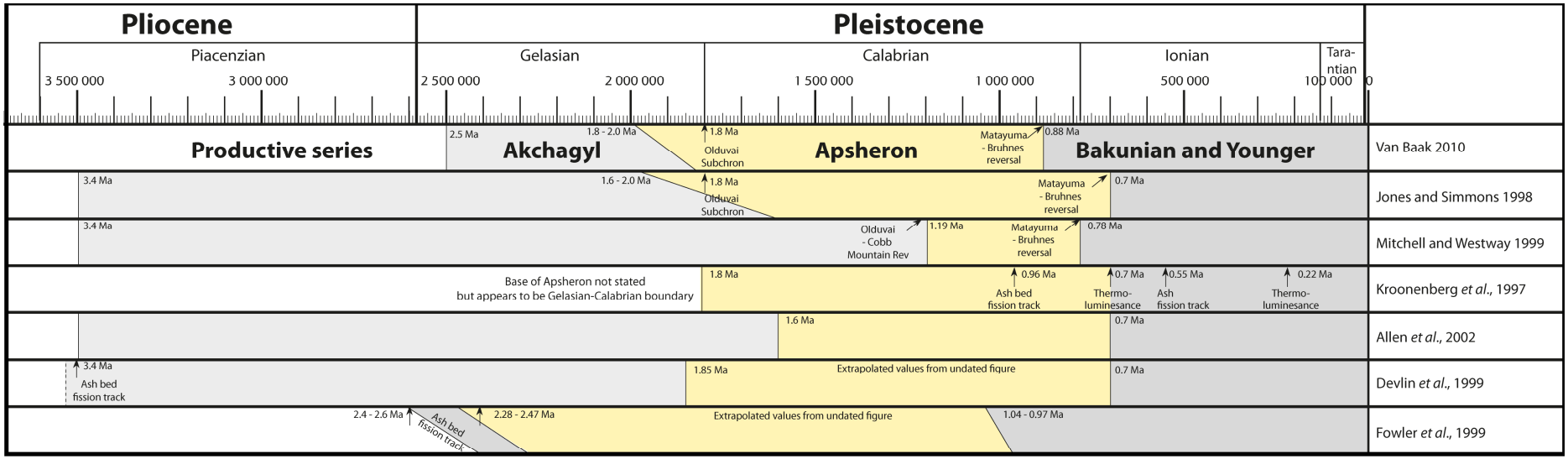

Bakunian and younger Formations	Ash fission track, within formation (0.55 Ma) Thermoluminescance at boundary (0.7 Ma)
Apsheron Formation	Ash fission track (0.96 Ma) Magnetic reversal, near top of formation (0.88 Ma) Magnetic reversal within the formation (1.8 Ma)
Akchagyl Formation	Ash fission track near base (2.4 - 2.6 Ma) Ash fission track, near base (3.4 Ma)

Figure 5.2 Summary of age estimates for the South Caspian Basin

Recommendations for further work

Towards an absolute Pleistocene chronology for the South Caspian Basin

A major limiting problem that each study in this thesis encountered was the poor age control in the South Caspian Pleistocene geological record. As discussed previously, this is challenging due to the isolated nature of the basin, endemic biostratigraphy, debate concerning the age of the base Pleistocene, and the scarcity of accessibility of Soviet-era research (see Nikiforova, 2004; Gibbard *et al.*, 2010). Several attempts have been made to address this issue (see Jones & Simmons, 1996; Zubakov, 2001), the most recent are the magnetostratigraphic study of van Baak (2010), and a comparable, integrated study in the lesser Caucasus (Joannin *et al.*, 2010). However no two published studies have produced the same results, and age estimates still vary wildly (Figure 5.2).

Radiometrically dated late Pliocene and early Pleistocene ash bands have been referred to in the literature (Jones & Simmons, 1996; Kroonenberg *et al.*, 1997; Devlin *et al.*, 1999), however they are essentially unpublished, the accuracy of these results is disputed, and ages are used inconsistently between citations (discussed in Mitchell & Westaway, 1999; van Baak, 2010). There is therefore a clear opportunity for renewed absolute dating of the Pleistocene successions of the South Caspian Basin. Apsheron Formation outcrops are inter-bedded with volcanic tuffs, which are present throughout the succession (Chapter 2), and provide a high-resolution, untapped tephrochronology database. Pleistocene age, fine grained, ash beds can be dated using either fission track analysis (outlined in Westgate & Briggs, 1980), or by radiometric $^{40}Ar/^{39}Ar$ methods (e.g. Joannin *et al.*, 2010). If absolute dates can be established, these should then be integrated with other data: magnetostratigraphic records(van Baak, 2010), and endemic biostratigraphy, (Nikiforova, 2004; Osipova, 2009), to produce a robust age model for the South Caspian Pleistocene epoch. Ash beds occur throughout the Apsheron Formation, however the most important are located close to a major regression surface in the upper portion of the onshore succession (identified in chapter 2), as this marker horizon can be regionally calibrated between both onshore and offshore areas. Absolute date spikes within the Apsheron Formation would address several outstanding regional geological questions, regarding the formation's age and rate of sedimentation, subsidence in the South Caspian Basin as a whole, and the timing of glacial – interglacial cycles with warm or cool periods. Furthermore it would provide a valuable tool to calibrate and test the frequency of the cyclical, probably palaeoclimatic, sedimentary processes, and models that this thesis highlights (discussed above).

Integrating stable isotope data with sequence stratigraphy

The topic of 'climate versus tectonics' forms a perpetual theme throughout this thesis, which could be further addressed with additional, climatically sensitive, tectonically insensitive data. Studies in other basins for instance, have integrated climate proxy data (stable isotopes of oxygen and carbon) with sequence stratigraphy, (essentially a combination of climate, tectonics and accommodation space generation) to identify non-eustatic deepening and shallowing events (e.g. Kukla & Cílek, 1996; Álvaro *et al.*, 2000; Rasmussen, 2004). Although these studies are not directly applicable to the Pleistocene South Caspian Basin, which is not impacted by eustacy, a similar approach could still be applied. Tectonic deepening of the basin has been suggested by other studies, though not proven (Degens & Paluska, 1979) and isolated tectonic pulses have been identified in offshore data (chapter 2, and discussed above) and might therefore be expected in the onshore sedimentary record.

A palaeoclimate record could be collected from the same mud-prone successions of this thesis (chapter 3). Possible data sources include carbon and oxygen-stable isotope proxies, from intact macro fossils or microfossils, and the separate records of temperature and depth-sensitive ostracods and pollen preserved within mudstone facies (Jones & Simmons, 1996). In addition to this, stable isotopes of strontium, or molybdenum within the mudstones could also be employed to track variations in continental weathering (Dasch, 1969; Siebert *et al.*, 2003), and could be used as a proxy record of wet and dry climatic periods, or varying uplift of the Greater Caucasus. Care should be taken to identify any periods of non-deposition, i.e. progressive unconformities, which would compromise the record.

Besides testing for, and identifying tectonic pulses in the Pleistocene geological record, the results would address several interesting questions: [1] the idea of sudden versus gradual deepening events, and the response time of relative lake levels to climatic changes; [2] a test of the model, suggested in chapter 2, of mud colour, driven by climatic fluctuations; [3] a resolution of the debate on timings of warm or cool periods, with increases in river activity and weathering (discussed in chapter 3).

5.2. SUMMARY AND CONCLUSIONS

This thesis set out to identify the relative controls of tectonic, sedimentary and climatic processes on Pleistocene fold growth strata in the South Caspian Basin. Its results add to the scientific understanding of the regional geology and of tectono-sedimentary processes in general.

The main finding which is recurrent throughout all three studies, is the strong influence of repetitive (climate-driven) lake level on Pleistocene – present-day South Caspian stratigraphy. This contrasts with the comparatively subdued and longer term effects of tectonic fold uplift, which is outpaced by high sedimentation rates. The repetitive sedimentary cycles are suggested to represent orbital Milankovic cycles of 40,000 years (obliquity) and 100,000 years (eccentricity), of which eccentricity is the most apparent. However this suggestion is not fully verified as South Caspian geochronology is as yet still unconstrained.

The section below summarises the topic of each chapter and reiterates the secondary conclusions of this thesis.

Chapter 1 investigated the syntectonic burial history of several folds in the South Caspian Basin, and searched for seismic scale, climatic and tectonic signals in their growth strata.

The South Caspian anticlines are identified as buckle folds which grew via limb rotation at a slow, constant or gradually changing rate. During uplift they were buried at fluctuating sedimentation rates.

Progressive unconformities within the fold growth strata developed over a regionally extensive area, during falling stage, and low-stand systems tracts, and were driven by climatically dry periods of low river activity, falling relative water level, and sedimentary hiatuses which reoccurred at rates in agreement with a 100,000 year, orbital eccentricity cycle.

High overall sedimentation rates may have played a role in blanketing and suppressing fold growth over million year time-scales.

Chapter 2 described early Pleistocene facies of the Apsheron Formation, and investigated the impact of fold uplift on its deposition.

The Apsheron Formation represents a series of depositional environments stretching from coastal nearshore to offshore shelf. The sedimentary succession fluctuates on a 25 – 100 m-scale between coarse, nearshore facies and mud-dominated, offshore shelf facies. Sedimentation in offshore muds was dominated by suspension settling with minor reworking by bottom water currents, whereas proximal sandy and shelly lithofacies show wave and storm dominated nearshore depositional processes.

The study identifies a gradual shallowing-upwards trend to the Apsheron Formation, and a regionally important sequence boundary which divides the succession into a deep offshore mud dominated section, and shallower nearshore section.

Although the Apsheron Formation was deposited during active fold uplift, this process seems to have been of minor influence, indicating that burial rates along the NW South Caspian Basin margin were generally in

excess of uplift rates along the folds. Climate change was apparently a far more influential driver on sedimentation.

Several repetitive sedimentary cycles are identified within the Apsheron Formation, which may be orbital in nature and indicative of climatic forcing; sedimentary sequences reoccur at timescales which are consistent with a 100,000 year eccentrity cycle, whereas 25 – 50 m-scale mudstone coloured banding, appears to repeat along a 41,000 year obliquity series.

Chapter 3 examined, the seismic scale morphology, evolution, and kinematics of mass transport deposits in fold growth strata.

A large proportion of Pleistocene – present-day sedimentary succession along the western margin of the South Caspian Basin consists of remobilised sediment, emplaced as mass transport deposits and -complexes, which range from 10,000 to 50,000 m in lateral extent, but are potentially much larger. The largest of these deforms the present-day lake bed.

Mass transport deposit morphology typically includes an extensional domain with elaborate, convex upslope headwall scarps, filled with blocky debris. Their headwall morphology classifies most as 'slope-bound' though novel exceptions exist which display no headwall scarp, which this thesis terms 'whole wedge failures'. Basal shear surfaces commonly run along multiple bedding planes, and are laterally terminated along headwall, lateral and frontal ramps. Compressive domains contain extensive and complex thrust and fold sheets, and are classified as 'frontally confined'.

Several novel, unreported features, are described; these are: 1) divergently oriented mass transport deposit headwall lobes 2) whole wedge failures 3) restraining bends in the lateral margin, and 4) an increase in throw along thrust faults towards the mass transport deposit toe.

Many of the mass transport complexes contain syndepositional structures indicative of episodic failure, evolving kinematics, and potentially changes between compressive and extensional strain. They also show interactions with contemporaneously active geological structures: Basin slope-generated landslides were influenced by a nearby fold, which controlled their evolution and extent, and created long-lived, syntectonically changing, sediment corridors, whilst mud volcanoes acted as rigid obstacles which deflected landslides around them along curved lateral ramps.

Landslides were initiated along two types of slope: inclined fold flanks, and the western basin margin, which appears to have generated the majority of the failures.

The triggers that generated the South Caspian Basin landslides are elusive; however several known slope failure mechanisms operated in the basin during their emplacement.

Mass transport deposits are not detected in seismic data beneath the Pliocene – Pleistocene boundary, and a regional tectonic or climatic change occurring at this time may have contributed to a regime of sedimentary instability. This is speculated to be related to a regional, second-order stratigraphic trend and tectonic changes occurring in the basin around this time.

6. Reference list

ABDULLAEV, T.I., FALT, L.M., AKHUNDOV, A., VAN GRAAS, G.W., KVAMME, T., FLOLO, L.H., MEHMANDAROV, K., NARIMANOV, A.A., OLSEN, T.S. & SELJESKOG, G. (1998) A Reservoir Model for the Main Pliocene Reservoirs of the Bahar Field in the Caspian Sea, Azerbaijan. *Petroleum Geoscience*, **4,** 259.

ABDULLAYEV, N.R. (2000) Seismic Stratigraphy of the Upper Pliocene and Quaternary Deposits in the South Caspian Basin. *Journal of Petroleum Science and Engineering*, **28,** 207-226.

ABRAMS, M.A. & NARIMANOV, A.A. (1997) Geochemical Evaluation of Hydrocarbons and Their Potential Sources in the Western South Caspian Depression, Republic of Azerbaijan. *Marine and Petroleum Geology*, **14,** 451-468.

ABREU, V., NUMMEDAL, D., SELF, D., WARE, P. & WITMER, R. (2000) Miocene/Quaternary Sequence Stratigraphy of the Caspian Sea Region: Interplay of Deltaic Systems and Climatic Control on Non-Marine Depositional Sequences. *AAPG Bulletin*, **84,** 1395-1519.

ABREU, V. & NUMMEDAL, D. (2007) Miocene to Quaternary Sequence Stratigraphy of the South and Central Caspian Basins. In: *Oil and Gas of the Greater Caspian Area* (Ed. by P. O. Yilmaz & G. H. Isaksen), *Aapg Studies in Geology*, 65 - 86.

ALLEN, M.B., JONES, S., ISMAIL-ZADEH, A., SIMMONS, M. & ANDERSON, L. (2002) Onset of Subduction as the Cause of Rapid Pliocene-Quaternary Subsidence in the South Caspian Basin. *Geology*, **30,** 775-778.

ALLEN, M.B., VINCENT, S.J., ALSOP, G.I., ISMAIL-ZADEH, A. & FLECKER, R. (2003) Late Cenozoic Deformation in the South Caspian Region: Effects of a Rigid Basement Block within a Collision Zone. *Tectonophysics*, **366,** 223-239.

ALLEN, M.B., JACKSON, J.A. & WALKER, R.T. (2004) Late Cenozoic Reorganization of the Arabia-Eurasia Collision and the Comparison of Short-Term and Long-Term Deformation Rates. *Tectonics*, **23,** TC2008.

ALLEN, M.B. & ARMSTRONG, H.A. (2008) Arabia–Eurasia Collision and the Forcing of Mid-Cenozoic Global Cooling. *Palaeogeography, Palaeoclimatology, Palaeoecology*, **265,** 52-58.

ÁLVARO, J., VENNIN, E., MUÑOZ, A., SÁNCHEZ-VALVERDE, B. & OJEDA, J. (2000) Interplay of Orbital Forcing and Tectonic Pulses in the Cambrian Iberian Platform, Ne Spain. *International Journal of Earth Sciences*, **89,** 366-376.

AMIROV, E. (2008) Full Depositional Cycles and Oxygen 18 Isotopes in Marine Upper Baku Regiostage Succession in the Western Flank of the South Caspian Depression. *EGU Annual Meeting 2008*, Geophysical Research Abstracts. Vienna. **10,** EGU2008-A-00045.

AMOS, C.C., KNAPP, C.C. & KNAPP, J.H. (2008) Seafloor Deformation in the South Caspian Sea: A Potential Proxy for Gas Hydrate Dissociation and Climate Change. *AGU fall meeting*. San Francisco**,** OS33A-1327.

ANADÓN, P., CABRERA, L., COLOMBO, F., MARZO, M. & RIBA, O. (1986) Syntectonic Intraformational Unconformities in Alluvial Fan Deposits, Eastern Ebro Basin Margins (North East Spain). In: *Foreland Basins* (Ed. by P. A. Allen & P. Homewood), *Special Publications of the International Association of Sedimentologists*, **8**, 259-271.

APOL'SKIY, O.P. (1974) Origin of the Black Sea and South Caspian Sea Troughs. *Geotectonics*, **5,** 310-311.

ARTYUSHKOV, E.V. (2007) Formation of the Superdeep South Caspian Basin: Subsidence Driven by Phase Change in Continental Crust. *Russian Geology and Geophysics*, **48,** 1002-1014.

ASCHOFF, J.L. & SCHMITT, J.G. (2008) Distinguishing Syntectonic Unconformity Types to Enhance Analysis of Growth Strata: An Example from the Cretaceous, Southeastern Nevada, USA. *Journal of Sedimentary Research*, **78,** 608.

BALLATO, P., NOWACZYK, N.R., LANDGRAF, A., STRECKER, M.R., FRIEDRICH, A. & TABATABAEI, S.H. (2008) Tectonic Control on Sedimentary Facies Pattern and Sediment Accumulation Rates in the Miocene Foreland Basin of the Southern Alborz Mountains, Northern Iran. *Tectonics*, **27,** TC6001.

BARLEY, B. (1999) Deepwater Problems around the World. *The Leading Edge*, **18,** 488-494.

BELOPOLSKY, A.V. & TALWANI, M. (2007) Assessment of the Greater Caspian Region Petroleum Reservoirs and Thier Role in World Energy. In: *Oil and Gas of the Greater Caspian Area* (Ed. by P. O. Yilmaz & G. H. isaksen), *Aapg Studies in Geology*, 5-7. American Association of Petroleum Geologists.

BENSON, L.V. & THOMPSON, R.S. (1987) Lake-Level Variation in the Lahontan Basin for the Past 50,000 Years. *Quaternary Research*, **28,** 69-85.

BERBERIAN, M. (1983) The Southern Caspian: A Compressional Depression Floored by a Trapped, Modified Oceanic Crust". *Canadian Journal of Earth Sciences*, **20,** 163-183.

BIROT, P. (1937) Thesis - Recherches Sur La Morphologie Des Pyrénées Orientales Franco-Espagnoles, University of Paris, 311 pages.

BRITISH PETROLEUM (2010) Map of Apsheronian Palaeo Shelf Break Traces, Unpublsihed internal report.

BROWN, A.R. (2004) *Interpretation of Three-Dimensional Seismic Data*, 7 edn. Society of Exploration Geophysicists, Tulsa, Oklahoma.

BULL, S., CARTWRIGHT, J. & HUUSE, M. (2009) A Review of Kinematic Indicators from Mass-Transport Complexes Using 3d Seismic Data. *Marine and Petroleum Geology*, **26,** 1132-1151.

BURBANK, D., MEIGS, A. & BROZOVIC, N. (1996) Interactions of Growing Folds and Coeval Depositional Systems. *Basin Research*, **8,** 199-223.

BURYAKOVSKY, L.A., CHILINGAR, G.V. & AMINZADEH, F. (2001a) Geology of Azerbaijan and the South Caspian Basin. In: *Petroleum Geology of the South Caspian Basin* (Ed. by L. A. Buryakovsky, G. V. Chilingar & F. Aminzadeh), 2-16. Gulf Professional Publishing.

BURYAKOVSKY, L.A., CHILINGAR, G.V. & AMINZADEH, F. (2001b) Onshore Oil and Gas Fields. In: *Petroleum Geology of the South Caspian Basin* (Ed. by L. Buryakovsky, G. V. Chilingar & F. Aminzadeh), 32-52. Gulf Professional Publishing.

BUTLER, R.W.H. & LICKORISH, W.H. (1997) Using High-Resolution Stratigraphy to Date Fold and Thrust Activity: Examples from the Neogene of South-Central Sicily. *Journal of Geological Society*, **154,** 633-643.

BUTLER, R.W.H. & MCCAFFREY, W.D. (2010) Structural Evolution and Sediment Entrainment in Mass-Transport Complexes: Outcrop Studies from Italy. *Journal of the Geological Society*, **167,** 617-631.

BUTLER, R.W.H. & TURNER, J.P. (2010) Gravitational Collapse at Continental Margins: Products and Processes; an Introduction. *Journal of the Geological Society*, **167,** 569-570.

CARROLL, A.R. & BOHACS, K.M. (1999) Stratigraphic Classification of Ancient Lakes: Balancing Tectonic and Climatic Controls. *Geology*, **27,** 99.

CARTER, R.M. (1975) A Discussion and Classification of Subaqueous Mass-Transport with Particular Application to Grain-Flow, Slurry-Flow, and Fluxoturbidites. *Earth Science Reviews*, **11,** 145-147.

CASTELLTORT, S., GUILLOCHEAU, F., ROBIN, C., ROUBY, D., NALPAS, T., LAFONT, F. & ESCHARD, R. (2003) Fold Control on the Stratigraphic Record: A Quantified Sequence Stratigraphic Study of the Pico Del Aguila Anticline in the South-Western Pyrenees (Spain). *Basin Research*, **15,** 527-551.

CASTELLTORT, S., POCHAT, S. & VAN DEN DRIESSCHE, J. (2004) How Reliable Are Growth Strata in Interpreting Short-Term (10 S to 100 S Ka) Growth Structures Kinematics? *Comptes rendus-Géoscience*, **336,** 151-158.

CATUNEANU, O., ABREU, V., BHATTACHARYA, J.P., BLUM, M.D., DALRYMPLE, R.W., ERIKSSON, P.G., FIELDING, C.R., FISHER, W.L., GALLOWAY, W.E., GIBLING, M.R., GILES, K.A., HOLBROOK, J.M., JORDAN, R., KENDALL, C.G.S.C., MACURDA, B., MARTINSEN, O.J., MIALL, A.D., NEAL, J.E., NUMMEDAL, D., POMAR, L., POSAMENTIER, H.W., PRATT, B.R., SARG, J.F., SHANLEY, K.W., STEEL, R.J., STRASSER, A., TUCKER, M.E. & WINKER, C. (2009) Towards the Standardization of Sequence Stratigraphy. *Earth-Science Reviews*, **92,** 1-33.

CHEEL, R.J. & LECKIE, D.A. (1993) Hummocky Cross-Stratification. *Sedimentology review*, **1,** 103-122.

COE, A.L. (2003) *The Sedimentary Record of Sea-Level Change*. Cambridge Univ Pr.

COLLINSON, J.D., MOUNTNEY, N.P. & THOMPSON, D.B. (2006) *Sedimentary Structures*, 3 edn. Terra Publishing, Harpenden, England.

DASCH, E.J. (1969) Strontium Isotopes in Weathering Profiles, Deep-Sea Sediments, and Sedimentary Rocks. *Geochimica et Cosmochimica Acta*, **33,** 1521-1552.

DAVIES, R.J. & STEWART, S.A. (2005) Emplacement of Giant Mud Volcanoes in the South Caspian Basin: 3d Seismic Reflection Imaging of Their Root Zones. *Journal of Geological Society*, **162,** 1.

DAVIES, R.J. & CLARK, I.R. (2006) Submarine Slope Failure Primed and Triggered by Silica and Its Diagenesis. *Basin Research*, **18,** 339-350.

DAVIS, D.M., SUPPE, J. & DAHLEN, F.A. (1983) Mechanics of Fold-and-Thrust Belts and Accretionary Wedges. *Journal of Geophysical Research*, **88,** 1153-1172.

DEGENS, E.T. & PALUSKA, A. (1979) Tectonic and Climatic Pulses Recorded in Quaternary Sediments of the Caspian Black Sea Region. *Sedimentary Geology*, **23,** 149-163.

DEVLIN, W.J., COGSWELL, J.M., GASKINS, G.M., ISAKSEN, G.H., PITCHER, D.M., PULS, D.P., STANLEY, K.O. & WALL, G.R.T. (1999) South Caspian Basin: Young, Cool, and Full of Promise. *GSA Today*, **9,** 1–9.

DIACONESCU, C.C. & KNAPP, J.H. (2000) Buried Gas Hydrates in the Deepwater of the South Caspian Sea, Azerbaijan: Implications for Geo-Hazards. *Energy Exploration & Exploitation*, **18,** 385-400.

DIACONESCU, C.C., KIECKHEFER, R.M. & KNAPP, J.H. (2001) Geophysical Evidence for Gas Hydrates in the Deep Water of the South Caspian Basin, Azerbaijan. *Marine and Petroleum Geology*, **18,** 209-221.

DIACONESCU, C.C. (2002) Gas Hydrates of the South Caspian Sea, Azerbaijan: Drilling Hazards and Sea Floor Destabilizers. *Offshore Technology Conference*. Houston, Texas. 14036**,** 1-7.

DIMITROV, L.I. (2002) Mud Volcanoes--the Most Important Pathway for Degassing Deeply Buried Sediments. *Earth-Science Reviews*, **59,** 49-76.

DOGLIONI, C. & PROSSER, G. (1997) Fold Uplift Versus Regional Subsidence and Sedimentation Rate. *Marine and Petroleum Geology*, **14,** 179-190.

DOTT JR, R.H. & BOURGEOIS, J. (1982) Hummocky Stratification: Significance of Its Variable Bedding Sequences. *Bulletin of the Geological Society of America*, **93,** 663.

DUGAN, B. & STIGALL, J. (2010) Origin of Overpressure and Slope Failure in the Ursa Region, Northern Gulf of Mexico. In: *Submarine Mass Movements and Their Consequences* (Ed. by D. C. Mosher, L. Moscardelli, C. D. P. Baxter, R. Urgeles, R. C. Shipp, J. D. Chaytor & H. J. Lee), 167-178. Springer.

EFFIMOFF, I. (2000) The Oil and Gas Resource Base of the Caspian Region. *Journal of Petroleum Science and Engineering*, **28,** 157-159.

EGAN, S.S., MOSAR, J., BRUNET, M.F. & KANGARLI, T. (2009) Subsidence and Uplift Mechanisms within the South Caspian Basin: Insights from the Onshore and Offshore Azerbaijan Region. In: *South Caspian to Central Iran Basins* (Ed. by M.-F. Brunet, M. Wilmsen & J. W. Granath), *Geological Society Special Publications*, **312**, 219. The Geological Society, London.

ERSLEV, E.A. (1991) Trishear Fault-Propagation Folding. *Geology*, **19,** 617.

EVANS, R.J., STEWART, S.A. & DAVIES, R.J. (2008) The Structure and Formation of Mud Volcano Summit Calderas. *Journal of the Geological Society*, **165,** 769.

FARRELL, S.G. (1984) A Dislocation Model Applied to Slump Structures, Ainsa Basin, South Central Pyrenees. *Journal of Structural Geology*, **6,** 727-736.

FIELD, M.E., GARDNER, J.V. & PRIOR, D.B. (1999) Geometry and Significance of Stacked Gullies on the Northern California Slope. *Marine Geology*, **154,** 271-286.

FINCH, E., HARDY, S. & GAWTHORPE, R.L. (2003) Discrete Element Modelling of Contractional Fault-Propagation Folding above Rigid Basement Fault Blocks. *Journal of Structural Geology*, **25,** 515-528.

FISCHER, A.G. & BOTTJER, D.J. (1991) Orbital Forcing and Sedimentary Sequences. *Journal of Sedimentary Research*, **61,** 1063-1069.

FORD, M., WILLIAMS, E.A., ARTONI, A., VERGES, J. & HARDY, S. (1997) Progressive Evolution of a Fault-Related Fold Pair from Growth Strata Geometries, Sant Llorenc De Morunys, Se Pyrenees. *Journal of Structural Geology*, **19,** 413-441.

FOWLER, S.R., MILDENHALL, J., ZALOVA, S., RILEY, G., ELSLEY, G., DESPLANQUES, A. & GULIYEV, F. (2000) Mud Volcanoes and Structural Development on Shah Deniz. *Journal of Petroleum Science and Engineering*, **28,** 189-206.

FREY, R.W. & PEMBERTON, S.G. (1984) Trace Fossil Facies Models. In: *Facies Models* (Ed. by R. G. Walker), 189-208. Geological Association of Canada Publications.

FREY-MARTINEZ, J., CARTWRIGHT, J. & HALL, B. (2005) 3d Seismic Interpretation of Slump Complexes: Examples from the Continental Margin of Israel. *Basin Research*, **17,** 83-108.

FREY-MARTÍNEZ, J., CARTWRIGHT, J. & JAMES, D. (2006) Frontally Confined Versus Frontally Emergent Submarine Landslides: A 3d Seismic Characterisation. *Marine and Petroleum Geology*, **23,** 585-604.

GAFEIRA, J., LONG, D., SCRUTTON, R. & EVANS, D. (2010) 3d Seismic Evidence of Internal Structure within Tampen Slide Deposits on the North Sea Fan: Are Chaotic Deposits That Chaotic? *Journal of the Geological Society*, **167,** 605-616.

GAMBERI, F., ROVERE, M. & MARANI, M. (2011) Mass-Transport Complex Evolution in a Tectonically Active Margin (Gioia Basin, Southeastern Tyrrhenian Sea). *Marine Geology*, **279,** 98-110.

GARDNER, J.V., PRIOR, D.B. & FIELD, M.E. (1999) Humboldt Slide -a Large Shear-Dominated Retrogressive Slope Failure. *Marine Geology*, **154,** 323-338.

GAWTHORPE, R.L., HALL, M., SHARP, I.R. & DREYER, T. (2000) Tectonically Enhanced Forced Regressions: Examples from Growth Folds in Extensional and Compressional Settings, the Miocene of the Suez Rift and the Eocene of the Pyrenees. In: *Sedimentary Responses to Forced Regressions* (Ed. by D. Hunt & R. Gawthorpe), *Geological Society Special Publications*, 177-191. The Geological Society, London.

GAWTHORPE, R.L. & HARDY, S. (2002) Extensional Fault-Propagation Folding and Base-Level Change as Controls on Growth-Strata Geometries. *Sedimentary Geology*, **146,** 47-56.

GEE, M.J.R., GAWTHORPE, R.L. & FRIEDMANN, J.S. (2005) Giant Striations at the Base of a Submarine Landslide. *Marine Geology*, **214,** 287-294.

GEOMAPAPP. Retrieved 01/03/2011, 2011, from http://www.geomapapp.org.

GEOSPATIAL RESEARCH LIMITED (2008) Geological Map of Azerbaijan. R. R. Jones. Durham.

GHENEA, C. (1970) Stratigraphy of the Upper Pliocene-Lower Pleistocene Interval in the Dacic Basin (Romania). *Palaeogeography, Palaeoclimatology, Palaeoecology*, **8,** 165-174.

GHIGLIONE, M.C. & RAMOS, V.A. (2005) Progression of Deformation and Sedimentation in the Southernmost Andes. *Tectonophysics*, **405,** 25-46.

GIBBARD, P.L., HEAD, M.J. & WALKER, M.J.C. (2010) Formal Ratification of the Quaternary System/Period and the Pleistocene Series/Epoch with a Base at 2.58 Ma. *Journal of Quaternary Science*, **25,** 96-102.

GINSBURG, G. & SOLOVIEV, V. (1994) Mud Volcano Gas Hydrates in the Caspian Sea. *Bulletin of the Geological Society of Denmark*, **41,** 95-100.

GODDARD, E., TRASK, P., DE FORD, R., ROVE, O., SINGEWALD JR, J. & OVERBECK, R. (1995) Rock Color Chart, Geological Society of America. Boulder, Colorado.

GOLONKA, J. (2007) Geodynamic Evolution of the South Caspian Basin. In: *Oil and Gas of the Greater Caspian Area* (Ed. by P. O. Yilmaz & G. H. isaksen), *Aapg Studies in Geology*, 17-41. American Association of Petroleum Geologists.

GRANATH, J., SOOFI, K., BAGANZ, O. & BAGIROV, E. (2007) Gravity Modelling and Its Implications to the Tectonics of the South Caspian Basin. In: *Oil and Gas of the Greater Caspian Area* (Ed. by P. O. Yilmaz & G. H. isaksen), *Aapg Studies in Geology*, 43-46. American Association of Petroleum Geologists.

GREEN, T., ABDULLAYEV, N.R., HOSSACK, J., RILEY, G. & ROBERTS, A.M. (2009) Sedimentation and Subsidence in the South Caspian Basin, Azerbaijan. In: *South Caspian to Central Iran Basins* (Ed. by M.-F. Brunet, M. Wilmsen & J. W. Granath), *Geological Society Special Publications*, **312**, 241-260. The Geological Society, London.

GRIM, R. (1951) The Depositional Environment of Red and Green Shales. *Journal of Sedimentary Research*, **21,** 226.

GUEST, B., GUEST, A. & AXEN, G. (2007a) Late Tertiary Tectonic Evolution of Northern Iran: A Case for Simple Crustal Folding. *Global and Planetary Change*, **58,** 435-453.

GUEST, B., HORTON, B.K., AXEN, G.J., HASSANZADEH, J. & MCINTOSH, W.C. (2007b) Middle to Late Cenozoic Basin Evolution in the Western Alborz Mountains: Implications for the Onset of Collisional Deformation in Northern Iran. *Tectonics*, **26,** TC6011.

GURGEY, K. (2003) Correlation, Alteration, and Origin of Hydrocarbons in the Gca, Bahar, and Gum Adasi Fields, Western South Caspian Basin: Geochemical and Multivariate Statistical Assessments. *Marine and Petroleum Geology*, **20,** 1119-1139.

HALL, J.K. (2002) Bathymetric Compilations of the Seas around Israel 1: The Caspian and Black Seas. *Geological Society of Israel, (GSI) Current research*, **13,** 105-108.

HAMPSON, G.J. (2010) Sediment Dispersal and Quantitative Stratigraphic Architecture across an Ancient Shelf. *Sedimentology*, **57,** 96-141.

HAMPTON, M.A., LEE, H.J. & LOCAT, J. (1996) Submarine Landslides. *Reviews of Geophysics*, **34,** 33-59.

HARDY, S. & POBLET, J. (1994) Geometric and Numerical Model of Progressive Limb Rotation in Detachment Folds. *Geology*, **22,** 371.

HARDY, S., POBLET, J., MCCLAY, K. & WALTHAM, D. (1996) Mathematical Modelling of Growth Strata Associated with Fault-Related Fold Structures. In: *Modern Developments in Structural Interpretation, Validation, and Modelling* (Ed. by P. G. Buchanan & D. A. Nieuwland), *Geological Society Special Publications*, **99**, 265-282. The Geological Society, London.

HARDY, S., DUNCAN, C., MASEK, J. & BROWN, D. (1998) Minimum Work, Fault Activity and the Growth of Critical Wedges in Fold and Thrust Belts. *Basin Research*, **10,** 365-373.

HEINIO, P. & DAVIES, R.J. (2006) Degradation of Compressional Fold Belts: Deep-Water Niger Delta. *AAPG Bulletin*, **90,** 753-770.

HEINIO, P. & DAVIES, R.J. (2009) Trails of Depressions and Sediment Waves Along Submarine Channels on the Continental Margin of Espirito Santo Basin, Brazil. *Geological Society of America Bulletin*, **121,** 698-711.

HINDS, D.J., ALIYEVA, E., ALLEN, M.B., DAVIES, C.E., KROONENBERG, S.B., SIMMONS, M.D. & VINCENT, S.J. (2004) Sedimentation in a Discharge Dominated Fluvial-Lacustrine System: The Neogene Productive Series of the South Caspian Basin, Azerbaijan. *Marine and Petroleum Geology*, **21,** 613-638.

HJELSTUEN, B.O., ELDHOLM, O. & FALEIDE, J.I. (2007) Recurrent Pleistocene Mega-Failures on the Sw Barents Sea Margin. *Earth and Planetary Science Letters*, **258,** 605-618.

HOLLINGSWORTH, J., JACKSON, J.A., WALKER, R.T. & NAZARI, H. (2008) Extrusion Tectonics and Subduction in the Eastern South Caspian Region since 10 Ma. *Geology*, **36,** 763-766.

HOOGENDOORN, R.M., BOELS, J.F., KROONENBERG, S.B., SIMMONS, M.D., ALIYEVA, E., BABAZADEH, A.D. & HUSEYNOV, D. (2005) Development of the Kura Delta, Azerbaijan; a Record of Holocene Caspian Sea-Level Changes. *Marine Geology*, **222,** 359-380.

HOSTERMAN, J.W. & WHITLOW, S.I. (1980) Munsell Color Value as Related to Organic Carbon in Devonian Shale of the Appalachian Basin, US Geological Survey. **Open File Report 80-660,** 333-335.

HOWIE, J.M., ROBINSON, N., RIVIERE, M., LYON, T. & MANLEY, D. (2005) Developing the Long-Term Seismic Strategy for Azeri-Chirag-Gunashli, South Caspian Sea, Azerbaijan. *The Leading Edge*, **24,** 934-939.

HUVENNE, V.A.I., CROKER, P.F. & HENRIET, J.P. (2002) A Refreshing 3d View of an Ancient Sediment Collapse and Slope Failure. *Terra Nova*, **14,** 33-40.

ILSTAD, T., MARR, J.G., ELVERH I, A. & HARBITZ, C.B. (2004) Laboratory Studies of Subaqueous Debris Flows by Measurements of Pore-Fluid Pressure and Total Stress. *Marine Geology*, **213,** 403-414.

INAN, S., YALCIN, M.N., GULIEV, I.S., KULIEV, K. & FEIZULLAYEV, A.A. (1997) Deep Petroleum Occurrences in the Lower Kura Depression, South Caspian Basin, Azerbaijan: An Organic Geochemical and Basin Modeling Study. *Marine and Petroleum Geology*, **14,** 731-762.

JACKSON, J.A., PRIESTLEY, K., ALLEN, M.B. & BERBERIAN, M. (2002) Active Tectonics of the South Caspian Basin. *Geophysical journal international(Print)*, **148,** 214-245.

JOANNIN, S., CORNÉE, J.-J., MÜNCH, P., FORNARI, M., VASILIEV, I., KRIJGSMAN, W., NAHAPETYAN, S., GABRIELYAN, I., OLLIVIER, V., ROIRON, P. & CHATAIGNER, C. (2010) Early Pleistocene Climate Cycles in Continental Deposits of the Lesser Caucasus of Armenia Inferred from Palynology, Magnetostratigraphy, and 40ar/39ar Dating. *Earth and Planetary Science Letters*, **291,** 149-158.

JONES, R.W. & SIMMONS, M.D. (1996) A Review of the Stratigraphy of Eastern Paratethys (Oligocene-Holocene). *Bull. Nat. Hist. Mus.(Geol. Suppl.)*, **52,** 25-49.

JUHÁSZ, E., KOVÁCS, L.Ó., MÜLLER, P., TÓTH-MAKK, A., PHILLIPS, L. & LANTOS, M. (1997) Climatically Driven Sedimentary Cycles in the Late Miocene Sediments of the Pannonian Basin, Hungary. *Tectonophysics*, **282,** 257-276.

KALANI, M., KHODABAKHSH, S. & AMIRBEHBOUDI, C. (2008) Seismic Expression and Inferred Depositional Environments of Plio-Pleistocene Sedimentary Sequences in the Southwestern Caspian Sea. *Geo-Marine Letters*, **28,** 31-41.

KAPLIN, P.A. & SELIVANOV, A.O. (1995) Recent Coastal Evolution of the Caspian Sea as a Natural Model for Coastal Responses to the Possible Acceleration of Global Sea-Level Rise. *Marine Geology*, **124,** 161-175.

KATZ, B., RICHARDS, D., LONG, D. & LAWRENCE, W. (2000) A New Look at the Components of the Petroleum System of the South Caspian Basin. *Journal of Petroleum Science and Engineering*, **28,** 161-182.

KEIGHLEY, D., FLINT, S., HOWELL, J. & MOSCARIELLO, A. (2003) Sequence Stratigraphy in Lacustrine Basins: A Model for Part of the Green River Formation (Eocene), Southwest Uinta Basin, Utah, U.S.A. *Journal of Sedimentary Research*, **73,** 987-1006.

KENDALL, C.G.S.C. (2003) Sepm Sequence Stratigraphy Web, Sequence Stratigraphy Nomenclature. Retrieved 06/03/2011, 2011, from http://sepmstrata.org.

KNAPP, C.C., KNAPP, J.H. & CONNOR, J.A. (2004) Crustal-Scale Structure of the South Caspian Basin Revealed by Deep Seismic Reflection Profiling. *Marine and Petroleum Geology*, **21,** 1073-1081.

KÖNIG, I., DRODT, M., SUESS, E. & TRAUTWEIN, A.X. (1997) Iron Reduction through the Tan-Green Color Transition in Deep-Sea Sediments. *Geochimica et Cosmochimica Acta*, **61,** 1679-1683.

KOPF, A., DEYHLE, A., LAVRUSHIN, V.Y., POLYAK, B.G., GIESKES, J.M., BUACHIDZE, G.I., WALLMANN, K. & EISENHAUER, A. (2003) Isotopic Evidence (He, B, C) for Deep Fluid and Mud Mobilization from Mud Volcanoes in the Caucasus Continental Collision Zone. *International Journal of Earth Sciences*, **92,** 407-425.

KOSAREV, A. (2005) Physico-Geographical Conditions of the Caspian Sea. In: *The Caspian Sea Environment* (Ed. by A. Kosianoy & A. Kosarev), **5P**, 5-31. Springer-Verlag, Berlin.

KOYI, H.A. & VENDEVILLE, B.C. (2003) The Effect of Décollement Dip on Geometry and Kinematics of Model Accretionary Wedges. *Journal of Structural Geology*, **25,** 1445-1450.

KRIJGSMAN, W., STOICA, M., VASILIEV, I. & POPOV, V. (2010) Rise and Fall of the Paratethys Sea During the Messinian Salinity Crisis. *Earth and Planetary Science Letters*, **290,** 183-191.

KROONENBERG, S.B., RUSAKOV, G.V. & SVITOCH, A.A. (1997) The Wandering of the Volga Delta: A Response to Rapid Caspian Sea-Level Change. *Sedimentary Geology*, **107,** 189-209.

KROONENBERG, S.B., BADYUKOVA, E.N., STORMS, J.E.A., IGNATOV, E.I. & KASIMOV, N.S. (2000) A Full Sea-Level Cycle in 65years: Barrier Dynamics Along Caspian Shores. *Sedimentary Geology*, **134,** 257-274.

KUKLA, G. & CÍLEK, V. (1996) Plio-Pleistocene Megacycles: Record of Climate and Tectonics. *Palaeogeography, Palaeoclimatology, Palaeoecology*, **120,** 171-194.

KUPRIN, P.N. (2002) Apsheron Threshold and Its Role in the Processes of Sedimentation and Formation of Hydrological Regimes in the Southern and Middle Caspian Basins. *Water Resources*, **29,** 473-484.

LEWIS, K.B. (1971) Slumping on a Continental Slope Inclined at 1°-4°. *Sedimentology*, **16,** 97-110.

LICKORISH, W.H., FORD, M., BÜRGISSER, J. & COBBOLD, P.R. (2002) Arcuate Thrust Systems in Sandbox Experiments: A Comparison to the External Arcs of the Western Alps. *Geological Society of America Bulletin*, **114,** 1089-1107.

LISLE, R.J. (1999) Predicting Patterns of Strain from Three-Dimensional Fold Geometries: Neutral Surface Folds and Forced Folds. In: *Forced Folds and Fractures* (Ed. by J. W. Cosgrove & M. S. Ameen), *Geological Society Special Publications*, **169**, 213-221. The Geological Society, London.

LIU, X. & GOULTY, N.R. (1999) Comparison of 2d Filters for Suppressing Noise in Common Shot Gathers. *first break*, **17,** 105-110.

LOCAT, J. & LEE, H.J. (2002) Submarine Landslides: Advances and Challenges. *Canadian Geotechnical Journal*, **39,** 193-212.

LUCENTE, C.C. & PINI, G.A. (2003) Anatomy and Emplacement Mechanism of a Large Submarine Slide within a Miocene Foredeep in the Northern Apennines, Italy: A Field Perspective. *American Journal of Science*, **303,** 565-602.

MACEDO, J. & MARSHAK, S. (1999) Controls on the Geometry of Fold-Thrust Belt Salients. *Geological Society of America Bulletin*, **111,** 1808-1822.

MAMEDOV, A.V. (1997) The Late Pleistocene-Holocene History of the Caspian Sea. *Quaternary International*, **41-42,** 161-166.

MANGINO, S. & PRIESTLEY, K. (1998) The Crustal Structure of the Southern Caspian Region. *Geophysical Journal International*, **133,** 630-648.

MARQUES, F.O. & COBBOLD, P.R. (2002) Topography as a Major Factor in the Development of Arcuate Thrust Belts: Insights from Sandbox Experiments. *Tectonophysics*, **348,** 247-268.

MARTEL, A.T. & GIBLING, M.R. (1991) Wave Dominated Lacustrine Facies and Tectonically Controlled Cyclicity in the Lower Carboniferous Horton Bluff Formation, Nova Scotia, Canada. In: *Lacustrine Facies Analysis* (Ed. by P. Anadon, L. Cabrera & K. Kelts), *International Association of Sedimentologists, Special Publication*, **13**, 223-243. Blackwell Scientific, Oxford.

MARTINSEN, O. & BAKKEN, B. (1990) Extensional and Compressional Zones in Slumps and Slides in the Namurian of County Clare, Ireland. *Journal of the Geological Society*, **147,** 153-164.

MARTINSEN, O. (1994) Mass Movements. *The Geological Deformation of Sediments: London, Chapman & Hall***,** 127-165.

MASAFERRO, J.L., BULNES, M., POBLET, J. & EBERLI, G.P. (2002) Episodic Folding Inferred from Syntectonic Carbonate Sedimentation: The Santaren Anticline, Bahamas Foreland. *Sedimentary Geology*, **146,** 11-24.

MASLIN, M., OWEN, M., DAY, S. & LONG, D. (2004) Linking Continental-Slope Failures and Climate Change: Testing the Clathrate Gun Hypothesis. *Geology*, **32,** 53-56.

MASSON, D.G., HUGGETT, Q.J. & BRUNSDEN, D. (1993) The Surface Texture of Saharan Debris Flow Deposit and Some Speculations on Submarine Debris Flow Processes. *Sedimentology*, **40,** 583-598.

MASSON, F., ANVARI, M., DJAMOUR, Y., WALPERSDORF, A., TAVAKOLI, F., DAIGNIÈRES, M., NANKALI, H. & VAN GORP, S. (2007) Large-Scale Velocity Field and Strain Tensor in Iran Inferred from Gps Measurements: New Insight for the Present-Day Deformation Pattern within Ne Iran. *Geophysical Journal International*, **170,** 436-440.

MAZZANTI, P. & BLASIO, F.V. (2010) Peculiar Morphologies of Subaqueous Landslide Deposits and Their Relationship to Flow Dynamics. In: *Submarine Mass Movements and Their Consequences* (Ed. by D. C. Mosher, L. Moscardelli, C. D. P. Baxter, R. Urgeles, R. C. Shipp, J. D. Chaytor & H. J. Lee), 141-151. Springer.

McBride, E.F. (1974) Significance of Color in Red, Green, Purple, Olive, Brown, and Gray Beds of Di Funta Group, Northeastern Mexicon. *Jounal of sedimentary petrology*, **44,** 760-773.

McCaig, A.M. & McClelland, E. (1992) Palaeomagnetic Techniques Applied to Thrust Belts. *Thrust Tectonics: London, Chapman and Hall***,** 209–216.

McClay, K.R. (1992) *Thrust Tectonics*. Chapman & Hall.

McHugh, C.M.G., Damuth, J.E. & Mountain, G.S. (2002) Cenozoic Mass-Transport Facies and Their Correlation with Relative Sea-Level Change, New Jersey Continental Margin. *Marine Geology*, **184,** 295-334.

Mitchell, J. & Westaway, R. (1999) Chronology of Neogene and Quaternary Uplift and Magmatism in the Caucasus: Constraints from K–Ar Dating of Volcanism in Armenia. *Tectonophysics*, **304,** 157-186.

Mitra, S. (1990) Fault-Propagation Folds: Geometry, Kinematic Evolution, and Hydrocarbon Traps. *AAPG Bulletin*, **74,** 921-945.

Mitra, S. (2003) A Unified Kinematic Model for the Evolution of Detachment Folds. *Journal of Structural Geology*, **25,** 1659-1673.

Mohrig, D., Whipple, K.X., Hondzo, M., Ellis, C. & Parker, G. (1998) Hydroplaning of Subaqueous Debris Flows. *Geological Society of America Bulletin*, **110,** 387-394.

Morley, C.K. (2007) Development of Crestal Normal Faults Associated with Deepwater Fold Growth. *Journal of Structural Geology*, **29,** 1148-1163.

Morley, C.K. (2009) Growth of Folds in a Deep-Water Setting. *Geosphere*, **5,** 59-89.

Morton, A., Allen, M.B., Simmons, M., Spathopoulos, F., Still, J., Hinds, D., Ismail-Zadeh, A. & Kroonenberg, S. (2003) Provenance Patterns in a Neotectonic Basin: Pliocene and Quaternary Sediment Supply to the South Caspian. *Basin Research*, **15,** 321-337.

Moscardelli, L., Wood, L. & Mann, P. (2006) Mass-Transport Complexes and Associated Processes in the Offshore Area of Trinidad and Venezuela. *AAPG Bulletin*, **90,** 1059-1088.

Moscardelli, L. & Wood, L. (2008) New Classification System for Mass Transport Complexes in Offshore Trinidad. *Basin Research*, **20,** 73-98.

Mosher, D.C., Moscardelli, L., Baxter, C.D.P., Urgeles, R., Shipp, R.C., Chaytor, J.D. & Lee, H.J. (2010) Introduction to Submarine Mass Movements and Their Consequences. In: *Submarine Mass Movements and Their Consequences* (Ed. by D. C. Mosher, L. Moscardelli, C. D. P. Baxter, R. Urgeles, R. C. Shipp, J. D. Chaytor & H. J. Lee), *Advances in Natural and Technological Hazards Research*, **28**, 1-8. Springer Netherlands.

Mulder, T. & Cochonat, P. (1996) Classification of Offshore Mass Movements. *Journal of Sedimentary Research*, **66,** 43-57.

Mullins, H.T., Hinchey, E.J., Wellner, R.W., Stephens, D.B., Anderson Jr, W.T., Dwyer, T.R. & Hine, A.C. (1996) Seismic Stratigraphy of the Finger Lakes: A Continental Record Ofheinrich Event Hl and Laurentide Ice Sheet Instability. *Subsurface geologic investigations of New York Finger Lakes: impliations for Late Quaternary deglaciation and environmental change***,** 1.

Nadirov, R.S., Bagirov, E., Tagiyev, M. & Lerche, I. (1997) Flexural Plate Subsidence, Sedimentation Rates, and Structural Development of the Super-Deep South Caspian Basin. *Marine and Petroleum Geology*, **14,** 383-400.

Nemec, W. (1990) Aspects of Sediment Movement on Steep Delta Slopes. *Coarse-Grained Deltas*, **10,** 29-73.

Nikiforova, K.V. (2004) The Pliocene and Pleistocene of the European Part of the Commonwealth of Independent States. In: *The Pleistocene Boundary and the Beginning of the Quaternary* (Ed. by J. van Couvering), 221-226. Cambridge Univ Press.

Nio, S.D. & Yang, C.S. (1991) Diagnostic Attributes of Clastic Tidal Deposits: A Review. *Clastic Tidal Sedimentology***,** 3–28.

Norris, R.D. (1986) Taphonomic Gradients in Shelf Fossil Assemblages: Pliocene Purisima Formation, California. *PALAIOS*, **1,** 256-270.

Nummedal, D., Clifton, H.E., Abreu, V., Bati, Z., Demchick, T., Fornaciari, M., Riley, G., Narimanov, A.A., Sayili, A. & Stein, J. (2000). *Sedimentological Response to Climate Cycles During the Pliocene of the South Caspian Basin*.

O´Brien, N. & Kemp, A.E.S. (1996) Shale Lamination and Sedimentary Processes. *Palaeoclimatology and Palaeoceanography from Laminated Sediments***,** 23-36.

Osborne, M.J. & Swarbrick, R.E. (1997) Mechanisms for Generating Overpressure in Sedimentary Basins: A Reevaluation. *AAPG Bulletin*, **81,** 1023-1041.

Osipova, E.M. (2009) Development Stages of the Quaternary Molluscan Fauna in the South Urals Region. *Stratigraphy and Geological Correlation*, **17,** 663-666.

Panin, G.N. (2005) The Caspian Sea Level Fluctuations as an Example of Local/Global Climatic Change. *Translation of unknown russian paper.*

Patton, T.L. (2004) Numerical Models of Growth-Sediment Development above an Active Monocline. *Basin Research*, **16,** 25-39.

Perissoratis, C., Piper, D.J.W. & Lykousis, V. (2000) Alternating Marine and Lacustrine Sedimentation During Late Quaternary in the Gulf of Corinth Rift Basin, Central Greece. *Marine Geology*, **167,** 391-411.

Planke, S., Svensen, H., Hovland, M., Banks, D. & Jamtveit, B. (2003) Mud and Fluid Migration in Active Mud Volcanoes in Azerbaijan. *Geo-Marine Letters*, **23,** 258-268.

Poblet, J. & Stuart, H. (1995) Reverse Modelling of Detachment Folds; Application to the Pico Del Aguila Anticline in the South Central Pyrenees (Spain). *Journal of Structural Geology*, **17,** 1707-1724.

POBLET, J., MCCLAY, K.R., STORTI, F. & MUÑOZ, J.A. (1997) Geometries of Syntectonic Sediments Associated with Single-Layer Detachment Folds. *Journal of Structural Geology*, **19,** 369-381.

POCHAT, S., CASTELLTORT, S., CHOBLET, G. & VAN DEN DRIESSCHE, J. (2009) High-Resolution Record of Tectonic and Sedimentary Processes in Growth Strata. *Marine and Petroleum Geology*, **26,** 1350-1364.

POPOV, G. (1970) Significance of Fresh Water Molluscs for Correlation of Continental and Marine Pleistocene of Ponto Caspian. *Palaeogeography, Palaeoclimatology, Palaeoecology*, **8,** 251-260.

POPOV, S.V., SHCHERBA, I.G., ILYINA, L.B., NEVESSKAYA, L.A., PARAMONOVA, N.P., KHONDKARIAN, S.O. & MAGYAR, I. (2006) Late Miocene to Pliocene Palaeogeography of the Paratethys and Its Relation to the Mediterranean. *Palaeogeography, Palaeoclimatology, Palaeoecology*, **238,** 91-106.

POSAMENTIER, H.W. & VAIL, P.R. (1988) Eustatic Controls on Clastic Deposition - Sequence and Systems Tracts Models, . In: *Sea-Level Changes: An Integrated Approach:*
(Ed. by C. K. Wilgus, B. S. Hastings, H. W. Posamentier, J. C. Van Wagoner, C. A. Ross & C. G. S. C. Kendall), **42**, 125-154. SEPM, Special Publication

POSAMENTIER, H.W. & KOLLA, V. (2003) Seismic Geomorphology and Stratigraphy of Depositional Elements in Deep-Water Settings. *Journal of Sedimentary Research*, **73,** 367-388.

POTTER, P.E., MAYNARD, J.B. & PRIOR, W.A. (1980) *The Sedimentology of Shale*, 1 edn. Springer Verlag, New York.

PRIESTLEY, K., BAKER, C. & JACKSON, J. (1994) Implications of Earthquake Focal Mechanism Data for the Active Tectonics of the South Caspian Basin and Surrounding Regions. *Geophysical Journal International*, **118,** 111-141.

PRIOR, D.B., BORNHOLD, B.D. & JOHNS, M.W. (1984) Depositional Characteristics of a Submarine Debris Flow. *Journal of Geology*, **92,** 707-727.

PROKOPENKO, A.A., HINNOV, L.A., WILLIAMS, D.F. & KUZMIN, M.I. (2006) Orbital Forcing of Continental Climate During the Pleistocene: A Complete Astronomically Tuned Climatic Record from Lake Baikal, Se Siberia. *Quaternary Science Reviews*, **25,** 3431-3457.

RAMSAY, J.G. (1967) *Folding and Fracturing of Rocks*. McGraw-Hill, New York.

RASMUSSEN, E.S. (2004) The Interplay between True Eustatic Sea-Level Changes, Tectonics, and Climatic Changes: What Is the Dominating Factor in Sequence Formation of the Upper Oligocene-Miocene Succession in the Eastern North Sea Basin, Denmark? *Global and Planetary Change*, **41,** 15-30.

RATZOV, G., SOSSON, M., COLLOT, J., MIGEON, S., MICHAUD, F., LOPEZ, E. & GONIDEC, Y. (2007) Submarine Landslides Along the North Ecuador – South Colombia Convergent Margin: Possible Tectonic Control. In: *Submarine Mass Movements and Their Consequences* (Ed. by V. Lykousis, D. Sakellariou & J. Locat), *Advances in Natural and Technological Hazards Research*, **27**, 47-55. Springer Netherlands.

READING, H.G. & COLLINSON, J.D. (1996) Lakes. In: *Sedimentary Environments: Processes, Facies and Stratigraphy* (Ed. by H. G. Reading), 154-231. Blackwell, Oxford.

REYNOLDS, A.D., SIMMONS, M.D., BOWMAN, M.B.J., HENTON, J., BRAYSHAW, A.C., ALI-ZADE, A.A., GULIYEV, I.S., SULEYMANOVA, S.F., ATEAVA, E.Z. & MAMEDOVA, D.N. (1998) Implications of Outcrop Geology for Reservoirs in the Neogene Productive Series; Apsheron Peninsula, Azerbaijan. *AAPG Bulletin*, **82,** 25-49.

RIBA, O. (1976) Syntectonic Unconformities of the Alto Cardener, Spanish Pyrenees: A Genetic Interpretation. *Sedimentary Geology*, **15,** 213-233.

RICHARDS, K., LEROY, S.A.G., ARPE, K., MARRET, F., HOOGENDOORN, R.M. & KROONENBERG, S.B. (2012) Fluctuations in Caspian Sea Level During the Quaternary: New Evidence from Palynology, Ostracods and Climate Modelling. *3rd International Symposium on the Geology of the Black Sea Region*. N. Anitai & A. Seghedi. Bucharest, Romania.

RIGGS, S.R., CLEARY, W.J. & SNYDER, S.W. (1995) Influence of Inherited Geologic Framework on Barrier Shoreface Morphology and Dynamics. *Marine Geology*, **126,** 213-234.

ROBERTS, K.S., DAVIES, R.J. & STEWART, S.A. (2010) Structure of Exhumed Mud Volcano Feeder Complexes, Azerbaijan. *Basin Research*, **22,** 439-451.

ROBERTS, K.S., DAVIES, R.J., STEWART, S.A. & TINGAY, M. (2011a) Structural Controls on Mud Volcano Vent Distributions: Examples from Azerbaijan and Lusi, East Java. *Journal of the Geological Society*, **168,** 1013-1030.

ROBERTS, K.S., STEWART, S.A., DAVIES, R.J. & EVANS, R.J. (2011b) Sector Collapse of Mud Volcanoes, Azerbaijan. *Journal of the Geological Society*, **168,** 49.

ROBINSON, N., FORD, A., HOWIE, J., MANLEY, D., RIVIERE, M., STEWART, S. & THOMAS, R. (2005) 4d Time-Lapse Monitoring of Chirag Field. *The Leading Edge*, **24,** 928-932.

ROGERS, H. (2011) Personal Communication.

RUDDIMAN, W.F. (2006) Orbital Changes and Climate. *Quaternary Science Reviews*, **25,** 3092-3112.

RYCHAGOV, G.I. (1997) Holocene Oscillations of the Caspian Sea, and Forecasts Based on Palaeogeographical Reconstructions. *Quaternary International*, **41,** 167-172.

SALVINI, F. & STORTI, F. (2002) Three-Dimensional Architecture of Growth Strata Associated to Fault-Bend, Fault-Propagation, and Décollement Anticlines in Non-Erosional Environments. *Sedimentary Geology*, **146,** 57-73.

SAWYER, D.E., FLEMINGS, P.B., DUGAN, B. & GERMAINE, J.T. (2009) Retrogressive Failures Recorded in Mass Transport Deposits in the Ursa Basin, Northern Gulf of Mexico. *Journal of Geophysical Research*, **114,** B10102.

SCHMOKER, J.W. (1981) Determination of Organic-Matter Content of Appalachian Devonian Shales from Gamma-Ray Logs. *AAPG Bulletin*, **65,** 1285-1298.

SCHNEIDER, C.L., HUMMON, C., YEATS, R.S. & HUFTILE, G.L. (1996) Structural Evolution of the Northern Los Angeles Basin, California, Based on Growth Strata. *Tectonics*, **15,** 341-355.

SCHNELLMANN, M., ANSELMETTI, F.S., GIARDINI, D. & MCKENZIE, J.A. (2005) Mass Movement-Induced Fold-and-Thrust Belt Structures in Unconsolidated Sediments in Lake Lucerne (Switzerland). *Sedimentology*, **52,** 271-289.

SCHOLZ, C.A. (1995) Deltas of the Lake Malawi Rift, East Africa: Seismic Expression and Exploration Implications. *AAPG Bulletin*, **79,** 1679-1679.

SCHOLZ, C.A. (2002) Applications of Seismic Sequence Stratigraphy in Lacustrine Basins. In: *Tracking Environmental Change Using Lake Sediments: Physical and Chemical Techniques* (Ed. by W. M. Last & J. P. Smol), 7-22. Kluwer Academic, Dordrecht.

SCHULZ, H., VON RAD, U. & VON STACKELBERG, U. (1996) Laminated Sediments from the Oxygen-Minimum Zone of the Northeastern Arabian Sea. In: *Palaeoclimatology and Plaeoceanography from Laminated Sediments* (Ed. by A. E. S. Kemp), *Geological Society Special Publications*, **116**, 185-207. The Geological Society, London.

ŞENGÖR, A.M.C. (1990) A New Model for the Late Palaeozoic–Mesozoic Tectonic Evolution of Iran and Implications for Oman. In: *The Geology and Tectonics of the Oman Region* (Ed. by A. Robertsen, M. Searle & A. Ries), *Geological Society Special Publications*, **49**, 797-831. The Geological Society, London.

SHAW, J.H., NOVOA, E. & CONNORS, C.D. (2004) Structural Controls on Growth Stratigraphy in Contractional Fault-Related Folds. In: *Thrust Tectonics and Hydrocarbon Systems* (Ed. by K. McClay), *Aapg Memoir*, **82**, 400–412.

SHIKALIBEILY, E.S. & GRIGORIANTS, B.V. (1980) Principal Features of the Crustal Structure of the South-Caspian Basin and the Conditions of Its Formation. *Tectonophysics*, **69,** 113-121.

SIEBERT, C., NAGLER, T.F., VON BLANCKENBURG, F. & KRAMERS, J.D. (2003) Molybdenum Isotope Records as a Potential New Proxy for Paleoceanography. *Earth and Planetary Science Letters*, **211,** 159-171.

SMITH-ROUCH, L.S. (2006) Oligocene–Miocene Maykop/Diatom Total Petroleum System of the South Caspian Basin Province, Azerbaijan, Iran, and Turkmenistan. *USGS Bulletin*, United States Geological Survey. Reston, Virginia**,** 1-27.

SOLEIMANY, B., POBLET, J., BULNES, M. & SABAT, F. (2011) Fold Amplification History Unravelled from Growth Strata: The Dorood Anticline, Nw Persian Gulf. *Journal of the Geological Society*, **168,** 219-234.

SOUQUE, C., FISHER, Q.J., CASEY, M. & BENTHAM, P. (2010) Structural Controls on Mechanical Compaction within Sandstones: An Example from the Apsheron Peninsula, Azerbaijan. *Marine and Petroleum Geology*, **27,** 1713-11724.

STEWART, S.A. & DAVIES, R.J. (2006) Structure and Emplacement of Mud Volcano Systems in the South Caspian Basin. *AAPG Bulletin*, **90,** 771-786.

STORTI, F. & MCCLAY, K.R. (1995) Influence of Syntectonic Sedimentation on Thrust Wedges in Analogue Models. *Geology*, **23,** 999.

STORTI, F. & POBLET, J. (1997) Growth Stratal Architectures Associated to Decollement Folds and Fault-Propagation Folds. Inferences on Fold Kinematics. *Tectonophysics*, **282,** 353-373.

STRAYER, L.M., ERICKSON, S.G., SUPPE, J. & MCCLAY, K.R. (2004) Influence of Growth Strata on the Evolution of Fault-Related Folds–Distinct-Element Models. In: *Thrust Tectonics and Hydrocarbon Systems* (Ed. by K. R. McClay), *Aapg Memoir*, **82**, 18–29. American Association of Petroleum Geologists.

SUPPE, J. (1983) Geometry and Kinematics of Fault-Bend Folding. *American Journal of Science*, **283,** 684-721.

SUPPE, J., CHOU, G.T. & HOOK, S.C. (1992) Rates of Folding and Faulting Determined from Growth Strata. In: *Thrust Tectonics* (Ed. by K. R. McClay), **1052121**, 106-121. London: Chapman & Hall.

SVITOCH, A.A. & YANINA, T.A. (2007) Data on Stratotypes of the Neopleistocene-Holocene Regional and Local Subdivisions in the Caspian Region. *Stratigraphy and Geological Correlation*, **15,** 536-552.

SVITOCH, A.A. (2010a) The Neoeuxinian Basin of the Black Sea and the Khvalinian Transgression of the Caspian Sea. *Quaternary International*, **225,** 230-234.

SVITOCH, A.A. (2010b) Palaeogeographical History of the Aral Sea. In: *The Aral Sea Environment* (Ed. by A. G. Konstianoy & A. N. Kosarev), *The Handbook of Environmental Chemistry*, **7**, 22-44. Springer-Verlag, Berlin Heidelberg, Germany.

SYLVESTER, A.G. (1988) Strike-Slip Faults. *Geological Society of America Bulletin*, **100,** 1666-1703.

TALBOT, M.R. & ALLEN, P.A. (1996) Lakes. In: *Sedimentary Environments: Processes, Facies and Stratigraphy* (Ed. by H. Reading), 83-124. Blackwell, Oxford.

TALLING, P.J., WYNN, R.B., MASSON, D.G., FRENZ, M., CRONIN, B.T., SCHIEBEL, R., AKHMETZHANOV, A.M., DALLMEIER-TIESSEN, S., BENETTI, S. & WEAVER, P.P.E. (2007) Onset of Submarine Debris Flow Deposition Far from Original Giant Landslide. *Nature*, **450,** 541-544.

TAPPONNIER, P., RYERSON, F.J., VAN DER WOERD, J., MÉRIAUX, A.S. & LASSERRE, C. (2001) Long-Term Slip Rates and Characteristic Slip: Keys to Active Fault Behaviour and Earthquake Hazard. *Comptes Rendus de l'Academie des Sciences-Serie IIa-Sciences de la Terre et des Planetes*, **333,** 483-494.

TATAR, M., JACKSON, J., HATZFELD, D. & BERGMAN, E. (2007) The 2004 May 28 Baladeh Earthquake (Mw 6.2) in the Alborz, Iran: Overthrusting the South Caspian Basin Margin, Partitioning of Oblique Convergence and the Seismic Hazard of Tehran. *Geophysical Journal International*, **170,** 249-261.

TERRA NOVA (1990) Fiery Mountain Springs and Wells of Fire. *Terra Nova*, **2,** 415-416.

TINGAY, M., HEIDBACH, O., DAVIES, R. & SWARBRICK, R. (2008) Triggering of the Lusi Mud Eruption: Earthquake Versus Drilling Initiation. *Geology*, **36,** 639.

TORRES, M.A. (2007) The Petroleum Geology of Western Turkmenistan: The Gograndag–Okarem Province. *Oil and Gas of the Greater Caspian area. American Association of Petroleum Geologists Studies in Geology*, **55,** 109-132.

TUCKER, M.E. (1990) Carbonate Depositional Systems: Marene, Shallow Water and Lacustrine Carbonates. In: *Carbonate Sedimentology* (Ed. by M. Tucker, V. Wright & J. Dickson), 101-228. Blackwell Scientific, Oxford.

TUCKER, M.E. (2003) *Sedimentary Rocks in the Field*. Wiley.

TWISS, R.J. & MOORES, E.M. (1992) Structural Environments of Thrust Faults. In: *Structural Geology* (Ed. by R. J. Twiss & E. M. Moores), 100-106. WH Freeman and company.

ULOMOV, V.L., POLYAKOVA, T.P. & MEDVEDEVA, N.S. (1999) Seismogeodynamics of the Caspian Sea Region. *Izvestiya Physics of the Solid Earth*, **35,** 1036-1042.

URGELES, R., LOCAT, J., SAWYER, D.E., FLEMINGS, P.B., DUGAN, B. & BINH, N.T.T. (2010) History of Pore Pressure Build up and Slope Instability in Mud-Dominated Sediments of Ursa Basin, Gulf of Mexico Continental Slope. In: *Submarine Mass Movements and Their Consequences* (Ed. by D. C. Mosher, L. Moscardelli, C. D. P. Baxter, R. Urgeles, R. C. Shipp, J. D. Chaytor & H. J. Lee), 179-190. Springer.

VAIL, P.R., MITCHUM, R.M. & THOMPSON, S. (1977) Seismic Stratigraphy and Global Changes of Sea Level, Part 3: Relative Changes of Sea Level from Coastal Onlap. In: *Seismic Stratigraphy: Applications to Hydrocarbon Exploration* (Ed. by P. C. E), *Aapg Memoir*, **26**, 63–97. American Association of Petroleum Geololgists.

VAN BAAK, C.G.C. (2010) Glacio-Marine Transgressions of the Early and Middle Pleistocene Caspian Basin, Azerbaijan, Universieit Utrecht, Utrecht.

VAN WAGONER, J.C., POSAMENTIER, H.W., MITCHUM, R.M.J., VAIL, P.R., SARG, J.F., LOUTIT, T.S. & HARDENBOL, J. (1988) An Overview of the Fundamentals of Sequence Stratigraphy and Key Definitions. *Sea-Level Changes: An Integrated Approach: SEPM, Special Publication*, **42,** 39–45.

VARNES, D.J., SCHUSTER, R.L. & KRIZEK, R.J. (1978) Slope Movement Types and Processes.

VERGES, J., BURBANK, D.W. & MEIGS, A. (1996) Unfolding: An Inverse Approach to Fold Kinematics. *Geology*, **24,** 175-178.

VINCENT, S.J., ALLEN, M.B., ISMAIL-ZADEH, A.D., FLECKER, R., FOLAND, K.A. & SIMMONS, M.D. (2005) Insights from the Talysh of Azerbaijan into the Paleogene Evolution of the South Caspian Region. *Bulletin of the Geological Society of America*, **117,** 1513-1533.

VINCENT, S.J., DAVIES, C.E., RICHARDS, K. & ALIYEVA, E. (2010) Contrasting Pliocene Fluvial Depositional Systems within the Rapidly Subsiding South Caspian Basin; a Case Study of the Palaeo-Volga and Palaeo-Kura River Systems in the Surakhany Suite, Upper Productive Series, Onshore Azerbaijan. *Marine and Petroleum Geology*, **27,** 2079-2106.

WALKER, R.G. (1984) Shelf and Shallow Marine Sands. *Facies models*, **2,** 141-170.

WEIMER, P. (1990) Sequence Stratigraphy, Facies Geometries, and Depositional History of the Mississippi Fan, Gulf of Mexico. *AAPG Bull*, **74,** 425–453.

WEIMER, P. & SHIPP, C. (2004) Mass Transport Complex: Musing on Past Uses and Suggestions for Future Directions. *Offshore Technology Conference*. Houston, Texas**,** OTC 16752.

WESTGATE, J.A. & BRIGGS, N.D. (1980) Dating Methods of Pleistocene Deposits and Their Problems: V. Tephrochronology and Fission-Track Dating. *Geoscience Canada*, **7,** 3-10.

YUSIFOV, M. (2004) Seismic Interpretation and Classification of Mud Volcanoes of the South Caspian Basin, Offshore Azerbaijan, Texas A&M University.

YUSIFOV, M. & RABINOWITZ, P.D. (2004) Classification of Mud Volcanoes in the South Caspian Basin, Offshore Azerbaijan. *Marine and Petroleum Geology*, **21,** 965-975.

ZACHOS, J., PAGANI, M., SLOAN, L., THOMAS, E. & BILLUPS, K. (2001) Trends, Rhythms, and Aberrations in Global Climate 65 Ma to Present. *Science*, **292,** 686-693.

ZONENSTHAIN, L.P. & LE PICHON, X. (1986) Deep Basins of the Black Sea and Caspian Sea as Remnants of Mesozoic Back-Arc Basins. *Tectonophysics*, **123,** 181-211.

ZUBAKOV, V.A. (2001) History and Causes of Variations in the Caspian Sea Level: The Miopliocene, 7.1–1.95 Million Years Ago. *Water Resources*, **28,** 249-256.

7. Appendices

Appendix 1

Comparisons between published seismic lines and this study's interpretations

Appendix 2

Handheld gamma ray tool and specifications. Munsell Colours plotted against gamma ray count

Appendix 3

Munsell colour chart

Appendix 4

Photographic specimens of Apsheron Formation fossils

Appendix 5

Apsheron Formation dip-corrected palaeocurrent measurements

Appendix 6

Geological processes that affect slope stability and seismic mapping methodology for MTCs

Appendix 7

Alternative views along mass transport basal shear surfaces

Appendix 8

Kinematic indicators of South Caspian Mass Transport Deposits

Appendix 1. Comparisons between published seismic lines and Chapter 2

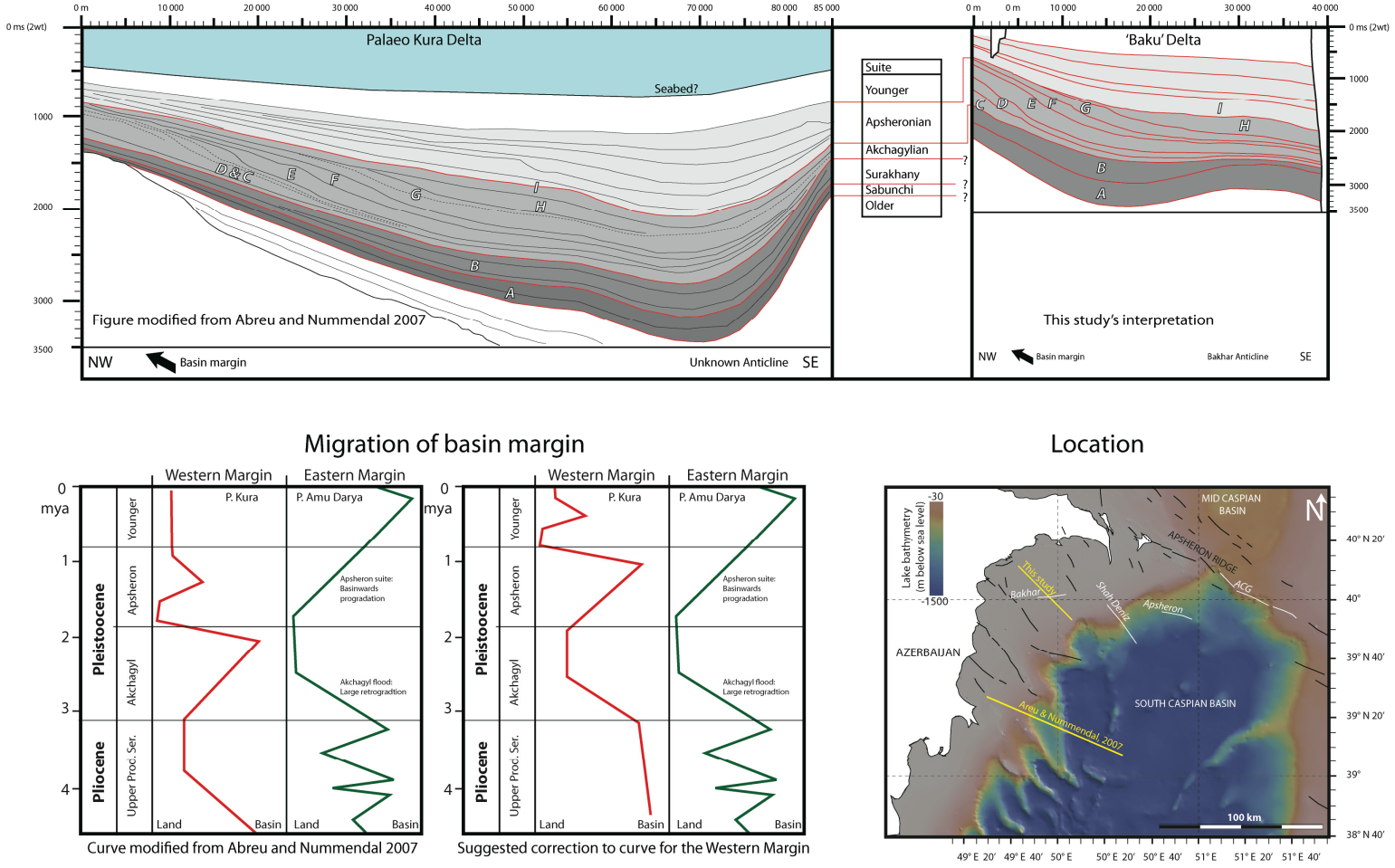

Appendix 1 Comparisons between published seismic lines and this study's interpretations. A1a) Sequence stratigraphy of the Palaeo Kura delta (from Abreu & Nummendal, 2007), and the 'Baku' delta (this study) showing outlines of sequence boundaries (black) and vertical positions of each suite (shaded greys). Age estimates of strata packages, and vertical time scales differ between each study. A1b) Published curves of the position of the coastline in this study's interval of interest (from Abreu and Nummendal, 2007). The original interpretation contains mismatching trends along the western and eastern margins of the basin. If the time estimates are corrected using the well picks from this study there is much more agreement between the curves. *To be printed on A3 landscape oriented paper*

Appendix 1 (continued)

The seismic stratigraphic interpretation of chapter 2, that that extends onto the western shelf margin is similar to a published line drawing from the Palaeo Kura delta which lies 70 km to the south (Abreu & Nummedal, 2007). Apsheronian sequences C – H, are clearly identifiable in both sections. However, both interpretations differ on age estimations by approximately 1 million years. Both this study and that of Abreu and Nummendal use well picks (from BP and ExxonMobil respectively) to date the seismic packages. The picks were allegedly defined using a combination of biostratigraphy, orbital tuning, and radiogenic dating but all data are unpublished and cannot be investigated. No radiogenic dating beyond ash bands in the Akchagyl and Apsheron Suites are present in the literature (Kroonenberg *et al.*, 1997; Devlin *et al.*, 1999) and what exists is Soviet era data and inaccessible. Similarly this study does not have access to the data or criteria used to define BP's proprietary well picks.

This discrepancy has implications for the sedimentation history in the basin and on further interpretations in this thesis. This study's data implies the Apsheronian is a regressive fourth-ordersequence with high rates of prograding sedimentation, whereas Abreu and Nummendal conclude that Apsheronian lake level remained approximately static, with relatively low sedimentation rates. Field observations from the Apsheron suite, (presented in chapter 3) show fifth or sixth-orderdepositional cycles, which show clear basinwards progradation over a succession of 850 m; a shallowing-upwards regressive sequence which favours the seismic stratigraphic interpretation of this study. In addition to this, Abreu and Nummendal show conflicting Apsheronian relative lake level trends between their seismic lines from the western and eastern margins of the basin, which are resolved by readjusting their well pick time estimates to those used in this study. This study is frequently cited in this thesis and its (time corrected) lake level curve is used in chapter 3.

Appendix 2. Handheld gamma ray tool and specifications

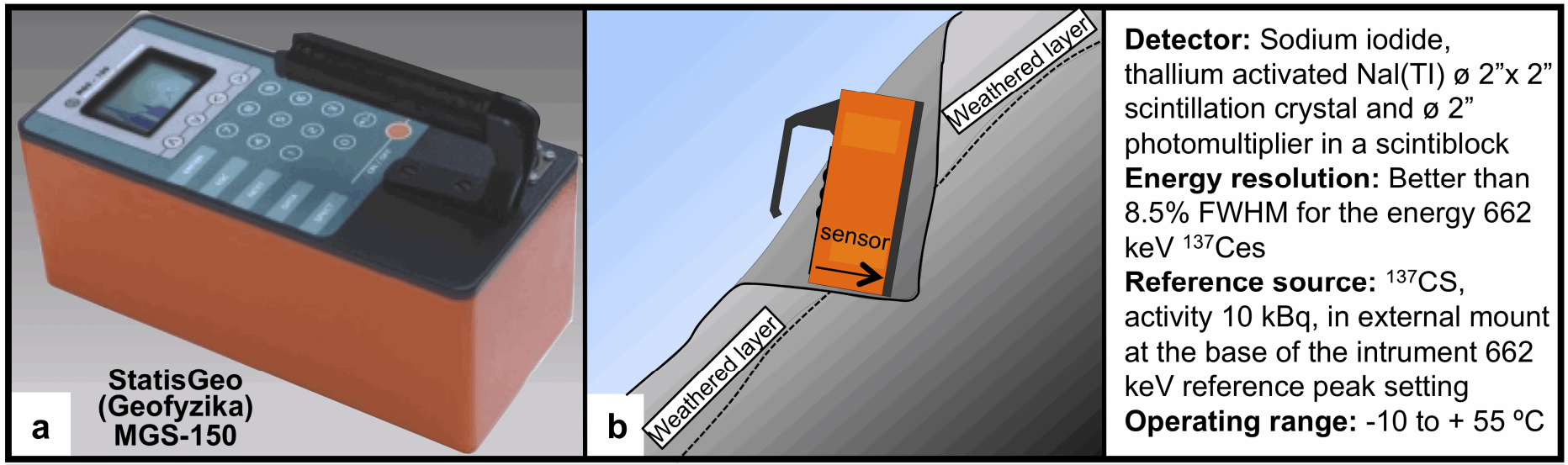

Appendix 2 [a – b] Handheld gamma ray tool and specifications, used to collect data presented in Figure 3.22. [c] Correlation chart of Munsell colours and gamma ray measurements. The chart shows no clear correlation. Ultimately the gamma ray data was barely used as the metre wide sample spacing appears to have aliased any fine-scale signal present within it. This data and methodology is included for completeness.

Appendix 3. Munsell colour chart

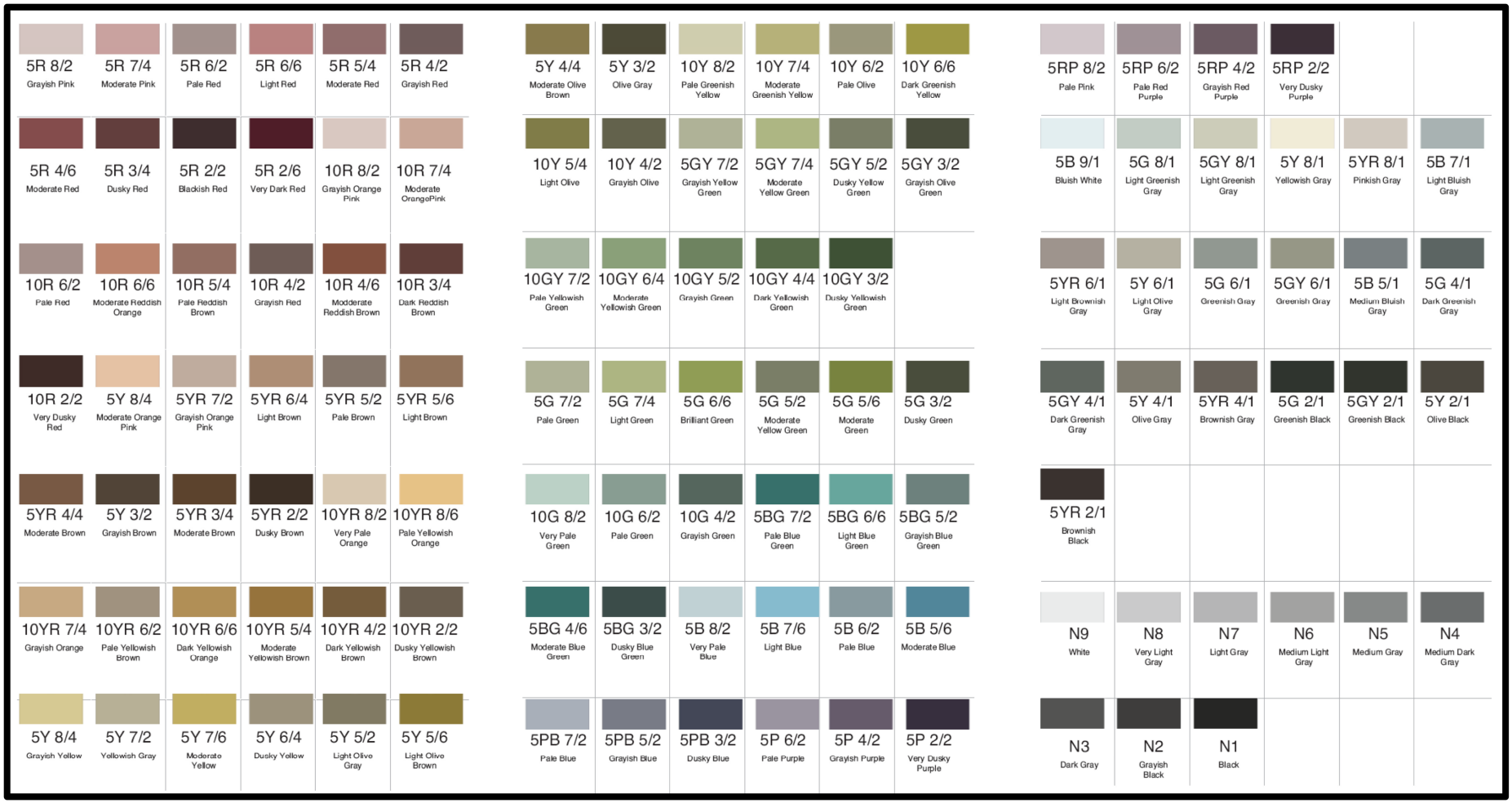

Appendix 3 Munsell colour chart (Munsell Colour Company, 2010)

Appendix 4. Photographic specimens of Apsheron Formation fossils

Appendix 4 Photographic specimens of bivalves, gastropods, trace fossils (top left), and fossilised wood (bottom right) observed in field outcrops of the Apsheron Formation

Appendix 5. Apsheron Formation dip-corrected palaeocurrent measurements

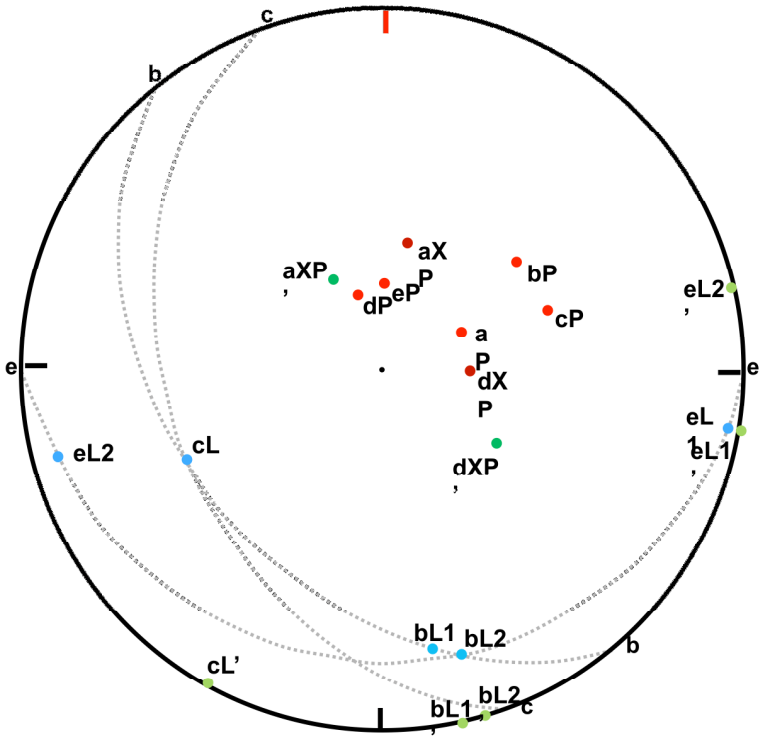

Appendix 5 Palaeocurrent measurements, plotted on a steronet and dip corrected

Corrected Palaeocurrent measurements for tectonic dip

MEASUREMENTS **name: measurement**	**orientation**	**log**
Cross bedding		
aP: Pole to bedding	154/20/SW	1b @ 5m
aXP: Pole to X bedding	100/30/S	
aXP': Pole to XB corrected	060/24/SE	
Paleocurrent direction	***150 °SSE***	
Ripple axes		
bP: Pole to bedding	140/40/SW	1b @ 20m
bL1: Ripple axis	176 °	
bL1':Corrected axis	168°	
Paleocurrent direction	***76°E/ 256 °W***	
bL2: Ripple axis	170 °	
bL2':Corrected axis	164°	
Paleocurrent direction	***74°E /254 ° W***	
Ripple axis		
cP: Pole to bedding	160/40/W	1b @ 30m
cL: Ripple axis	70 °	
cL':Corrected axis	168°	
Paleocurrent direction	***118°SE/298 °NW***	
Parting lineations		
eP: Pole to bedding	090/20/S	2 @ 50m
eL1: Parting lineation	100 °	
eL1':Corrected lineation	100°	
Paleocurrent direction	***100° E/280 °W***	
eL2: Parting lineation	75 °	
eL2':Corrected lineation	76°	
Paleocurrent direction	***76°E /278 °W***	

Appendix 6. Geological slope stability processes and seismic mapping methodology

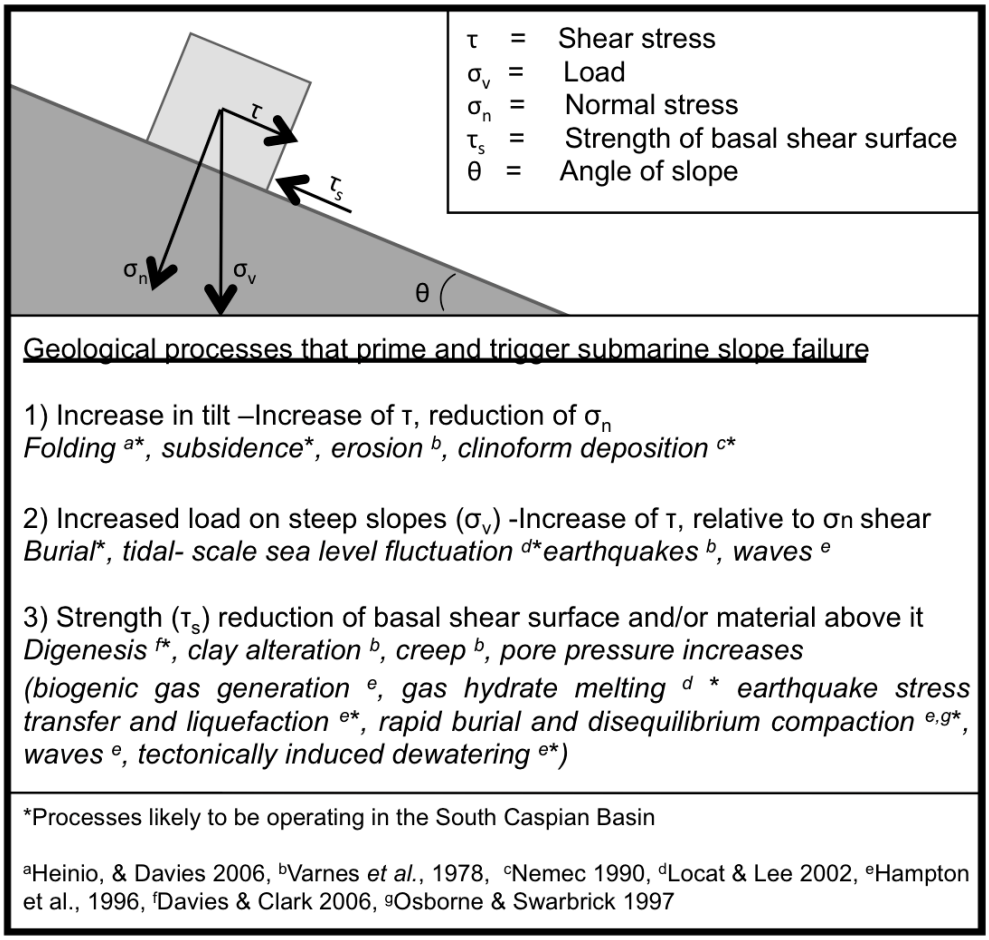

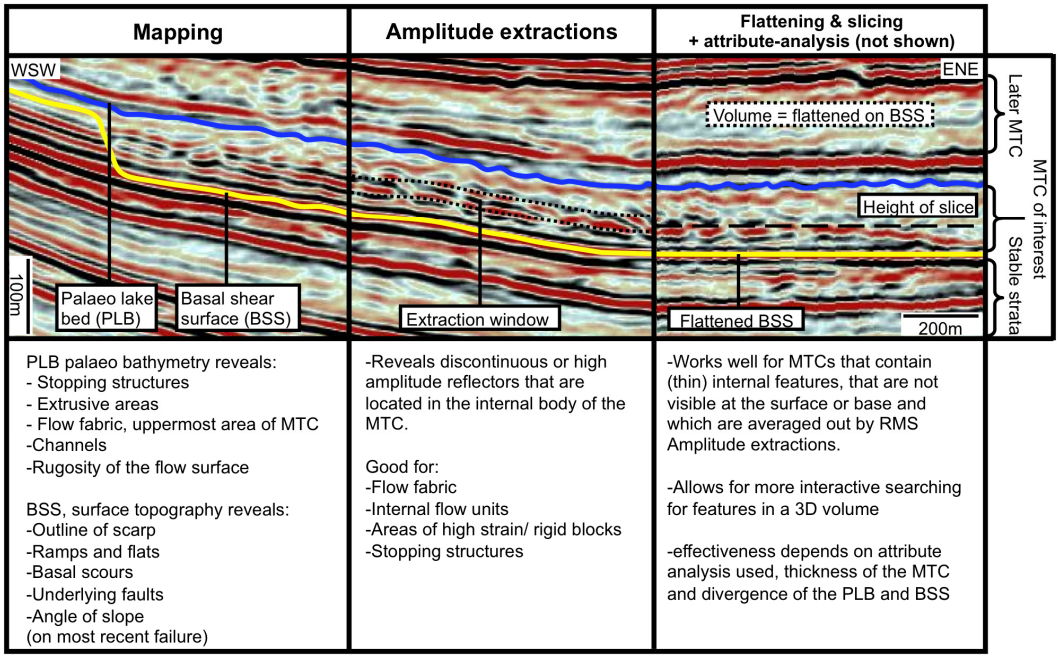

Appendix 6 [Upper] Cartoon summarising geological processes and their effects on slope stability along the South Caspian Basin margin. [lower] schematic explanation of each workflow for mapping mass transport deposits.

Appendix 7. Alternative views along mass transport basal shear surfaces

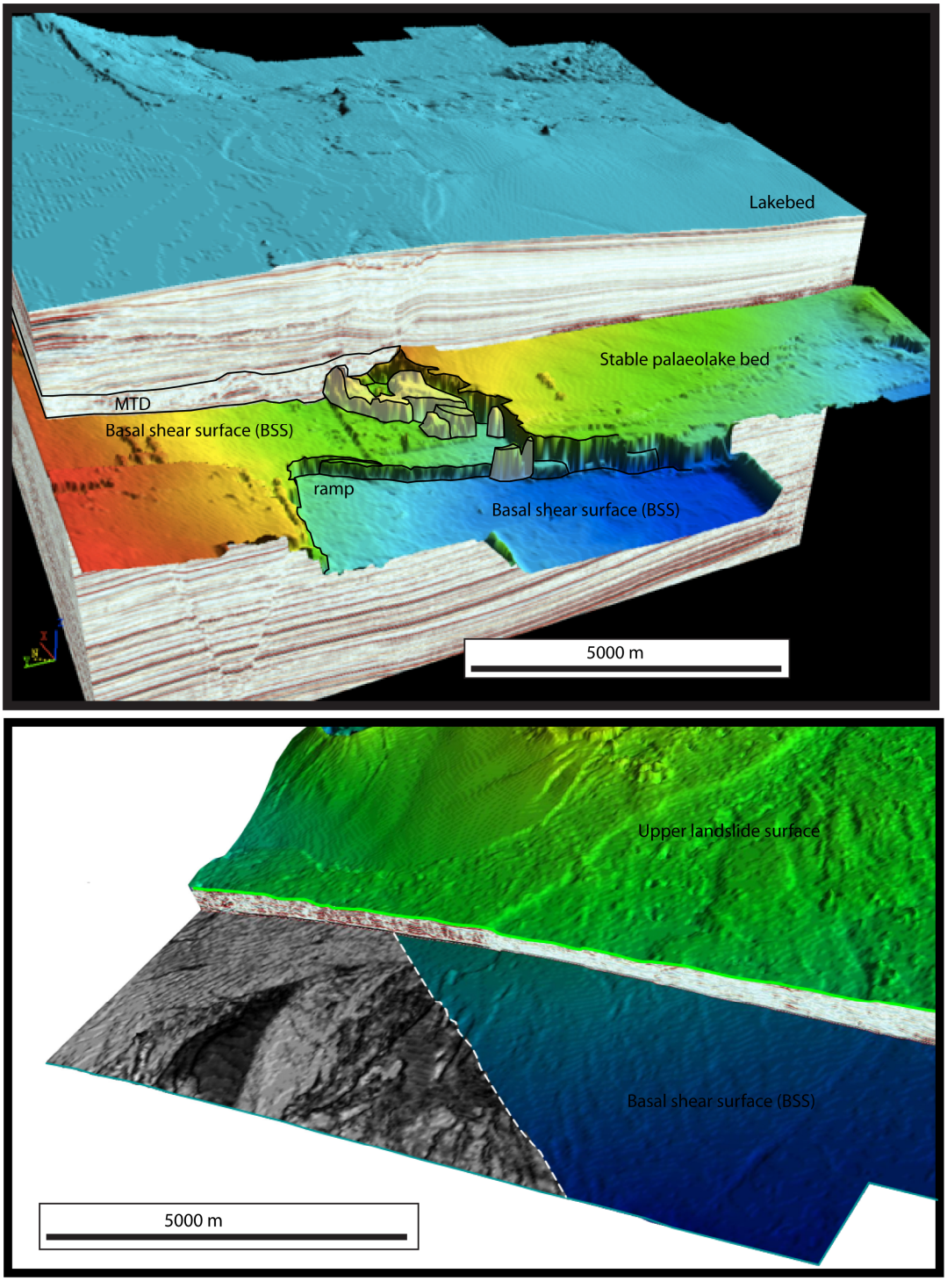

Appendix 7. Alternative views across mass transport complex basal shear surfaces. The upper image displays a complex ramp and flat morphology. The deposit contains several rafted blocks, which are highlighted in white. The same horizons are displayed in an alternative view on figure 4.3. The lower image depicts a dip-shaded perspective cut-out view across a landslide compressive domain. Information regarding the internal structure of this mass transport deposit is contained within the dip map of the landslide upper surface (green), dip map of the basal shear surface (blue) and amplitude extraction map taken 25 m above the basal shear surface (greyscale). Note the difference in detail between the amplitude extraction map and the basal shear surface dip map. The same mass transport deposit is shown in figure 4.9.

Appendix 8. Kinematic indicators of South Caspian Mass Transport Deposits

	Extensional Domain				Translational Domain					Compressive Domain				Other	
Name	- Crown cracks	- Headwall lobes	- Lateral margin ramps	- Convex up slope lineations	- Lateral shear zones	- Block raft orientation and shape	- Convex down slope lineations	- Erosional shadow remnants	- Basal grooves	- Basal scours	- Convex down slope thrust and fold traces	- Elongated lobes	- Out runner blocks	- Mud volcano flow orientations	-Over spilling material
MTC 1	×	×	×	×	×				×		×			×	
MTC 2					×						×				
MTD 3		×			×									×	
MTC 4		×	×	×	×									×	×
MTC 5			×		×									×	
MTC 6		×	×	×	×	×	×	×	×		×			×	
MTD 7											×	×	×	×	
MTD 8			×		×									×	
MTD 9		×	×	×	×									×	
MTD10		×	×	×	×									×	
MTD 11			×				×		×						
MTD 12											×	×			
MTC 13						×				×	×				
MTD 14											×			×	
MTD 15												×	×	×	
MTD 16												×			
MTC 17			×		×									×	
MTD 18			×						×						
MTD 19											×	×			
MTC A	×	×	×	×	×						×			×	
MTC B			×		×										
MTD C		×	×	×											
MTD D		×	×		×		×				×			×	
MTD E											×			×	
MTD F							×				×			×	
MTD G			×								×	×		×	
MTD H		×	×								×	×		×	
MTD I			×								×			×	
MTD J			×								×			×	

Appendix 8 List of kinematic and palaeo slope direction indicators present in each mass transport deposit and mass transport complex presented in chapter 4